

3-23-1962

A System for Recording Electromagnetic Atmospheric Noise in 30-50 CPS Region

James F. White

Follow this and additional works at: https://digitalrepository.unm.edu/ece_etds



Part of the [Electrical and Computer Engineering Commons](#)

Recommended Citation

White, James F.. "A System for Recording Electromagnetic Atmospheric Noise in 30-50 CPS Region." (1962).
https://digitalrepository.unm.edu/ece_etds/398

This Thesis is brought to you for free and open access by the Engineering ETDs at UNM Digital Repository. It has been accepted for inclusion in Electrical and Computer Engineering ETDs by an authorized administrator of UNM Digital Repository. For more information, please contact disc@unm.edu.

UNIVERSITY OF NEW MEXICO-UNIVERSITY LIBRARIES



A14429 094948

378.789

Un30wh

1962

cop. 2

RECORDING ELECTROMAGNETIC ATMOSPHERIC NOISE

-

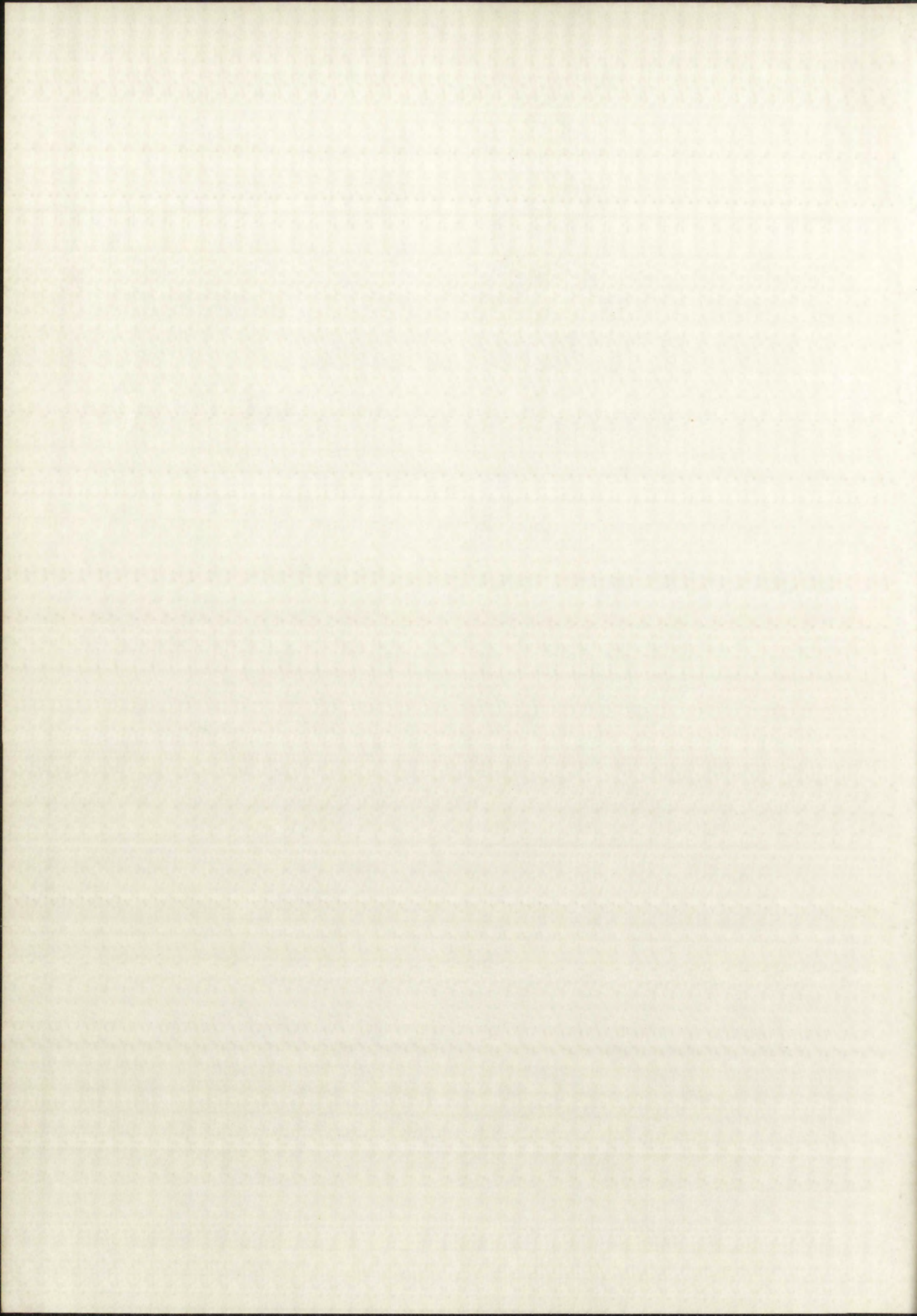
WHITE

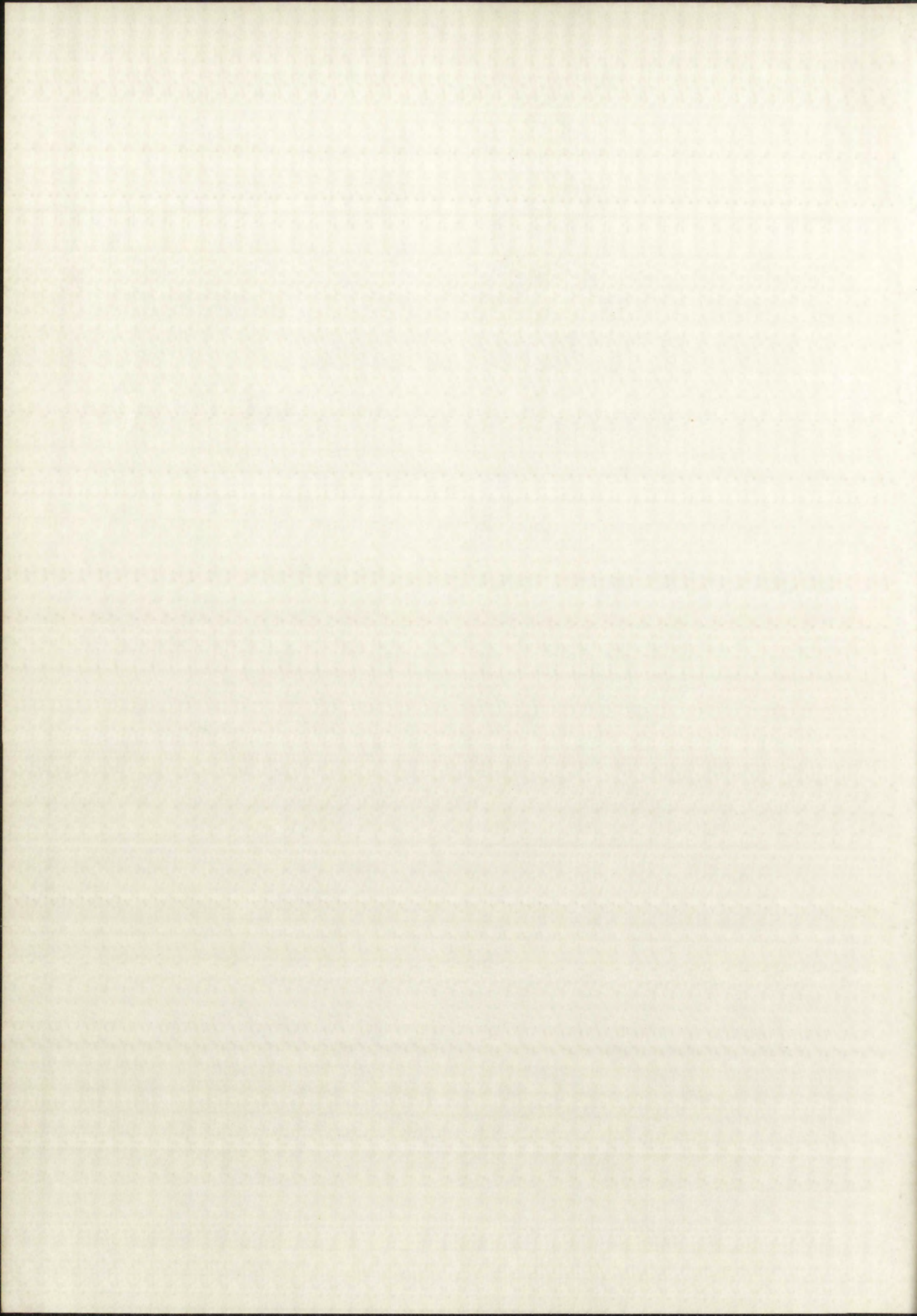
THE LIBRARY
UNIVERSITY OF NEW MEXICO

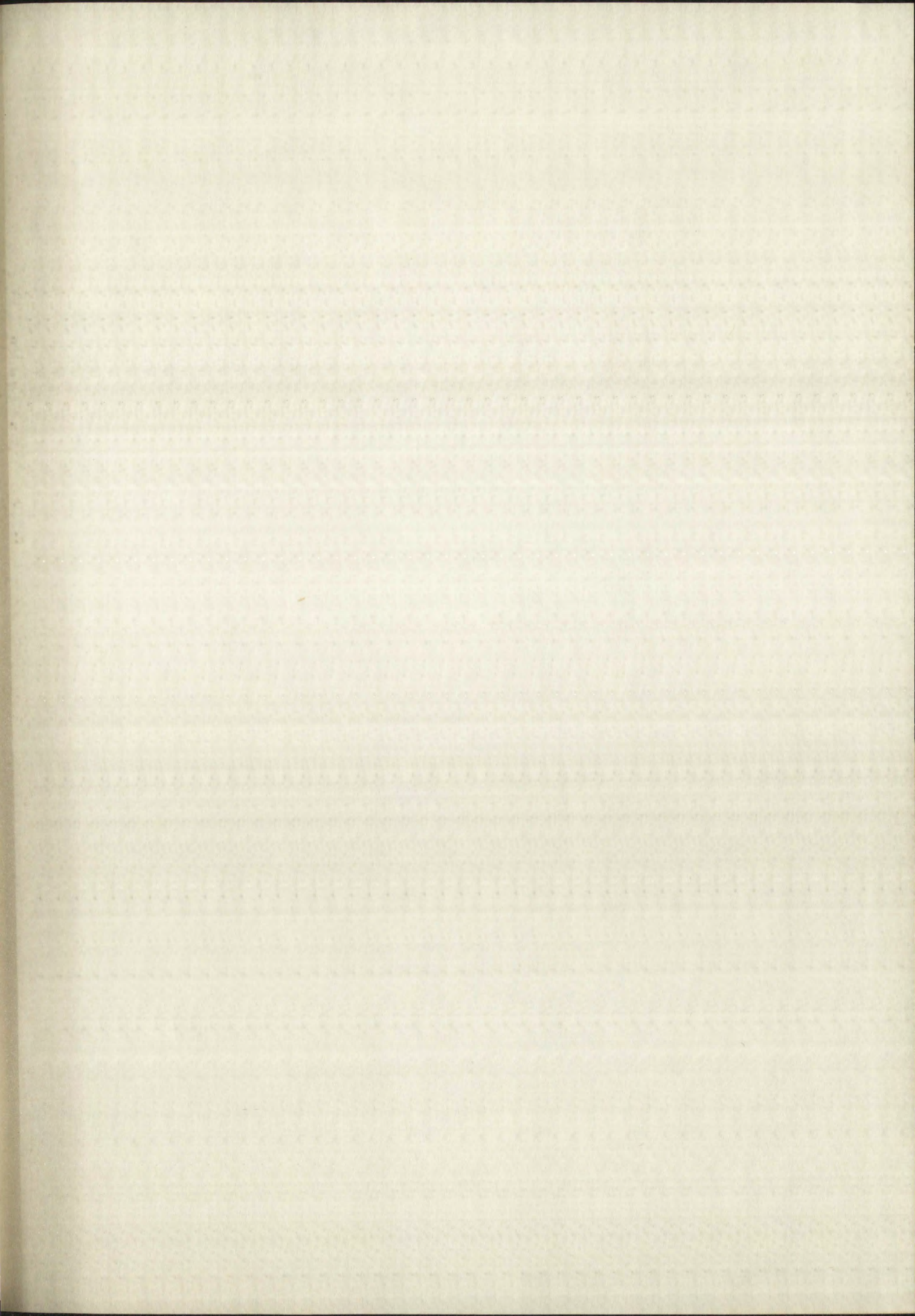


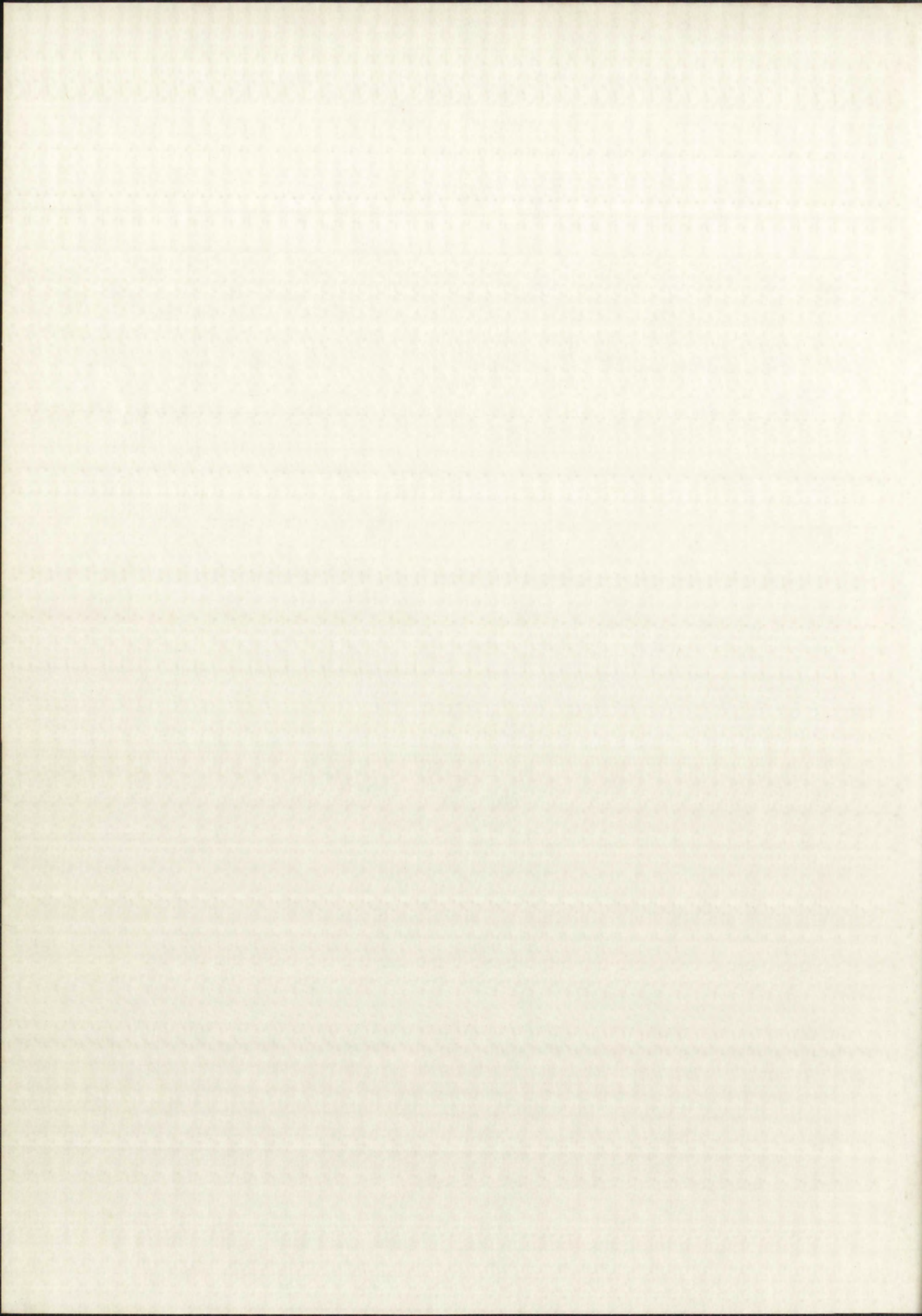
Call No.
378.789
Un30wh
1962
cop.2

Accession
Number
291589









ERASE BOND

GILBERT

• COTTON FIBRE

UNIVERSITY OF NEW MEXICO LIBRARY

MANUSCRIPT THESES

Unpublished theses submitted for the Master's and Doctor's degrees and deposited in the University of New Mexico Library are open for inspection, but are to be used only with due regard to the rights of the authors. Bibliographical references may be noted, but passages may be copied only with the permission of the authors, and proper credit must be given in subsequent written or published work. Extensive copying or publication of the thesis in whole or in part requires also the consent of the Dean of the Graduate School of the University of New Mexico.

This thesis by James F. White
has been used by the following persons, whose signatures attest their acceptance of the above restrictions.

A Library which borrows this thesis for use by its patrons is expected to secure the signature of each user.

NAME AND ADDRESS

DATE

MANUSCRIPT THESIS

Unpublished theses submitted to the Manuscript and Library Services and deposited in the University of New Mexico Library are open for inspection, but are not to be used without the express written permission of the author. Reproduction of the text of the thesis or any part thereof may be made for personal use only. The University of New Mexico Library reserves the right to make copies of the thesis for its own use. Extensive copying or publication of the thesis in whole or in part requires also the consent of the University of New Mexico.

This thesis by James L. White
has been used by the following persons who sign their names in
acceptance of the above restrictions:

A Library which borrows this thesis for use by its patrons is
expected to secure the signature of each user.

NAME AND ADDRESS DATE

A SYSTEM FOR RECORDING ELECTROMAGNETIC ATMOSPHERIC
NOISE IN 3-50 cps REGION

by

James F. White

A Thesis

Submitted in Partial Fulfillment of the
Requirements for the Degree of
Master of Science in Electrical Engineering

The University of New Mexico

1962

WOLFE
JAN 1962

A SYSTEM FOR RECORDING AND ANALYZING THE ACTIVITY OF

NOTES IN THE RECORD



James T. Wolfe

Submitted in Partial Fulfillment of the

Requirements for the Degree of

Master of Science in Electrical Engineering

The University of New Mexico

1962

WOLFE

This thesis, directed and approved by the candidate's committee, has been accepted by the Graduate Committee of the University of New Mexico in partial fulfillment of the requirements for the degree of

MASTER OF SCIENCE

Stuart A. Northrop
Dean

March 23, 1962
Date

Thesis committee


Shirley Entez
Chairman

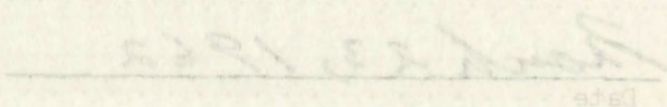
Ruben J. Kelly

R. D. Moore


This thesis, directed and approved by the candidate's committee, has been accepted by the Graduate Committee of the University of New Mexico in partial fulfillment of the requirements for the degree of

MASTER OF SCIENCE

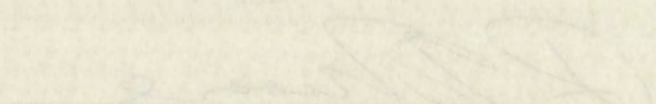

Dean


Date

Thesis committee


Chairman





378.789
Un 30 wh
1962
cop. 2

CONTENTS

	Page
ACKNOWLEDGMENTS	iii
LIST OF FIGURES	iv
CHAPTER	
1. INTRODUCTION	1
A. Historical Background	1
B. The Status of ELF Noise Data	9
C. The Need for ELF Noise Investigation	11
D. The Noise Data	12
E. Instrumentation	13
2. THE OVERALL SYSTEM	15
3. INDIVIDUAL UNITS OF THE SYSTEM	20
A. Tape Recorder	20
B. Oscillator	30
C. Multivibrator	34
D. Switch	36
E. Amplifier	39
F. Pre-amplifier	43
G. Antenna	45
4. FINAL SYSTEM DESIGN AND PERFORMANCE	48
A. Description of the System	48
B. Overall Performance Tests	54
C. Design Considerations	61
5. DATA-COLLECTING SITE	62
6. DATA SAMPLES	68
7. CONCLUSION	72
APPENDIX	
A. Twin-T Filters	74
B. Tape Recording	98
C. Modulation	112
D. Antenna	128
LIST OF REFERENCES	137

291589

ACKNOWLEDGMENTS

LIST OF FIGURES

CHAPTER

1. INTRODUCTION

1	A. Historical Background
3	B. The Status of ELF Noise Data
11	C. The Need for ELF Noise Investigation
15	D. The Noise Data
15	E. Introduction

2. THE OVERALL SYSTEM

3. INDIVIDUAL UNITS OF THE SYSTEM

20	A. Tape Recorder
20	B. Oscillator
21	C. Multiplicator
25	D. Switch
29	E. Amplifier
45	F. Pre-amplifier
45	G. Antenna

4. FINAL SYSTEM DESIGN AND PERFORMANCE

48	A. Description of the System
54	B. Overall Performance Tests
61	C. Design Considerations

5. DATA-COLLECTING SITE

6. DATA SAMPLES

7. CONCLUSION

APPENDIX

74	A. Twin-T Filters
98	B. Tape Recording
111	C. Modulation
128	D. Antenna

LIST OF REFERENCES

ACKNOWLEDGMENTS

The author expresses his sincere appreciation to Dr. Wallace L. Anderson, who suggested the subject of this paper, to Professor A. Erteza, who supervised the development of this paper, and to the United States Navy, which sponsored this research effort. Sincere appreciation is also extended to Professor R. K. Moore for his support and encouragement.

A special note of gratitude is extended to my wife, Lorraine, and my children.

The author is indebted to his undergraduate assistant, Mr. Dennis V. Brockway, for his untiring help and cooperation.

The author also wishes to thank Governor Esquipula Jojola, Governor of the Isleta Pueblo, for his permission to use the data-collection site on the Isleta Indian Reservation.

The author is appreciative of the conscientious work of the typist, Miss Amelia J. Montoya, and of the draftsman, Mr. Terry L. Anna.

The author has been...
Mr. William L. White...
paper, in 1914...
ment of this...
suggested this...
also extended...
encouragement...
A special...
Lorraine, and...

The author...
Mr. Dennis V. Brown...
The author...
Ugole, Governor...
has the data...
The author...
the typist, Miss...
Mr. Terry L. Anna...

W. L. White

LIST OF FIGURES

FIGURE	Page
1.1 A typical atmospheric waveform	6
2.1 Block diagram of data-collecting system	17
2.2 Block diagram of data-processing system	19
3.1 Block diagram of tape recorder in record mode before modification	23
3.2 Block diagram of tape recorder in playback mode before modification	24
3.3 Block diagram of tape recorder in record mode after modification	25
3.4 Block diagram of tape recorder in playback mode after modification	26
3.5 Schematic diagram of the oscillator	32
3.6 Oscillator frequency versus battery voltage for variations in temperature	33
3.7 Schematic diagram of the multivibrator	35
3.8 Schematic of the switch, "chopper"	37
3.9 Diagram of the switch output waveforms	38
3.10 Schematic diagram of the amplifier	40
3.11 Schematic diagram of the pre-amplifier	44
3.12 The antenna	47
4.1 Block diagram of data-collecting system	49
4.2 Schematic diagram of data-collecting system	50
4.3 Functional diagram of Test Point System	51
4.4 Schematic of Battery Test System	53

LIST OF FIGURES

FIGURES

- 1.1 A typical functional block diagram
- 1.2 Block diagram of data-collecting system
- 1.3 Block diagram of data-collecting system
- 2.1 Block diagram of data-collecting system in record mode before modification
- 2.2 Block diagram of data-collecting system in record mode before modification
- 2.3 Block diagram of data-collecting system in record mode after modification
- 2.4 Block diagram of data-collecting system in record mode after modification
- 2.5 Schematic diagram of the oscillator
- 2.6 Oscillator frequency versus battery voltage for variations in temperature
- 2.7 Schematic diagram of the amplifier
- 2.8 Schematic of the antenna
- 2.9 Diagram of the antenna system
- 2.10 Schematic diagram of the amplifier
- 2.11 Schematic diagram of the antenna
- 2.12 The antenna
- 3.1 Block diagram of data-collecting system
- 3.2 Schematic diagram of data-collecting system
- 3.3 Functional diagram of Test Point System
- 3.4 Schematic of battery test system

LIST OF FIGURES (Con't)

	Page
4.5 Tape recorder amplifier input versus battery voltage	56
Table 4-I Gain switch positions	58
4.6 Frequency response of receiver	60
5.1 Data-collecting site, $34^{\circ} 54' N$, $106^{\circ} 34' 30'' W$ (true)	64
5.2 Site location relative to Isleta Pueblo and Albuquerque, New Mexico	66
5.3 Data-collecting equipment at the site	67
6.1 Hourly recordings of atmospheric noise field strength versus frequency from 0900 to 1500 (MST) on August 21, 1961	69
6.2 Hourly recordings of atmospheric noise field strength versus frequency from 1800 to 2400 (MST) on September 15, 1961	70
6.3 Atmospheric noise field strength versus frequency during the hour 1000 to 1100 for the week August 21-25, 1961	71
A1 A "T" network	74
A2 Two T networks in parallel	78
A3 T network with R and C elements	79
A4 Twin-T network	80
A5 $ \beta $ versus ρ	91
A6 Twin-T network with voltage source and load	92
A7 D-C equivalent circuit of twin-T network with source and load	93
A8 High frequency equivalent circuit of twin-T network with source and load	94
A9 Capacity and resistance for null frequencies 0-50 cps	97

4.5 Tape recorder and voltage

Table 4.1 Gain and phase

4.6 Frequency response of amplifier

5.1 Data-collecting base (time)

5.2 Site location relative to later fault and Alhambra, New Mexico

5.3 Data-collecting equipment at the site

6.1 Hourly recordings of atmospheric noise (static) versus frequency from 0.00 to 1000 (MST) on August 11, 1981

6.2 Hourly recordings of atmospheric noise (static) versus frequency from 0.00 to 1000 (MST) on September 12, 1981

6.3 Atmospheric noise (static) versus frequency from 0.00 to 1000 for the week August 21-27, 1981

A1 A "T" network

A2 Two T networks in parallel

A3 T network with R and C elements

A4 Twin-T network

A5 |a| versus ω

A6 Twin-T network with voltage source and load

A7 D-C equivalent circuit of twin-T network with source and load

A8 High frequency equivalent circuit of twin-T network with source and load

A9 Capacity and resistance for unit capacitance

0-30 cps

LIST OF FIGURES (Con't)

	Page
B1 Interaction between tape speed and flux	98
B2 Recording head flux and tape speed versus time	100
B3 Playback tape speed versus time	102
B4 Playback signal frequency versus time	103
B5 Output voltage versus tape playback speed	106
B6 A non-symmetric capstan	107
B7 Tape playback speed versus time with non-symmetric capstan	108
Table B-I Signal frequencies at various tape speeds during playback	109
B8 Tape speed and signal frequency versus time during playback	110
C1 Single-ended switching	112
C2 Spectrum of single-ended switching	114
C3 Spectrum of single-ended switching after filtering by tape recorder	115
C4 Spectrum of single-ended switching used for analysis	116
C5 Bi-polar switching	117
C6 Bi-polar switching function	118
C7 Spectrum of bi-polar switching	119
C8 Transistor switch	120
C9 Equivalent circuit for transistor switch	121
C10 Spectrum of transistor switch after filtering by tape recorder	122
D1 Loop antenna configuration	129
Table D-I Capacity of a vertical antenna with variations in dimensions	132
D2 Values of the constant k for h'/m	135
D3 Antenna reactance versus frequency	136

LIST OF FIGURES (Cont.)

Page	
98	81. Interaction between tape speed and flux
100	82. Recording head flux and tape speed versus time
102	83. Playback tape speed versus time
103	84. Playback signal frequency versus time
106	85. Output voltage versus tape playback speed
107	86. A non-symmetric capacitor
108	87. Tape playback speed versus time with non-symmetric capacitor
109	Table A-1. Signal frequencies at various tape speeds during playback
110	88. Tape speed and signal frequency versus time during playback
112	89. Single-ended switching
114	90. Spectrum of single-ended switching
115	91. Spectrum of single-ended switching after filtering by tape recorder
116	92. Spectrum of single-ended switching used for analysis
117	93. Bi-polar switching
118	94. Bi-polar switching function
119	95. Spectrum of bi-polar switching
120	96. Transistor switch
121	97. Equivalent circuit for transistor switch
122	98. Spectrum of transistor switch after filtering by tape recorder
123	99. Loop antenna configuration
124	Table D-1. Capacity of a vertical antenna with variations in dimensions
125	D1. Values of the constant k for h/λ
126	D2. Antenna resistance versus frequency

1. Introduction

A. Historical Background

The electromagnetic noise spectrum extends from below 1 cps to above 3,000 mcs. Within this spectrum many phenomena of atmospheric noise have been observed. Those atmospherics which occur in the audio frequency region of the spectrum have been given not only descriptive but also subjective names by many different investigators. As a result, it is often difficult to determine from the literature what aspect of the noise phenomenon is being considered. In addition, references to low frequencies involved in certain experiments are vague. A brief history of atmospherics research is presented here in order to explain the terminology, to show the frequencies involved, and to give some indication of the many aspects of atmospheric noise.

Throughout this paper, VLF (Very Low Frequency) refers to the 3-30 kc region as defined at the Atlantic City Radio Convention 1947 [Tepley 1959]. The 1-3,000 cps range is called the ELF (Extremely Low Frequency) range [Wait 1960a, Wait and Carter 1960, Wait, 1960b]. The term "atmospherics" includes all atmospheric noises and, on the basis of the source of the noise, is subdivided into three parts, viz., whistlers, VLF emissions, and "sferics" [Helliwell, 1958].

Whistlers occur in the 1-30 kc region of the spectrum and consist of long descending tones with durations that vary from 2 to 3 seconds. They were first observed by Barkhausen in 1919. It is believed that they are due to the dispersion of lightning energy through the ionosphere guided along the earth's magnetic

flux lines [Helliwell, 1958] . Helliwell and Morgan [1959] mention several types of whistlers--pure tone, swishy, multiple, short, long, echo, and nose. Helliwell et al. [1956] observed that the whistler was not a homogeneous band of noise as previously observed, but was a rapid succession of discrete traces or pure tones. Each trace appeared at approximately 1500 cps and separated into two branches--one decreasing in frequency as usual, but the other increasing in frequency contrary to Eckersley's dispersion law. Helliwell calls this the "nose whistler" due to the characteristic shape of the two branches arising from the initial "nose" frequency. This disclosure was largely due to better frequency resolution provided by the spectrograph used in the analysis [Gruentz, 1951, Potter, 1945, Grierson, 1957] .

Another type of atmospheric is "VLF emissions"--a name first proposed by Gallet [1959] . These emissions occur in the same frequency range as whistlers and are thought to be generated in the exosphere [Helliwell, 1958] . Crary and Helliwell [1961] developed equations for the duct propagation of both whistlers and VLF emissions.

Finally, the last category of atmospherics is called "sferics." They are due to lightning sources and are propagated in the earth-ionosphere cavity by ground wave or by reflections. These sferics include tweeks, warbling, chirping, risers, hooks, hiss, and chorus. The name "dawn chorus" was introduced by Storey because it sounds like the warbling of birds at dawn. This chorus is a combination of short

link lines [Helliwell, 1958] [Helliwell and Morgan, 1959]

mention several types of whistles--pure tone, whistly, multiple, short, long, echo, and nose. Helliwell et al. [1956] observed

that the whistle was not a homogeneous band of noise as previously observed, but was a rapid succession of discrete traces of pure tones. Each trace appeared at approximately 1500 cps and separated into two branches--one decreasing in frequency as usual, but the other increasing in frequency

contrary to Rokerley's dispersion law. Helliwell calls this the "nose whistle", one of the characteristic shapes of the two branches arising from the initial "nose" frequency. This

dispersion was largely due to better frequency resolution provided by the spectrograph used in the analysis [Ortengren, 1951; Potter, 1945; Gjersten, 1951]

Another type of atmospheric is "VLF emissions"--a name first proposed by Galt [1959]. These emissions occur in the same frequency range as whistles and are thought to be generated in the exosphere [Helliwell, 1958]. Cary and

Helliwell [1961] developed equations for the duct propagation of both whistles and VLF emissions.

Finally, the last category of atmospheric is called "sferics". They are due to lightning sources and are propagated in the earth-ionosphere cavity by ground wave or by reflections. These sferics include twerks, warbling, chirping, rizers, hooks, hiss, and chorus. The name "dawn chorus" was introduced by Storey because it sounds like the warbling of birds at dawn. This chorus is a combination of short

(0.1 - 0.2 second) rising whistlers and warbling tones the occurrence of which increases near the auroral zone. Although the chorus has been known for many years, no systematic study has been made [Gallet and Helliwell, 1957]. Tweeks are musical sounds produced by long pulse trains as a result of the number of reflection paths between the ionosphere and earth. According to Helliwell [1958], they may be quite long (50-100 milliseconds) and are often mistaken for whistlers. Watts [1957b] concludes from his work that this is not associated with individual sferics or whistlers. His analysis shows that the greatest amplitude is centered around 3 kcs [Watts, 1957a]. Martin et al. [1960] have indicated that hiss is broadly centered around 8 kcs. Although chorus, hiss, and risers are heard during magnetic storms, their origin is unknown [Helliwell, 1958].

Tepley [1961b] refers to "hm" emissions--hydromagnetic emissions. These emissions occur in the 0.5 to 5 cps region and are single frequency oscillations which may vary slowly with time.

At the extreme low frequencies there exist small fluctuations in the geomagnetic field which are called geomagnetic micropulsations [Boothe et al., 1960]. These pulsations have been known since 1861. They have periods of several seconds to several minutes and, according to Campbell [1959], occur in two groups with periods of 1-3 minutes and 5-30 seconds and have flux densities approximating $1/3 \gamma$ with recordings as high as 40γ ($\gamma = 10^{-5}$ gauss = 10^{-9} webers/m²). Duffus et al. [1957] conclude from their observations that these

(0.1 - 0.2 second) rising whistles and whistling tones the

occurrence of which increases near the auroral zone. Although

the chorus has been known for many years, no systematic study

has been made [Gale and Helliwell, 1957]. Two aspects of interest

sounds produced by ionospheric waves as a result of the number

of reflection paths between the ionosphere and earth. According

to Helliwell [1956], they may be quite long (50-100 miles)

(seconds) and are often mistaken for whistlers. Watts [1957b]

concludes from his work that this is not associated with individual

dual auroral whistlers. His analysis shows that the greatest

amplitude is centered around 5 Kcs [Watts, 1957a]. Martin

et al. [1960] have indicated that this is probably centered

around 8 Kcs. Although chorus, hiss, and hiss are heard

during magnetic storms, their origin is unknown [Helliwell,

1958].

Topley [1961b] refers to "magnetic--hydromagnetic

emissions. These emissions occur in the 0.5 to 5 cps region

and are single frequency oscillations which vary slowly

with time.

At the extreme low frequencies there exist small fluctuations

in the geomagnetic field which are called geomagnetic

microfluctuations [Booth et al., 1960]. These fluctuations

have been known since 1961. They have periods of several seconds

to several minutes and, according to Campbell [1959], occur in

two groups with periods of 1-5 minutes and 5-30 seconds and

have flux densities approximating 10^{-5} with recordings as

high as 40γ ($\gamma = 10^{-5}$ gauss = 10^{-9} weber/m²). Booth et al.

[1957] conclude from their observations that these

micro-pulsations do not occur simultaneously everywhere as is "occasionally stated in the literature."

Earth currents, telluric, or magneto-telluric fields pertain, of course, to the E and H fields of the earth. These currents were discovered, according to Hopkins [1960], in ground return circuits of telegraph lines where potentials are sufficient to energize the system without batteries. These phenomena, of course, are also present in underwater communications cables. Although diurnal and seasonal variations have been investigated, variations of shorter periods--frequency range from .005 cps to 1 cps--have only recently been studied [Smith, et al., 1960].

Long delay echoes with a delay from 2 to 20 seconds were first observed by Van der Pol and Störmer in 1928. Budden has investigated this phenomenon with no success. Apparently there is no explanation for these long delay echoes. However, Storey, who has done theoretical work on whistler traces [Storey, 1957], believes that the long delay echo is not produced by whistler mode type propagation.

In general, most investigators attribute low frequency noise to thunder-storm activity [Gustafsson et al., 1960]. However, Gallet and Helliwell, [1959] believe that a portion of this noise originates in the ionosphere. Pierce [1960b] in considering the work of Large [1957], Large and Wormell [1958], Aarons [1956], and Willis [1948] concluded that above 20 cps the electric and magnetic fields are electromagnetic and due to sferics while below 20 cps the E and H fields are due to different sources, i.e., the E field is due

micro-pulsations of the geomagnetic field.

"Electromagnetic waves" in the ionosphere.

Earth currents, and their relation to the geomagnetic field.

Portals of cosmic rays, and their relation to the geomagnetic field.

Currents were observed in the ionosphere, and their relation to the geomagnetic field.

Ground return currents, and their relation to the geomagnetic field.

Insufficient to energize the ionosphere, and their relation to the geomagnetic field.

Phenomena, of course, and their relation to the geomagnetic field.

Long cables, although they are not, and their relation to the geomagnetic field.

been investigated, and their relation to the geomagnetic field.

range from 0.05 cps to 1 cps, and their relation to the geomagnetic field.

[Smith, et al., 1959] and their relation to the geomagnetic field.

Long delay echoes with a delay from 1 to 10 seconds were

first observed by Van der Pol and his group in 1930, and their relation to the geomagnetic field.

investigated this phenomenon with a view to its relation to the geomagnetic field.

there is no explanation for these long delay echoes, however.

Storey, who has done theoretical work on this phenomenon, believes that the long delay echoes are

[Storey, 1957], and their relation to the geomagnetic field.

produced by whistler mode waves, and their relation to the geomagnetic field.

In general, most investigators attribute the long delay echoes to

noise to thunder-storm activity, and their relation to the geomagnetic field.

However, Gallet and Helliwell [1955] believe that a part of

of this noise originates in the ionosphere, and their relation to the geomagnetic field.

in considering the work of [Storey, 1957], and their relation to the geomagnetic field.

[1958], and their relation to the geomagnetic field.

above 30 cps the electric field is considered to be due to the geomagnetic field.

magnetic and due to electric fields, and their relation to the geomagnetic field.

fields are due to different sources, and their relation to the geomagnetic field.

to moving space charges and the H field to ionosphere and earth currents. Campbell [1959] states that the interval in which the dominant signals change from those due to slow tail sferics to geomagnetic pulsations is in the 0.2 to 2.0 cps range. This agrees with Hopkins [1960] who has noticed that micropulsations occur below 0.2 cps and that signals due to sferics are above 2 cps. He further noted that there is very little energy in the transition band at 1 cps. Duffus, et al. [1957] have conducted experiments in this area of the spectrum between pulsations and atmospherics. Holzer and Deal [1956] also have investigated this spectral region.

According to Gustafsson, et al. [1960], the existence of natural electromagnetic radiation in the audio frequency range was first discussed by Menzel and Salisbury [1948]. Aarons and Henissart [1953] reported correlation between low frequency magnetic fluctuations and geomagnetic disturbances and solar phenomenon. In 1960, Aarons, et al. [1960] observed two bands of noise which correlated with geomagnetic disturbances, viz., 600-950 cps centered at 750 cps (the gyro frequency of protons at 100 km) and 1.8 to 4.5 kcs. They were considering the possible source of low frequency radiation to be emissions due to protons revolving around geomagnetic field lines at the gyro frequency. However, Gustafsson, et al. [1960] in their experimentation found no correlation between low-frequency noise and magnetic activity or between 20 to 200 cps range and solar noise at 200 mc during SID (Sudden Ionosphere Disturbance). A year later, Pierce [1961] observed that SID had no effect in the 10 to 20 kc range but that attenuation increased below 10 kcs and decreased above 20 kcs.

to moving space of the ...
with the dominant ...
stages to geomagnetic ...
range. This agrees ...
microflashes occur ...
stages are above ...
little energy in the ...
[1951] have conducted ...
between pulsations ...
also have investigated ...
According to ...
natural electromagnetic ...
was first discussed by ...
and Hannasert [1955] ...
magnetic fluctuations ...
phenomenon. In 1950 ...
of noise which ...
600-950 cps centered ...
at 100 km) and 1.5 ...
possible source of ...
to protons revolving ...
frequency. However ...
mentation found no ...
magnetic activity ...
at 300 mc during ...
later, Pierce [1961] ...
to 30 kc range but ...
observed above 30 ...

In addition to observations mentioned above, considerable interest has been shown in spheric waveforms. For the purpose of discussion, a typical waveform is shown in Figure 1.1.

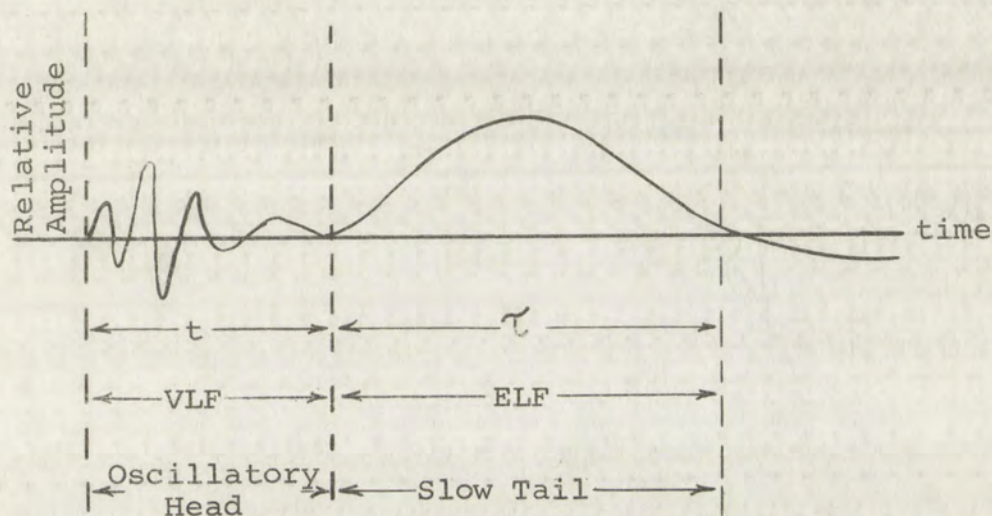


Figure 1.1 A typical atmospheric waveform

These waveforms are usually amplified with wide-band receivers and displayed on an oscilloscope for photographic purposes. Wide-band equipment is necessary if both the VLF and ELF portions of the waveform are to be observed.

Watson-Watt, et al., [1937] observed the presence of the slow tail and also the increased separation of the head and tail with increase in propagation distance. They used the time duration " t " and " $\frac{\tau}{2}$ " as parameters in what was apparently the first detailed study of the slow tail. Hepburn and Pierce [1953] also investigated the slow tails and measured " $\frac{\tau}{4}$ ".

Appleton and Chapman [1937] noticed that all these waveforms had characteristic patterns and that frequencies around 2 kcs

In addition to showing that the system has been used in the past, the system has been used in the past in the past.



Figure 1-1. A typical atmospheric wave.

These waveforms are usually recorded with a wide-band receiver and displayed on an oscilloscope for photographic purposes. Wide-band equipment is required to detect the VLF and ELF portions of the waveform and to be sensitive.

Watson-Walt, et al., [1951] observed the presence of the slow tail and also the increased duration of the head and tail with increase in propagation distance. They used the time duration "f" and "g" as parameters in which was exponentially the first detailed study of the slow tail. Yeh and Pao [1952] also investigated the slow tail and reported that all these waveforms had characteristic patterns and their frequencies around 1 Mc.

were either originally missing or highly attenuated. In order to determine the cause of this apparent absorption at 2 kcs, Chapman and Edwards [1950] simultaneously recorded waveforms and frequency spectrum. Subsequent observations by Chapman and Matthews [1953], Chapman and Jolley [1954], and Chapman and Macario [1956] showed that there was in fact an absorption at 2 kcs. This effect contradicted the Austin-Cohen law [1911] which says that attenuation decreases with frequency. Actually this law was based on observations of VLF propagation above 12 kcs. In 1957, Wait [1957] theoretically established this absorption band at 1 to 3 kcs.

The attenuation coefficient " α " in the ELF region is quite low. Chapman and Macario [1956] from their amplitude spectra measurements, found " α " to be 1 db/1000km at 100 cps. Tepley [1959] has also experimentally determined " α " and dispersion in the ELF region. In addition to these studies of " α ," substantial work has been done on the waveform patterns themselves. Chapman and Pierce [1957] observed the different waveforms as a function of geographical location where distance and lower ionosphere conditions were considered the same. In addition, Hepburn [1958] classified waveforms according to source, distance, and geographical effects. See also Hepburn [1957a] and [1957b].

Hepburn and Pierce [1953] established experimentally an empirical law for " t " and " $\frac{T}{4}$ " as a function of distance for both night and day. They also worked out values of ionosphere height and conductivity using Hales' [1948] theory. These figures were later revised by Hepburn [1957b]. Liebermann's

were either originally missed or highly attenuated. In order to determine the cause of this, Chapman and Mattheus [1952] and Chapman and Mattheus [1953] simultaneously recorded waveforms and frequency spectra. Subsequent observations by Chapman and Mattheus [1952], Chapman and Topley [1954], and Chapman and Mattheus [1955] showed that there was in fact an absorption at 2 Mc. This effect contradicted the Appleton-Cohen law [1911] which says that attenuation decreases with frequency. Actually this law was based on observations of VLF propagation above 12 Mc. In 1957, Wait [1957] theoretically established this absorption band at 1 to 5 Mc. The attenuation coefficient "Q" in the ELF region is quite low. Chapman and Mattheus [1955] from their amplitude spectra measurements, found "Q" to be 1 to 100 km at 100 cps. Topley [1955] has also experimentally determined "Q" and dispersion in the ELF region. In addition to these studies of "Q", substantial work has been done on the waveform patterns themselves. Chapman and Prince [1957] observed the different waveforms as a function of geographical location, wave distance and lower ionosphere conditions were considered the same. In addition, Heppner [1958] classified waveforms according to source, distance, and geographical effects. See also Heppner [1957a] and [1957b].

Heppner and Prince [1957] established experimentally an empirical law for "Q" and "Q'" as a function of distance for both night and day. They also worked out values of ionosphere height and conductivity using Heale's [1948] theory. These studies were later revised by Heppner [1957c]. Liebermann's

[1956a] experimental results for slow tail propagation fit his theory [Liebermann, 1956b] for values of ionosphere heights and conductivity which did not agree with those of Hepburn and Pierce [1953] or Hepburn [1957]. Pierce [1960b] states that these different results have never been resolved. However, Wait [1960b] indicates that the different results are reconcilable if it is remembered that Hales' [1948] theory is only good for narrow band type of signals, i.e., quasi-monochromatic.

In addition to the observation of "t" and " $\frac{\tau}{2}$," the polarity of the slow tails has also been of interest. Liebermann [1956a] was apparently the first to observe two types of slow tail pulses. The normal tail is shown in Figure 1.1. The "anomalous" tail is initially positive-going but completes a full cycle in the period " τ " before tapering off. Whitson [1960] reported an apparent phase reversal of ELF waveform--positive-going at St. Johns, Newfoundland and negative-going at Thule, Greenland. He states that further investigation is necessary before such a reversal can be considered a reality. Taylor [1961] noted that the positive-going tails had more well defined relationship between such parameters as radiated energy, peak field strength, $\frac{\tau}{2}$, and frequency of the spectral peak than the negative-going tails. Tepley [1961a], who also considered the polarity of slow tails, believes that the negative polarity is due to intra-cloud discharge, not to propagation effects, and that the positive polarity tail is due to regular cloud-to-ground discharge.

Experimental evidence of propagation as a function of direction has been obtained. Lutkins [1939] was the first to

[1955] experimental results for the first time.

His theory [1955] was that the tail of the distribution

and conductivity which is a function of the temperature

curve [1955] is a function of the temperature.

These different results have been obtained by different

ways [1955] and it is not clear whether they are correct

since it is not possible to obtain a definite answer

for narrow band type of materials.

In addition to the above results, it has been found

that the polarity of the slow tail of the distribution

[1955] was apparently the same for all the materials

tail polarities. The polarities of the slow tail of the

"anomalous" tail is not the same for all the materials

tail cycle in the period of the tail of the distribution.

[1955] reported an experiment which showed that the

positive-going at low temperatures and negative-going

at high temperatures. He stated that further investigation

necessary before such a generalization can be made.

Taylor [1955] noted that the positive-going tail of the

defined relationship between the tail of the distribution

peak field strength and the temperature of the material

the negative-going tail. Taylor [1955] also stated that

the polarity of slow tail of the distribution is not the

same for all the materials.

is due to inter-atomic distances and the temperature

and that the positive-going tail of the distribution is

ground discharge.

Experimental evidence of the existence of a tail of the

direction has been obtained. Taylor [1955] and others

observe that waveforms from the west contained more oscillations and were smoother than those from the east. Crombie [1958] found that VLF signals were attenuated less in West-to-East propagation. Barber and Crombie [1959] showed that ionosphere reflection depends on the direction of propagation. This, of course, supports the experimental evidence.

Other aspects of atmospheric noise such as the electrostatic field and lightning itself have been observed and studied. Watt [1960] finds that in fair weather the electrostatic field is approximately 100 v/m and in foul weather as high as 4,000 v/m. During fair weather, the static E field fluctuations are around 1 v/m [Pierce 1955]. The duration of field changes due to lightning is as long as one second [Pierce 1960b]. Lutkin [1939] has measured fields up to 600 v/m at a distance of 5 km from a storm. Wilson [1920] found that the field changes due to a nearby thunderstorm were usually positive. Lightning has been found to occur on the average of 100 strokes/sec over the earth [Liebermann 1956a]. This average over the earth's surface also agrees with Davis [1961].

B. The Status of ELF Noise Data

Regardless of the numerous investigations of atmospheric noise, the experimental data in the ELF region is rather limited [Wait and Carter, 1960; Wait, 1960d; Watt, 1960]. The experimentation that has been done in this region has been "incidental to the reception of higher frequencies" [Liebermann 1956a], in connection with recording of slow tails [Wait, 1960b; 1960e], and in geomagnetic work at frequencies below 0.1 cps

operative that was...
the were...
that the signals were...
Barber and...
depends of the...
reports the experimental...

Other aspects of...
static field and...
water [1900]...
is approximately 100...
During late...
1 v/m [place 1955]...
lightning is as...
[1950] has measured...
from a storm...
a steady...
been found to...
earth [Lieberman 1955]...
surface also agrees with...

B. The status of...
Regardless of the...
noise, the experimental...
limited [Wall and...
experimentation that...
"incidental to the...
1955a] in connection...
1950e] and in connection...

[Goldberg, 1956] . Duffus, et al. [1958] refer to their experiment in 1957 as being conducted in the "somewhat neglected frequency range 0.1 to 30 cps." The meagerness of noise information in the ELF region is indicated by the fact that the International Radio Consultative Committee Compilations extend down to only 10 kcs.

This lack of ELF noise data is a hindrance to experimenters in developing receiving equipment and to theoretical investigators in analyzing their work. In discussing his system for spheric observations, Whitson [1960] mentions that it was made flexible because the nature and magnitude of sferics in the arctic were unknown. Pierce [1960a] maintains that further theoretical work in ELF propagation is "academic" as long as experimental observations remain "so scanty."

In contrast to the experimental work in the ELF region, considerable attention has been given to theoretical work by Schumann [1952a, 1954a, 1954b] , Wait [1956] , and Liebermann [1957] . One aspect of these studies has been the development of the mode theory in which the earth and ionosphere are considered as a resonant cavity. The resonant frequencies of this cavity were apparently first suggested by Schumann [1952b] . The first three Schumann mode frequencies--10.6, 18.3, and 25.9 cps--were also determined by Wait [1960a] .

In spite of the theoretical work on the mode frequencies, there has been practically no effort made toward securing experimental evidence of their reality. At the time of this literature survey, Balser and Wagner [1960] reported their unsuccessful experiment to observe these resonant frequencies.

[Goldberg 1950] ...

... in 1950 ...

... frequency range ...

... from the ...

... included Radio ...

... to only 10 ...

... This lack of ...

... in developing ...

... factors as ...

... astatic observations ...

... astatic were ...

... theoretical work ...

... experimental observations ...

... In contrast to ...

... considerable attention ...

... Schumann [1951, 1952, 1953, 1954, 1955, 1956, 1957, 1958, 1959, 1960, 1961, 1962, 1963, 1964, 1965, 1966, 1967, 1968, 1969, 1970, 1971, 1972, 1973, 1974, 1975, 1976, 1977, 1978, 1979, 1980, 1981, 1982, 1983, 1984, 1985, 1986, 1987, 1988, 1989, 1990, 1991, 1992, 1993, 1994, 1995, 1996, 1997, 1998, 1999, 2000, 2001, 2002, 2003, 2004, 2005, 2006, 2007, 2008, 2009, 2010, 2011, 2012, 2013, 2014, 2015, 2016, 2017, 2018, 2019, 2020, 2021, 2022, 2023, 2024, 2025]

... One aspect of ...

... of the mode theory ...

... considered as a ...

... this cavity were ...

... The first three ...

... ops were also ...

... In spite of the ...

They concluded that further experimentation was necessary at frequencies nearer to the fundamental 10.6 cps.*

C. The Need for ELF Noise Investigation

The absence of information in the ELF region does not of itself constitute a need for further physical research. However, as pointed out in the previous section, this situation has hampered theoretical work and has had a bearing on experimentation. Many researchers in atmospheric noise have expressed the need for further investigations in the lower VLF and the ELF regions of the spectrum.

In 1957, Watt and Maxwell [1957] emphasized the importance of knowing not only the character of atmospheric noise but also the level when determining system performance. They show that the limiting noise factor in VLF communications is atmospheric noise rather than man-made or thermal noise and conclude that the "need for a detailed investigation of the statistical character of atmospheric noise is readily apparent." Anderson [1961] demonstrated that natural noise is also the basic limitation in the 1 to 1,000 cps region and pointed out that system attenuation figures in this region must be related to expected noise power to have "practical significance." Evaluating the expected noise power proved to be a problem since the noise data (1 to 1,000 cps range) published in the literature had a wide range of values and was difficult to interpret.

*In 1961, after the investigation discussed in this paper was in progress, Fitchen, et al. [1961] reported evidence of resonance at 9 cps while, according to Raemer [1961], Balser and Wagner (in a subsequent experiment) reported 8 cps as did Maple [1961].

They concluded that the noise was not a simple tone.

The noise was not a simple tone.

The noise was not a simple tone.

The noise was not a simple tone.

The noise was not a simple tone.

The noise was not a simple tone.

The noise was not a simple tone.

The noise was not a simple tone.

The noise was not a simple tone.

The noise was not a simple tone.

The noise was not a simple tone.

The noise was not a simple tone.

The noise was not a simple tone.

The noise was not a simple tone.

The noise was not a simple tone.

The noise was not a simple tone.

The noise was not a simple tone.

The noise was not a simple tone.

The noise was not a simple tone.

The noise was not a simple tone.

The noise was not a simple tone.

The noise was not a simple tone.

The noise was not a simple tone.

The noise was not a simple tone.

The noise was not a simple tone.

The noise was not a simple tone.

The noise was not a simple tone.

The noise was not a simple tone.

In addition to the importance of noise data in the analysis of communication system performance, other manifestations of atmospheric noise are considered important. For example, more detailed results are urgently needed on ELF propagation [Pierce, 1960a]. More measurements are required to accurately fix the source of the noise and to determine the dependence or independence of the propagation path upon geomagnetic or geographical effects [Wait, 1960b].

Perhaps the main motivation for further research in the ELF and the lower VLF region arises from the implications even at the present state of knowledge. The extremely low attenuation in this region of the spectrum implies world-wide communication systems. The fact that these frequencies penetrate the ionosphere because of magneto-ionic phenomena further implies space communications [Wait, 1960c]. Other less spectacular, but nevertheless important, possibilities have also been considered. The correlation between atmospheric and the atmosphere potential gradient at sea suggest a means of measuring world-wide thunderstorm activity [Holzer and Deal, 1956]. In addition, the ELF radiated from lightning can serve as a thunderstorm location system [Wait, 1960b].

D. The Noise Data

The conclusions reached as a result of this literature review are (1) that very little data has been obtained in the ELF region and (2) that a need for further data exists. This investigation was undertaken to contribute to the fulfillment

In addition to the... of... atmospheric noise... detailed results... 1960s... source of the noise... effects [Wait, 1960]... ELF and the lower... at the present state... ionosphere because of... space communication... but nevertheless... considered... atmosphere potential... ing world-wide... In addition, the... thunderstorm location... [Wait, 1960]

The conclusions reached as a result of... review are (1) that... ELF region and (2) that... investigation was... [Wait, 1960]

of this need by seeking evidence of the Schumann frequencies and by securing noise amplitude data in the 0 to 50 cps region.

The noise data were recorded for approximately 30 minutes and are considered representative of the noise activity for the hour during which they were taken. During the data processing, the output of each of 10 filters is rectified and integrated. This output is expressed in field strength units. Thus the data are available for plotting purposes in units of field strength for each frequency for each hour recorded. Sample plots of the data are given in Chapter 6.

E. Instrumentation

Although information in the literature concerning instrumentation is lacking in detail, the overall systems are generally given or are discernible. This is the case since the instrumentation approach is determined largely by the particular aspect of the noise phenomenon that is being investigated. In the study of waveform patterns, for example, the display on an oscilloscope is photographed. Information on attenuation as a function of frequency and distance can be obtained by a simultaneous oscilloscope display of the spheric waveform and its spectrum. In whistler experimental work, the spectrograph is the main research instrument.

Amplitude versus frequency information is often provided by a sweeping or scanning filter and a pen recorder arrangement. This method provides a permanent but not a readily reproducible record of the data. It has only been comparatively recently that data has been recorded and stored on magnetic tape. This

of this used by seeing a light on the screen.

and by recording the position of the light on the screen.

The noise level is a function of the frequency of the noise.

and are considered as a function of the frequency of the noise.

the noise level is a function of the frequency of the noise.

therefore, the output of the system is a function of the frequency of the noise.

in general, the output of the system is a function of the frequency of the noise.

Thus the data are available for a certain number of frequencies.

which are plotted on a graph of the noise level versus the frequency of the noise.

plots of the data are given in Figure 1.

Figure 1 shows the noise level versus the frequency of the noise.

Figure 2 shows the noise level versus the frequency of the noise.

Figure 3 shows the noise level versus the frequency of the noise.

Figure 4 shows the noise level versus the frequency of the noise.

Figure 5 shows the noise level versus the frequency of the noise.

Figure 6 shows the noise level versus the frequency of the noise.

Figure 7 shows the noise level versus the frequency of the noise.

Figure 8 shows the noise level versus the frequency of the noise.

Figure 9 shows the noise level versus the frequency of the noise.

Figure 10 shows the noise level versus the frequency of the noise.

Figure 11 shows the noise level versus the frequency of the noise.

Figure 12 shows the noise level versus the frequency of the noise.

Figure 13 shows the noise level versus the frequency of the noise.

Figure 14 shows the noise level versus the frequency of the noise.

Figure 15 shows the noise level versus the frequency of the noise.

Figure 16 shows the noise level versus the frequency of the noise.

Figure 17 shows the noise level versus the frequency of the noise.

Figure 18 shows the noise level versus the frequency of the noise.

means of recording data has the distinct advantage that the data can be repeatedly processed. In addition, the magnetic tape can be played back at speeds which are many times the recording speed. This method eases the filtering requirements and saves processing time. The recording of the data on magnetic tape implies that the frequency range of the data is within the response of the recorder.

The frequency range of interest in this investigation was below the lower limit of the response of the available tape recorder. The system discussed in this paper was devised to make the recorder compatible with the data. This system is quite different than those discussed in the literature. Essentially the noise data is frequency translated to within the frequency range of the recorder during the record mode and restored to its original position in the spectrum during the play-back mode. A synchronizing signal ensures proper demodulation during play-back independent of tape speed. This signal also is a means of monitoring frequency variations due to speed changes. In this manner, excursions outside of the filter bandwidths are observed. Lastly, this synchronizing signal is available as a control signal for a servo system to automatically control motor speed during play-back if necessary.

means of recording data has the distinct advantage that the data can be repeatedly processed. In addition, the magnetic tape can be played back at speeds which are many times the recording speed. This method meets the listening requirements and saves processing time. The recording of the data on magnetic tape implies that the frequency range of the data is within the response of the recorder. The frequency range of interest in this investigation was below the lower limit of the response of the available tape recorder. The system discussed in this paper was devised to make the recorder compatible with the data. This system is quite different than those discussed in the literature. Essentially the noise data is frequency translated so within the frequency range of the recorder during the record mode and restored to its original position in the spectrum during the play-back mode. A synchronizing signal ensures proper demodulation during play-back independent of tape speed. This signal also is a means of monitoring frequency variations due to speed changes. In this manner, excursions outside of the filter bandwidths are observed. Lastly, this synchronizing signal is available as a control signal for a servo system to automatically control motor speed during play-back if necessary.

2. The Overall System

Several design criteria are incorporated in the system. These criteria are due to environmental conditions and to the desire for flexibility. Inasmuch as the natural electromagnetic noise is the desired data, man-made noise and interference are eliminated by recording in remote locations free of such artificial noise sources. The data-taking system itself is battery-operated to eliminate power transforming equipment and its associated noise and to facilitate transporting the equipment to these remote sites. All components of the system function properly at temperatures up to approximately 40°C. This upper temperature limit allows data-taking during the summer months and in relatively warm weather.

In order to incorporate the greatest possible flexibility in the system, the data is recorded on magnetic tape. Thus the data is permanently preserved in a form that can be repeatedly recovered. This permits processing the same information by more than one method.

In the development of any data-collecting system it is essential that the design be compatible with a feasible data-processing system. In the final analysis the main concern is whether or not the data can be recovered in an economical manner. Perhaps one of the most direct methods of data recovery is by filtering. This is particularly so in this case since the relative activity at different frequencies in the 0 to 50 cps range is desired. This display of data can be directly compared with the Schumann mode frequencies.

Considering the various types of filters, the Wien-Bridge and Twin-T were selected largely on the basis of economy, i.e., being composed of resistance and capacitance. The Wien-Bridge was rejected since there is no common ground for the input and output.

A complete discussion of the Twin-T filter is given in Appendix A. Figure A9 in Appendix A shows that the resistance and capacitance required for frequencies in the 0 to 50 cps range have values that are readily available.

The ability to filter a particular frequency was experimentally verified. Equivalent circuit Q's on the order of 25 were readily attained. The selective amplifier used permitted adjusting the "Q" to any desired value less than maximum (25).

This paper is concerned with the data-collecting system. However, the basic idea involved is inherently related to the method of modulating and demodulating during data-collecting and data-processing. Consequently, the basic idea is briefly described here before proceeding with a detailed discussion of the data-collecting system.

A block diagram of the data-collecting system is shown in Figure 2.1. The data-signal, as shown in this figure, is fed through a switch and is interrupted or "chopped" at a rate determined by the oscillator. The multivibrator is synchronized by the oscillator and drives the switch. The data is recorded on the data-track of the tape as sidebands about the switching frequency. Simultaneously, the oscillator signal is recorded on the synchronizing (sync) track of the duo-track tape of the magnetic tape recorder.

Considering the values of α and β and γ were selected and γ was rejected since there was no change in the output. A complete discussion of the data-collecting system is given in Appendix A. Figure 2.1 shows the data-collecting system and capacitance required for the system. The data-collecting range have values of the order of 10^{-10} to 10^{-12} farads. The ability to filter a particular frequency was easily verified. Equations (2.1) and (2.2) were readily attained. The results of the data-collecting system adjusting the "Q" to any desired value were shown in Figure 2.2. This paper is concerned with the data-collecting system. However, the basic data-collecting system is a method of modulating and demodulating the data and data-processing. Consequently, the data-collecting system described here before presented with a detailed discussion of the data-collecting system. A block diagram of the data-collecting system is shown in Figure 2.1. The data-collecting system is shown in Figure 2.1 through a switch and is represented as "data-collecting" determined by the oscillator. The data-collecting system by the oscillator and the data-collecting system on the data-collecting system. The data-collecting system frequency. Simultaneously, the data-collecting system on the systemized data-collecting system. magnetic tape recorder.

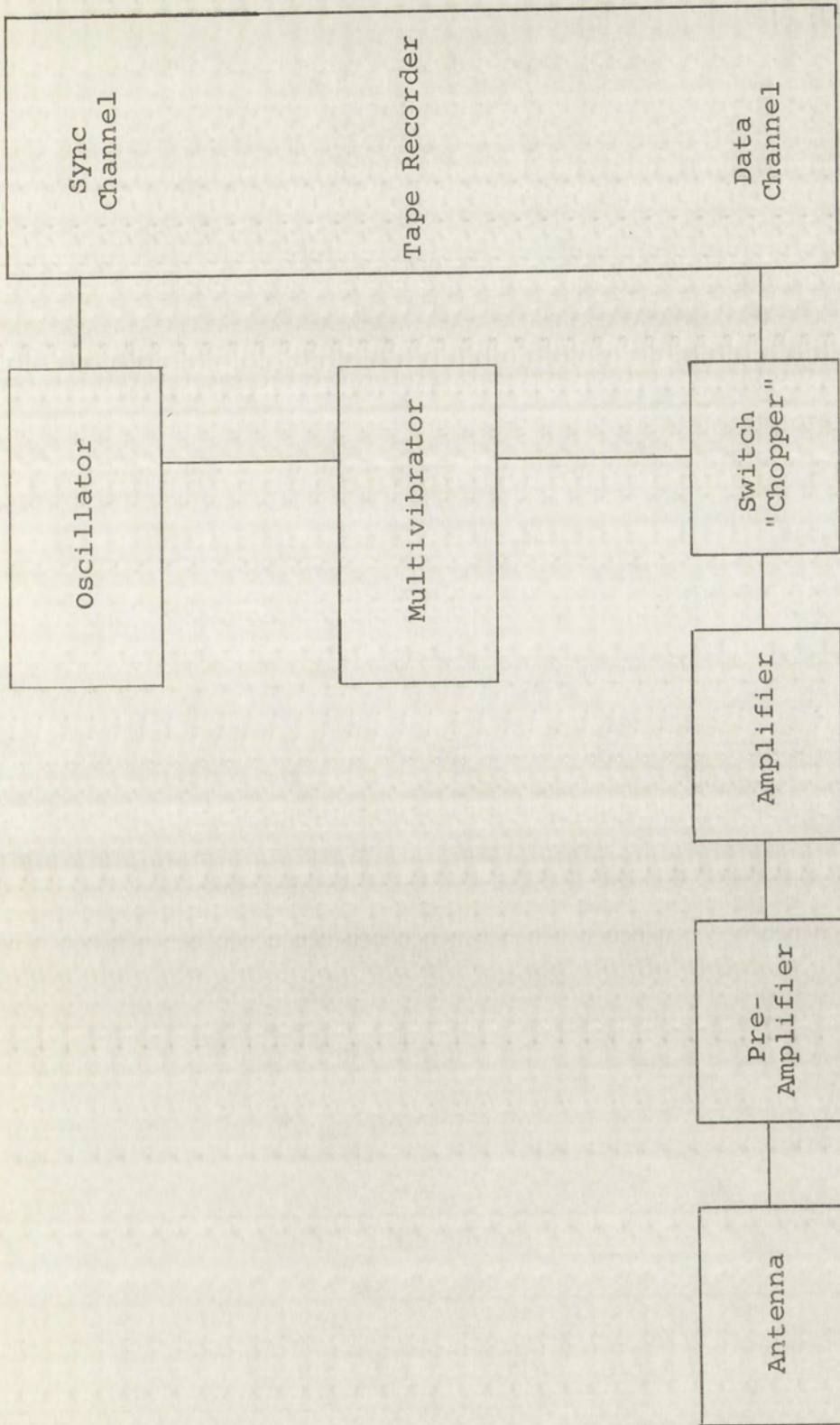
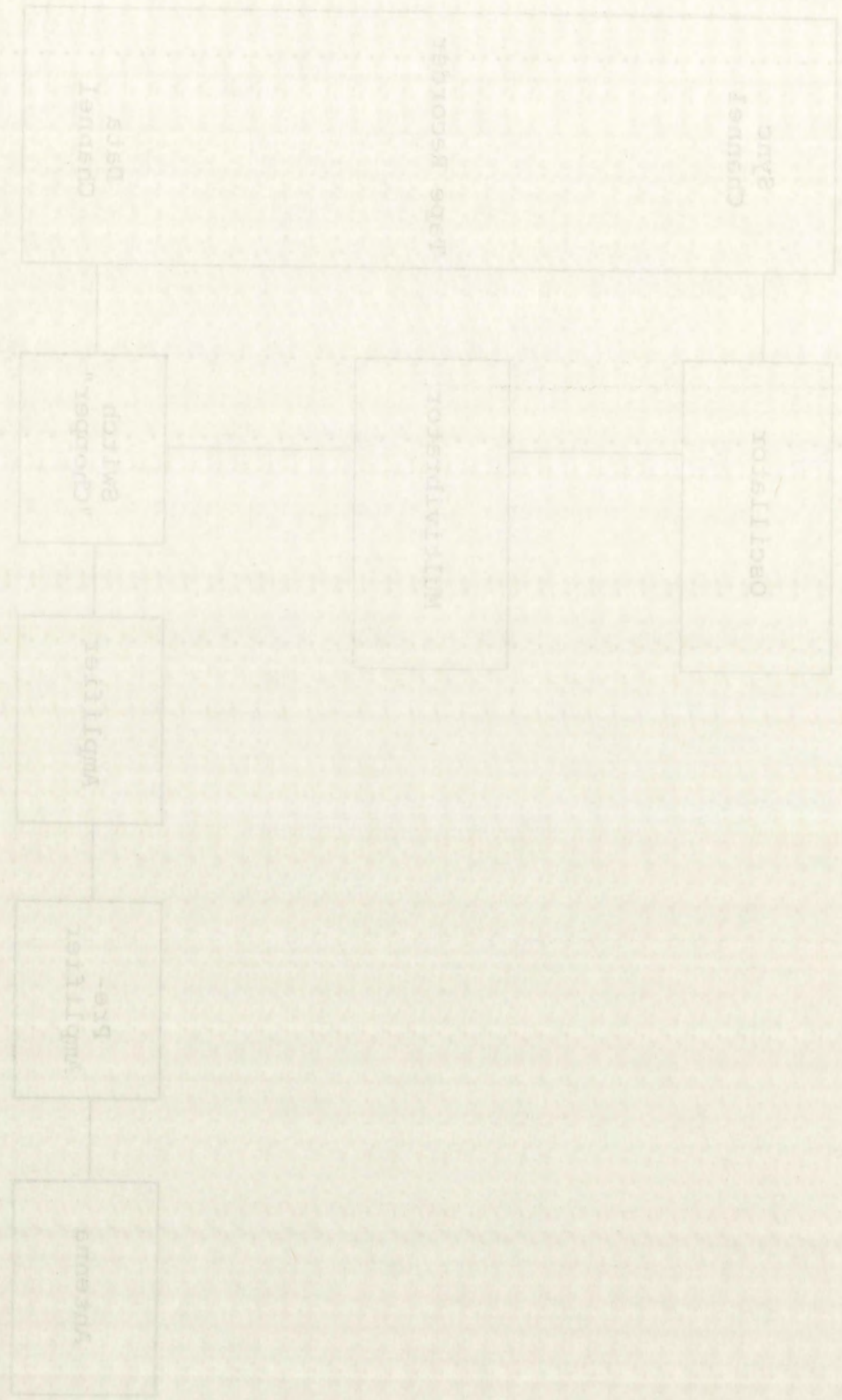


Figure 2.1 Block diagram of data-collecting system

Figure 5. Block diagram of the proposed system.



During data-processing (Figure 2.2), the output of the data-track is fed through the switch and interrupted or "chopped" at a rate determined by the signal from the sync-track. The low-pass filter removes the fundamental and harmonics of the switching frequency and passes the original data spectrum.

Thus in this system the sync signal and the data carrier are always of the same frequency and phase regardless of speed variations of the tape recorder during recording or playback. Since the sync signal is actually the demodulating frequency and the data carrier frequency is the original modulating frequency, the modulating and demodulating frequencies are always of the same frequency and phase. It is analytically shown in Appendix C that such similarity in frequency and in phase of both the modulating and demodulating carriers is a necessary requirement for this type of demodulation.

During data processing, the carrier frequency is

data-clock is fed through the switching mechanism at a rate determined by the sampling rate of the clock.

low-pass filter, removes the fundamental and harmonics of the

switching frequency and passes the original data stream.

Thus in this system the data stream is

always of the same frequency and phase regardless of the

variations of the data stream.

Since the sync signal is actually the demodulated

and the data carrier frequency is the original modulation

frequency, the modulation and demodulation frequencies are

always of the same frequency and phase. It is relatively

shown in Appendix C that such similarity in frequency and

phase of both the modulation and demodulation carrier is

necessary requirement for this type of demodulation.

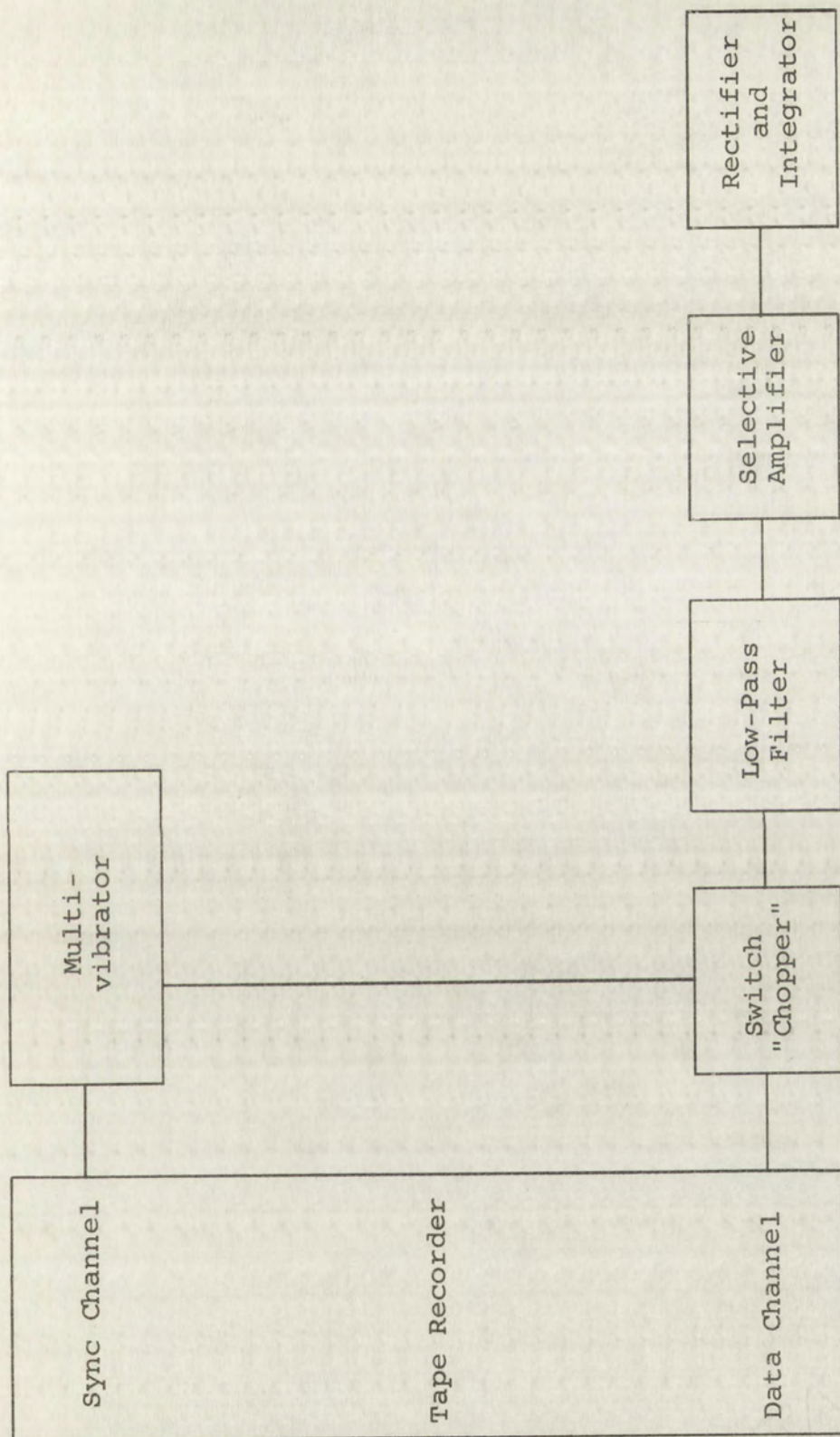
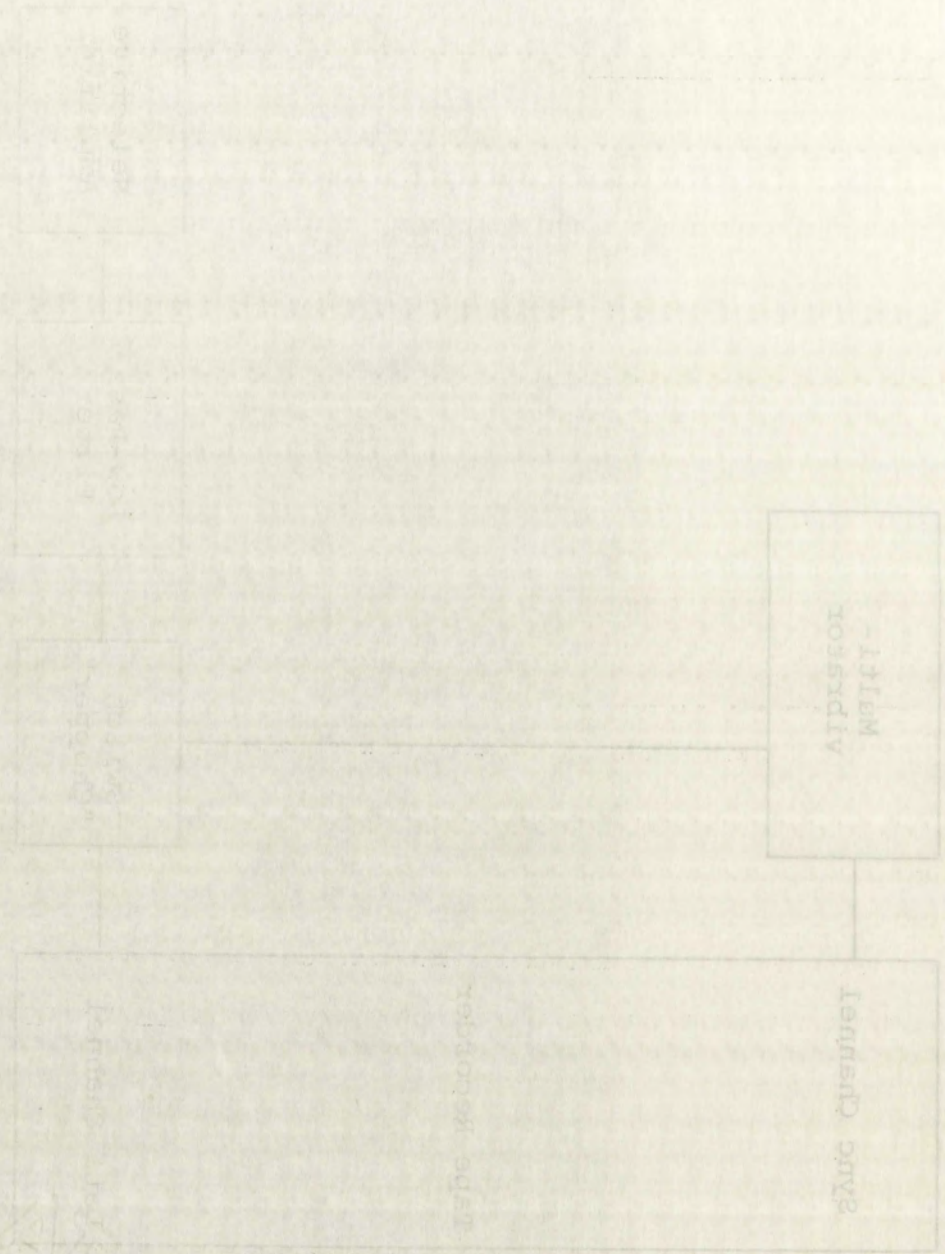


Figure 2.2 Block diagram of data-processing system

FIGURE 1. Schematic diagram of the proposed model.



3. Individual Units of the System

A. Tape Recorder

The initial requirement, portability, can be met in either of two ways--using an a-c operated recorder with a battery-powered converter or a battery-operated recorder. The converter arrangement was rejected because the possibility of noise-free operation is not guaranteed with either mechanical or solid-state type converters.

The decision to use a battery-operated tape recorder necessitated an investigation into the effect of speed characteristics upon reproduction. This is particularly so for a battery-operated tape recorder since speed specifications while usually not available are generally less stringent than a-c operated machines. It is shown in Appendix B that the percentage frequency change is proportional to the percentage speed variation. Since filtering during the data-processing is to be accomplished with circuit Q's up to 40, the maximum speed variation must be within approximately 0.6%.

A survey of available recorders showed that the frequency response was approximately 150 to 5,000 cps at the slow tape speeds. Obviously some means of frequency translation is necessary to place the data in the response region of the recorder. In addition, the method of accomplishing this translation must be compatible with speed variations inherent in the recorder and with the demodulation system.

Frequency translation immediately suggests a switching technique. A complete discussion of both single-ended and

bi-polar switching as a modulation method is presented in Appendix C. The conclusion reached in this discussion is that single-ended switching is much simpler and more economical.

To ensure that this switching-type modulation system would be compatible with a similar demodulation system, an inquiry into the demodulation process was made as shown in Appendix C. This inquiry shows that demodulation by switching can be accomplished provided the modulating and demodulating carriers are of the same frequency and phase.

In view of the frequency and phase requirements, demodulation by envelope detection was considered. However, the switching method offered several advantages in spite of the necessity for incorporating a synchronizing track along with the data track on the recording tape. The synchronizing signal and modulated carrier arising from the same frequency source and simultaneously recorded and played back, always fulfill the frequency and phase requirements simply because they are both simultaneously subjected to the same tape speed variations. In addition, the synchronizing signal provides a means for monitoring circuit operation during data-processing since the data undergoes the same percentage variation in frequency as the synchronizing signal due to speed variations.

The Steelman Model 2-7111 portable tape recorder was selected largely on the basis of economy. This is a two-speed ($1\frac{7}{8}$ and $3\frac{3}{4}$ ips), two-track record and playback machine. It is completely transistorized and battery-operated. Since mid-frequency response occurs at 1000 cps at the slow speed, this frequency was selected for switching. At the slow

of point switching at a rate of 1000 per second. The
Appendix C. The above was verified by the following
and a good example of the type of work that can be
to ensure that the data is of the highest quality
be compatible with a 1000 per second rate of 1000
into the demodulation process was used as a guide.
This inquiry shows that the data is of the highest
accomplished provided the following conditions are
are of the same frequency and phase.
In view of the frequency and phase relationship
tion by a single device or by a single device, the
switching action of the device is of the order of
necessary for the operation of the device, the
the data track on the recording tape. The system
and modulated carrier signal from the transmitter
and a suitable frequency and phase relationship
the frequency and phase relationship of the carrier
both simultaneously and the same rate of operation
In addition, the system is a good example of a
monitoring circuit which is a good example of a
data under the same conditions as the frequency and
synchronizing signal to the carrier wave.
The system is a good example of a system which
selected frequency of the carrier wave. This is a
speed (117X8 and 117X8) and the carrier wave is
medium. The system is a good example of a system
since the frequency response of the system is of the
speed, this frequency was selected as a guide.

speed approximately 32 minutes of recording time is obtained by using 300 ft. of 1/2 mil tape a 1/4 inch wide.

Several modifications were necessary to adapt the tape recorder to the system. The extent of these modifications can be seen in Figures 3.1 and 3.4 which are block diagrams before and after the modifications were made. The first consideration in adapting the recorder to the system was the feasibility of using the erase head as a recording head for the 1 kc synchronizing signal (sync signal). Using this method gave excessive inter-channel modulation regardless of the head position. This was due apparently to the large air-gap in the erase head core. Replacing the erase head with a regular recording head and leaving the bias oscillator disabled gave satisfactory results. In fact, tests indicated that inter-channel modulation was approximately -40db.

Results of these tests further showed that the impedance to the sync head was 6 k-ohms and that it required approximately 1.0 volts for satisfactory level of recording. However, in the play-back mode, the output of this head was approximately 4 mv. To reduce the amplitude requirement for the oscillator in the data-collecting system, this 250/1 voltage ratio is made up during data processing by an additional amplifier. The phone jack which normally shunts the speaker was connected directly to the sync head to serve as "sync in" and "sync out" terminals in the record and play-back modes, respectively.

The effects of disabling the bias oscillator were investigated. The purpose of this oscillator is to remove any residual magnetism on the magnetic tape which causes noise and

seems approximately 10% of the total length of the tape.

Several models have been proposed for the tape.

referred to the system. The extent of the tape is

be seen in Figure 1. The tape is a continuous

and after the modification is made. The tape is

in adjusting the location of the tape.

using the tape. The tape is a continuous

ing signal (input signal) and the tape is

inter-channel modulation. The tape is

was due apparently to the tape. The tape is

registering the error head with a tape. The tape is

leaving the tape. The tape is a continuous

in fact, these indicated that the tape is

approximately 4000.

Results of these tests indicate that the tape is

to the sync head was 0.5 cm and that the tape is

1.0 volts for satisfactory tape. The tape is

the play-back mode. The output of the tape is

4 mv. To reduce the tape, the tape is

in the data-collecting system. The tape is

up during data processing by an additional system. The

phone jack which normally is used for the tape is

directly to the sync head. The tape is

terminals in the record and the tape is

The effects of these tests indicate that the tape is

gated. The purpose of this experiment is to remove the

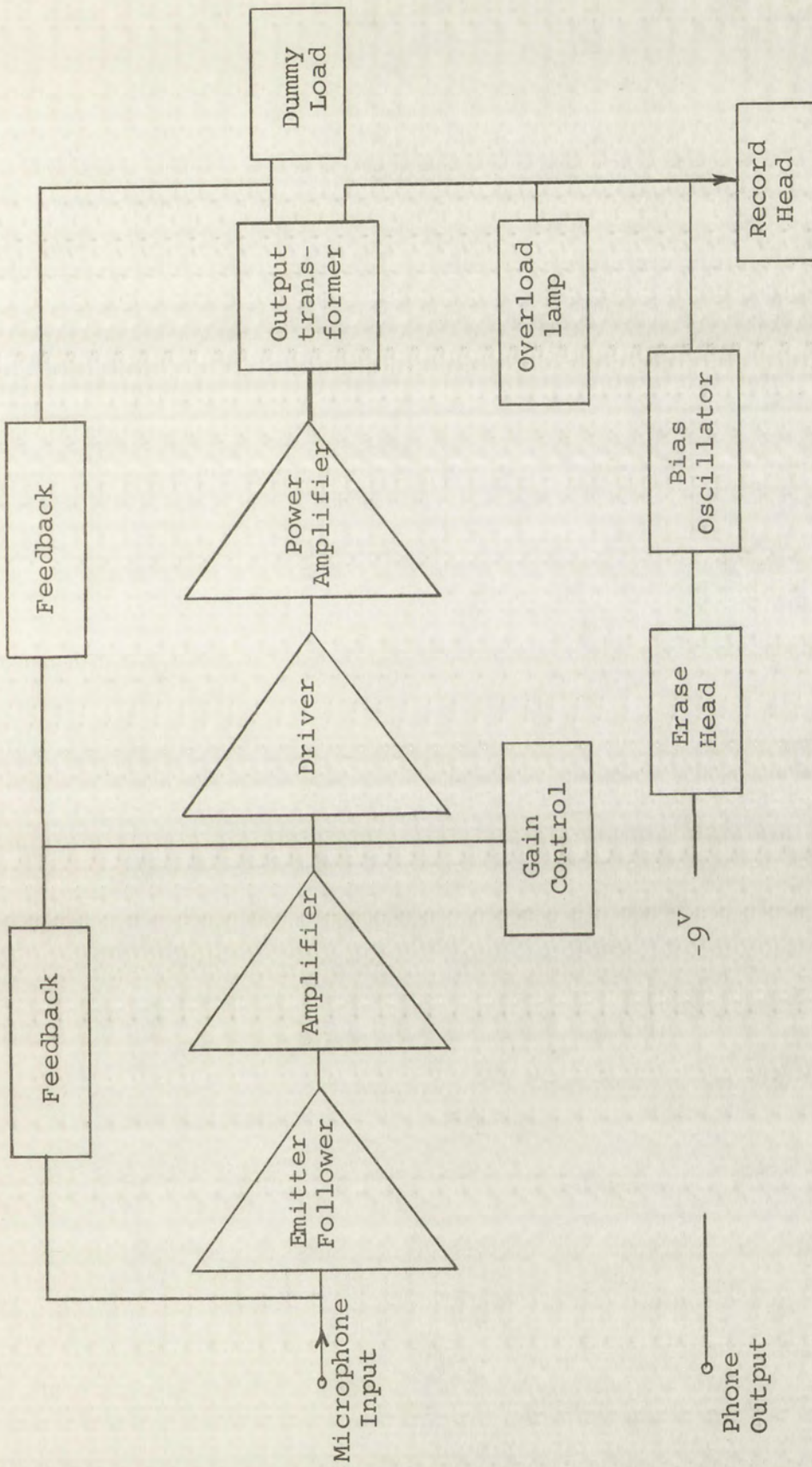
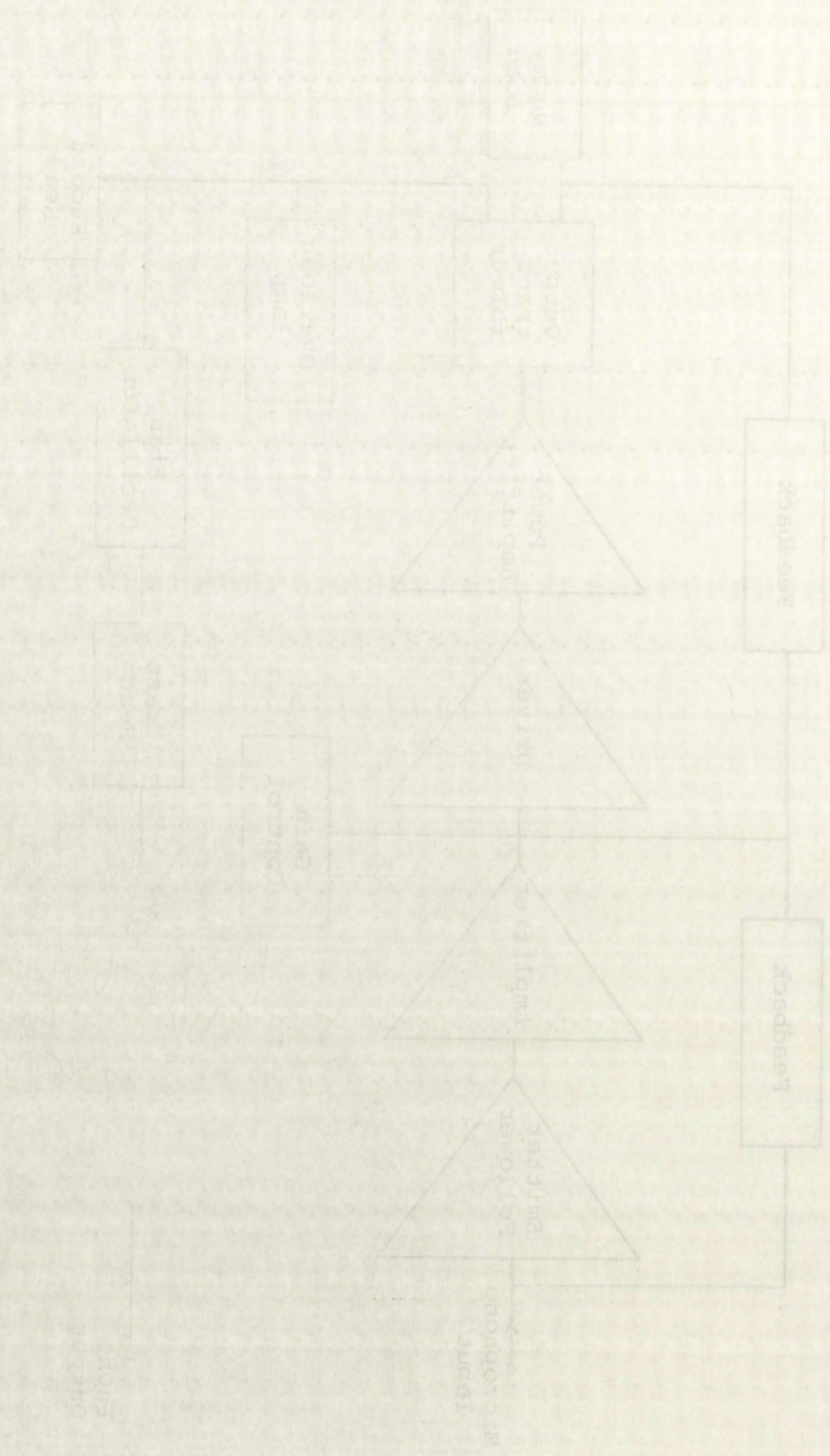


Figure 3.1 Block diagram of tape recorder in record mode before modification

Figure 1. Block diagram of a typical digital communication system.



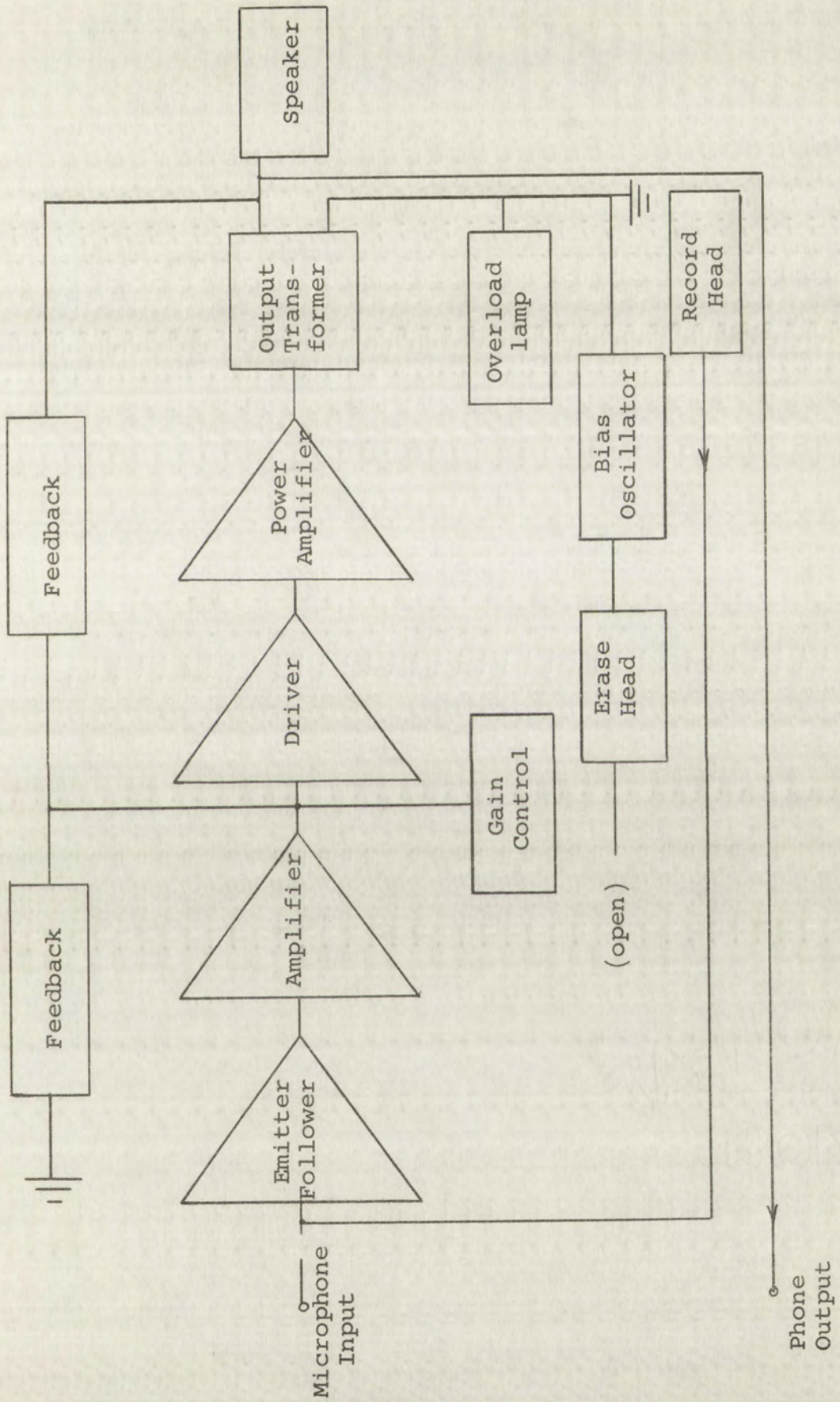


Figure 3.2 Block diagram of tape recorder in playback mode before modification

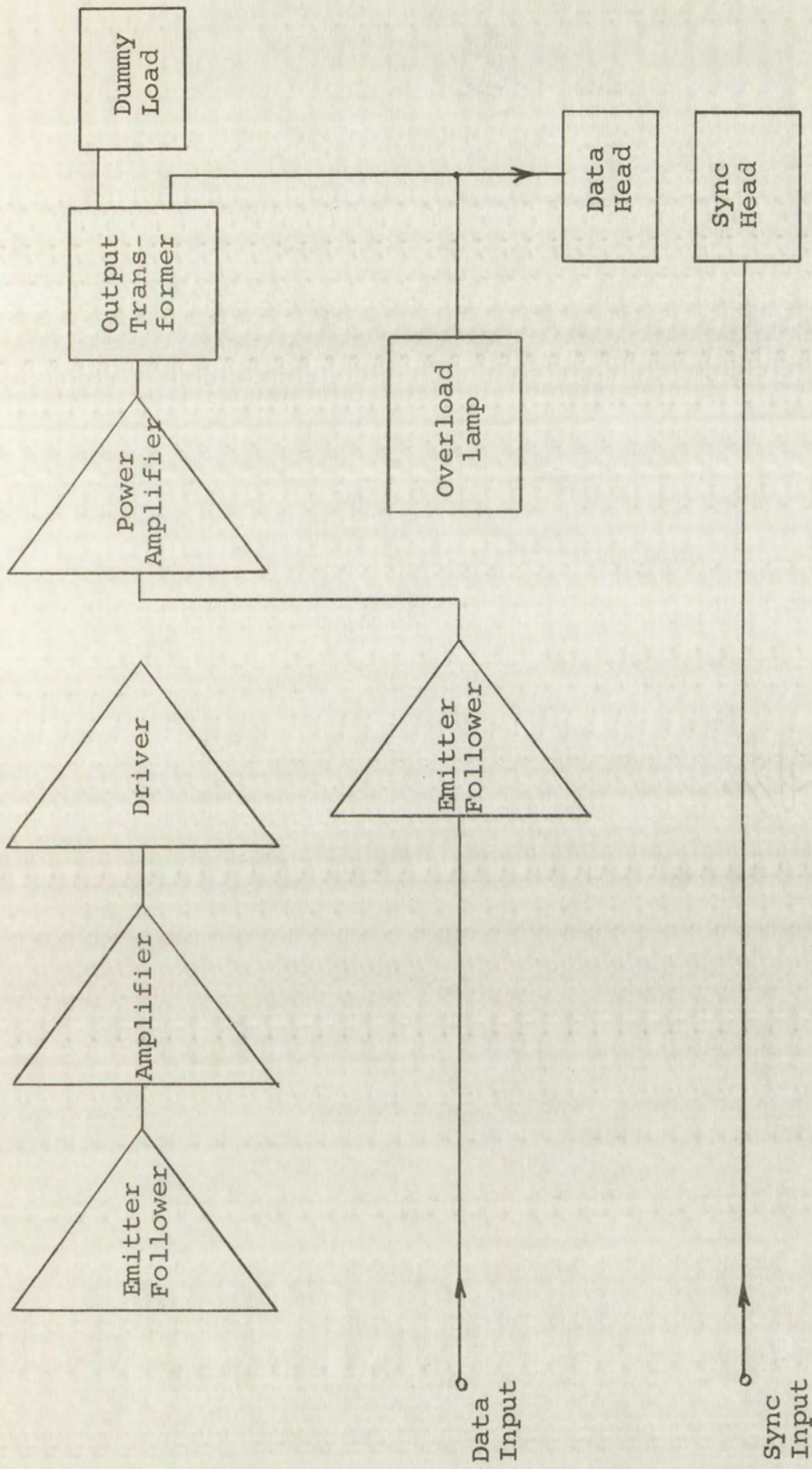


Figure 3.3 Block diagram of tape recorder in record mode after modification

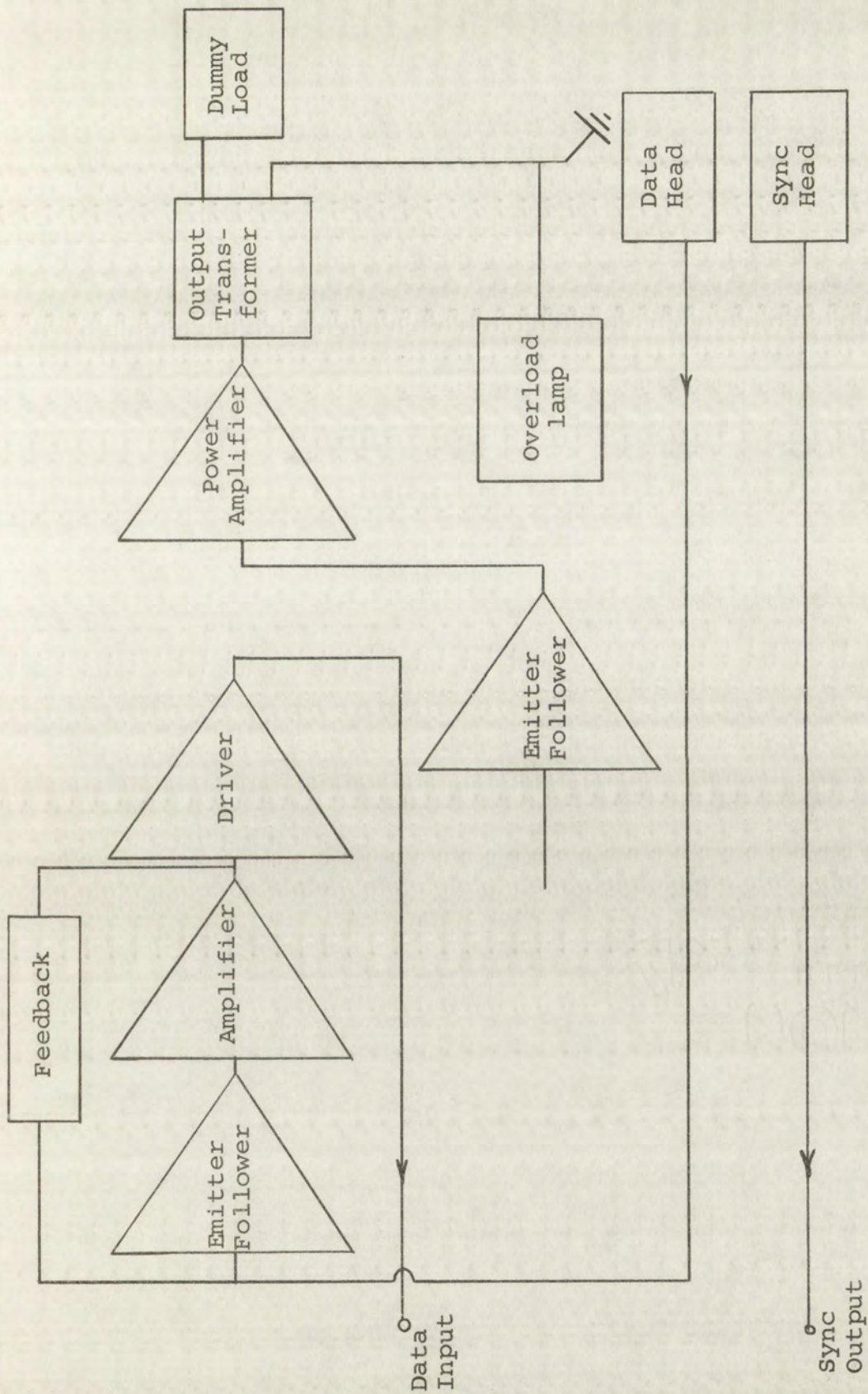


Figure 3.4 Block diagram of tape recorder in playback mode after modification

nonlinearities. Tests indicate that the linearity characteristics on record and play-back are satisfactorily preserved when the tape is de-magnetized prior to recording. Thus, as a matter of procedure all tapes are bulk-erased before recording.

The output of the switch when fed into the low-level input terminals of the recorder overloaded its amplifier. This amplifier consisted of an input emitter follower, common emitter voltage amplifier, and a common emitter driver feeding a pushpull power amplifier. The input impedance of this power amplifier is 2700 ohms. A 2.5 volt (peak-to-peak) signal at the input of this amplifier gives a 13 volt (peak-to-peak) signal at the collector side of the output transformer and causes the "overload lamp" to just come on. The overload lamp is in shunt with the regular record head (hence to be referred to as the data head) and is connected to a secondary of the power amplifier output transformer. Tests indicate that this overload lamp gives an accurate indication of overloading in the power amplifier.

The output of the switch was in excess of 1.25 volts (peak) with an impedance of 56 k-ohms. This indicated that impedance matching between the switch and power amplifier was necessary. To this end several modifications were made.

The speaker was removed and the speaker dummy-load was connected at the function switch so that it remained in the circuit in both the record and play-back mode instead of the record mode only. This change insured that the reflected impedance as seen by the power amplifier remained the same in both modes as before.

nonlinearities. Tests indicate that the linearity character-

istics on record and play-back are satisfactorily preserved

when the tape is de-magnetized prior to recording. Thus, as a

matter of procedure all tapes are half-erased before recording.

The output of the switch when fed into the low-level input

terminals of the recorder overloaded its amplifier. This

amplifier consisted of an input emitter-follower, common

emitter voltage amplifier, and a common emitter driver feeding

a pushpull power amplifier. The input impedance of this power

amplifier is 2700 ohms. A 2.5 volt (peak-to-peak) signal at the

input of this amplifier gives a 15 volt (peak-to-peak) signal

at the collector side of the output transformer and causes the

"overload lamp" to just come on. The overload lamp is in shunt

with the regular record head (heads to be referred to as the

data head) and is connected to a secondary of the power amplifier

output transformer. Tests indicate that this overload lamp

gives an accurate indication of overloading in the power

amplifier.

The output of the switch was in excess of 1.25 volts

(peak) with an impedance of 50 k-ohms. This indicated that

impedance matching between the switch and power amplifier was

necessary. To this end several modifications were made.

The speaker was removed and the speaker dummy-load was

connected at the function switch so that it remained in the

circuit in both the record and play-back mode instead of the

record mode only. This change insured that the reflected

impedance as seen by the power amplifier remained the same in

both modes as before.

An emitter follower installed in the place vacated by the speaker served as an impedance matching device between the switch and the power amplifier. Actually the emitter follower loaded the switch such that the overload lamp just came on when the switch was saturated, i.e., the modulation on the switch was maximum. Thus monitoring the overload lamp was as effective as monitoring the switch itself. With this modification the first three stages were not used in the record mode. Therefore the function switch on the recorder was rewired so that in the record mode (1) the microphone jack (hence referred to as the data input jack) was connected to the emitter follower and power amplifier, and (2) the battery power was removed from the first three stages.

Connecting the switch to the power amplifier through the emitter follower worked satisfactorily. However, in the playback mode, a 12 kc oscillation was present in the output even when no tape was being run.

In the original circuitry there were two feedback circuits-- (1) the main feedback circuit around the power amplifier and the third stage, and (2) the microphone compensating feedback circuit around the first and second stages during record and from the second stage to ground during playback. Opening the main feedback circuit reduced the magnitude of the oscillation somewhat. The instability was caused by the feedback from the second stage to ground. The function switch was modified to put this feedback circuit around the first two stages during the playback mode and open the circuit in the record mode. This modification did not effect the response in the region of interest--1000 + 50 cps.

The speed of the tape recorder motor is set by an electro-mechanical governor. The supply voltage indicator lamp is energized by transformer coupled pulses due to the governor contacts. Thus, the operation of the governor can be monitored. This lamp extinguishes when the battery voltage drops to approximately 50% of its normal value.

12/10/1914

B. Oscillator

Theoretically there are no criteria for choosing a type of oscillator for this application other than that it produces a sinusoidal output and is stable. However, for practical reasons, there are a few requirements that the oscillator must satisfy.

The oscillator must function properly at temperatures up to 40°C. This upper temperature limit was mentioned previously as being applicable to the whole system.

The supply voltage required must be of such value that the physical size and configuration of available batteries is suitable for portability. In addition, the current drain must be minimal for reasonably long battery life.

The output of the oscillator must be of sufficient amplitude to synchronize a multivibrator. This amplitude should not be a critical function of battery voltage. In addition, the waveform should be relatively undistorted.

The output impedance should be sufficiently low to preclude loading by the multivibrator, tape recorder synchronizing channel, and the oscillator test point. This test point is to be incorporated so that the output of the oscillator can be monitored continuously or at the discretion of the operator.

The oscillator frequency should be such that it falls within the flat response region of the tape recorder. This frequency must also be such that reasonably small components can be used for convenient packaging and construction.

The frequency stability should be within .025 per unit bandwidth for the range of tolerance of battery voltage

which will produce sufficient output to synchronize the multivibrator. Provisions for frequency adjustment should be incorporated.

A Colpitts transistor oscillator shown in Figure 3.5 was finally selected since it was in harmony with the specifications. As mentioned before, the frequency of 1000 cps was chosen on the basis of the tape recorder response. At this frequency the physical size of the elements is still suitable for packaging. The battery, to supply approximately 9 ma at 22.5 volts for a reasonable length of time, can also be physically accommodated in a small portable system.

The output voltage varies from 1.0 to 1.5 volts (peak) for a corresponding change in battery voltage from 19.5 to 22.5 volts. The output impedance is approximately 170 ohms. These output characteristics permit driving the sync head directly. This output voltage range is also adequate to synchronize the multivibrator throughout the adjustable frequency range of the oscillator--960 to 1300 cps.

The variation of frequency versus battery voltage with temperature as a parameter, presented in Figure 3.6, is within 1.8% over a 19.5 to 22.5 voltage range. The upper temperature limit satisfies the temperature specification for the system.

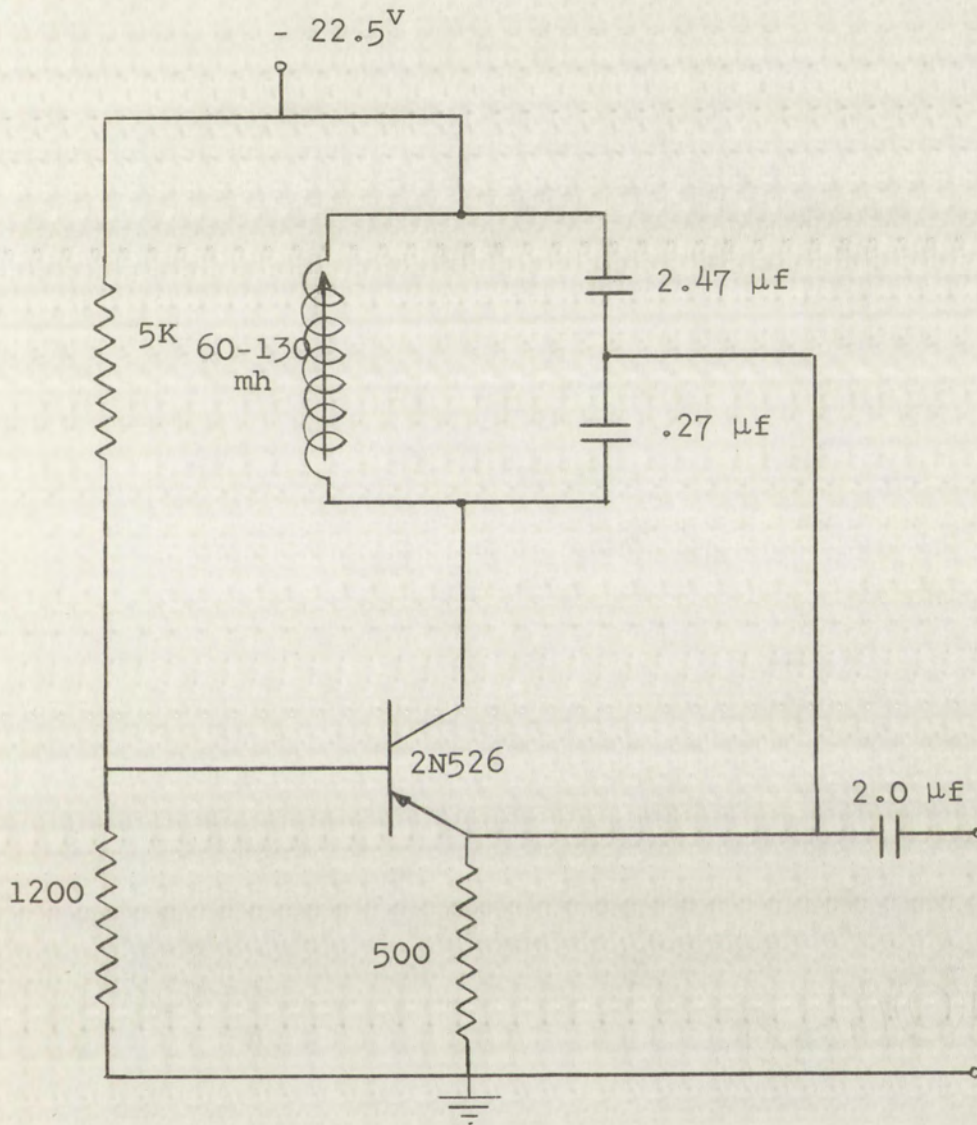


Figure 3.5 Schematic diagram of the oscillator

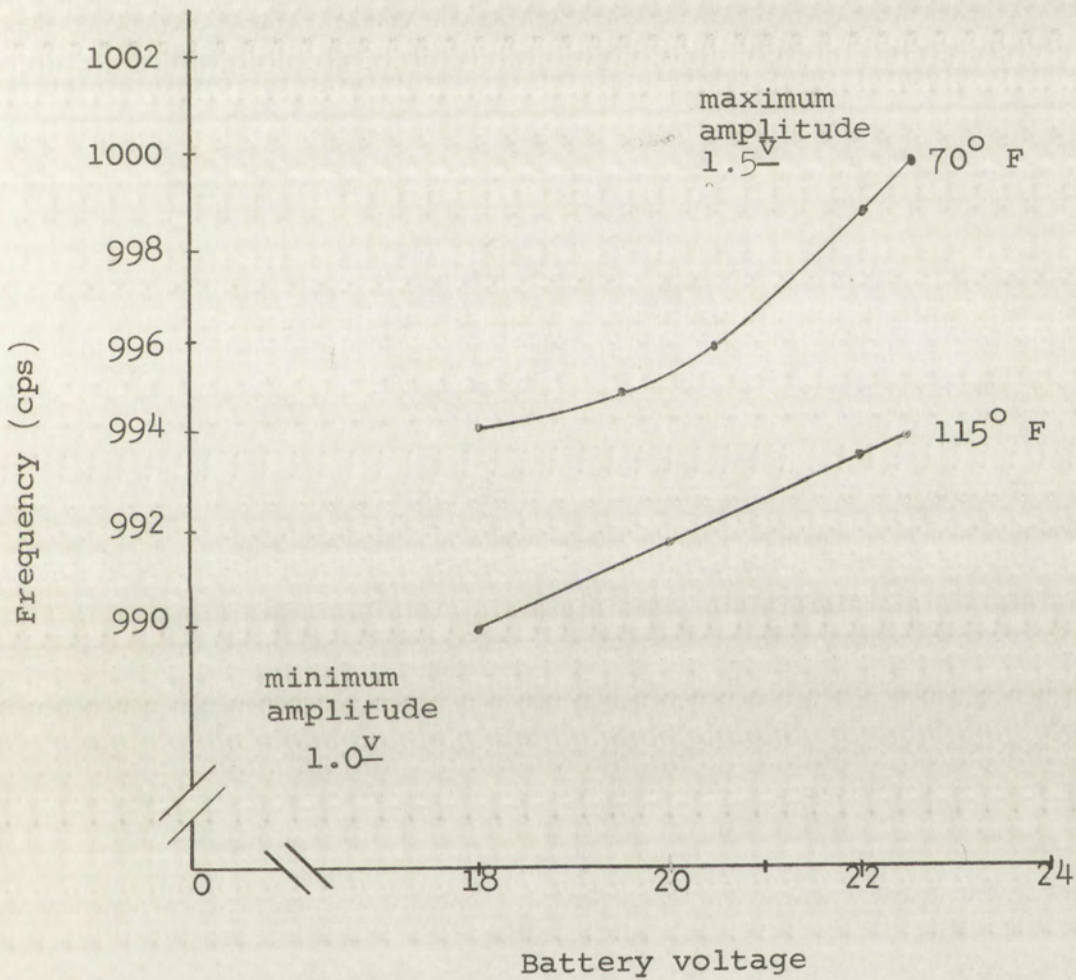


Figure 3.6 Oscillator frequency versus battery voltage for variations in temperature

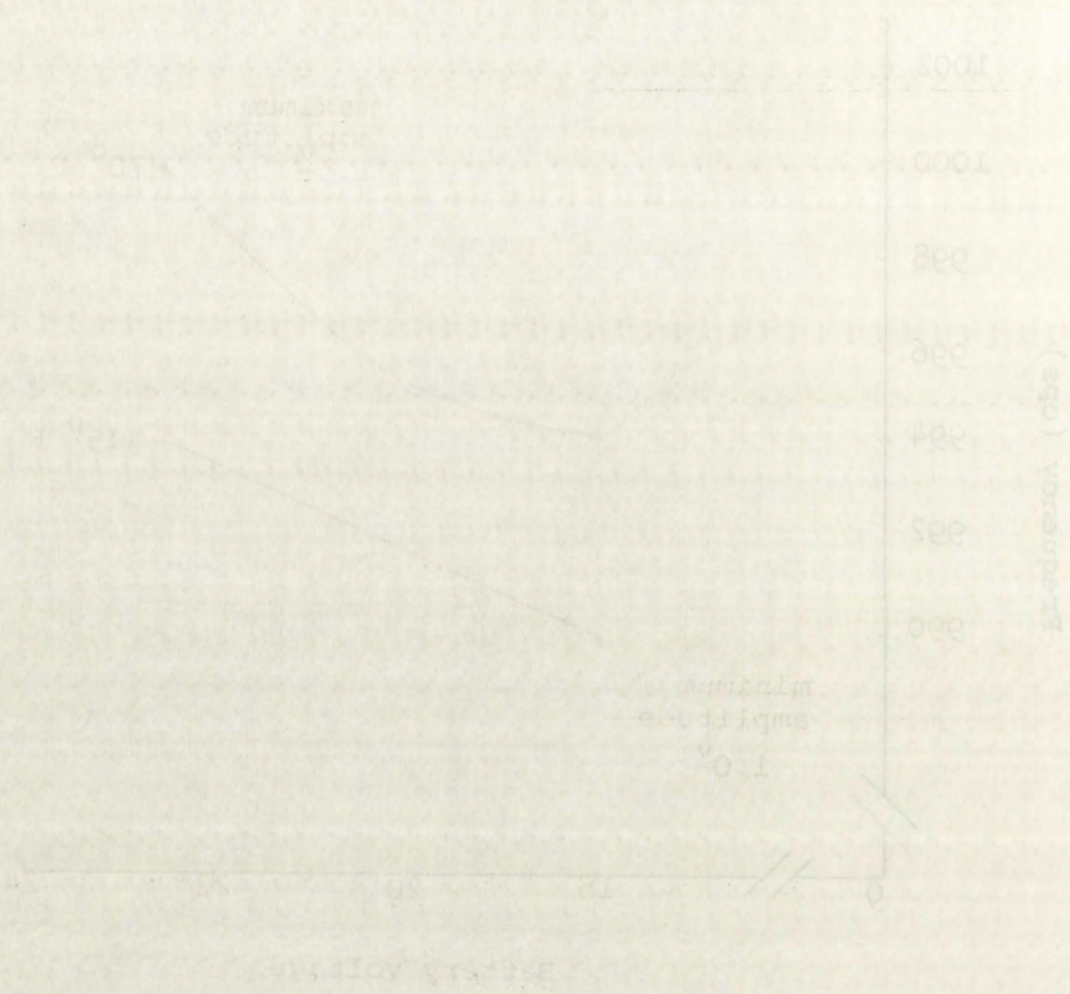


Figure 3.6 Oscillator response versus frequency for variations in frequency

C. Multivibrator

The function of the multivibrator is to drive the switch at a rate determined by the oscillator. The output waveform should be symmetrical and have sufficient amplitude over a reasonable battery voltage range to drive the switch properly. Here as throughout the system the physical sizes of batteries and parts are a consideration.

The circuit which was finally developed is shown in Figure 3.7. The output waveform is symmetrical and at least 4 volts (peak-to-peak) for a supply voltage range of 7 to 9 volts. This signal is adequate to drive the switch.

The multivibrator is free-running at approximately 1000 cps with no sync input. With maximum battery voltage (9 volts) on the multivibrator, the output of the oscillator (1.0 to 1.5 volts) is sufficient for synchronizing the multivibrator over the frequency range 960 to 1300 cps. In addition, the sync input impedance is approximately 1200 ohms which results in negligible loading of the oscillator.

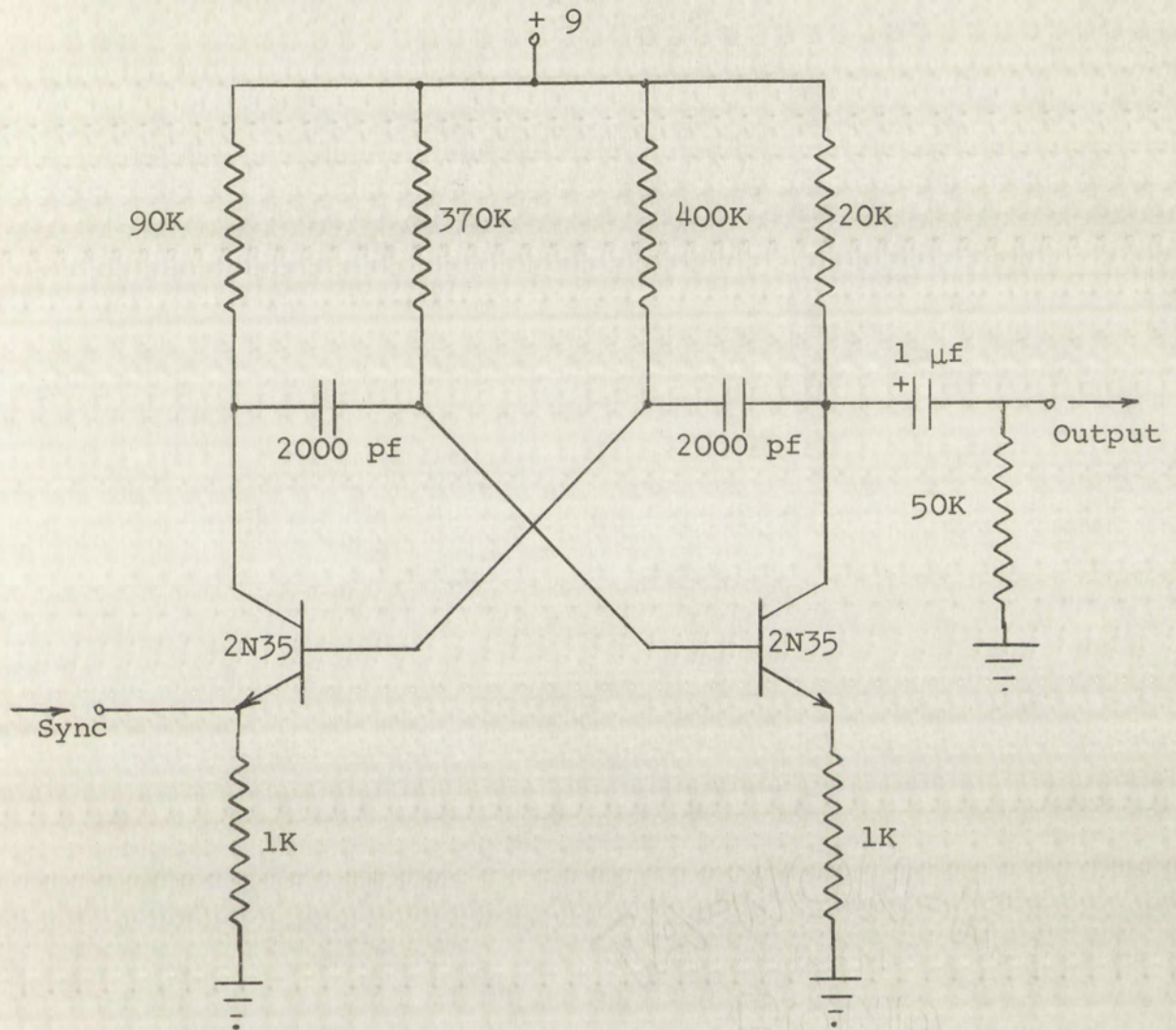


Figure 3.7 Schematic diagram of the multivibrator

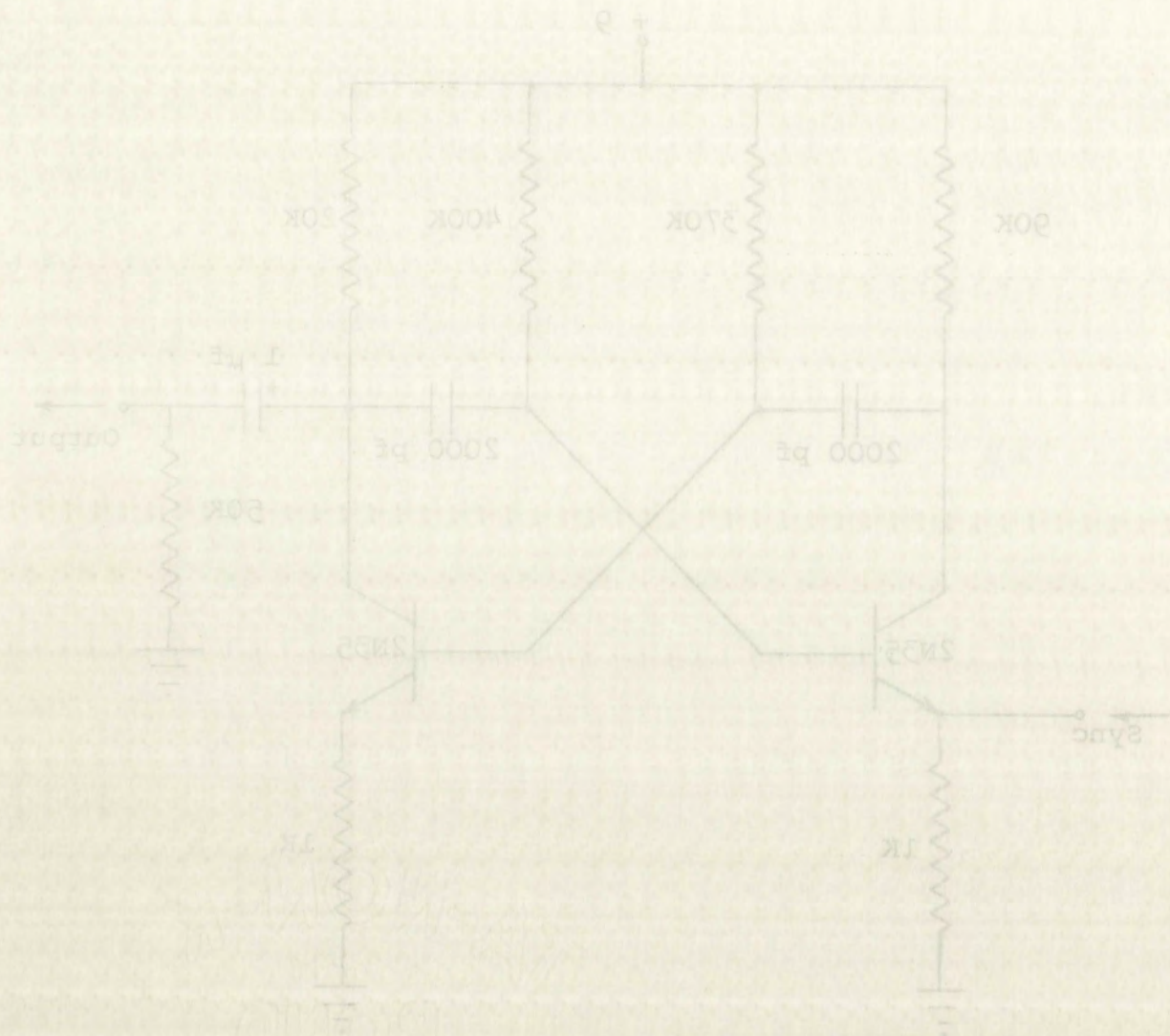


Figure 3-7 Schematic diagram of the multivibrator

D. Switch

The function of the switch is to interrupt or "chop" the data at the oscillator frequency. As mentioned before, this switching can be accomplished by either of two basic methods--single-ended and bi-polar. ~~The single-ended~~ method was selected primarily because of simplicity. A complete analytical discussion of the switching technique is given in Appendix C.

The final circuit design is shown in Figure 3.8. As mentioned previously in the Tape Recorder section (3A), an emitter follower was installed in the tape recorder as a matching device between the power amplifier of the recorder and the switch. To prevent overdriving this power amplifier, the "match" was such that saturation of the switch caused the overload lamp to come on. This indication serves as a means of monitoring and setting the amplifier gain.

With the tape recorder connected, the switch has a 0.5 volt (peak-to-peak) output in the emitter circuit. This means, of course, that data-signals of 1.0 volts (peak-to-peak) can be satisfactorily chopped without saturating the switch. These waveforms are shown in Figure 3.9.

The switch requires a 4.0 volt square wave at the base for proper operation. This was really a specification applied to and fulfilled by the multivibrator. The input impedance for the data circuit is approximately 50 k-ohms. This impedance does not load the amplifier. That there should be no such loading was actually a design requirement on the switch because the type of amplifier had already been selected.

D. Switch

The function of the switch is to interrupt or "chop" the data at the oscillator frequency. As mentioned before, this switching can be accomplished by either of two basic methods--single-ended and bi-polar. The single-ended method was selected primarily because of simplicity. A complete analytical discussion of the switching technique is given in Appendix C. The final circuit design is shown in Figure 3.8. As mentioned previously in the Tape Recorder section (3A), an emitter follower was installed in the tape recorder as a matching device between the power amplifier of the recorder and the switch. To prevent overdriving this power amplifier, the "match" was such that saturation of the switch caused the overload lamp to come on. This indication serves as a means of monitoring and setting the amplifier gain.

With the tape recorder connected, the switch has a 0.5 volt (peak-to-peak) output in the emitter circuit. This means of course, that data-signals of 1.0 volts (peak-to-peak) can be satisfactorily chopped without saturating the switch. These waveforms are shown in Figure 3.9.

The switch requires a 4.0 volt square wave at the base for proper operation. This was really a specification applied to and fulfilled by the multivibrator. The input impedance of the data circuit is approximately 50 k-ohms. This impedance does not load the amplifier. That there should be no such loading was actually a design requirement on the switch because the type of amplifier had already been selected.

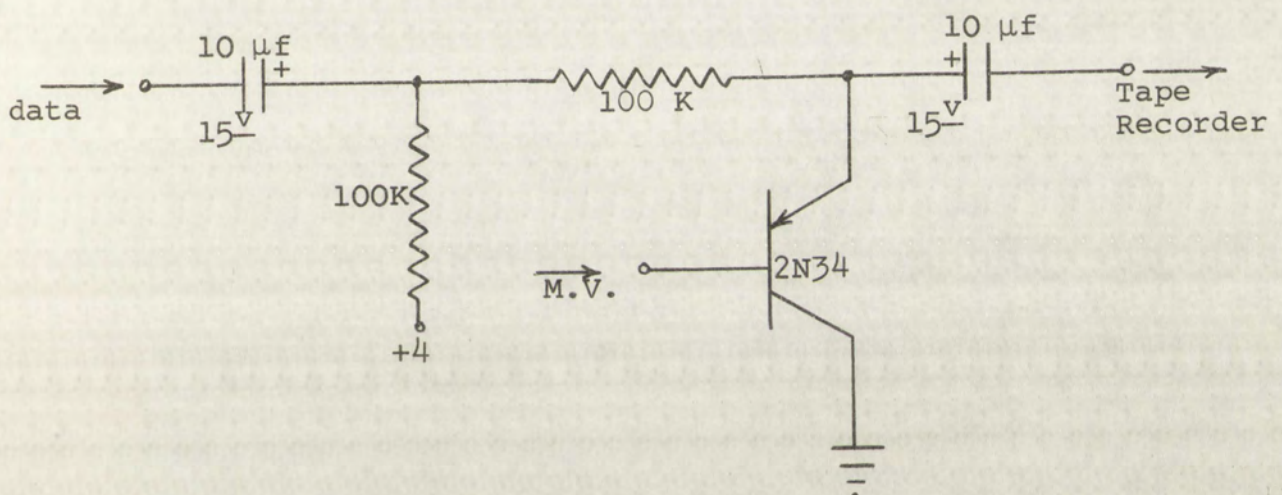


Figure 3.8 Schematic of the switch, "chopper"

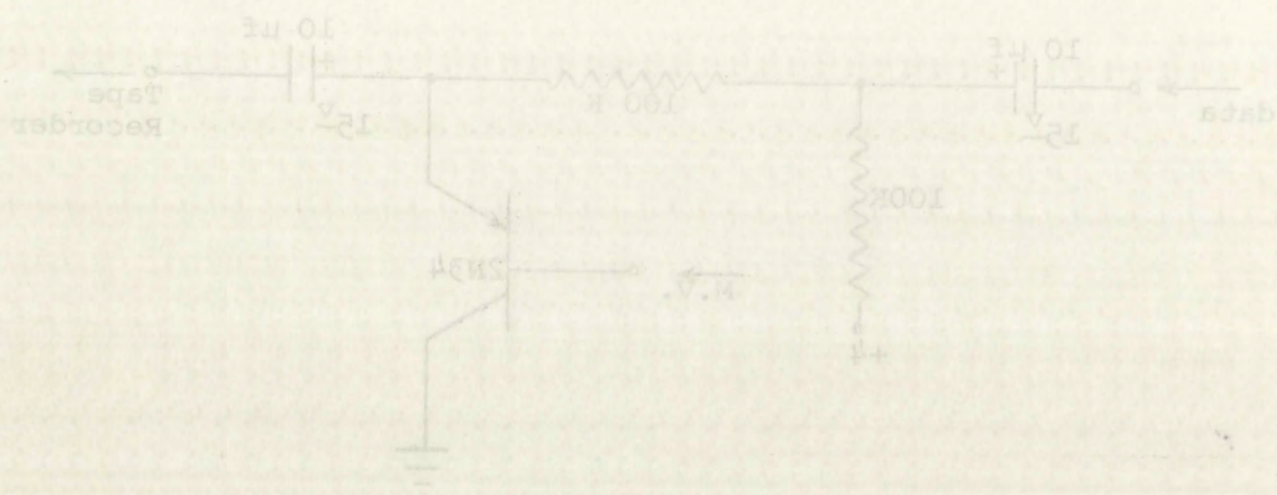
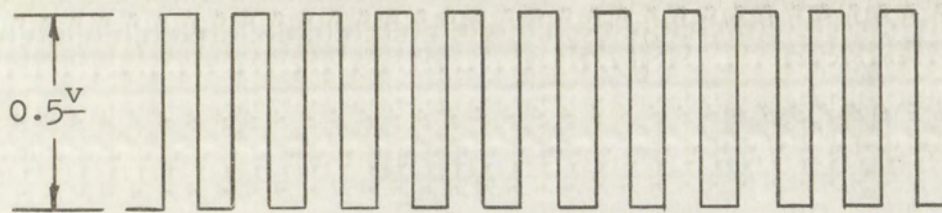
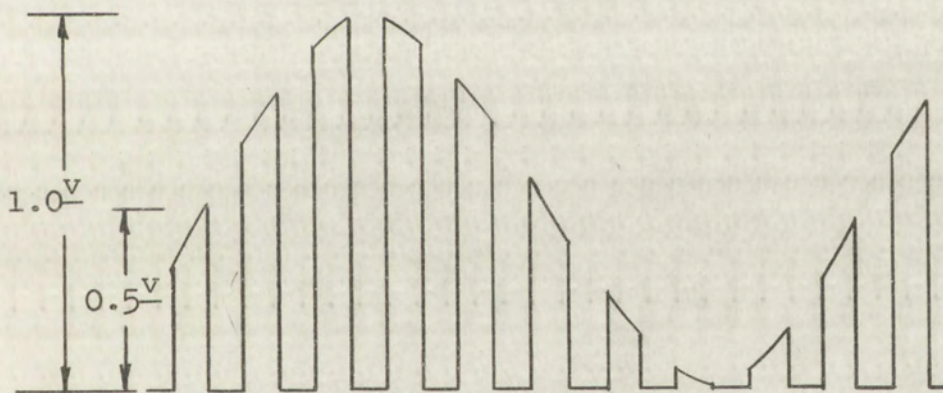


Figure 2.8 Schematic of the switch, "chopper"



Switch output with no data

(a)



Switch output with arbitrary data

(b)

Figure 3.9. Diagram of the switch output waveforms



Switch output with no data

(a)



Switch output with arbitrary data

(b)

Figure 3.3 Diagram of the switch output waveforms

E. Amplifier

The requirements stipulated for the amplifier were based on the assumption that very low signal strengths would be encountered. This assumption also necessitated a low noise figure requirement.

The circuit in Figure 3.10 was finally selected largely on the basis of low noise figure. Direct coupling throughout the circuit affords economy of parts and space. The overall gain is approximately 1000 over the range of 3 cps to 30 kcs. Thus, with the selection of this amplifier, the specifications for the system were altered from 0 to 50 cps to 3 to 50 cps. Mercury batteries are used because of their low-noise and constant terminal voltage characteristic. The low drain on these batteries makes possible about 1500 hours of service.

The circuit has good stability over a large temperature range. In fact, satisfactory performance can be secured at temperatures around 45°C. The stability is also good for large variations in transistor characteristics. This facilitates interchangeability.

Due to feedback the input impedance is essentially the impedance of the input capacitor and series resistor. Thus, with the gain in the X1000 position, the input impedance is essentially 470 ohms. With a low impedance source (much lower than 470 ohms), the input current is a function of the input series resistance. This fact is evident since the input resistance differs by a factor of ten and the gain differs by the same factor. The 4.7 k-ohm input resistance was permanently removed since only the gain X1000 is of interest.

E. amplifier

The experimental results show that the amplifier is capable of the assumption that very low noise level would be encountered. This was verified by the results of the noise figure measurement.

The circuit in Figure 11 is a typical example of the basis of low noise figure. It is a common emitter circuit which affords economy of parts and space. The overall gain is approximately 1000 over the range of 50 to 1000 cycles per second with the selection of this amplifier. The gain of the amplifier system were altered from 10 to 1000 by the use of the mercury batteries are used because of their low noise and constant terminal voltage characteristics. The use of these batteries makes possible about 100 hours of service. The circuit has good stability even at large temperature range. In fact, satisfactory performance can be obtained at temperatures around 45°C. The sensitivity is also good for large variations in transistor characteristics. This is due to interchanging ability.

Due to feedback the input impedance is generally high. Impedance of the input capacitor and series resistor must be with the gain in the 1000 position. The input impedance is essentially 40 ohms. With a low impedance source much lower than 40 ohms, the input current is a function of the input series resistance. This fact is evident from the input resistance differs by a factor of ten and the gain follows by the same factor. The 4.7 k-ohm input resistance was permanently removed since only the gain 1000 is of interest.

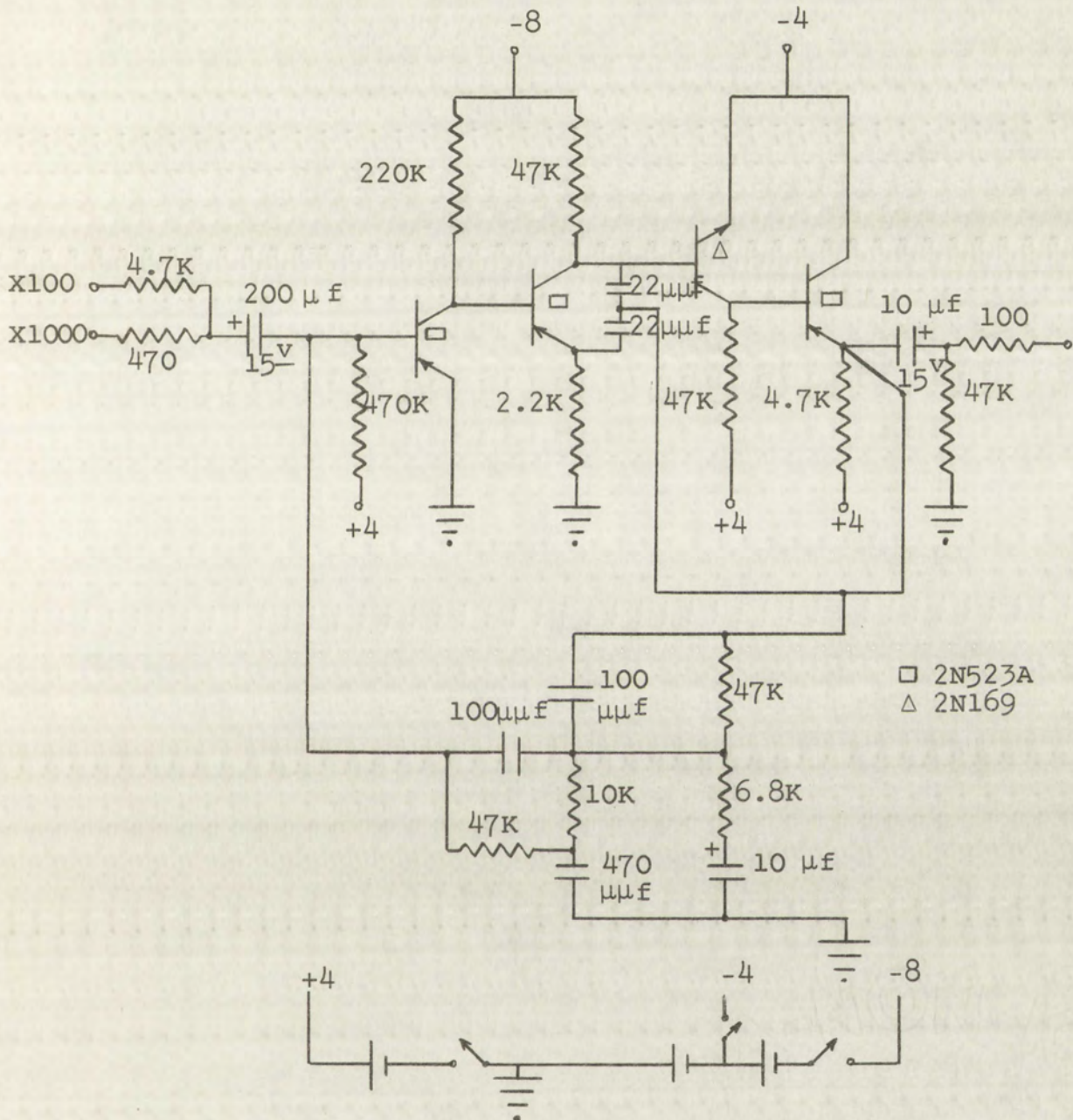


Figure 3.10 Schematic diagram of the amplifier

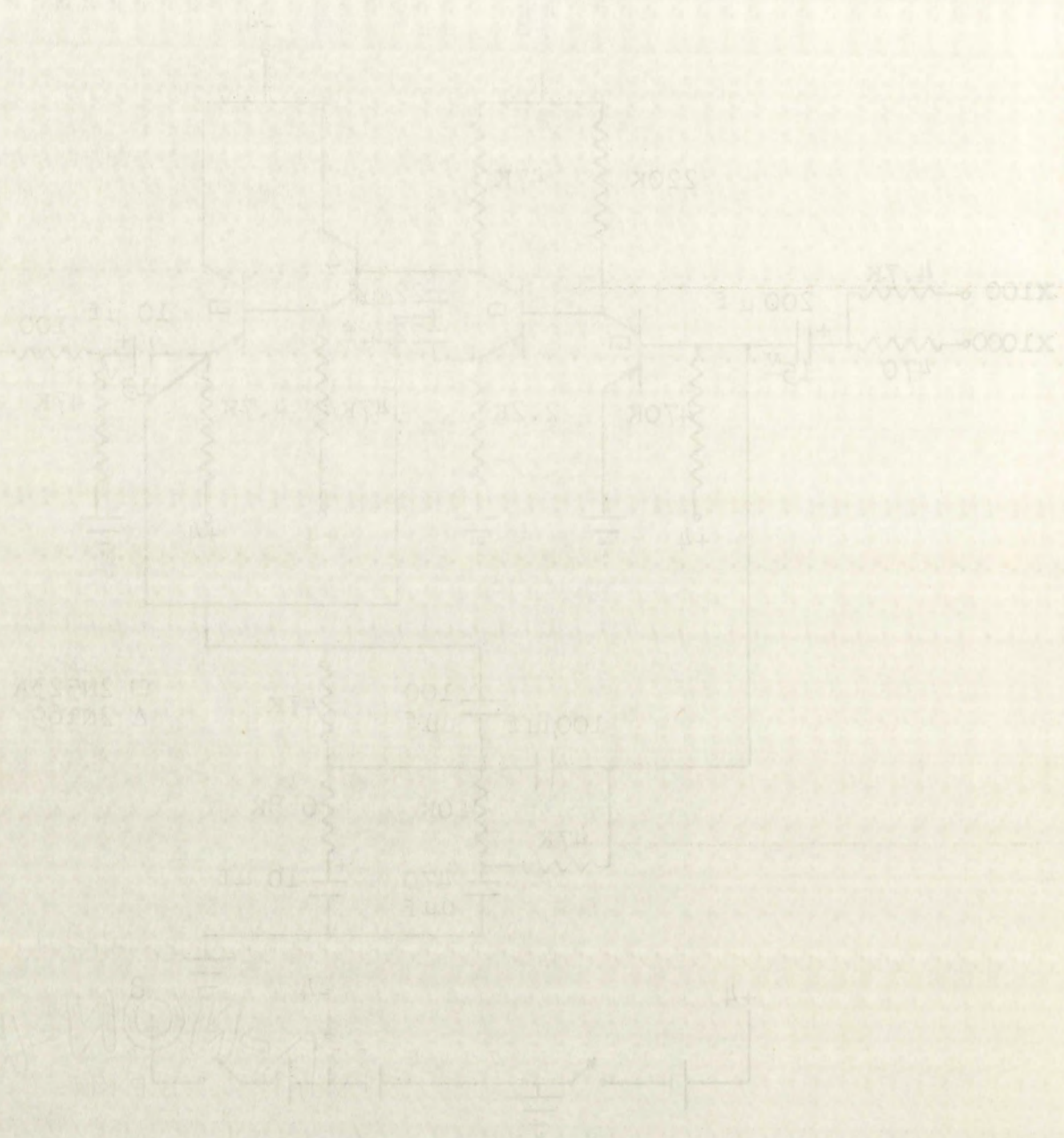


Figure 3.10 Schematic diagram of one amplifier

The no-load maximum undistorted output with a 1 kc test signal was 3.1 volts (peak) for a 3.45 mv (peak) input from a low impedance source. This is a gain of approximately 900 in the X1000 position. Clipping occurs for loads less than 7 k-ohms.

The measured output impedance was approximately 1800 ohms. Under no-load conditions the output has an inherent load--the 10 uf capacitor and 47 k-ohm resistor. This "no-load" condition can be incorporated in the switch. The input impedance of the switch was designed with this in mind. In the final system, the switch, Figure 3.8, is connected directly to the emitter of the last stage in the amplifier. With this connection the gain of the amplifier in the X1000 position is approximately 970. The gain variation from 5 to 1000 cps is about 0.5 db.

The basic feedback circuit is from the output to the input of the amplifier. This feedback circuit consists of a lead-lag circuit connected to the amplifier output in series with a bridge-T circuit connected to the amplifier input. The necessary magnitude of the feedback voltage is controlled primarily by the lead-lag circuit. This circuit also provides the necessary phase-lag at the lower frequencies. However, the phase-lead that is introduced is excessive in the 10 to 50 kcs region.

The bridge-T network while having very little effect on the magnitude of the feedback voltage introduces a phase-lag that increases with frequency to 34 kcs. Beyond 34 kcs, this phase-lag changes quickly to a phase-lead that increases with frequency. The net effect of the lead-lag and bridge-T circuits

The no-load maximum output voltage was 100 V. The signal was 2.1 V. The input impedance was 100 k Ω . The output impedance was 100 Ω . The measured output impedance was 100 Ω . Under no-load conditions the output was 100 V. 10 nF capacitor and 10 k Ω resistor. The output can be incorporated in a circuit. The switch was designed with this in mind. In the final system the switch, Figure 5.6, is connected directly to the output of the last stage in the amplifier. With this connection the gain of the amplifier in the 1000 position is approximately 100. The gain variation from 5 to 1000 is about 0.5 dB. The basic feedback circuit is shown in Figure 5.7. of the amplifier. This feedback circuit consists of a feedback circuit connected to the amplifier output. The bridge-T circuit connected to the amplifier output. The magnitude of the feedback voltage is proportional to the magnitude of the lead-lag circuit. This circuit provides a phase-lag at the lower frequencies. However, the phase-lag that is introduced is excessive in the 10 to 1000 range. The bridge-T network which has a very small phase-lag at the magnitude of the feedback voltage and produces a phase-lag that increases with frequency. The net effect of the lead-lag and bridge-T network phase-lag changes only to a phase-lag that increases with frequency. The net effect of the lead-lag and bridge-T network

is that in the 26 to 52 kcs region the phase-lead increases rapidly and is excessive. This excessive phase-lead causes instability at the higher frequencies.

A second feedback circuit is connected from the output of the amplifier to the second stage. The output voltage of the amplifier is injected into the emitter and collector of this second stage through 22 uuf capacitors. Due to the small capacitance, this feedback circuit is effective only at the higher frequencies above approximately 26 kcs. The additional phase-lag introduced by this feedback circuit reduces the overall phase-lead at the higher frequencies and provides high frequency stability.

The low noise figure of from 2.4 to 5 db is the culmination of several factors. Perhaps the foremost of these factors is that the germanium transistors have an inherently low noise characteristic. To further reduce the noise, the first stage is operated at very low collector voltage and current. And finally, the mercury batteries themselves possess a low noise performance rating.

is that in the 20 to 50 Kcs region the phase-lead increases rapidly and is excessive. This excessive phase-lead causes instability at the higher frequencies.

A second feedback circuit is connected from the output of the amplifier to the second stage. The output voltage of the amplifier is injected into the emitter and collector of this second stage through 22 and 23 capacitors. Due to the small capacitance, this feedback circuit is effective only at the higher frequencies above approximately 20 Kcs. The additional phase-lead introduced by this feedback circuit reduces the overall phase-lead at the higher frequencies and provides high frequency stability.

The low noise figure of from 2.4 to 5 db is the culmination of several factors. Perhaps the foremost of these factors is that the germanium transistors have an inherently low noise characteristic. To further reduce the noise, the first stage is operated at very low collector voltage and current. And finally, the mercury batteries themselves possess a low noise performance rating.

F. Pre-Amplifier

The most stringent requirement for the pre-amplifier is a high impedance input. This came about because the antenna had at this point already been determined. The antenna impedance as a function of frequency is shown in Figure D3 of Appendix D. To prevent loading the antenna and to secure a reasonable signal-to-noise ratio at the input, a high impedance device is necessary.

The usual type of transistor is immediately eliminated from consideration in the pre-amplifier because of the high impedance level required. An electrometer tube was considered and finally selected. Tubes of this type are available which have low-potential electrodes. The low-voltages and low current drain make them suitable for portable equipment. The extremely small grid currents (as low as 10^{-17} amperes) permits inserting very large resistance (on the order of 1000 megohms) in the grid circuit.

The Victoreen type 5800 tube was incorporated in the circuit shown in Figure 3.11. This tube has the following parameters at the operating point: $\mu = 1$, $r_p = 66$ k-ohm, and $g_m = 15 \mu$ -mhos.

The output impedance of the electrometer stage is considerably higher than the input impedance of the following amplifier stage. To improve this mismatch and at the same time prevent low frequency loss, a direct coupled emitter follower arrangement is used. The overall gain is approximately 0.5 from 3 to 50 cps. Most of the loss is in the emitter follower.

F. Pre-Amplifier

The most stringent requirement for the pre-amplifier is a high impedance input. This came about because the antenna had at this point already been determined. The antenna impedance as a function of frequency is shown in Figure D3 of Appendix D. To prevent loading the antenna and to secure a reasonable signal-to-noise ratio at the input, a high impedance device is necessary. The usual type of transistor is immediately eliminated from consideration in the pre-amplifier because of the high impedance level required. An electrometer tube was considered and finally selected. Tubes of this type are available which have low potential electrodes. The low-voltages and low current drain make them suitable for portable equipment. The extremely small grid currents (as low as 10^{-17} amperes) permits inserting very large resistance (on the order of 1000 megohms) in the grid circuit.

The Victoreen type 5800 tube was incorporated in the circuit shown in Figure 3.11. This tube has the following parameters at the operating point: $\mu = 1$, $r_p = 66 \text{ k-ohms}$, and $g_m = 15 \text{ mhos}$.

The output impedance of the electrometer stage is considerably higher than the input impedance of the following amplifier stage. To improve this mismatch and at the same time prevent low frequency loss, a direct coupled emitter follower arrangement is used. The overall gain is approximately 0.5 from 5 to 50 cps. Most of the loss is in the emitter follower.

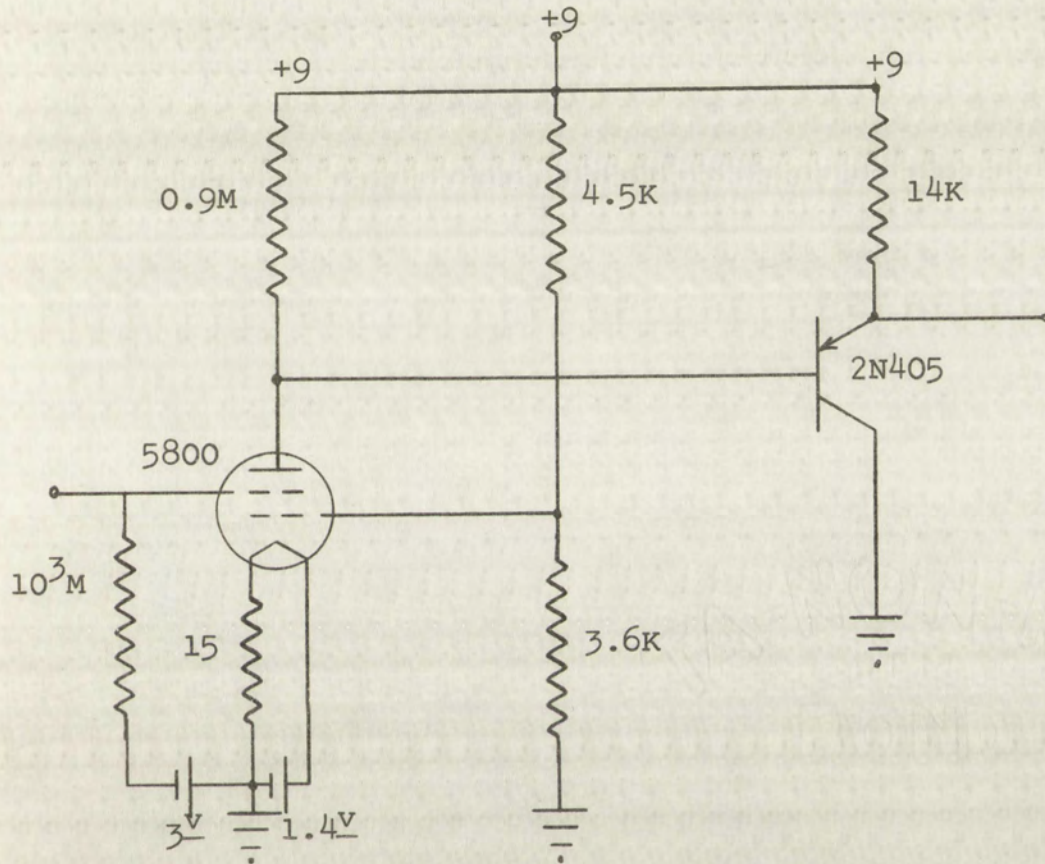


Figure 3.11 Schematic diagram of the pre-amplifier

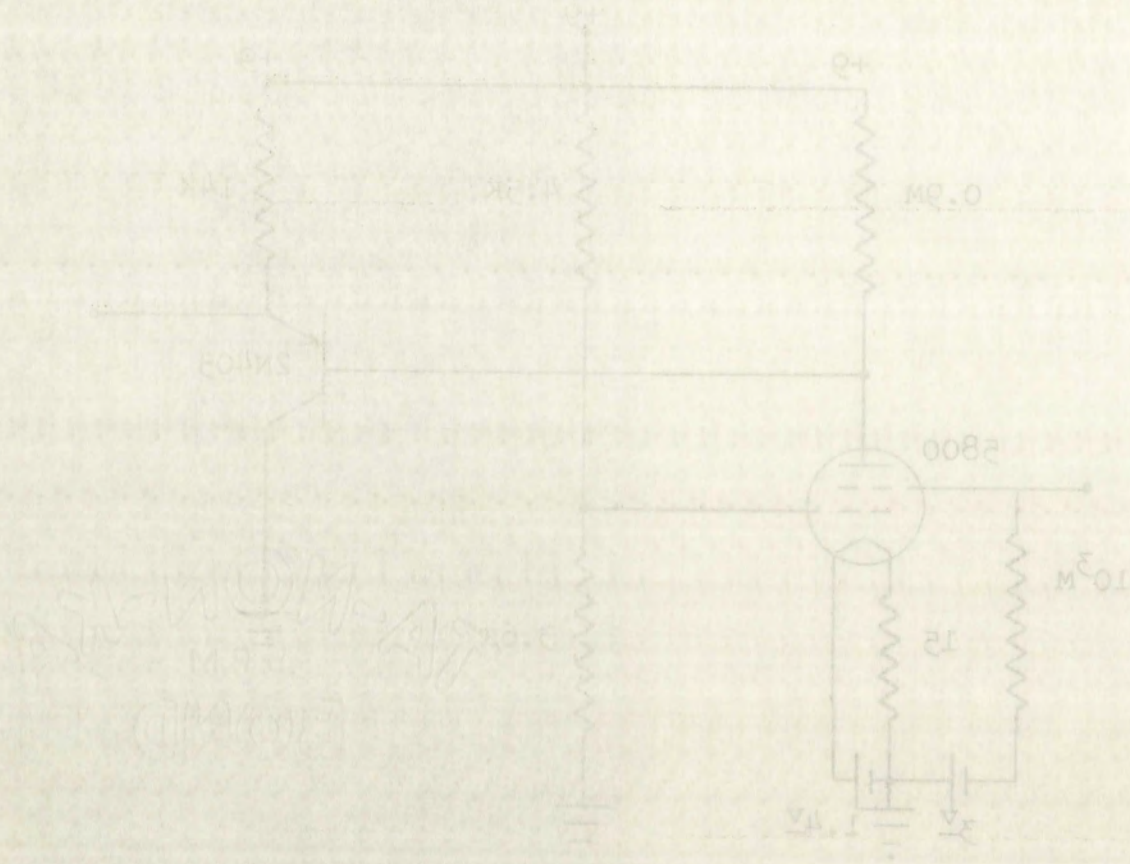


Figure 3.11 Schematic diagram of the pre-amplifier

G. Antenna

The portability requirement imposed upon the overall system implies that both the weight and the configuration of the antenna must permit ease of handling. Since the loop antenna is independent of shape, it would seem to meet this portability requirement. However, this antenna has a low efficiency and is subject to "night effect" and microseisms. In addition, voltages are induced in this antenna by wind motion.

Assuming $1 \mu v$ output from a loop antenna at 10 cps where $\lambda = 3 \times 10^7$ meters, calculations shown in Appendix D indicate that a circular loop 10 meters in radius requires 16,000 turns. Calculations for other loop dimensions show that the "area-turns" (AN) product is simply too large to meet the size and weight required for portability. Considering core material to further reduce the AN-product shows that as this product becomes reasonable the weight of the core material becomes excessive.

The capacitance and impedance of a vertical antenna are given in Appendix D. The conclusion that can be drawn here is that the capacitance is quite low and the impedance is very high in the frequency range of interest. Efforts are usually directed to reducing this impedance by increasing the capacitance.

The capacitance of a vertical antenna can be increased by increasing the length or the diameter or both. Increasing the length is more effective. Doubling the length has approximately the same effect as increasing the diameter ten times. Reducing the actual height of the antenna above ground also increases

The possibility of reducing the weight of the antenna must permit basic of handling. Since the antenna is independent of shape, it would seem to meet this other requirement. However, this antenna is subject to "night effect" and "missile" are induced in this antenna by induction. Assuming 1 v output from a loop antenna in the where $\lambda = 3 \times 10^7$ meters, calculations show that a circular loop 10 meters in radius requires 100 turns. Calculations for other loop dimensions show that the (AN) product is simply too large to meet the weight and weight required for portability. Considering core materials to further reduce the AN-product shows that the product becomes unreasonable the weight of the core material becomes excessive. The capacitance and inductance of a vertical antenna are given in Appendix B. The conclusion that can be drawn here is that the capacitance is quite low and the impedance is very high in the frequency range of interest. Efforts are now directed to reducing this impedance by increasing the capacitance.

The capacitance of a vertical antenna can be increased by increasing the length or the diameter of the antenna. The length is more effective. Doubling the length has about the same effect as increasing the diameter ten times. Reducing the actual height of the antenna above ground also increases

the capacitance. In addition to altering the dimensions and height, the vertical antenna can be top-loaded with inductance and/or capacitance to lower the impedance. However, this method is not conducive to portability.

A Hall-effect device was briefly considered as a sensor or antenna. While this device is relatively independent of frequency it is considerably noisier than either a vertical or a loop antenna.

All factors considered, the vertical antenna was finally selected. The antenna completely assembled and erected is shown in Figure 3.12. The 30 ft. overall length telescope into a portable length of 10 ft. The 4.5 inch insulator is permanently mounted on the base plate. The bottom of the antenna is bolted to the insulator fitting for raising and lowering. Four copper rods are used as stakes for the nylon guy lines. These rods and the base plate are electrically connected and serve as the ground system.

Calculations given in Appendix D show that the antenna capacitance is approximately 93 ~~pf~~ fd. A graph of antenna reactance as a function of frequency is also presented in Appendix D (Figure D3). It can be seen from this graph that the antenna coupling device should have a high input impedance.

the capacitance. In addition to the capacitance, the vertical distance between the antenna and the ground plane is not conducive to portability. A Hall-effect device was initially used as a means of antenna. While this device is relatively independent of frequency as is considerably smaller than a loop antenna, a loop antenna.

All factors considered, the vertical antenna was selected. The antenna completely assembled and mounted is shown in Figure 3.12. The antenna is mounted on a portable length of 10 ft. The antenna is mounted on the base plate. The bottom of the antenna is bolted to the insulator fitting for the antenna and the antenna rods are used as stakes for the antenna. The antenna the base plate are electrically connected and serve as the ground system.

Calculations given in Appendix B show that the capacitance is approximately 22 pF. A graph of capacitance as a function of frequency is also presented in Appendix B (Figure B2). It can be seen from this graph that the antenna coupling device should have a high impedance.

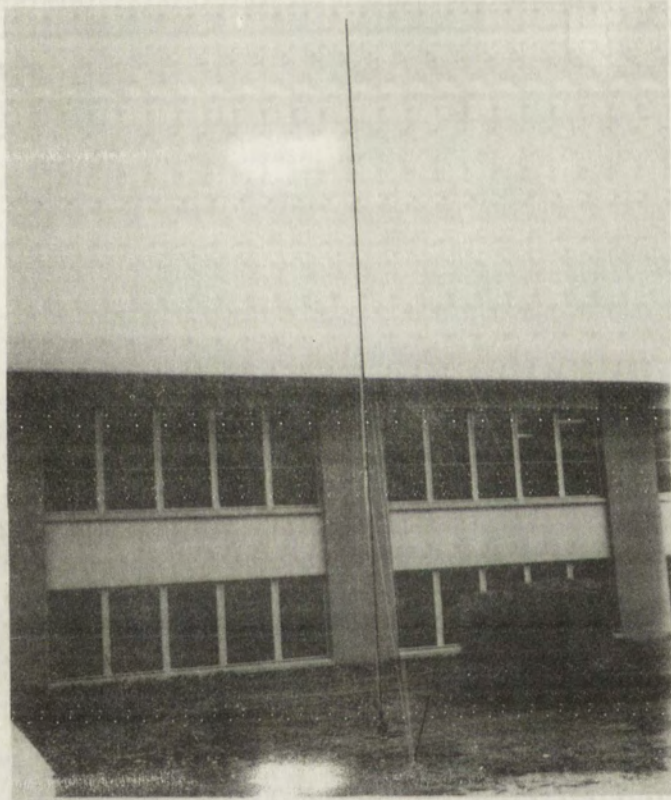


Figure 3.12 The Antenna

WOMEN
M. J. 272
BOLD

4. Final System Design and Performance

A. Description of the System

The data-collecting system is shown diagrammatically in Figure 4.1 and schematically in Figure 4.2. Referring to these figures it can be seen that the 1000 cps sinusoidal oscillator drives the sync head and the multivibrator. The sync head energizes the sync-track on the duo-track magnetic tape. In the playback mode, the sync-track provides a synchronizing signal. The astable multivibrator, synchronized by the oscillator, provides the necessary square wave to drive the switch which in turn interrupts the data-channel at the oscillator rate.

The data signals from the antenna are fed to the amplifier section when the test-record switch is in the "record" position. The output of the amplifier section is interrupted or "chopped" by the switch before being recorded on the data-track of the tape.

The outputs of the oscillator, multivibrator, switch, and amplifier section are made available at the test point on the front panel of the receiver through a test switch. This permits checking and monitoring the important components of the system. See Figure 4.3.

In the "test" position of the test-record switch, a 1000 cps test signal from the oscillator, properly attenuated in the attenuator, is injected into the amplifier section through the dummy antenna. Since the attenuation factor is constant, the performance of the amplifier section can be checked at the test

A. Description of the System

The data-collecting system is shown in Figure 4.1.

Figure 4.1 and schematically in Figure 4.2.

These figures it can be seen that the test section and the

oscillator drives the sync head and the sync head

sync head energizes the sync track on the data disk magnetic

tape. In the playback mode, the sync track energizes a

rising signal. The test section is energized by the

oscillator, provides the necessary square wave to drive the

switch which in turn energizes the data-collecting section.

oscillator rate.

The data signals from the antenna are fed to the amplifier

section when the test section switch is in the "test" position.

The output of the amplifier section is energized by the

by the switch before being recorded on the data disk on the

tape.

The outputs of the oscillator, multi-vibrator, switch, and

amplifier section are made available at the test point on the

front panel of the receiver through a test section. This permits

checking and monitoring the important components of the system.

See Figure 4.3.

In the "test" position of the test section switch a 4000

cps test signal from the oscillator, properly attenuated in the

attenuator, is injected into the amplifier section through the

dummy antenna. Since the attenuation factor is constant, the

performance of the amplifier section can be checked in the test

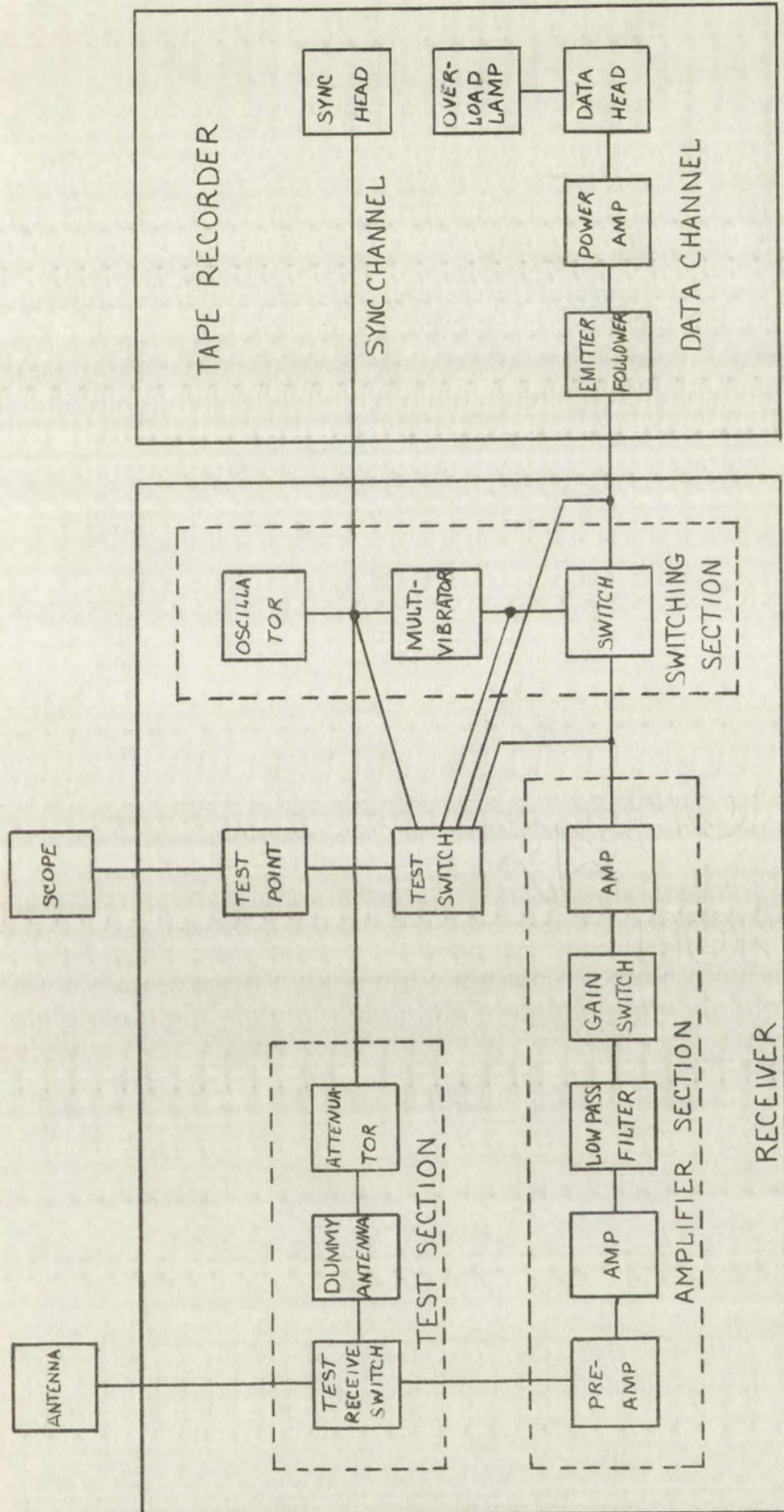


Figure 4.1 Block diagram of data-collecting system



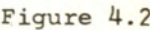


Figure 4.2 Schematic diagram of data-collecting system



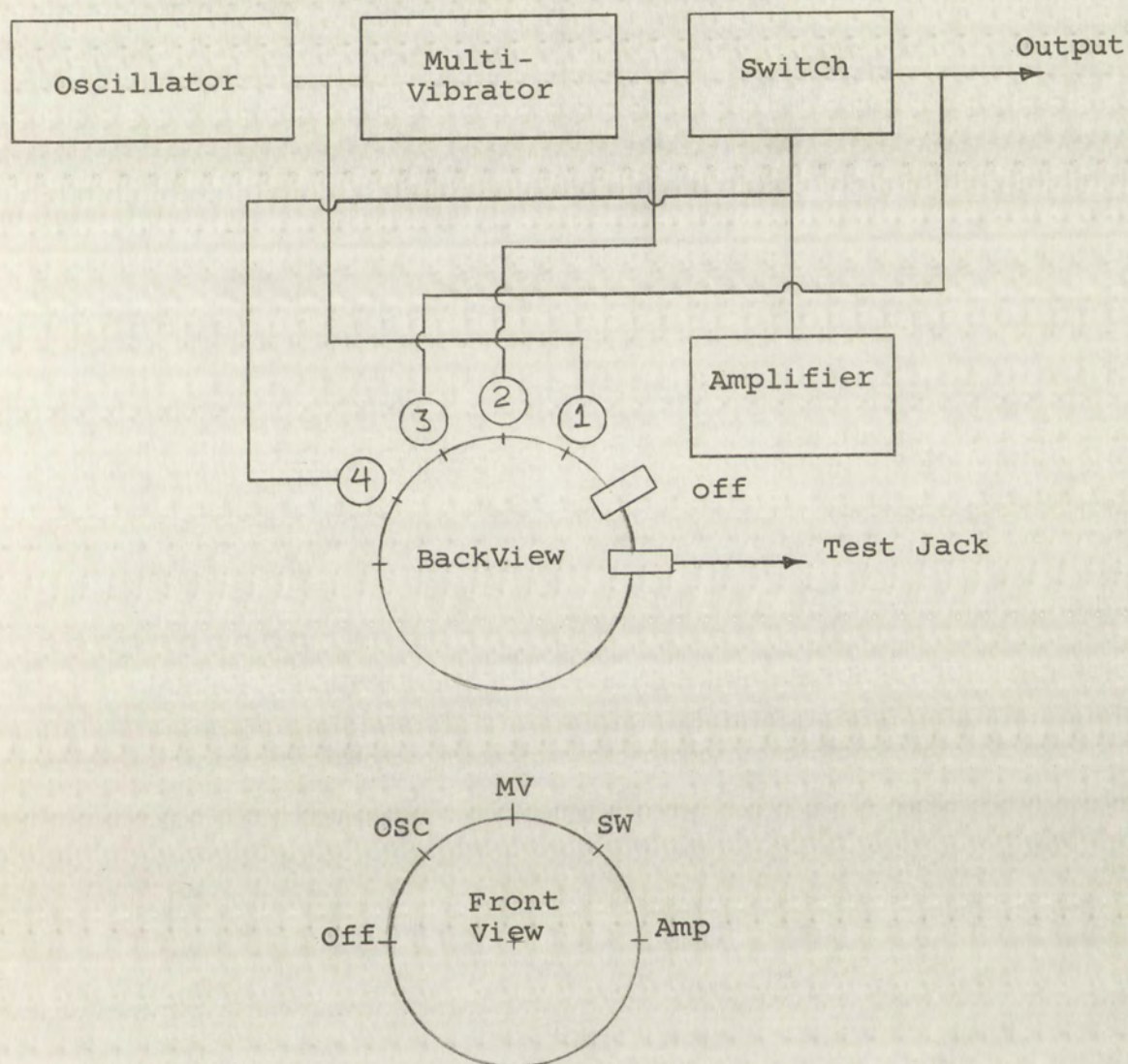


Figure 4.3 Functional diagram of Test Point System

point. A Tektronix Type 321 transistorized portable oscilloscope is connected to the test point for checking the system before and during the data-collecting process.

The batt-test switch provides an additional means of checking the components in the receiver. This switch permits measuring the battery voltages under load conditions on the front panel voltmeter. See Figure 4.4.

point. A Tektronix Type 521 characterized portable oscilloscope is connected to the test point for checking the system before and during the data-collecting process.

The batt-test switch provides an additional means of checking the components in the receiver. This switch permits measuring the battery voltages under load conditions on the front panel voltmeter. See Figure 4.4.

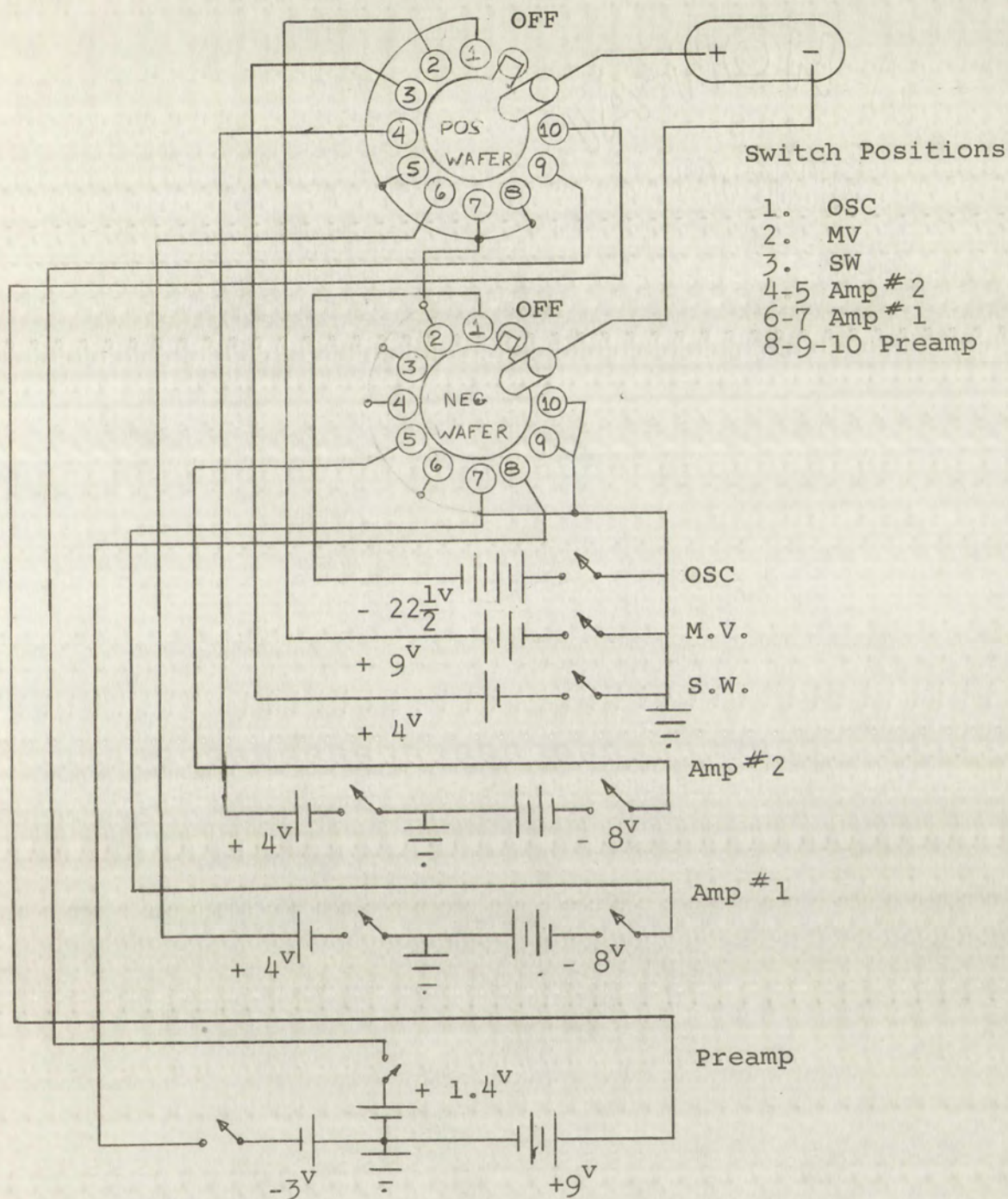


Figure 4.4 Schematic of Battery Test System

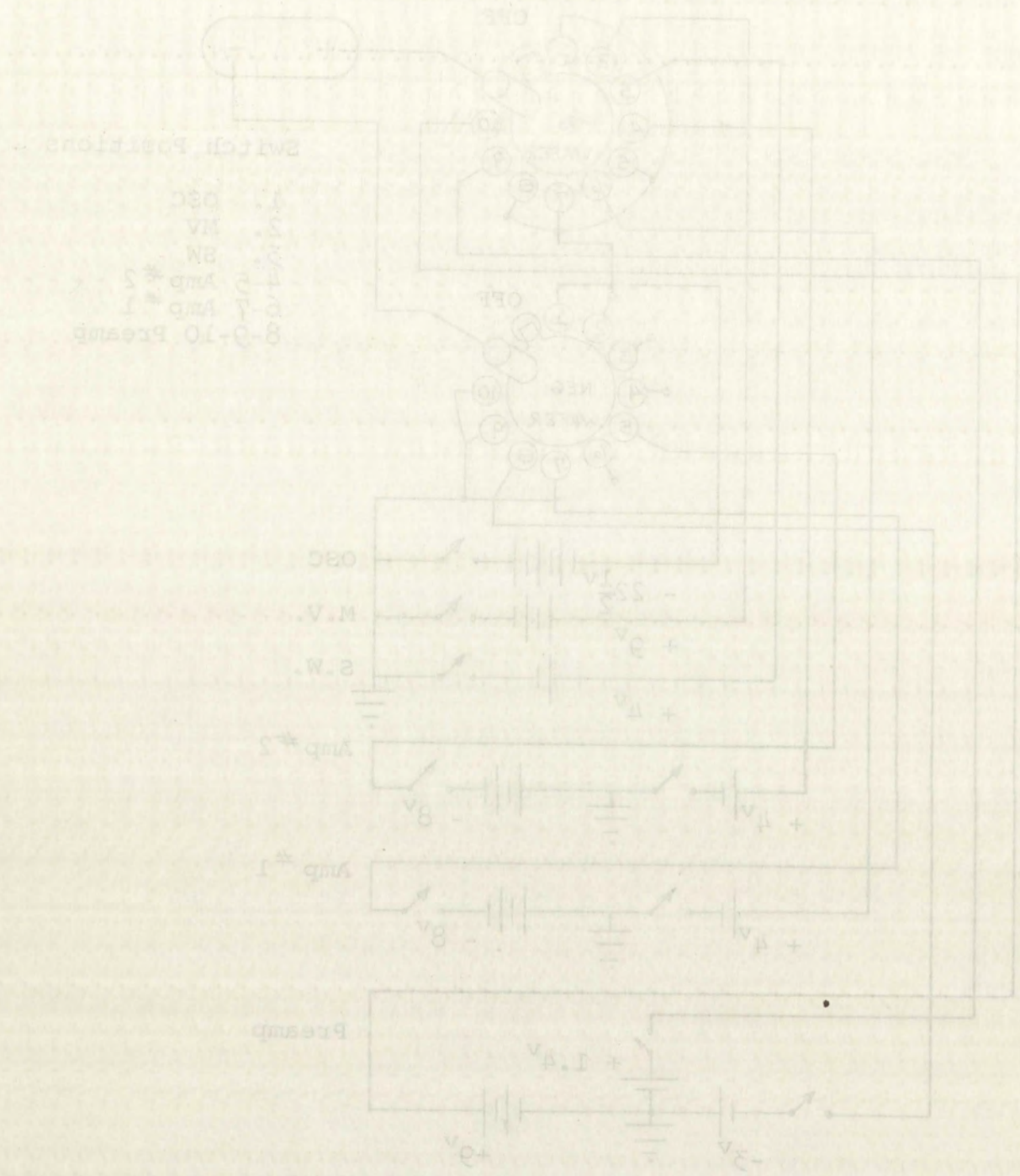


Figure 4.4 Schematic of Battery Test System

B. Overall Performance Tests

The variation of oscillator frequency versus battery voltage with temperature as the parameter has previously been shown in Figure 3.6. A battery voltage of 19.5 volts, down 3 volts from the design value of 22.5 volts, gives a frequency change of 5 cps at 21°C and 9 cps at 46°C. Thus at 21°C the frequency decreases 0.5% and at 46°C, 0.9%.

The oscillator frequency increases approximately 0.1% when the multivibrator is turned on. Subsequently energizing the switch and tape recorder causes no further change in frequency. However, connecting the sync head causes the frequency to increase about 0.2%. This "pulling" effect is independent of the oscillator battery voltage.

The magnitude of the oscillator output is relatively independent of the multivibrator, switch, and sync head. In other words, there are no "loading" effects on amplitude. The mechanical stability is verified by the fact that there was no discernible frequency change after four field trips.

Synchronization of the multivibrator is maintained throughout the multivibrator and oscillator battery voltage ranges 6.4 to 9.0 and 18 to 22.5 volts, respectively. With the multivibrator and switch battery voltages equal to or greater than 6.4 and 3.5 volts respectively, variations of the oscillator battery voltage (18 to 22.5 volts) have no influence on the amplitude of the switch output. This is another way of saying that although the magnitude of the multivibrator output is a function of battery voltage, this output does not effect

The variation of oscillator frequency versus battery

voltage with temperature as the parameter has previously been shown in Figure 5.1. A battery voltage of 12.5 volts, down 3 volts from the design value of 15.5 volts, gives a frequency change of 5 cps at 21°C and 9 cps at 40°C. Thus at 21°C the frequency decreases 0.5% and at 40°C, 0.9%.

The oscillator frequency increases approximately 0.1% when the multivibrator is turned on. Subsequently energizing the switch and tape recorder causes no further change in frequency. However, connecting the sync head causes the frequency to increase about 0.3%. This "pulling" effect is

independent of the oscillator battery voltage.

The magnitude of the oscillator output is relatively

independent of the multivibrator, switch, and sync head. In other words, there are no "loading" effects on amplitude. The mechanical stability is verified by the fact that there was no discernible frequency change after four field trips.

Synchronization of the multivibrator is maintained through-

out the multivibrator and oscillator battery voltage ranges

6.4 to 9.0 and 18 to 22.5 volts, respectively. With the

multivibrator and switch battery voltages equal to or greater than 6.4 and 3.5 volts respectively, variations of the

oscillator battery voltage (18 to 22.5 volts) have no influence on the amplitude of the switch output. This is another way of saying that although the magnitude of the multivibrator output is a function of battery voltage, this output does not effect

the switch output provided this battery voltage is equal to or greater than 6.4 volts. Actually this battery voltage is normally 7.3 volts and because of light loading does not vary appreciably from this value. Maintaining the battery voltage of the switch equal to or greater than 3.5 volts ensures proper switching.

Thus by maintaining the battery voltages on the oscillator, multivibrator, and switch equal to or greater than 19.5, 7.3, and 3.7 volts, respectively, proper performance of the switching section is assured. Under these conditions the output of the switch is maintained at 0.5 volts (peak-to-peak).

The design voltage for the data-channel in the tape recorder is 8.04 volts due to 6 batteries at 1.34 volts each. Under these conditions a sinusoid of 0.52 volts (rms) is required to light the overload lamp in the tape recorder. Tests show (Figure 4.5) that when the battery voltage reduces to 6.6 volts a sinusoid of 0.67 volts (rms) is required to light this overload lamp. In the test procedure, an adjustable fraction of the oscillator output is injected into the tape recorder data-channel, the amplitude of this voltage is not only an indication of the battery voltage but also an indication of the data-channel operation.

The change in signal voltage from 0.52 to 0.67 volts represents a 3 db drop in the data-channel gain. However, under actual field conditions the injected voltage is relatively constant at 0.52 volts with a very rapid and noticeable change when the mercury batteries become exhausted.

the switch output provided this battery voltage is equal to or greater than 0.4 volts. Actually this battery voltage is normally 1.5 volts and because of light loading does not vary appreciably from this value. Maintaining the battery voltage of the switch equal to or greater than 0.5 volts ensures proper switching.

Thus by maintaining the battery voltages on the oscillator, multiplier, and switch equal to or greater than 1.5, 1.5, and 0.5 volts, respectively, proper performance of the switching section is assured. Under these conditions the output of the switch is maintained at 0.5 volts (peak-to-peak).

The design voltage for the data-channel in the tape recorder is 8.04 volts due to 6 batteries at 1.34 volts each. Under these conditions a sinusoid of 0.52 volts (rms) is required to light the overload lamp in the tape recorder. Tests show (Figure 4.5) that when the battery voltage reduces to 6.6 volts a sinusoid of 0.67 volts (rms) is required to light this overload lamp. In the test procedure, an adjustable fraction of the oscillator output is injected into the tape recorder data-channel, the amplitude of this voltage is not only an indication of the battery voltage but also an indication of the data-channel operation.

The change in signal voltage from 0.52 to 0.67 volts represents a 3 db drop in the data-channel gain. However, under actual field conditions the injected voltage is relatively constant at 0.52 volts with a very rapid and noticeable change when the mercury batteries become exhausted.

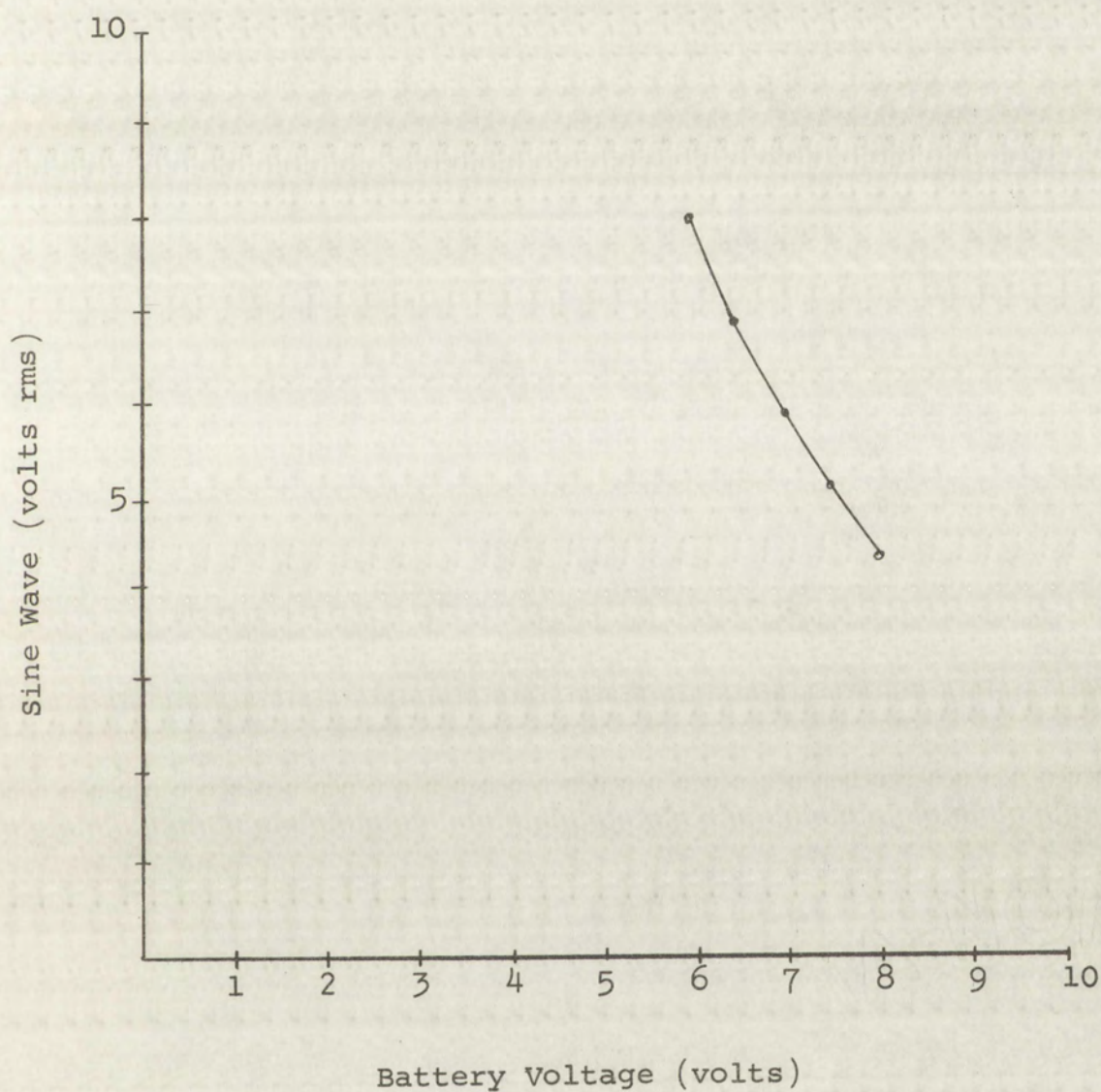


Figure 4.5 Tape recorder amplifier input versus battery voltage

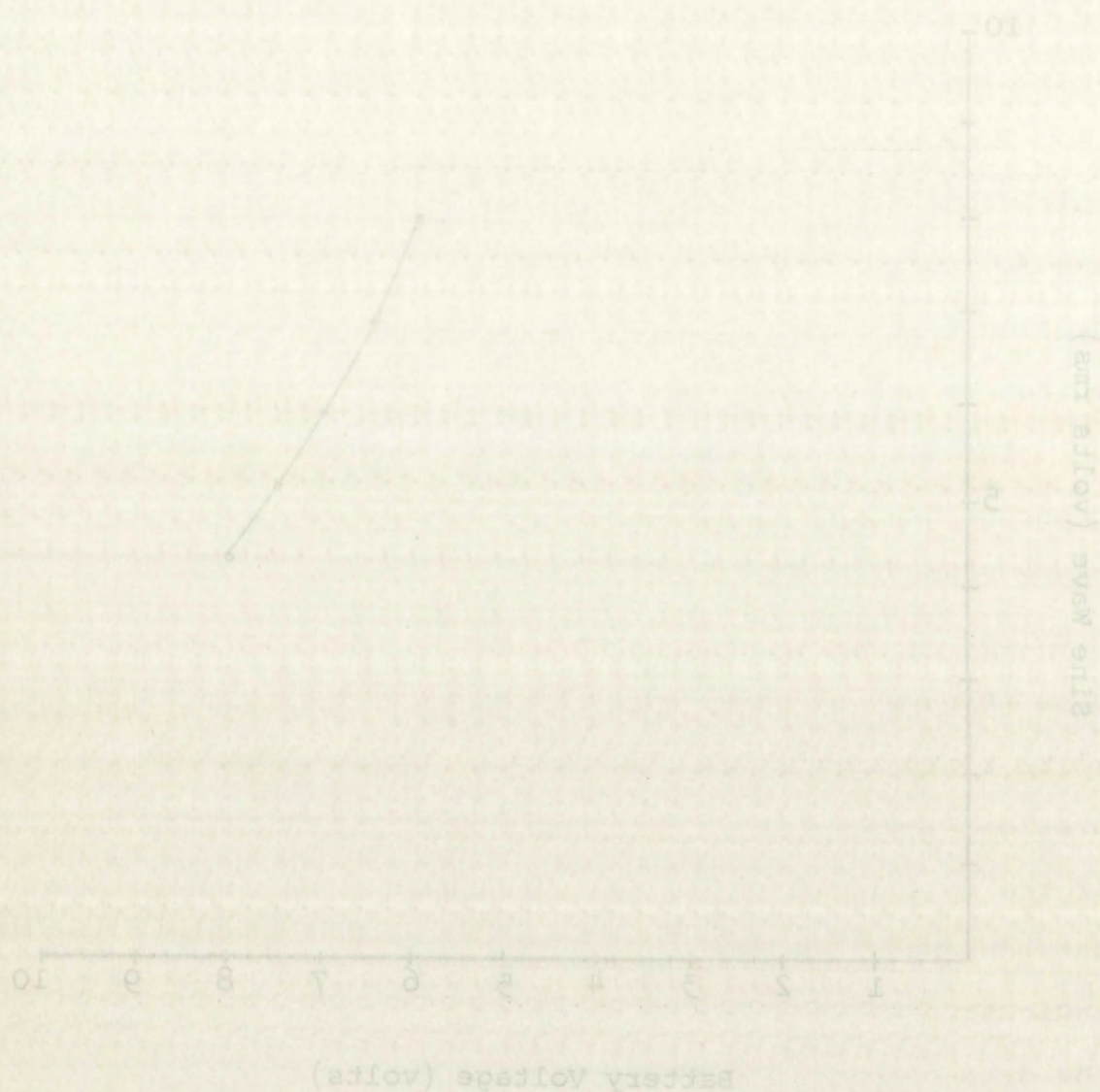


Figure 4.5 Tape recorder amplifier input versus battery voltage

Since 13 volts is required at the driving side of the output transformer to light the overload lamp, the voltage gain through the data-channel of the tape recorder is approximately 17. This, of course, includes the gain of the emitter follower which is approximately 0.9. The overload lamp circuit is itself independent of the battery voltage and therefore constitutes a relatively constant reference.

The attenuator, dummy antenna, and test-record switch comprise the test section. The attenuator is essentially a voltage divider permanently connected to the oscillator output. The output of this divider is 8.06×10^{-5} that of the oscillator. The dummy antenna is a 93 μpf capacitor which is electrically equivalent to the antenna. When the test-record switch is in the "test" position the output from the divider is injected into the amplifier section through the dummy antenna.

The output of the amplifier section and the oscillator can be measured at the test point on the front panel by using the test switch. Thus, in the "test" position the gain of the amplifier section is readily determined by the relation

$$k = \frac{e_o \text{ (amplifier section)}}{e_o \text{ (oscillator)} 8.06 \times 10^{-5}} .$$

The gain of the amplifier section for the various positions of the gain switch is shown in Table 4-I. The performance of the amplifier section is checked by determining the gain at positions 1, 5, and 9. With all battery voltages at design values, the gain at positions 1, 5, and 9 is 47.69, 627, and 6535, respectively. Permitting a 3 db reduction in gain, these become 35.5, 467, and 4865, respectively.

Position	Gain
1	47.6
2	83.3
3	157.
4	334.
5	547.
6	1006.
7	2080.
8	3640.
9	5700.

Table 4-I Gain switch positions

Position	Gain
1	47.6
2	85.3
3	157.
4	324.
5	547.
6	1006.
7	2080.
8	3640.
9	5700.

Table 4-1 Gain switch positions

In data-collecting, position 1 of the gain switch is used almost exclusively to prevent saturating or overdriving the switch. In this position the gain is 35.5 to 47.69. This upper limit is with external supplies giving the required design voltages. The gain never exceeds 41 with fresh batteries. Measurements with the test circuit show a gain of 36 to 41, a 1.2 db variation. The usual reading is 36 or 37.

Since the test procedure employs 1000 cps for gain determination, some method of correlating this gain with the actual frequency response is necessary. The frequency response, when the gain is 36 according to the test circuit, is shown in Figure 4.6. This response is the result of injecting signals through the dummy antenna at three voltage levels--70, 44, and 5 mv (rms). The 70 and 44 mv input signals give 100 and 50% saturation of the switch respectively. The 5 mv signal was the minimum obtainable from the signal generator without external voltage division. External voltage division can be done but not without sacrificing accuracy due to 60 cps pickup.

In data-collecting position 1 of the gain switch is used almost exclusively to prevent saturating or overdriving the switch. In this position the gain is 35.5 to 47.6. This upper limit is with external supplies giving the required design voltages. The gain never exceeds 47 with fresh batteries. Measurements with the test circuit show a gain of 35 to 41.5 \pm 1.2 db variation. The usual reading is 35 or 37.

Since the test procedure employs 1000 cps for gain determination, some method of correlating this gain with the actual frequency response is necessary. The frequency response, when the gain is 35 according to the test circuit, is shown in Figure 4.6. This response is the result of injected signals through the dummy antenna at three voltage levels - 70, 44, and 5 mv (rms). The 70 and 44 mv input signals give 100 and 50% saturation of the switch respectively. The 5 mv signal was the minimum obtainable from the signal generator without external voltage division. External voltage division can be done but not without sacrificing accuracy due to 60 cps pickup.

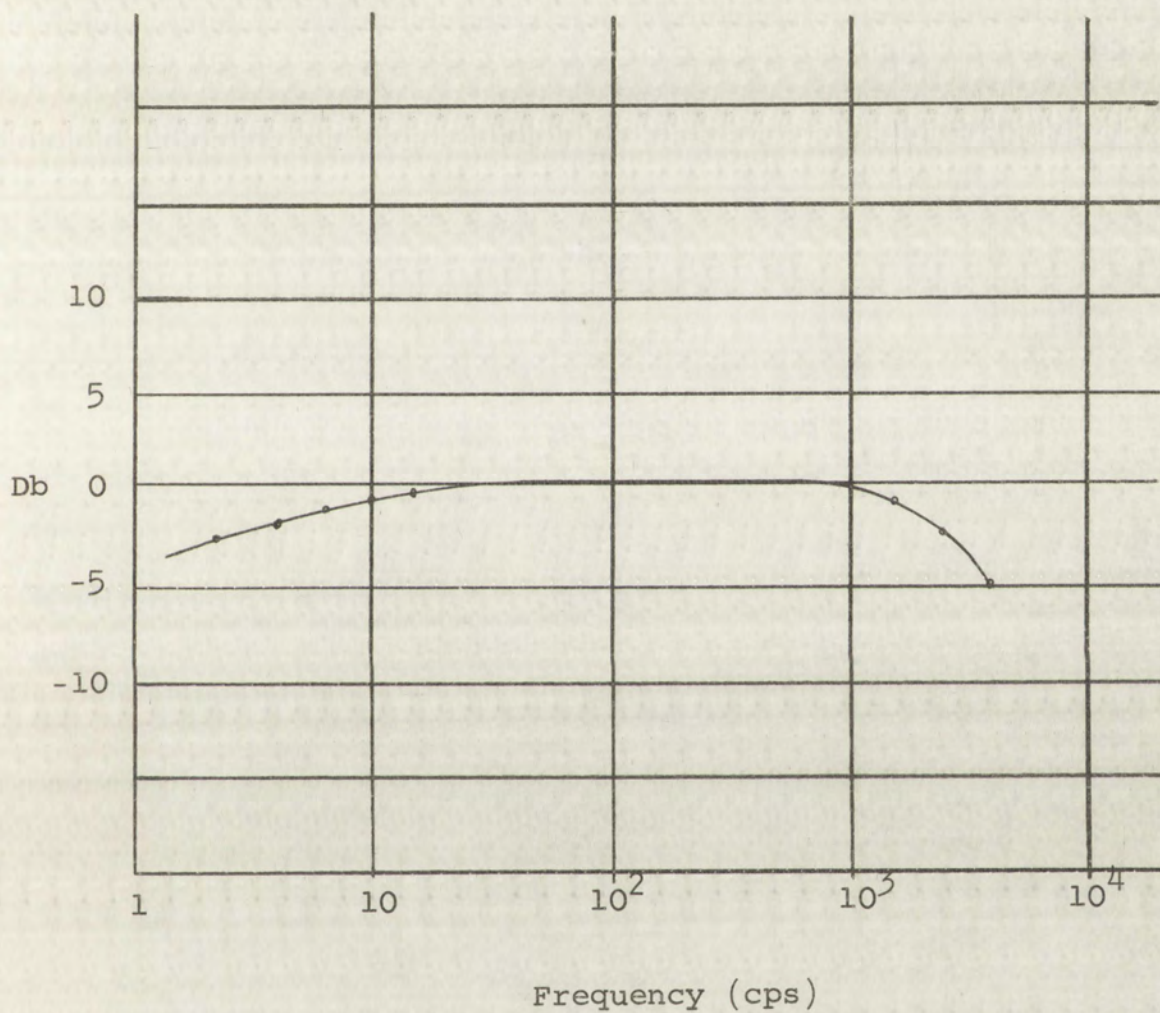


Figure 4.6 Frequency response of receiver

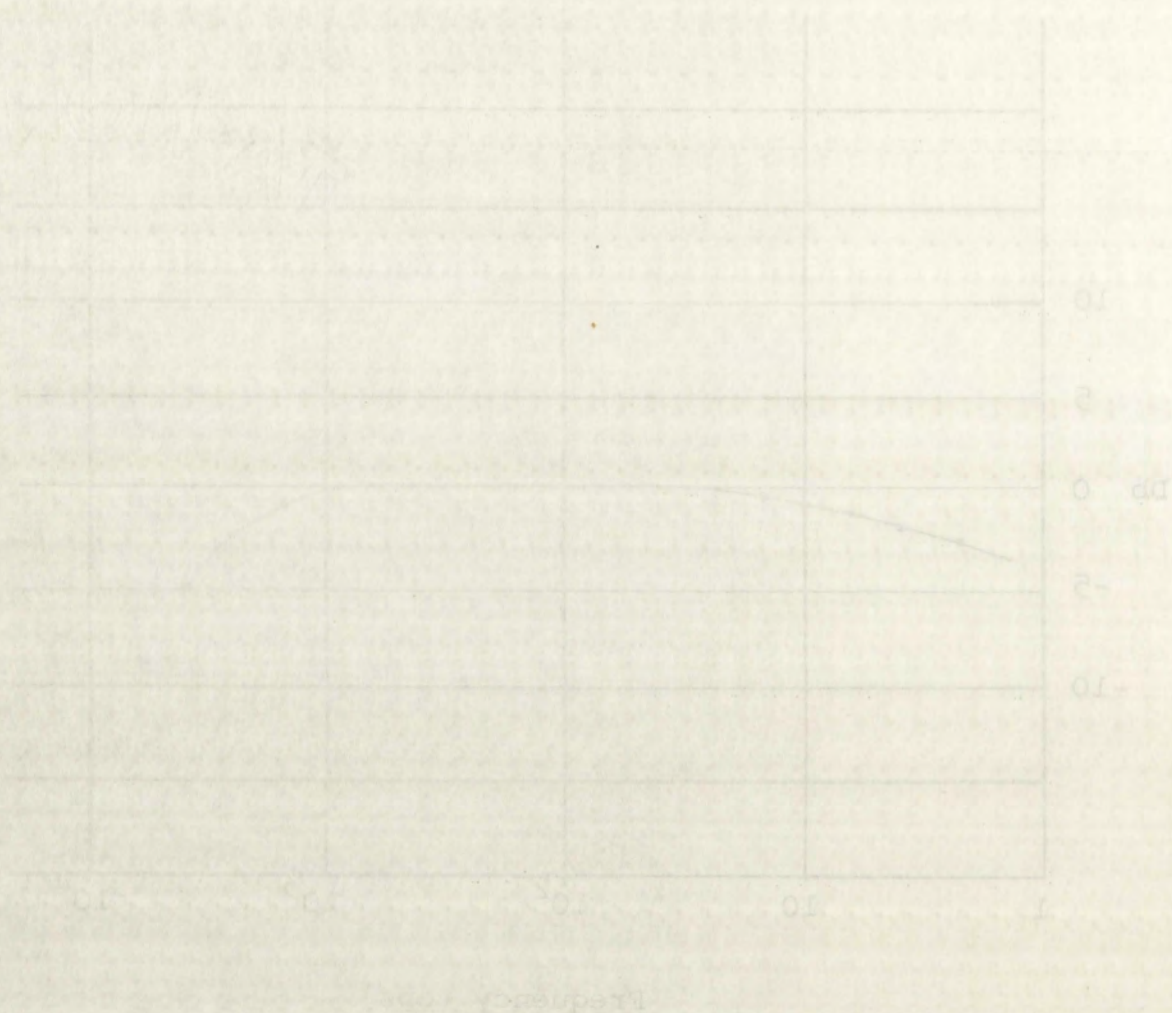


Figure 4.6 Frequency response of receiver

C. Design Considerations

The system for collecting data actually evolved from a series of engineering considerations. The objective to secure electromagnetic noise-data in the 0 to 50 cps region suggested remote sites free from man-made interference. This, in turn, required that the equipment be portable. The speed and response characteristics of the portable tape recorder motivated the synchronizing and switching technique.

The test circuit which finally evolved was based on a compromise method of calibration. Recording a calibration signal simultaneously with the data, or prior to the data, would require another oscillator in the 0 to 50 cps range or frequency division from the 1000 cps oscillator. However, either method was not compatible with compactness and portability. The solution was to reduce the magnitude of the 1000 cps oscillator output and apply it to the data-taking system through a dummy antenna. By adhering to certain gain limitations, the response to this test signal can be correlated with the response to signals in the 0 to 50 cps region.

Other considerations included the gain switch, the low pass filter, and the tape recorder. The 9-position gain switch evolved from a series of field test on the levels of the data-signals. The low pass filter provides a "roll-off" of the response at 2000 cps. This ensures against the possibility of strong high-frequency signals overloading the receiver. The extensive modifications necessary to adapt the tape recorder to the system have been previously discussed.

5. Data-Collecting Site

The selection of the data-collecting site was based upon several requirements. The most important requirement was freedom from man-made interference. While this, to a certain extent, implies a remote location, distance and traveling time were to be minimized. Finally the site must be accessible by at least a jeep-type vehicle.

An initial survey of available maps indicated that the distance factor was favored by the mesa area between the Rio Grande and the Manzano Mountains southeast of Albuquerque. The approach to this area is via Highway 47 which runs along the valley on the eastside of the river. Since the east mesa rises 300-500 feet from the valley rather abruptly, access routes were limited and in some case quite primitive.

The latest available maps of this area were based on 1952-54 information. As a result, the initial survey trip disclosed that there was no assurance that various landmarks and primitive roads existed as shown. This was not particularly unusual in itself, but it did indicate that a careful investigation of all landmarks must be made before the site was finally selected. As a result of this policy, a water well, driven by a gasoline engine, was discovered. This disclosure had a direct bearing on site finally selected.

Several approaches to the mesa were made from various points along Highway 47. These were too far and involved too much travel time. The only two approaches which seemed to be suitable were on the Isleta Indian Reservation. Permission to

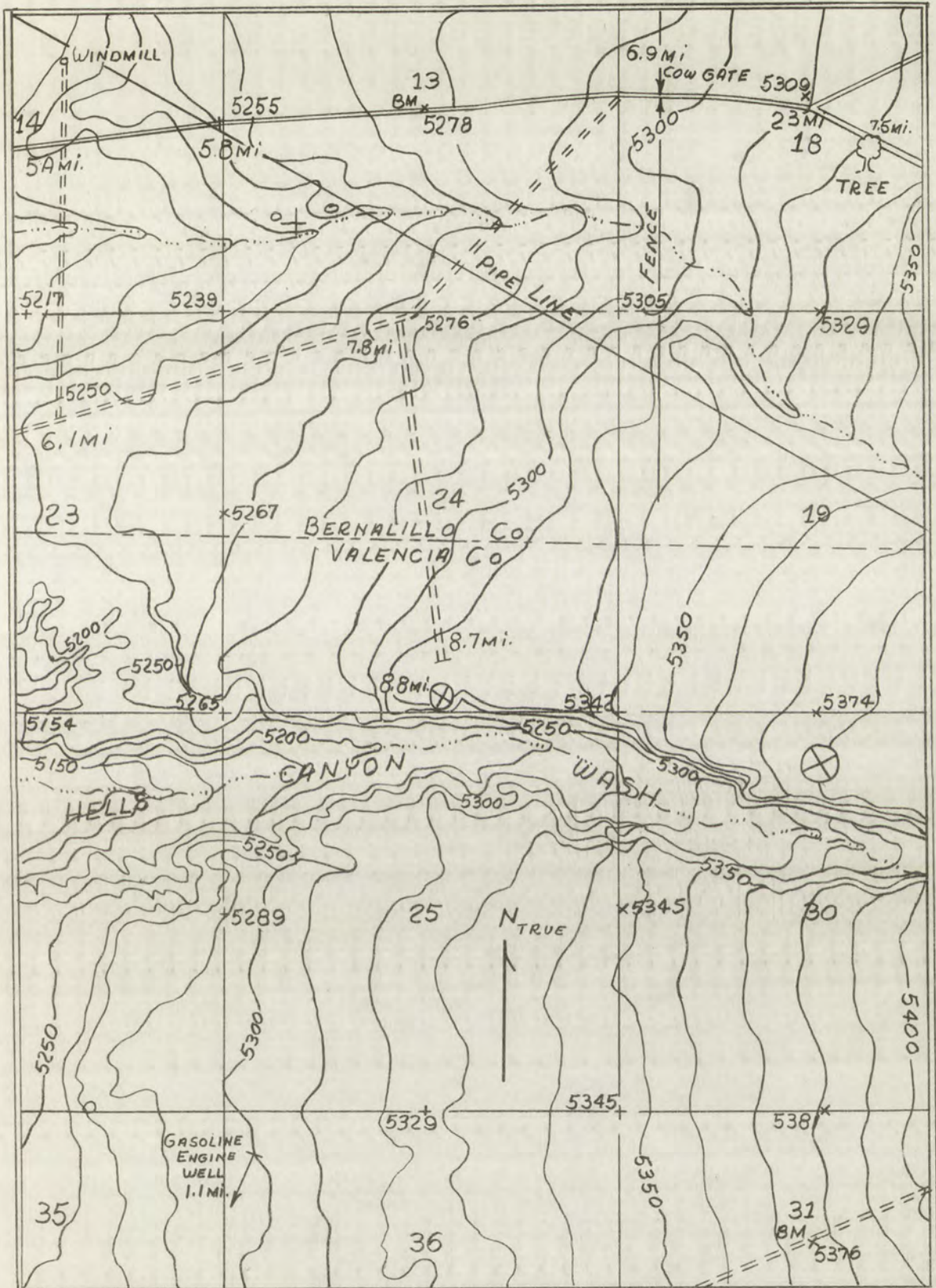
explore this section of the mesa and to use a site, later found there, was obtained from Governor Esquipula Jojola, Governor of Isleta Pueblo.

The area shown in Figure 5.1 is within the Isleta Reservation. The north and south boundaries of the reservation are 4 and 6 miles, respectively, from the site. There is a gradually rising elevation to the foot of the Manzano Mountains 13 miles to the east of Highway 47. This area is devoid of trees except where labelled on the map. A scrub tree (height less than 3 feet) area begins approximately 2 miles west of the mountains. A power line runs roughly north and south along Highway 47 and the west side of the mesa. The dominant feature of this area is Hells Canyon which extends from the Manzano Mountains to the Rio Grande River. The character of the terrain varies quite markedly on either side of this canyon.

The area south of the canyon was immediately rejected as a site location. Here the terrain is very sandy and traveling is difficult. In addition, the distance is excessive whether entrance to the area is made from Isleta or from Chical Indian School. Nevertheless this area was investigated in order to verify landmarks on the maps. The gasoline engine driven well was discovered on this trip.

On the north side of the canyon the terrain is, of course, sandy but is much firmer. The area east of Hubbell Springs was unsuitable because of the proximity to the mountains and possible mining activity. The site finally selected was on the north rim of Hells Canyon. Here the terrain is slightly elevated, free from scrub trees, and quite firm. It is about

explore this section of the map and see what was there. There was observed from the top of the mesa a view of the area of interest. The area shown in Figure 2 is within the same area. The north and south boundaries of the area are 1.5 and 6 miles respectively. The area is situated at an elevation of 10,000 feet above the sea level. The area is bounded by the east of Highway 27. The area is bounded by the west of the mesa. A power line runs roughly north and south along Highway 27 and the west side of the mesa. The boundary between the area and the mesa is the Santa Fe River. The character of the terrain within the area is markedly on either side of the river. The area south of the canyon was immediately adjacent to a site located. Here the terrain is very sandy and very dry. In addition, the distance is excessive. The entrance to the area is made from the east or from the south. Nevertheless this area was investigated in order to verify landmarks on the map. The geological and mineralogical was discovered on this trip. On the north side of the canyon the terrain is of course sandy but is much firmer. The area east of the canyon was unsuitable because of the proximity to the mesa. The possible mining activity. The site finally selected was on the north rim of Santa Fe Canyon. Here the terrain is slightly elevated, free from steep crests, and quite firm. It is about



SCALE: 1 GRID DIVISION = 1 MILE

Figure 5.1 Data-collecting site, $34^{\circ} 54' N$, $106^{\circ} 34' 30'' W$ (True)

8.8 miles from the Isleta turn-off and 20.8 miles from the city of Albuquerque. It is shown in Figure 5.2 that the distance to the nearest power line is 4 miles and to the gasoline-engine well is 2.35 miles.

The rough condition of the road from Isleta turn-off to the site necessitated packaging the equipment in wooden boxes padded with 3 inches of packing material to protect the equipment from shock. A total of 2,000 miles was travelled on surveying and data-collecting trips.

The arrangement of the equipment at the recording site is shown in Figure 5.3. The small tarpaulin was required to keep the direct rays of the sun off the equipment. The temperature under this tarpaulin, which was monitored continuously, varied from 72° to 99°F.

8.8 miles from the latest turn-off and 20.5 miles from the shore of Albuquerque. It is shown in Figure 5.2 that the distance to the nearest power line is 5 miles and to the nearest engine well is 2.35 miles.

The rough condition of the road from the turn-off to the site necessitated packaging the equipment in wooden boxes padded with 3 inches of packing material to protect the equipment from shock. A total of 2,000 miles was travelled on highways and data-collecting trips. The arrangement of the equipment at the recording site is shown in Figure 5.3. The small tarpaulin was required to keep the direct rays of the sun off the equipment. The tarpaulin under this tarpaulin, which was mounded considerably, varied from 72° to 99°.

NOV-74
BOMB

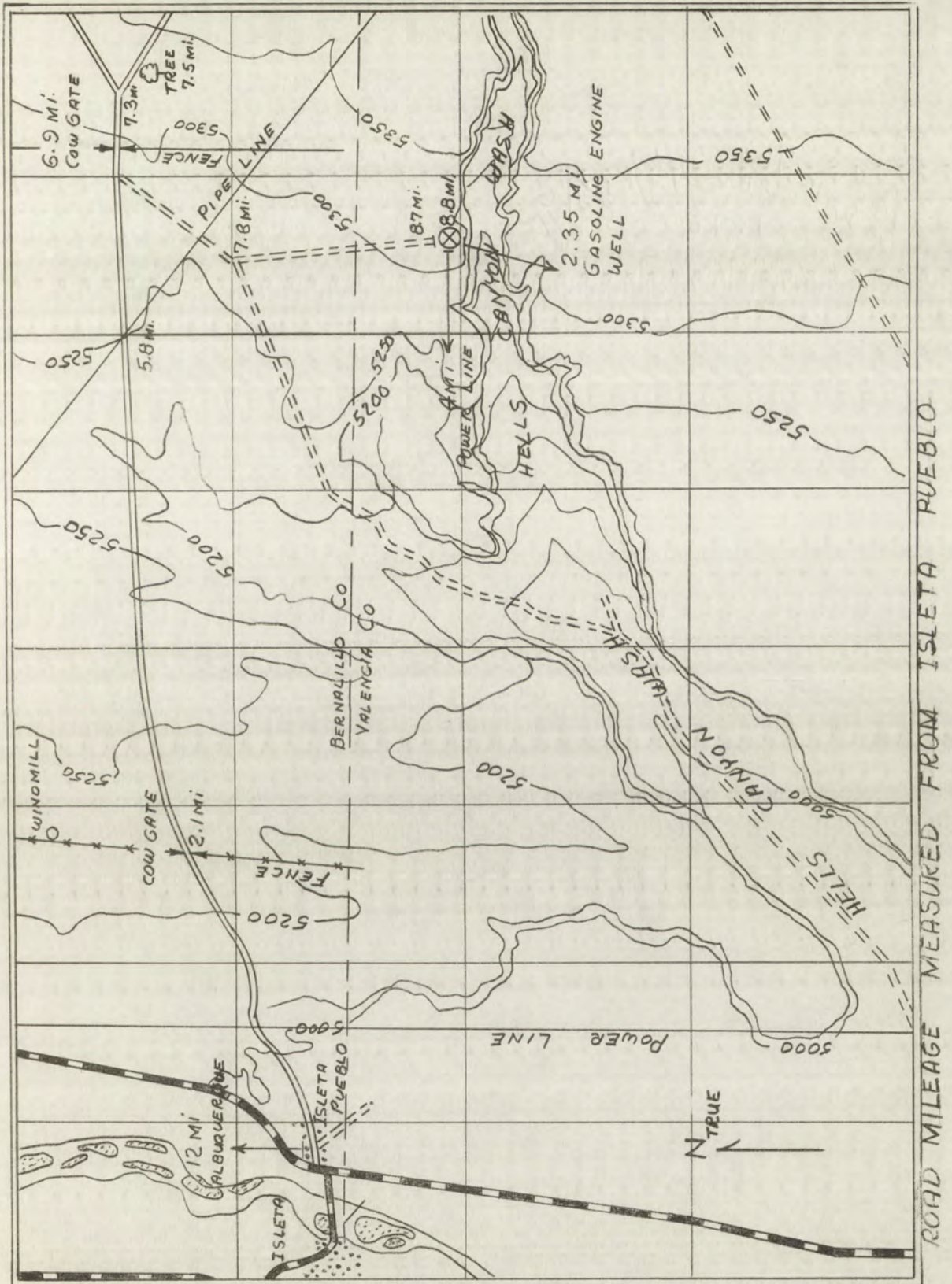


Figure 5.2 Site location relative to Isleta Pueblo and Albuquerque, New Mexico

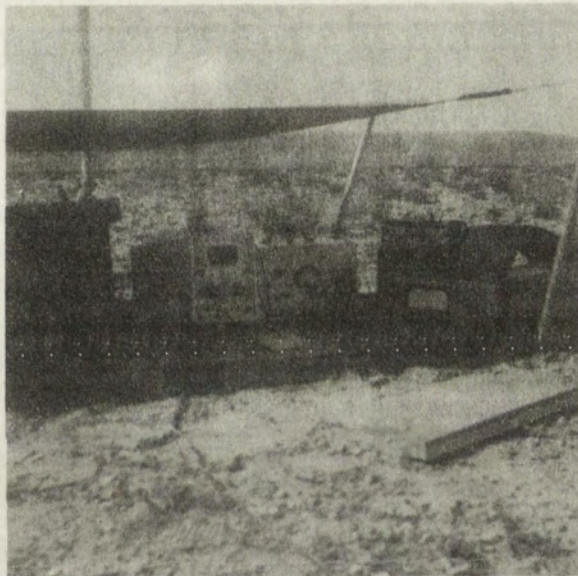


Figure 5.3 Data-collecting equipment at the site.



Figure 5.3 Data collected equipment at the site.

6. Data Samples

The data was recorded during daylight hours from August 1 to September 8, 1961, and during evening hours from September 11 to September 15, 1961. During this period, 240 rolls of magnetic tape were recorded. Since the time involved precludes any observable seasonal effect, the primary interest is in the diurnal variations of the mean values of field strength.

As can be seen in Figure 2.2, the data-processing system is essentially a filtering system. A particular frequency is selected by the selective amplifier, rectified, and integrated. Five similar circuits are connected to the output of the low-pass filter. This arrangement permits processing five different frequencies simultaneously. The output voltage of the integrator is expressed as a mean value over the integration period. Since the gain of the recording and processing systems are known, the mean value is restated as the mean peak value of the field strength in millivolts per meter (mv/m).

The duration of each magnetic tape is 32 minutes. The mean peak value of field strength for each frequency is considered as representative of the noise activity at that frequency during the hourly period in which the roll of tape was taken. Thus the basic unit for plotting purposes is the mean peak value of field strength per frequency per hour.

No attempt is made here to discuss the data samples shown in Figure 6.1 to 6.3. These samples are simply presented to show the manner in which the data will be plotted when completely processed.

6. Data Samples

The data was recorded during daylight hours from August 1 to September 8, 1961; and during evening hours from September 11 to September 15, 1961. During this period, 240 rolls of magnetic tape were recorded. Since the time involved precludes any observable seasonal effect, the primary interest is in the diurnal variations of the mean values of field strength. As can be seen in Figure 5.2, the data-processing system is essentially a filtering system. A particular frequency is selected by the selective amplifier, rectified, and integrated. Five similar circuits are connected to the output of the low pass filter. This arrangement permits processing five different frequencies simultaneously. The output voltage of the integrator is expressed as a mean value over the integration period. Since the gain of the recording and processing systems are known, the mean value is repeated as the mean peak value of the field strength in millivolts per meter (mV/m).

The duration of each magnetic tape is 35 minutes. The mean peak value of field strength for each frequency is considered as representative of the noise activity at that frequency during the hourly period in which the roll of tape was taken. Thus the basic unit for plotting purposes is the mean peak value of field strength per frequency per hour.

No attempt is made here to discuss the data samples shown in Figure 6.1 to 6.5. These samples are simply presented to show the manner in which the data will be plotted when completely processed.

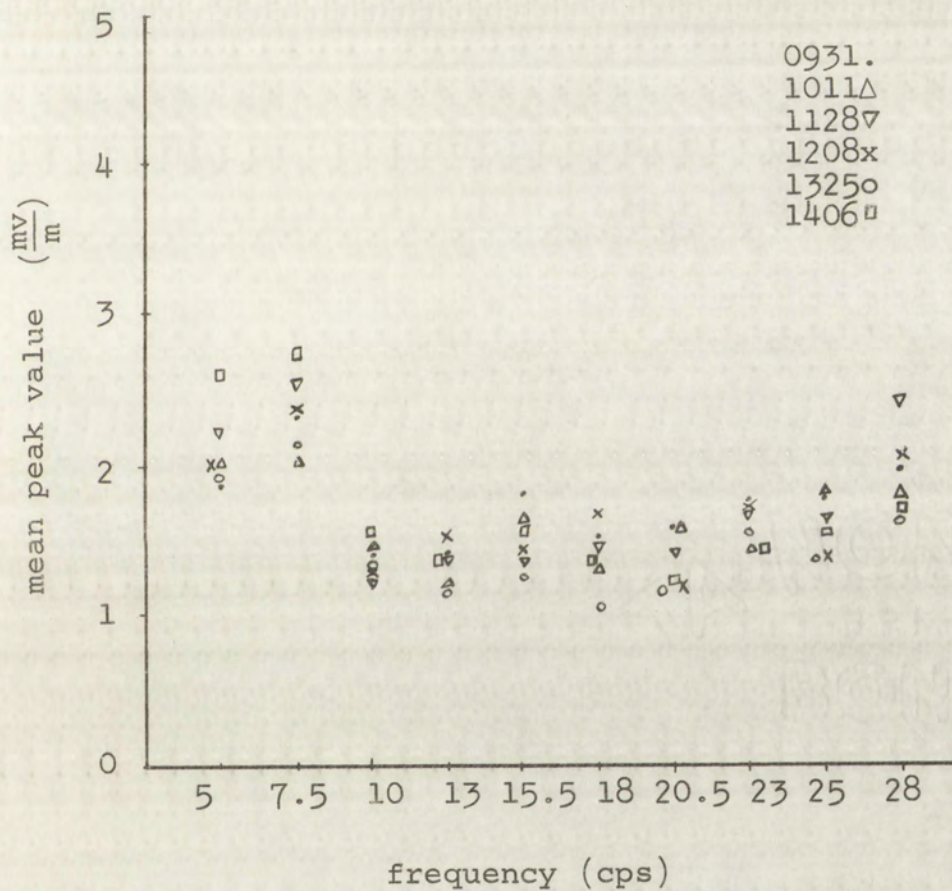


Figure 6.1 Hourly recordings of atmospheric noise field strength versus frequency from 0900 to 1500 (MST) on August 21, 1961

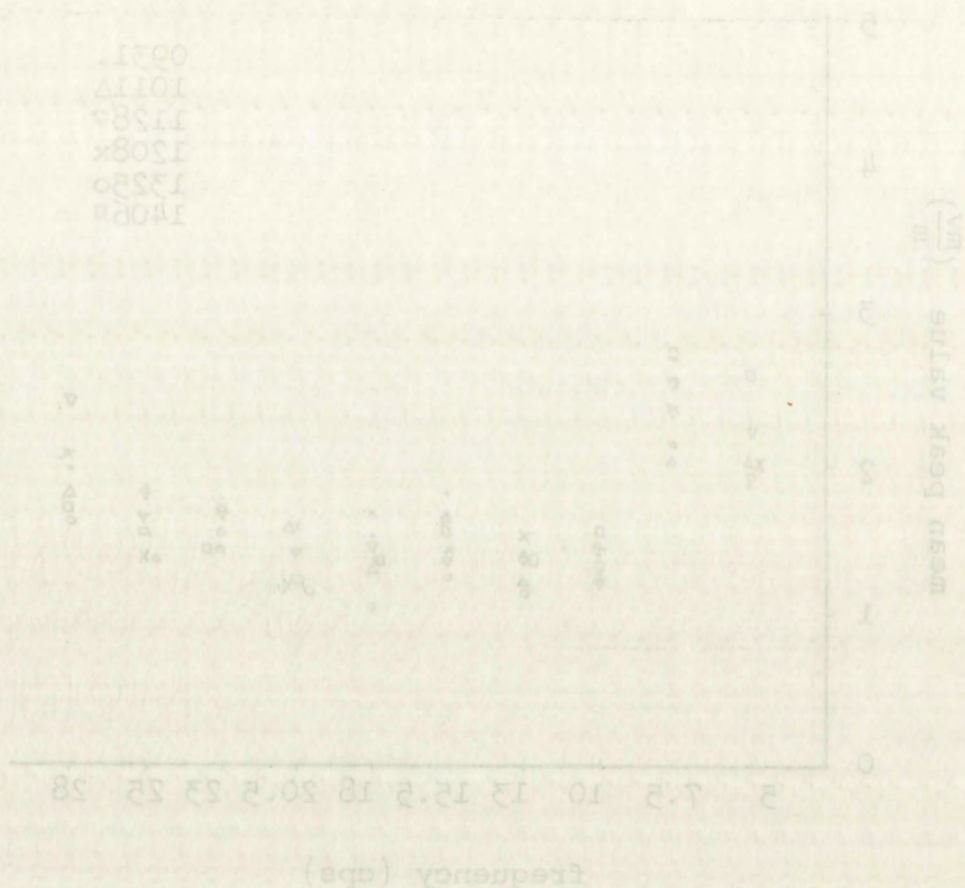


Figure 6.1 Hourly recordings of atmospheric noise field strength versus frequency from 0900 to 1500 (MST) on August 21, 1961

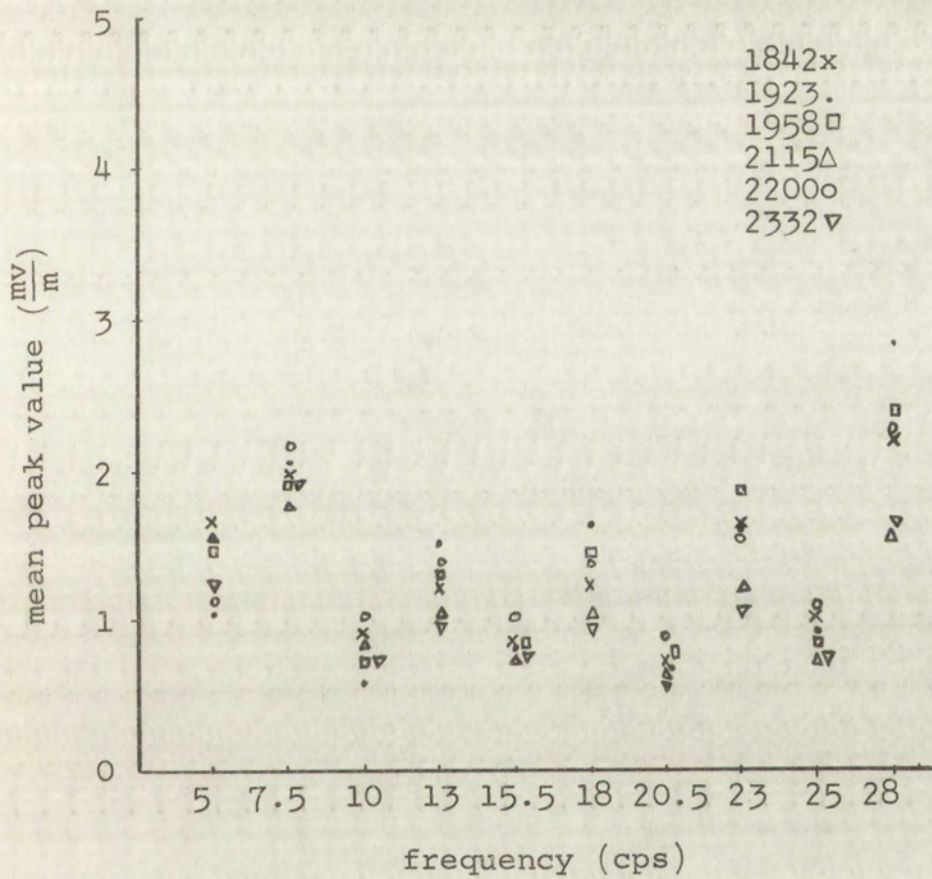


Figure 6.2 Hourly recordings of atmospheric noise field strength versus frequency from 1800 to 2400 (MST) on September 15, 1961

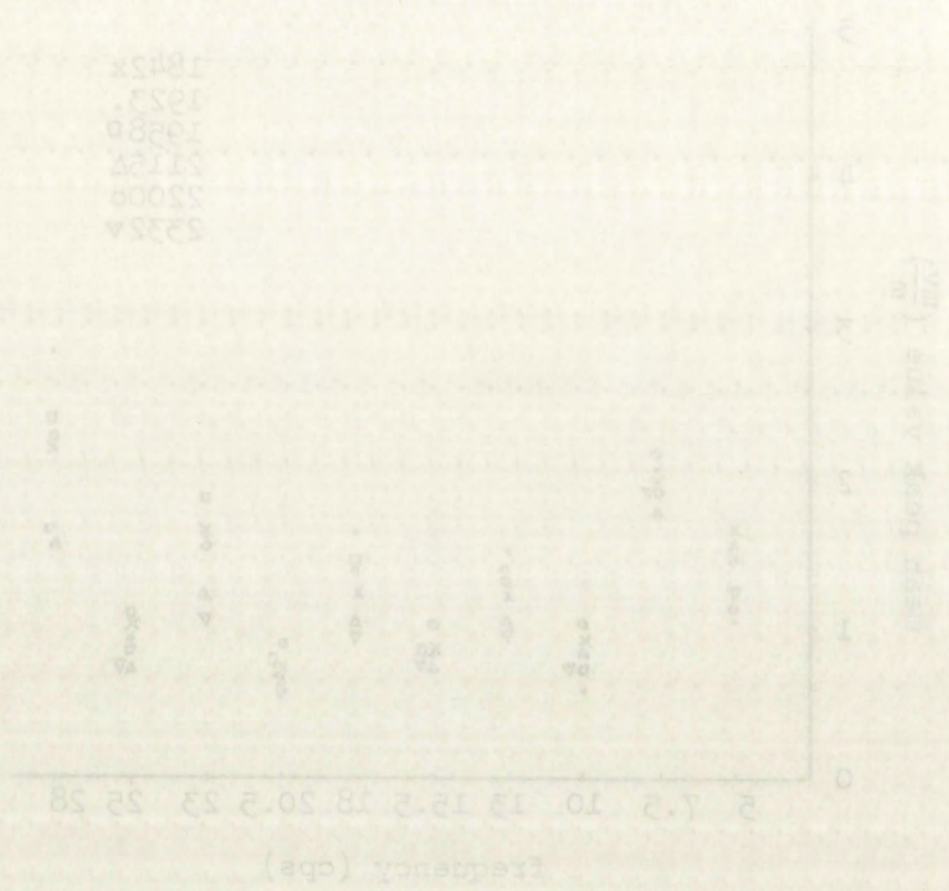


Figure 6.2. Hourly recording of atmospheric noise field strength versus frequency from 1800 to 2400 (MST) on September 15, 1961.

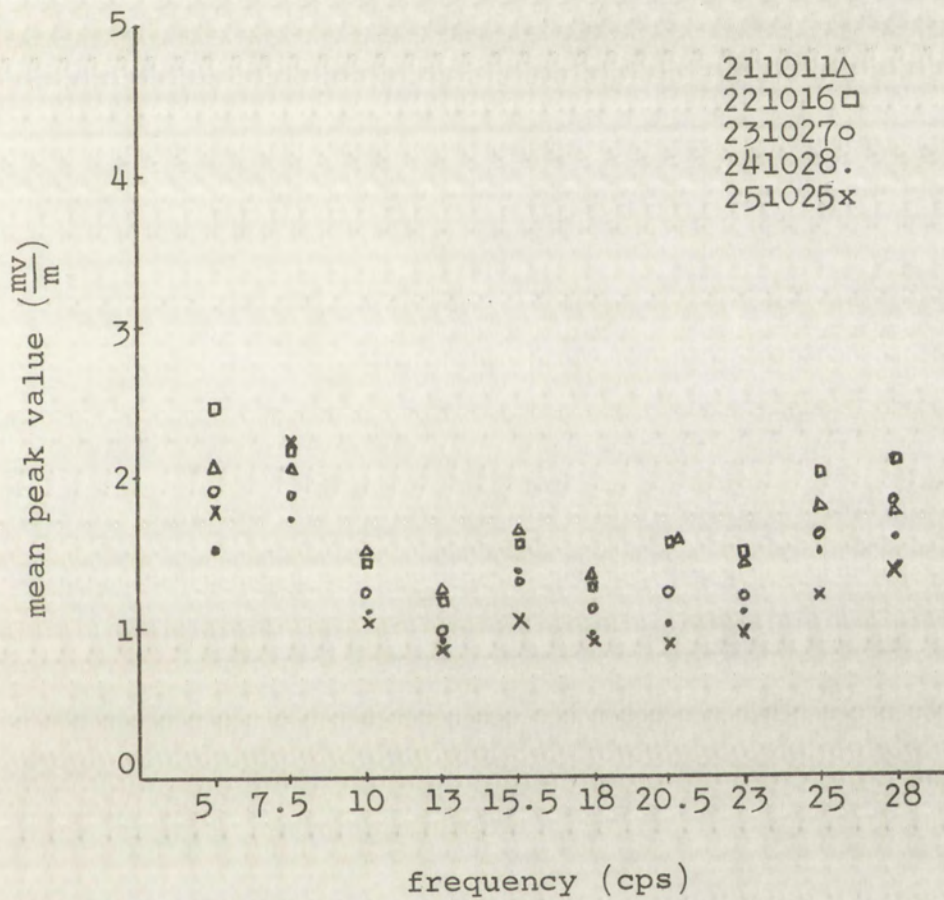
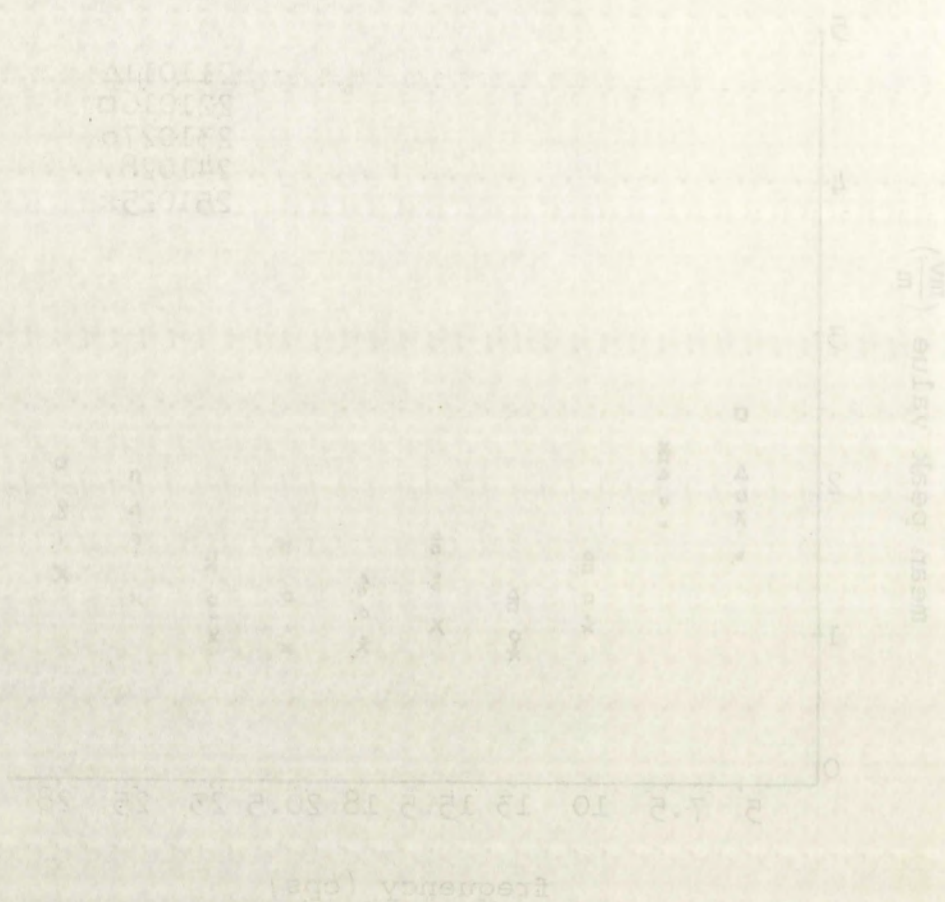


Figure 6.3 Atmospheric noise field strength versus frequency during the hour 1000 to 1100 (MST) for the week August 21-25, 1961

Figure 6.5 Atmospheric noise field strength versus frequency during the hour 1000 to 1100 (GMT) for the week August 21-25, 1981



7. Conclusions

The purpose of this investigation is to develop instrumentation to secure noise data in the 3 to 50 cps portion of the spectrum and, at the same time, to seek evidence of the Schumann frequencies in this region. The instrumentation used in this investigation is discussed fully in Chapter 4. Briefly, a frequency translation technique is employed during recording. During playback the data is again translated and restored to its normal position in the spectrum. A test signal is used to ensure that in the record mode the gain is maintained within 1.2 db. Under this restriction, test tapes recorded at frequencies in the 3 to 50 cps range indicate the gain from the antenna input during record to the receiver output during playback. The overall response in this frequency range is the response of the receiver, i.e., within 3 db.

During data processing, the inputs of 10 filters are connected to the receiver. The output of each of these 10 filters is amplified, rectified, and integrated. The gain of each filter channel is carefully determined so that the output of each integrator can be put in terms of the input to the filter channel. Since the filter input is the receiver output and the gain from the antenna to the receiver output is known, the integrator output can be expressed in terms of the antenna input. Considering the effective height of the antenna, this antenna input can be denoted in field strength units.

In the complete recording and recovery process, the noise data is subjected to two variations with known limits. These

variations are due to the frequency response of the receiver and changes in the receiver gain. Thus the data from a particular tape will vary as the response in Figure 4.6, while the data from different tapes will be within 1.2 db at the most. Samples of the noise data are presented in Chapter 6.

The system for data-collecting described in this paper was utilized during the daylight hours from August 1 to September 8, 1961 and during the evening hours from September 11 to September 15, 1961. In addition to these operational periods, that portion of the system involved in data-processing has been in daily (8 to 11 hours) continuous operation since November 25, 1961.

The data-samples are shown in Chapter 6 to demonstrate the manner in which the data will be plotted in a subsequent report. This report will be issued when the data have been completely processed. While nothing conclusive can be drawn from these samples, it is interesting to note that the greater activity in the 5 to 10 cps region agrees with the findings of Fitchen, et al. [1961], Balser and Wagner as reported by Raemer [1961], and Maple [1961].

variations are due to the following reasons: (1) the

and changes to the system are as follows: (1) the

data will vary in the response to the system. (2) the

data from different tapes will be within 1.5 dB of the mean.

Sample of the noise data is given in Figure 1.

The system for data collection and processing is as follows:

was utilized during the daylight hours from August 1 to

September 8, 1961 and during the evening hours from September 11

to September 15, 1961. In addition to these operations,

periods, that portion of the system involved in data processing

has been in daily (8 to 11 hours) continuous operation since

November 25, 1961.

The data samples are given in Chapter 5 of this report.

The manner in which the data will be used in a subsequent

report. This report will be based upon the data from the

completely processed. While the conclusions can be drawn

from these samples, it is interesting to note that the

activity in the 2 to 10 cps region agrees with the findings of

Fitcher et al. (1961). Baker and Baker as reported by Kerner

(1961) and Miller (1961).

Appendix A

Twin-T Filters

General Network Analysis

We shall discuss here the general approach of network analysis in considering the twin-T filter.

The single "T" network shown in Figure A1

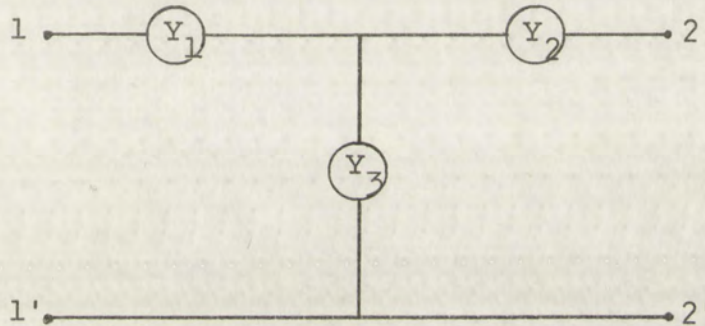


Figure A1 A "T" network

may be considered using the "y" or "short-circuit" parameters. The equations for this network take the form

$$\begin{aligned} y_{11}V_1 + y_{12}V_2 &= I_1 \\ y_{21}V_1 + y_{22}V_2 &= I_2 \end{aligned} \tag{A-1}$$

where

$$\begin{aligned} y_{11} &= \left. \frac{I_1}{V_1} \right|_{V_2 = 0}; & y_{12} &= \left. \frac{I_1}{V_2} \right|_{V_1 = 0} \\ y_{21} &= \left. \frac{I_2}{V_1} \right|_{V_2 = 0}; & y_{22} &= \left. \frac{I_2}{V_2} \right|_{V_1 = 0} \end{aligned} \tag{A-1a}$$

General Network Analysis

We shall discuss next the general approach of network

analysis in considering the "T" circuit.
The single "T" network shown in Figure A-1



Figure A-1. A "T" network.

may be considered using the "Y" or "short-circuit" parameters. The equations for these parameters are the following:

$$\begin{aligned} Y_{11}V_1 + Y_{12}V_2 &= I_1 \\ Y_{21}V_1 + Y_{22}V_2 &= I_2 \end{aligned} \quad (A-1)$$

where

$$\begin{aligned} Y_{11} &= \left. \frac{I_1}{V_1} \right|_{V_2=0} \\ Y_{12} &= \left. \frac{I_1}{V_2} \right|_{V_1=0} \\ Y_{21} &= \left. \frac{I_2}{V_1} \right|_{V_2=0} \\ Y_{22} &= \left. \frac{I_2}{V_2} \right|_{V_1=0} \end{aligned} \quad (A-2)$$

Equations (A-1) may be written in Matrix form

$$\begin{vmatrix} y_{11} & y_{12} \\ y_{21} & y_{22} \end{vmatrix} \begin{vmatrix} V_1 \\ V_2 \end{vmatrix} = \begin{vmatrix} I_1 \\ I_2 \end{vmatrix}, \quad (\text{A-2})$$

which is easier to manipulate to obtain other circuit parameters such as "z."

If the circuit elements are combined in impedance form the circuit equations take the form

$$z_{11}I_1 + z_{12}I_2 = V_1 \quad (\text{A-3})$$

$$z_{21}I_1 + z_{22}I_2 = V_2$$

where

$$z_{11} = \left. \frac{V_1}{I_1} \right|_{I_2 = 0}; \quad z_{12} = \left. \frac{V_1}{I_2} \right|_{I_1 = 0} \quad (\text{A-3a})$$

$$z_{21} = \left. \frac{V_2}{I_1} \right|_{I_2 = 0}; \quad z_{22} = \left. \frac{V_2}{I_2} \right|_{I_1 = 0}$$

Equations (A-3a) define the "z" parameters on the "open circuit" basis. Equation (A-3) can be put in matrix form

$$\begin{vmatrix} z_{11} & z_{12} \\ z_{21} & z_{22} \end{vmatrix} \begin{vmatrix} I_1 \\ I_2 \end{vmatrix} = \begin{vmatrix} V_1 \\ V_2 \end{vmatrix}. \quad (\text{A-4})$$

Equations (A-1) may be written in Matrix form

$$(A-2) \quad \begin{bmatrix} V_1 \\ V_2 \end{bmatrix} = \begin{bmatrix} z_{11} & z_{12} \\ z_{21} & z_{22} \end{bmatrix} \begin{bmatrix} I_1 \\ I_2 \end{bmatrix}$$

which is easier to manipulate to obtain other circuit parameters such as "z".

If the circuit elements are combined in impedance

form the circuit equations take the form

$$(A-3) \quad \begin{aligned} z_{11}I_1 + z_{12}I_2 &= V_1 \\ z_{21}I_1 + z_{22}I_2 &= V_2 \end{aligned}$$

where

$$(A-3a) \quad \begin{aligned} z_{11} &= \frac{V_1}{I_1} \Big|_{I_2=0} = \frac{V_1}{I_1} \Big|_{I_2=0} \\ z_{12} &= \frac{V_1}{I_2} \Big|_{I_1=0} = \frac{V_1}{I_2} \Big|_{I_1=0} \\ z_{21} &= \frac{V_2}{I_1} \Big|_{I_2=0} = \frac{V_2}{I_1} \Big|_{I_2=0} \\ z_{22} &= \frac{V_2}{I_2} \Big|_{I_1=0} = \frac{V_2}{I_2} \Big|_{I_1=0} \end{aligned}$$

Equations (A-3a) define the "z" parameters on the

"open circuit" basis. Equation (A-3) can be put in matrix

form

$$(A-4) \quad \begin{bmatrix} V_1 \\ V_2 \end{bmatrix} = \begin{bmatrix} z_{11} & z_{12} \\ z_{21} & z_{22} \end{bmatrix} \begin{bmatrix} I_1 \\ I_2 \end{bmatrix}$$

Although equation (A-2) is more convenient in combining two circuits in parallel since admittances are additive, it is desirable to use equations (A-4) for series connections. The "z" parameters may be found directly from the "y" parameters--matrix (A-4) can be obtained from matrix (A-2), and vice versa.

Given the y-matrix, the determinant is

$$\Delta y = y_{11}y_{22} - y_{12}y_{21} \quad (\text{A-5})$$

Defining Δ_{ij} as the cofactor of element α_{ij} , we have

$$\Delta_{ij} = (-1)^{i+j} M_{ij} \quad (\text{A-6})$$

where M_{ij} is the minor of element α_{ij} ¹ and

$$\begin{vmatrix} \Delta_{11} & \Delta_{12} \\ \Delta_{21} & \Delta_{22} \end{vmatrix} \quad (\text{A-7})$$

where

$$\Delta_{11} = y_{22} \quad \Delta_{21} = -y_{21}$$

$$\Delta_{12} = -y_{12} \quad \Delta_{22} = y_{11} \quad .$$

Dividing each element of (A-7) by Δy and transposing, (A-2) becomes

¹Seshu S. and N. Balabanian, Linear Network Analysis, John Wiley and Sons, Inc., 1959.

Although equation (A-2) is more convenient in combining two circuits in parallel, it is desirable to use equation (A-3) for additive series connections. The "x" parameters may be found directly from the "y" parameter matrix (A-4) and vice versa. The "x" parameters may be found directly from matrix (A-2), and vice versa. Given the y-matrix, the determinant

$$\Delta y = y_{11}y_{22} - y_{12}y_{21}$$

Defining Δ_{ij} as the cofactor of element y_{ij} , we have

$$\Delta_{ij} = (-1)^{i+j} M_{ji}$$

where M_{ji} is the minor of element y_{ji} .

$$\begin{vmatrix} \Delta_{11} & \Delta_{12} \\ \Delta_{21} & \Delta_{22} \end{vmatrix}$$

where

$$\Delta_{11} = y_{22} \quad \Delta_{21} = -y_{12}$$

$$\Delta_{12} = -y_{11} \quad \Delta_{22} = y_{11}$$

Dividing each element of (A-7) by Δy and transposing, (A-2) becomes

$$\begin{vmatrix} V_1 \\ V_2 \end{vmatrix} = \frac{1}{\Delta y} \begin{vmatrix} \Delta_{11} & \Delta_{21} \\ \Delta_{12} & \Delta_{22} \end{vmatrix} \begin{vmatrix} I_1 \\ I_2 \end{vmatrix} \quad (\text{A-8})$$

where $z_{11} = \frac{\Delta_{11}}{\Delta y}$, $z_{21} = \frac{\Delta_{12}}{\Delta y}$, etc.

Matrix (A-3) can then be written

$$\begin{vmatrix} V_1 \\ V_2 \end{vmatrix} = \begin{vmatrix} z_{11} & z_{12} \\ z_{21} & z_{22} \end{vmatrix} \begin{vmatrix} I_1 \\ I_2 \end{vmatrix} \quad (\text{A-9})$$

where $z_{11} = \frac{V_1}{I_1} \Big|_{I_2=0}$; $z_{21} = \frac{V_2}{I_1} \Big|_{I_2=0}$, and so on.

Defining the voltage transfer function (g_{21}) to be

$$g_{21} = \frac{V_2}{V_1} \Big|_{I_2=0},$$

we see that

$$g_{21} = \frac{V_2}{V_1} \Big|_{I_2=0} = \frac{z_{21}}{z_{11}} = \frac{\frac{-y_{21}}{\Delta y}}{\frac{y_{22}}{\Delta y}} = \frac{-y_{21}}{y_{22}}. \quad (\text{A-10})$$

Circuits in Parallel

The admittances for circuit shown in Figure A1 are defined in equations (A-1a). Putting these admittances in terms of the admittance of the circuit elements we have

$$\begin{bmatrix} V_1 \\ V_2 \end{bmatrix} = \begin{bmatrix} Z_{11} & Z_{12} \\ Z_{21} & Z_{22} \end{bmatrix} \begin{bmatrix} I_1 \\ I_2 \end{bmatrix} \quad (2-9)$$

$$\text{where } Z_{ij} = \frac{V_i}{I_j}$$

Matrix (Z_{ij}) can then be written

$$\begin{bmatrix} V_1 \\ V_2 \end{bmatrix} = \begin{bmatrix} Z_{11} & Z_{12} \\ Z_{21} & Z_{22} \end{bmatrix} \begin{bmatrix} I_1 \\ I_2 \end{bmatrix} \quad (2-10)$$

$$\text{where } Z_{ij} = \frac{V_i}{I_j}$$

Defining the voltage

$$V_{21} = \frac{V_2}{I_1} \quad I_2 = 0$$

we see that

$$V_{21} = \frac{V_2}{I_1} \quad I_2 = 0 \quad (2-11)$$

Circuits in Parallel

The admittance Y_{21} is defined in equations (2-11) in terms of the admittance of the circuit. We have

$$y_{11} = \frac{Y_1(Y_2 + Y_3)}{Y_1 + Y_2 + Y_3}, \quad (\text{A-11a})$$

$$y_{22} = \frac{Y_2(Y_1 + Y_3)}{Y_1 + Y_2 + Y_3}, \quad (\text{A-11b})$$

$$\text{and } y_{12} = y_{21} = \frac{-Y_1 Y_2}{Y_1 + Y_2 + Y_3} \quad (\text{A-11c})$$

Equation (A-11a) and (A-11b) can be obtained by inspection. The equations (A-11c) are found by solving the loop equations. To obtain the results indicated here, and in subsequent developments, y_{12} and y_{21} , are determined by assuming the loop currents in the same direction in the shunt branch.

Now we consider the total admittances when two circuits are in parallel (Figure A2).

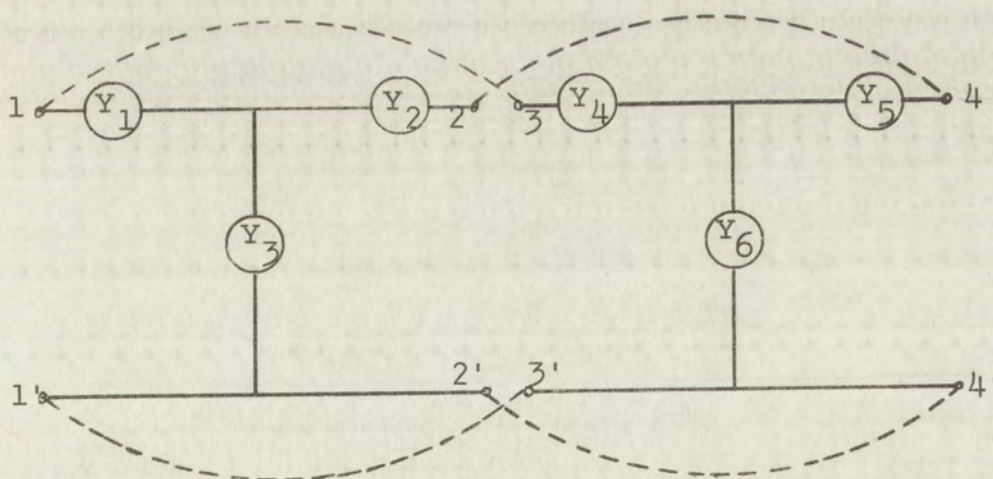


Figure A2 Two "T" networks in parallel

$$y_{12} = \frac{y_{12}}{y_{12}}$$

and $y_{12} = y_{12}$

Equation (A-14) and (A-15) are used in the inspection. The equations (A-14) and (A-15) are used in the inspection.

The loop equations are used to obtain the results. The loop equations are used to obtain the results. The loop equations are used to obtain the results.

Now we consider the loop equations and the results. The loop equations are used to obtain the results. The loop equations are used to obtain the results.

are in parallel (Figure A-1).

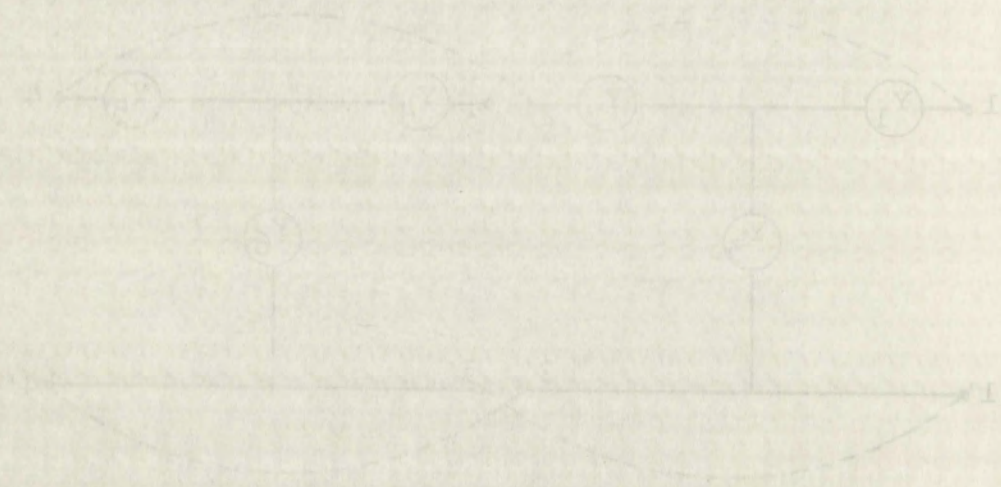


Figure A-1. Two parallel paths.

Since admittance in parallel are additive, the total admittances for the circuit in Figure A2 are

$$y_{11} = \frac{y_1(y_2 + y_3)}{y_1 + y_2 + y_3} + \frac{y_4(y_5 + y_6)}{y_4 + y_5 + y_6}, \quad (\text{A-12a})$$

$$y_{22} = \frac{y_2(y_1 + y_3)}{y_1 + y_2 + y_3} + \frac{y_5(y_4 + y_6)}{y_4 + y_5 + y_6}, \quad (\text{A-12b})$$

$$\text{and } y_{12} = y_{21} = \frac{-y_1 y_2}{y_1 + y_2 + y_3} - \frac{y_4 y_5}{y_4 + y_5 + y_6}. \quad (\text{A-12c})$$

The voltage transfer function (g_{21}) for the two circuits in parallel can be obtained by using equations (A-12b) and (A-12c) in equation (A-10).

Twin-T Network

Consider the two "T" networks shown in Figure A2 and Figure A3. The individual admittances of the

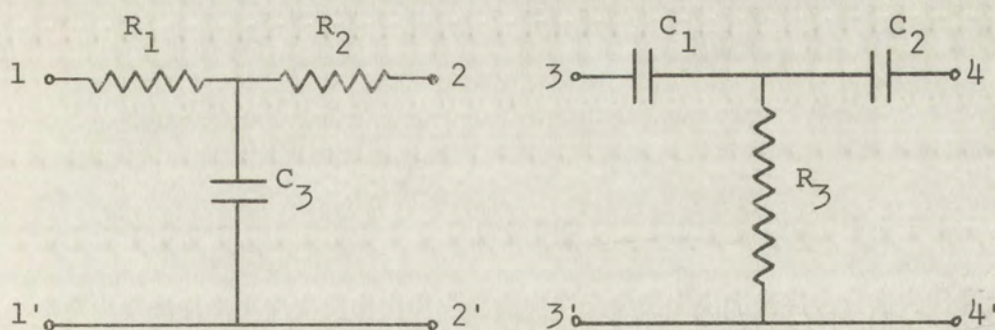


Figure A3 T networks with R and C elements

Since admittance is the reciprocal of impedance the total admittance is the sum of the admittances of the

$$Y_{11} = \frac{Y_1 + Y_2}{1 + Y_1 + Y_2}$$

$$Y_{22} = \frac{Y_1 + Y_2}{1 + Y_1 + Y_2}$$

and $Y_{12} = Y_{21} = \frac{Y_1 Y_2}{1 + Y_1 + Y_2}$

The voltage transfer function V_{21} for the circuit in parallel can be obtained by using equations (A-12b) and (A-13) in equation (A-11)

Twin-T Network

Consider the two T network shown in Figure A5 and Figure A5. The two T networks are identical.

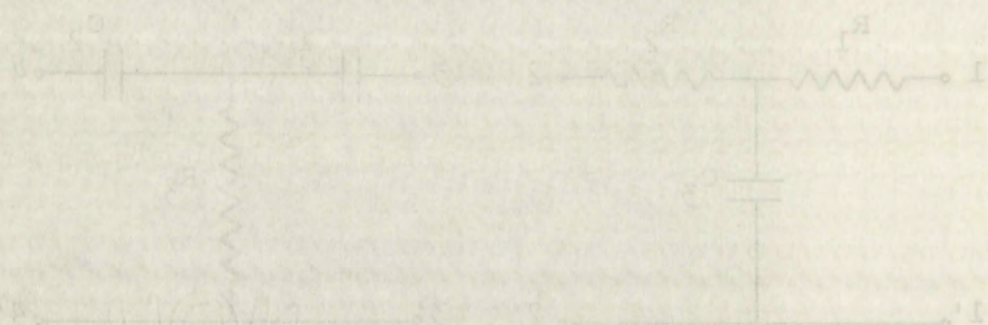


Figure A5. Twin-T network

circuit elements of Figure A3 are seen to be

$$\begin{aligned}
 Y_1 &= \frac{1}{R_1} & Y_4 &= sC_1 \\
 Y_2 &= \frac{1}{R_2} & Y_5 &= sC_2 \\
 Y_3 &= sC_3 & Y_6 &= \frac{1}{R_3}
 \end{aligned} \tag{A-13}$$

in the Laplace transform frequency domain. Putting the circuits in Figure A3 in parallel we have Figure A4.

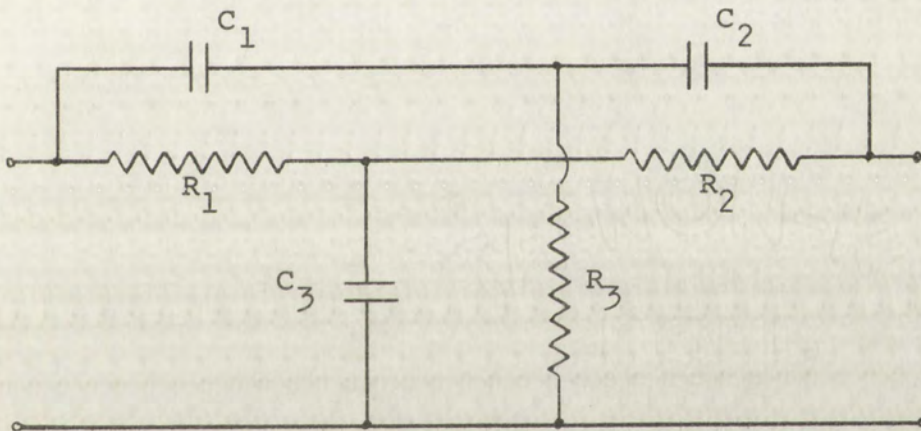


Figure A4 Twin-T network

The voltage transfer function (g_{21}) of Figure A2 is obtained by substituting (A-12b) and (A-12c) into (A-10)

$$g_{21} = \frac{Y_1 Y_2 (Y_4 + Y_5 + Y_6) + Y_4 Y_5 (Y_1 + Y_2 + Y_3)}{Y_2 (Y_1 + Y_3) (Y_4 + Y_5 + Y_6) + Y_5 (Y_4 + Y_6) (Y_1 + Y_2 + Y_3)} \tag{A-14}$$

Substituting (A-13) into (A-14) gives

$$g_{21} = \frac{\frac{1}{R_1} \cdot \frac{1}{R_2} \left[sC_1 + sC_2 + \frac{1}{R_3} \right] + (sC_1)(sC_2) \left[\frac{1}{R_1} + \frac{1}{R_2} + sC_3 \right]}{\frac{1}{R_2} \left(\frac{1}{R_1} + sC_3 \right) \left[sC_1 + sC_2 + \frac{1}{R_3} \right] + sC_2 \left(sC_1 + \frac{1}{R_3} \right) \left[\frac{1}{R_1} + \frac{1}{R_2} + sC_3 \right]} \quad (A-15)$$

Now simplifying (A-15), we have

$$g_{21} = \frac{(sR_3C_1 + sR_3C_2 + 1) + (s^2C_1C_2R_2R_3 + s^2C_1C_2R_1R_3 + s^3C_1C_2C_3R_1R_2R_3)}{(1 + sC_3R_1)(sC_1R_3 + sC_2R_3 + 1) + (s^2C_1C_2R_3 + sC_2)(R_2 + R_1 + sC_3R_1R_2)}$$

and

$$g_{21} = \frac{1 + s^2C_1C_2R_2R_3 + s^2C_1C_2R_1R_3 + sR_3C_1 + sR_3C_2 + s^3C_1C_2C_3R_1R_2R_3}{(1 + sC_3R_1)(1 + sC_1R_3 + sC_2R_3) + (s^2C_1C_2R_3 + sC_2)(R_2 + R_1 + sC_3R_1R_2)}$$

Now substituting

$$s = j\omega$$

$$\text{and } s^2 = -\omega^2$$

the transfer function becomes

$$g_{21} = \frac{[1 - \omega^2C_1C_2R_2R_3 - \omega^2C_1C_2R_1R_3] + j[\omega R_3C_1 + \omega R_3C_2 - \omega^3C_1C_2C_3R_1R_2R_3]}{(1 + j\omega C_3R_1)(1 + j\omega C_1R_3 + j\omega C_2R_3) + (-\omega^2C_1C_2R_3 + j\omega C_2)(R_2 + R_1 + j\omega C_3R_1R_2)} \quad (A-16)$$

The numerator of g_{21} in (A-16) has the form

$$\alpha + j\beta$$

If $g_{21} = 0$, then $\alpha = \beta = 0$. We then have

$$\alpha = 1 - \omega^2C_1C_2R_2R_3 - \omega^2C_1C_2R_1R_3 = 0$$

(A-17)

$$\omega_o^2 = \frac{1}{(R_1 + R_2)C_1C_2R_3}$$

$$g_{21} = \frac{\frac{1}{R_1} \cdot \frac{1}{sC_1} \cdot \frac{1}{R_2}}{\frac{1}{R_1} + \frac{1}{sC_1} + \frac{1}{R_2}}$$

(A-15)

Now simplifying (A-15)

$$g_{21} = \frac{(1/sC_1)(1/R_1)(1/R_2)}{(1/R_1) + (1/sC_1) + (1/R_2)}$$

and

$$g_{21} = \frac{(1/sC_1)(1/R_1)(1/R_2)}{(1/R_1) + (1/sC_1) + (1/R_2)}$$

Now substituting

$$s = j\omega$$

$$\text{and } s = -j\omega$$

the transfer function becomes

$$g_{21} = \frac{[1 - \omega^2 C_1^2 R_1^2 R_2^2]}{(1 + j\omega C_1 R_1)(1 + j\omega C_1 R_2)}$$

(A-16)



The numerator of g_{21} in (A-16) has the form

$$1 - \omega^2$$

If $g_{21} = 0$, then $1 - \omega^2 = 0$. We then have

$$\omega^2 = 1$$

(A-17)

$$\omega_0^2 = \frac{1}{(R_1 + R_2)C_1^2}$$

and

$$\beta = \omega R_3 C_1 + \omega R_3 C_2 - \omega^3 C_1 C_2 C_3 R_1 R_2 R_3 = 0 \quad (A-18)$$

$$\omega_o^2 = \frac{C_1 + C_2}{C_1 C_2 C_3 R_1 R_2}.$$

Combining (A-17) and (A-18)

$$\frac{1}{(R_1 + R_2) C_1 C_2 R_3} = \frac{C_1 + C_2}{C_1 C_2 C_3 R_1 R_2} \quad (A-19)$$

Separating variables,

$$\frac{\frac{R_1 R_2}{R_1 + R_2}}{R_3} = \frac{C_1 + C_2}{C_3} = n \quad (A-20)$$

where n is a real number $[0, \infty]$.

If we let

$$R_1 = R_2 = R \quad (A-21)$$

and $C_1 = C_2 = C,$

equation (A-20) becomes

$$\frac{R}{2R_3} = n = \frac{2C}{C_3} \quad (A-22)$$

By substituting the equalities (A-21) and (A-16),

g_{21} becomes

$$g_{21} = \frac{(1 - \omega^2 C^2 R R_3 - \omega^2 C^2 R R_3) + j(\omega R_3 C + \omega R_3 C - \omega^3 C^2 C_3 R^2 R_3)}{(1 + j\omega C_3 R)(1 + j\omega C R_3 + j\omega C R_3) + (-\omega^2 C^2 R_3 + j\omega C)(R + R + j\omega C_3 R^2)} \quad (A-23)$$

and

$$R = R_1 + R_2 + R_3 + \dots + R_n$$

(A-18)

Now

$$\frac{R}{C} = \frac{R_1 + R_2 + R_3 + \dots + R_n}{C}$$

Combining (A-17) and (A-18)

(A-19)

$$\frac{R_1 + R_2 + R_3 + \dots + R_n}{C} = \frac{R_1}{C} + \frac{R_2}{C} + \frac{R_3}{C} + \dots + \frac{R_n}{C}$$

Separating variables

(A-20)

$$\frac{R_1}{C} = \frac{R_1}{R_1 + R_2 + R_3 + \dots + R_n}$$

where n is a real number

If we let

$$R_1 = R_2 = R_3 = \dots = R_n = R$$

(A-21)

$$\text{and } C_1 = C_2 = C_3 = \dots = C_n = C$$

equation (A-20) becomes

(A-22)

$$\frac{R}{C} = n = \frac{R}{C}$$

By substituting the relations (A-21) and (A-22)

equation (A-21) becomes

$$\frac{R}{C} = \frac{(1 + j\omega C R)(1 + j\omega C R) \dots (1 + j\omega C R)}{(1 + j\omega C R)(1 + j\omega C R) \dots (1 + j\omega C R)}$$

(A-23)

According to (A-22)

$$R_3 = \frac{R}{2n} \quad \text{and} \quad C_3 = \frac{2C}{n} \quad . \quad (\text{A-24})$$

Relations (A-24) in (A-23) give

$$g_{21} = \frac{(1 - \omega^2 \frac{2C^2 R^2}{2n} - \omega^2 \frac{2C^2 R^2}{2n}) + j(\omega \frac{CR}{2n} + \omega \frac{CR}{2n} - \omega^3 \frac{C^3 R^3}{n^2})}{(1 + j\omega \frac{R^2 C}{n})(1 + j\omega \frac{CR}{2n} + j\omega \frac{CR}{2n}) + (-\omega^2 \frac{2C^2 R}{2n} + j\omega C)(R + R + j\omega \frac{R^2 2C}{n})} \quad (\text{A-25})$$

Collecting terms,

$$g_{21} = \frac{(1 - \omega^2 \frac{C^2 R^2}{n}) + j(\frac{\omega CR}{n} - \omega^3 \frac{R^3 C^3}{n^2})}{(1 + j\omega \frac{2RC}{n})(1 + j\omega \frac{RC}{n}) + (-\omega^2 \frac{RC^2}{2n} + j\omega C)(2R + j\omega \frac{2R^2 C}{n})} \quad (\text{A-26})$$

If $R_1 = R_2 = R$ and $C_1 = C_2 = C$, equation (A-17) becomes

$$\omega_o^2 = \frac{1}{2RC^2 R_3} \quad (\text{A-27})$$

and (A-18) becomes

$$\omega_o^2 = \frac{2C}{C^2 R^2 C_3} \quad . \quad (\text{A-28})$$

Substituting equations (A-24) into (A-27) and (A-28)

we have

$$\omega_o^2 = \frac{n}{R^2 C^2} \quad (\text{A-29})$$

$$\text{and } \omega_o^2 = \frac{n}{R^2 C^2} \quad \text{respectively.} \quad (\text{A-30})$$

According to (A-22)

$$R_1 = \frac{R}{Z_n} \text{ and } C_1 = \frac{ZC}{n} \quad (\text{A-24})$$

Relations (A-24) in (A-22) give

$$a_{21} = \frac{(1 + j\omega \frac{ZC}{n}) \left(1 + j\omega \frac{RC}{Z_n} + j\omega \frac{RC}{Z_n} + j\omega \frac{RC}{Z_n} \right) + j\omega \frac{RC}{Z_n} + j\omega \frac{RC}{Z_n} + j\omega \frac{RC}{Z_n}}{(1 + j\omega \frac{ZC}{n}) \left(1 + j\omega \frac{RC}{Z_n} + j\omega \frac{RC}{Z_n} + j\omega \frac{RC}{Z_n} \right) + j\omega \frac{RC}{Z_n} + j\omega \frac{RC}{Z_n} + j\omega \frac{RC}{Z_n}} \quad (\text{A-25})$$

Collecting terms

$$a_{21} = \frac{(1 + j\omega \frac{ZC}{n}) \left(1 + j\omega \frac{RC}{Z_n} + j\omega \frac{RC}{Z_n} + j\omega \frac{RC}{Z_n} \right) + j\omega \frac{RC}{Z_n} + j\omega \frac{RC}{Z_n} + j\omega \frac{RC}{Z_n}}{(1 + j\omega \frac{ZC}{n}) \left(1 + j\omega \frac{RC}{Z_n} + j\omega \frac{RC}{Z_n} + j\omega \frac{RC}{Z_n} \right) + j\omega \frac{RC}{Z_n} + j\omega \frac{RC}{Z_n} + j\omega \frac{RC}{Z_n}} \quad (\text{A-26})$$

If $R_1 = R$ and $C_1 = C$, equation (A-17) becomes

$$\omega_0^2 = \frac{1}{ZRC^2} \quad (\text{A-27})$$

and (A-18) becomes

$$\omega_0^2 = \frac{ZC}{C^2 R^2} \quad (\text{A-28})$$

Substituting equations (A-24) into (A-27) and (A-28)

we have

$$\omega_0^2 = \frac{n}{R^2 C^2} \quad (\text{A-29})$$

$$\text{and } \omega_0^2 = \frac{n}{R^2 C^2} \text{ respectively.} \quad (\text{A-30})$$

From (A-29) or (A-30)

$$R^2 C^2 = \frac{n}{\omega_o^2}, \quad (A-31)$$

$$RC = \frac{\sqrt{n}}{\omega_o},$$

and $R^3 C^3 = \frac{n\sqrt{n}}{\omega_o^3}.$

Substituting equations (A-31) in (A-26),

$$g_{21} = \frac{(1 - \frac{\omega^2}{\omega_o^2}) + j(\frac{\omega}{\omega_o} \frac{1}{\sqrt{n}} - \frac{\omega^3}{\omega_o^3} \frac{1}{\sqrt{n}})}{(1 + j \frac{\omega}{\omega_o} \frac{2}{\sqrt{n}})(1 + j \frac{\omega}{\omega_o} \frac{1}{\sqrt{n}}) + (-\frac{\omega^2}{\omega_o^2} \frac{1}{2R} + j \frac{\omega}{\omega_o} \frac{\sqrt{n}}{R})(\frac{2\sqrt{n}}{C\omega_o} + j \frac{\omega}{\omega_o^2} \frac{2}{C})} \quad (A-32)$$

Letting $\rho = \frac{\omega}{\omega_o}$, equation (A-32) becomes,

$$g_{21} = \frac{(1 - \rho^2) + j(\frac{\rho}{\sqrt{n}} - \frac{\rho^3}{\sqrt{n}})}{(1 + j\rho \frac{2}{\sqrt{n}})(1 + j\rho \frac{1}{\sqrt{n}}) + (-\frac{\rho^2}{2R} + j\rho \frac{\sqrt{n}}{R})(\frac{2\sqrt{n}}{\omega_o C} + j\rho \frac{2}{\omega_o C})} \quad (A-33)$$

Expanding the denominator gives,

$$g_{21} = \frac{(1 - \rho^2) + j \frac{\rho}{\sqrt{n}} (1 - \rho^2)}{(1 + j \frac{2\rho}{\sqrt{n}} + j \frac{\rho}{\sqrt{n}} - \frac{2\rho^2}{n}) + (-\frac{\rho^2 \sqrt{n}}{RC\omega_o} + j \frac{\rho 2n}{RC\omega_o} - j \frac{\rho^3}{RC\omega_o} - \frac{\rho^2 2\sqrt{n}}{RC\omega_o})} \quad (A-34)$$

Now $RC\omega_o = \sqrt{n}$ from (A-31). Using this relation, equation (A-34) becomes

$$p = \frac{1}{2} \left(1 + \frac{1}{\sqrt{2}} \right)$$

$$p = \frac{1}{2} \left(1 + \frac{1}{\sqrt{2}} \right)$$

$$p = \frac{1}{2} \left(1 + \frac{1}{\sqrt{2}} \right)$$

$$p = \frac{1}{2} \left(1 + \frac{1}{\sqrt{2}} \right)$$

Substituting equation (A-31) in (A-30)

$$\left(1 - \frac{1}{\sqrt{2}} \right) + \left(1 - \frac{1}{\sqrt{2}} \right) \sqrt{\frac{1}{2}} = \frac{1}{2}$$

$$p = \frac{1}{2} \left(1 + \frac{1}{\sqrt{2}} \right)$$

Setting $p = \frac{1}{2}$, equation (A-31) becomes

$$p = \frac{1}{2} \left(1 + \frac{1}{\sqrt{2}} \right)$$

Expanding the denominator gives

$$p = \frac{1}{2} \left(1 + \frac{1}{\sqrt{2}} \right)$$

Now $\frac{1}{\sqrt{2}} = \sqrt{2}/2$ from (A-31) Using this relation,

equation (A-34) becomes

$$p = \frac{1}{2} \left(1 + \frac{1}{\sqrt{2}} \right)$$

$$g_{21} = \frac{(1 - \rho^2) + j\frac{\rho}{\sqrt{n}}(1 - \rho^2)}{1 + j\frac{2\rho}{\sqrt{n}} + j\frac{\rho}{\sqrt{n}} - \frac{2\rho^2}{n} - \rho^2 + j\rho 2\sqrt{n} - j\frac{\rho^3}{\sqrt{n}} - \rho^2 2} \quad (\text{A-35})$$

Factoring the numerator and rearranging the denominator, (A-35) becomes

$$g_{21} = \frac{(1 - \rho^2)(1 + j\frac{\rho}{\sqrt{n}})}{1 - \rho^2 + j\frac{\rho}{\sqrt{n}} - j\frac{\rho^3}{\sqrt{n}} - 2\rho^2 - \frac{2\rho^2}{n} + j2\rho\sqrt{n} + j\frac{2\rho}{\sqrt{n}}} \quad (\text{A-36})$$

Now we operate on the denominator of (A-36) and obtain

$$\begin{aligned} & \left[(1 - \rho^2) + j\frac{\rho}{\sqrt{n}}(1 - \rho^2) \right] + \left[-2\rho^2 - \frac{2\rho^2}{n} + j(2\rho\sqrt{n} + \frac{2\rho}{\sqrt{n}}) \right], \\ & \left[(1 - \rho^2) + j\frac{\rho}{\sqrt{n}}(1 - \rho^2) \right] + j2\rho \left[j\rho + j\frac{\rho}{n} + (\sqrt{n} + \frac{1}{\sqrt{n}}) \right], \\ & \left[(1 - \rho^2) + j\frac{\rho}{\sqrt{n}}(1 - \rho^2) \right] + j2\rho(\sqrt{n} + \frac{1}{\sqrt{n}})(1 + j\frac{\rho}{\sqrt{n}}), \\ & (1 + j\frac{\rho}{\sqrt{n}})(1 - \rho^2) + j2\rho(1 + j\frac{\rho}{\sqrt{n}})(\sqrt{n} + \frac{1}{\sqrt{n}}), \\ & (1 + j\frac{\rho}{\sqrt{n}}) \left[(1 - \rho^2) + 2j\rho(\sqrt{n} + \frac{1}{\sqrt{n}}) \right], \end{aligned}$$

and

$$(1 + j\frac{\rho}{\sqrt{n}}) \left[(1 - \rho^2) + j2\rho(\frac{n+1}{\sqrt{n}}) \right]. \quad (\text{A-37})$$

Now putting the denominator (A-37) back into (A-36) we have

$$g_{21} = \frac{(1 - \rho^2)(1 + j\frac{\rho}{\sqrt{n}})}{(1 + j\frac{\rho}{\sqrt{n}}) \left[(1 - \rho^2) + j2\rho(\frac{n+1}{\sqrt{n}}) \right]} \quad (\text{A-38})$$

Dividing the numerator and denominator by $-(1 + j\frac{\rho}{\sqrt{n}})$, (A-38) becomes

(A-38) becomes

Dividing the numerator and denominator by \sqrt{A}

$$q_{21} = \frac{(1 + \frac{1}{\sqrt{A}}) \left[(1 - \frac{1}{\sqrt{A}}) + \frac{1}{\sqrt{A}} \right]}{(1 - \frac{1}{\sqrt{A}}) \left(1 - \frac{1}{\sqrt{A}} \right) + \frac{1}{\sqrt{A}}}$$

we have

Now putting the denominator in (A-38) back into (A-36)

$$(1 + \frac{1}{\sqrt{A}}) \left[(1 - \frac{1}{\sqrt{A}}) + \frac{1}{\sqrt{A}} \right]$$

and

$$(1 + \frac{1}{\sqrt{A}}) \left[(1 - \frac{1}{\sqrt{A}}) + \frac{1}{\sqrt{A}} \right]$$

$$(1 + \frac{1}{\sqrt{A}}) (1 - \frac{1}{\sqrt{A}}) + \frac{1}{\sqrt{A}}$$

$$\left[(1 - \frac{1}{\sqrt{A}}) + \frac{1}{\sqrt{A}} \right] \left[(1 - \frac{1}{\sqrt{A}}) + \frac{1}{\sqrt{A}} \right]$$

$$\left[(1 - \frac{1}{\sqrt{A}}) + \frac{1}{\sqrt{A}} \right] \left[(1 - \frac{1}{\sqrt{A}}) + \frac{1}{\sqrt{A}} \right]$$

$$\left[(1 - \frac{1}{\sqrt{A}}) + \frac{1}{\sqrt{A}} \right] \left[(1 - \frac{1}{\sqrt{A}}) + \frac{1}{\sqrt{A}} \right]$$

Now we operate on the denominator of (A-38) and obtain

(A-38)

$$q_{21} = \frac{(1 - \frac{1}{\sqrt{A}}) + \frac{1}{\sqrt{A}}}{(1 - \frac{1}{\sqrt{A}}) \left(1 - \frac{1}{\sqrt{A}} \right) + \frac{1}{\sqrt{A}}}$$

(A-35) becomes

Factoring the numerator and denominator

$$1 + \frac{1}{\sqrt{A}} = \frac{1}{\sqrt{A}} \left(\sqrt{A} + 1 \right)$$

(A-31)

$$g_{21} = \frac{\rho^2 - 1}{(\rho^2 - 1) - j2\rho\left(\frac{n+1}{\sqrt{n}}\right)} \quad (\text{A-39})$$

The optimum "n" will be that which gives the steepest slope of $|g_{21}|$ at ω_o . Now

$$|g_{21}| = \frac{\rho^2 - 1}{\left[(\rho^2 - 1)^2 + 4\rho^2\left(\frac{n+1}{\sqrt{n}}\right)^2\right]^{1/2}} \quad (\text{A-40})$$

and

$$\frac{\partial}{\partial \rho} |g_{21}| = \frac{-\frac{(\rho^2-1)}{2} \left[4\rho(\rho^2-1) + 8\rho\left(\frac{n+1}{\sqrt{n}}\right)^2 \right] + 2\rho \left[(\rho^2-1)^2 + 4\rho^2\left(\frac{n+1}{\sqrt{n}}\right)^2 \right]}{\left[(\rho^2-1)^2 + 4\rho^2\left(\frac{n+1}{\sqrt{n}}\right)^2 \right]^{3/2}} \quad (\text{A-41})$$

Relation (A-41) can be simplified by recalling that when $\omega = \omega_o$, $\rho = 1$ since $\rho = \frac{\omega}{\omega_o}$. Using this, (A-41) becomes

$$\left. \frac{\partial |g_{21}|}{\partial \rho} \right|_{\rho=1} = \frac{\sqrt{n}}{n+1} \quad (\text{A-42})$$

The optimum "n" will maximize (A-42). Therefore

$$\frac{d}{dn} \left(\left. \frac{\partial |g_{21}|}{\partial \rho} \right|_{\rho=1} \right) = \frac{-\sqrt{n} + \frac{1}{2}n^{-\frac{1}{2}}(n+1)}{(n+1)^2} = 0 \quad (\text{A-43})$$

$$\text{and } n = 1. \quad (\text{A-44})$$

For this value of n, the steepest slope of $|g_{21}|$, (A-42) will be

$$\left. \frac{\partial |g_{21}|}{\partial \rho} \right|_{\substack{\rho=1 \\ n=1}} = \pm \frac{1}{2} \quad (\text{A-45})$$

$$g_{21} = \frac{1}{(q^2 - 1) + 2q \frac{n}{\sqrt{n}} + 1} \quad (A-39)$$

The optimum "n" will be that which gives the steepest slope of $|g_{21}|$ at w_0 . Now

$$\left| \frac{d}{dn} |g_{21}| \right| = \frac{1}{\left[(q^2 - 1) + 2q \frac{n}{\sqrt{n}} + 1 \right]^2} \quad (A-40)$$

and

$$\frac{d}{dn} |g_{21}| = \frac{-\frac{2}{n} \left[(q^2 - 1) + 2q \frac{n}{\sqrt{n}} + 1 \right] + 2q \frac{1}{\sqrt{n}}}{\left[(q^2 - 1) + 2q \frac{n}{\sqrt{n}} + 1 \right]^3} \quad (A-41)$$

Relation (A-41) can be simplified by recalling that when $w = w_0$, $q = 1$ since $q = \frac{w}{w_0}$. Using this, (A-41) becomes

$$\frac{d}{dn} |g_{21}| \bigg|_{q=1} = \frac{\frac{1}{\sqrt{n}}}{n+1} \quad (A-42)$$

The optimum "n" will maximize (A-42). Therefore

$$\frac{d}{dn} \left(\frac{1}{\sqrt{n}} \right) \bigg|_{q=1} = \frac{-\frac{1}{2} n^{-\frac{3}{2}}}{(n+1)^2} = 0 \quad (A-43)$$

and $n = 1$. (A-44)

For this value of n, the steepest slope of $|g_{21}|$, (A-42) will be

$$\frac{d}{dn} |g_{21}| \bigg|_{q=1, n=1} = \frac{1}{2} \quad (A-45)$$

Also for $n = 1$,

$$R_3 = \frac{R}{2} \quad \text{and} \quad C_3 = 2C \quad (\text{A-46})$$

from (A-24).

If we let $n = 2$, however, the slope will be ± 0.472 but $C_3 = C$. Thus for a light sacrifice in slope, we are able to have $C_1 = C_2 = C_3$ which permits continuous variable tuning. Letting $n = \frac{1}{2}$, the slope will again be ± 0.472 but $R_1 = R_2 = R_3$.

The gain (β) of a twin-T network with zero input impedance, infinite output impedance, and $n = 1$ has been shown to be²

$$\beta = \frac{1}{1 - j \frac{4\rho}{\rho^2 - 1}} \quad (\text{A-47})$$

where

$$\rho = \frac{\omega}{\omega_o} = \frac{f}{f_o} \quad (\text{A-48})$$

The term

$$\frac{4\rho}{\rho^2 - 1} \quad (\text{A-49})$$

indicates the manner in which the magnitude and phases of " β " varies with " ρ ." When $\rho = 0$, (A-49) vanishes and

$$|\beta| = 1.$$

However when (A-49) is equal to unity,

$$|\beta| = \frac{\sqrt{2}}{2},$$

²Valley, G. E. Jr. and H. Wallman, Vacuum Tube Amplifiers, Vol. 18, Radiation Laboratory Series, McGraw-Hill Book Company, Inc., 1948.

$$|a| = \frac{\sqrt{2}}{2}$$

However when (A-49) is equal to unity,

$$|a| = 1.$$

of "a" varies with "q", when $q = 0$, (A-49) vanishes and

indicates the manner in which the magnitude and phase

$$\frac{4p}{q^2 - 1}$$

The term

$$p = \frac{\omega}{\omega_0} = \frac{f}{f_0}$$

where

$$a = \frac{1}{1 - \frac{4p}{q^2 - 1}}$$

shown to be

impedance, infinite output impedance, and a load impedance

The gain (a) of a tuned network with zero input

± 0.472 but $R_1 = R_2 = R_3 = R_4$, the ratio will again be

variable tuning. Letting $n = 4$, the ratio will again be

are able to have $C_1 = C_2 = C_3 = C_4$, which permits continuous

but $C_5 = C_6$. Thus for a fixed ratio in a circuit

If we let $n = 2$, however, the ratio will be 0.472

from (A-24).

$$R_3 = \frac{R}{2} \text{ and } C_3 = 2C$$

Also for $n = 1$,

and the response is 3 db down from $f = f_0$ which is taken here as the reference. Thus at the 3 db points

$$\frac{4\rho}{\rho^2 - 1} = 1$$

and $\rho \approx \frac{1}{4}$

or $\frac{f}{f_0} \approx \frac{1}{4}$.

(A-50)

Equation (A-47) may now be written as

$$\beta = \frac{1}{1 - j \frac{4}{\left(\frac{f}{f_0} - \frac{f_0}{f}\right)}} = \frac{1}{1 - j \frac{4f_0}{\left(f - \frac{f_0^2}{f}\right)}} ,$$
(A-51)

in which the frequencies at the $\frac{1}{2}$ -power points are

$$f_2 = \frac{f_0^2}{f}$$
(A-52)

and $f_1 = f$

Defining

$$Q = \frac{f_0}{f_2 - f} ,$$

then

$$Q = \frac{f_0}{\frac{f_0^2}{f} - f} = \frac{ff_0}{f_0^2 - f^2} ,$$
(A-53)

Using (A-50) and putting Q in terms of " f "

$$Q = \frac{4f^2}{16f^2 - f^2} \approx \frac{1}{4}$$
(A-54)

or $4 = \frac{1}{Q} .$

and the response is 3 db down from $f = 0$ which is taken here as the reference. Thus at the 3 db points

$$\frac{40}{f_0^2 - 1} = 1$$

$$\text{and } \frac{1}{f_0^2 - 1} = \frac{1}{4}$$

(A-50)

Equation (A-47) may now be written as

$$(A-51) \quad A = \frac{1}{f_0^2 - 1} = \frac{1}{f_0^2 - 1} \cdot \frac{f_0^2}{f_0^2} = \frac{f_0^2}{f_0^2 - 1} \cdot \frac{1}{f_0^2}$$

in which the frequencies at the $\frac{1}{2}$ -power points are

$$f_2 = \frac{f_0}{2}$$

(A-52)

$$\text{and } f_1 = f_0$$

Defining

$$Q = \frac{f_0}{f_2 - f_1}$$

then

$$(A-53) \quad Q = \frac{f_0}{f_2 - f_1} = \frac{f_0}{\frac{f_0}{2} - f_0} = \frac{f_0}{-\frac{f_0}{2}} = -2$$

Using (A-50) and putting Q in terms of " f "

$$(A-54) \quad Q = \frac{4f_0^2}{16f_0^2 - f_0^2} = \frac{4}{15}$$

$$\text{or } 4 = \frac{1}{Q}$$

Substituting this last relation into (A-51) gives

$$\beta = \frac{1}{1 - j \frac{1}{Q(\frac{f}{f_o} - \frac{f_o}{f})}} = \frac{1}{1 - j \frac{1}{\frac{Q}{f_o}(f - \frac{f_o^2}{f})}} . \quad (A-55)$$

We now show that " β " possesses geometric symmetry by considering the bracketed term in (A-55)

$$(f - \frac{f_o^2}{f}) \quad (A-56)$$

which is equal to $(f_1 - f_2)$ by equations (A-52).

In a geometric progression

$$a_1 + a_1 r + a_1 r^2 + \dots a_1 r^{n-1} \quad (A-57)$$

the ratio between successive terms is " r ," and the general expression for the n th term is

$$a_n = a_1 r^{n-1} .$$

Thus the relation between the ordered frequencies f_1 , f_x , and f_2 is

$$f_2 = f_1 r^2$$

or

$$r^2 = \frac{f_2}{f_1}$$

and by (A-52)

$$r^2 = \frac{\frac{f_o^2}{f}}{f} = \frac{f_o^2}{f^2} . \quad (A-58)$$

By referring to (A-57) we see that

$$f_x = f_1 r = f. \quad \left(\frac{f}{f_0}\right) = f_0 \quad (\text{A-59})$$

since $f_1 = f$ by (A-52).

Because the geometric mean of f_2 and f_1 is f_0 , the $|\beta|$ will be symmetric about the null frequency (f_0) when plotted against the logarithm of frequency or the logarithm of the frequency ratio "r."

Since

$$r = \frac{1}{\rho} \quad (\text{A-60})$$

by (A-50) and (A-58), it is more meaningful to use " ρ " as the parameter in plotting. From (A-48) we have

$$f = \rho f_0$$

which becomes

$$f_1 = \frac{1}{4} f_0 \quad (\text{A-61})$$

$$f_2 = 4 f_0$$

after substituting (A-50) and (A-52).

Considering equation (A-47), the phase angle of β is

$$\theta = \tan^{-1} \frac{4\rho}{\rho^2 - 1}. \quad (\text{A-62})$$

An examination of this relation shows that θ varies from 0 to $-\frac{\pi}{2}$ as ρ varies from 0 to 1, and from $\frac{\pi}{2}$ to 0 as ρ varies from 1 to ∞ . Figure A5 shows the $|\beta|$ and θ as functions of ρ .

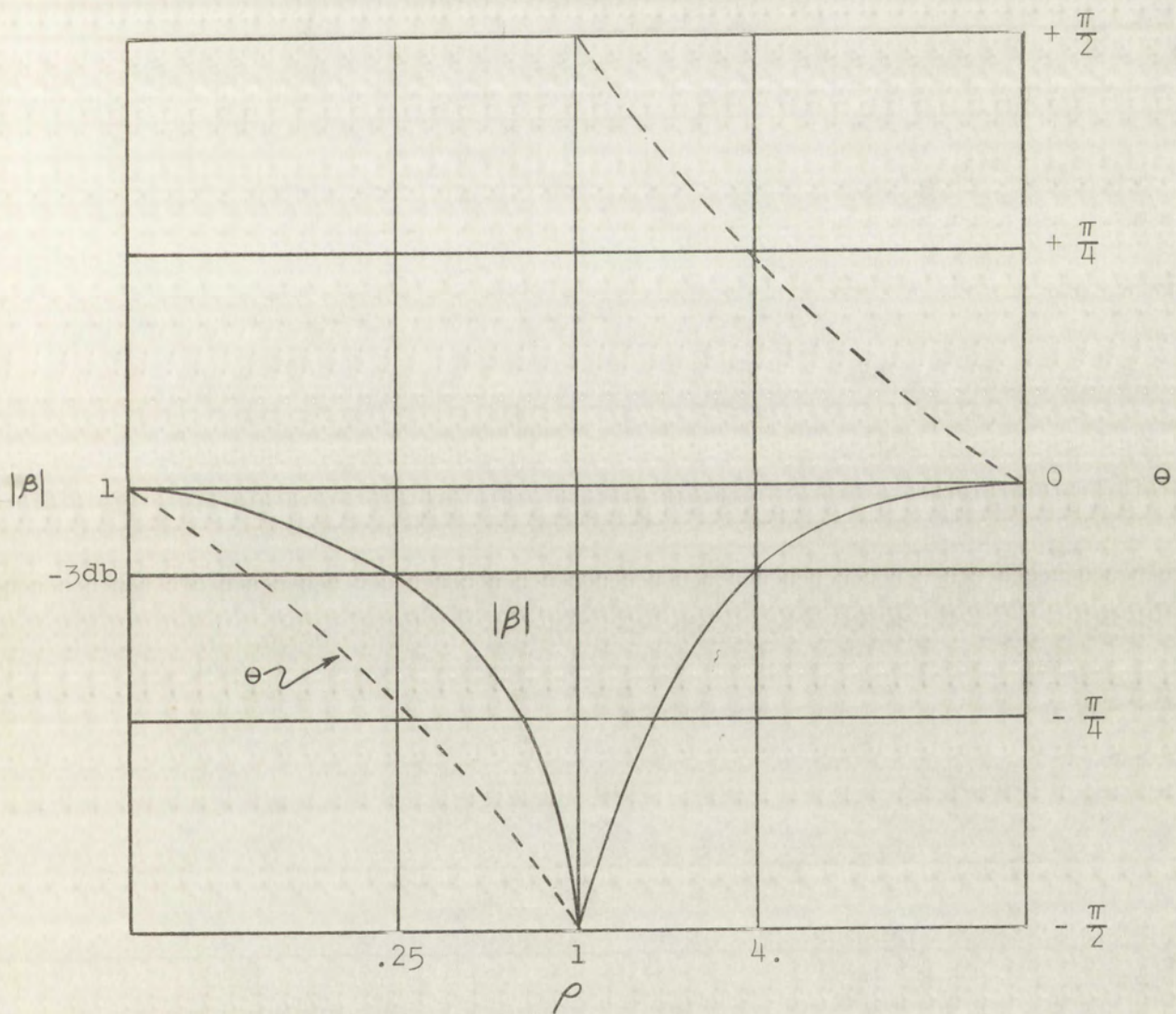


Figure A5 $|\beta|$ versus ρ

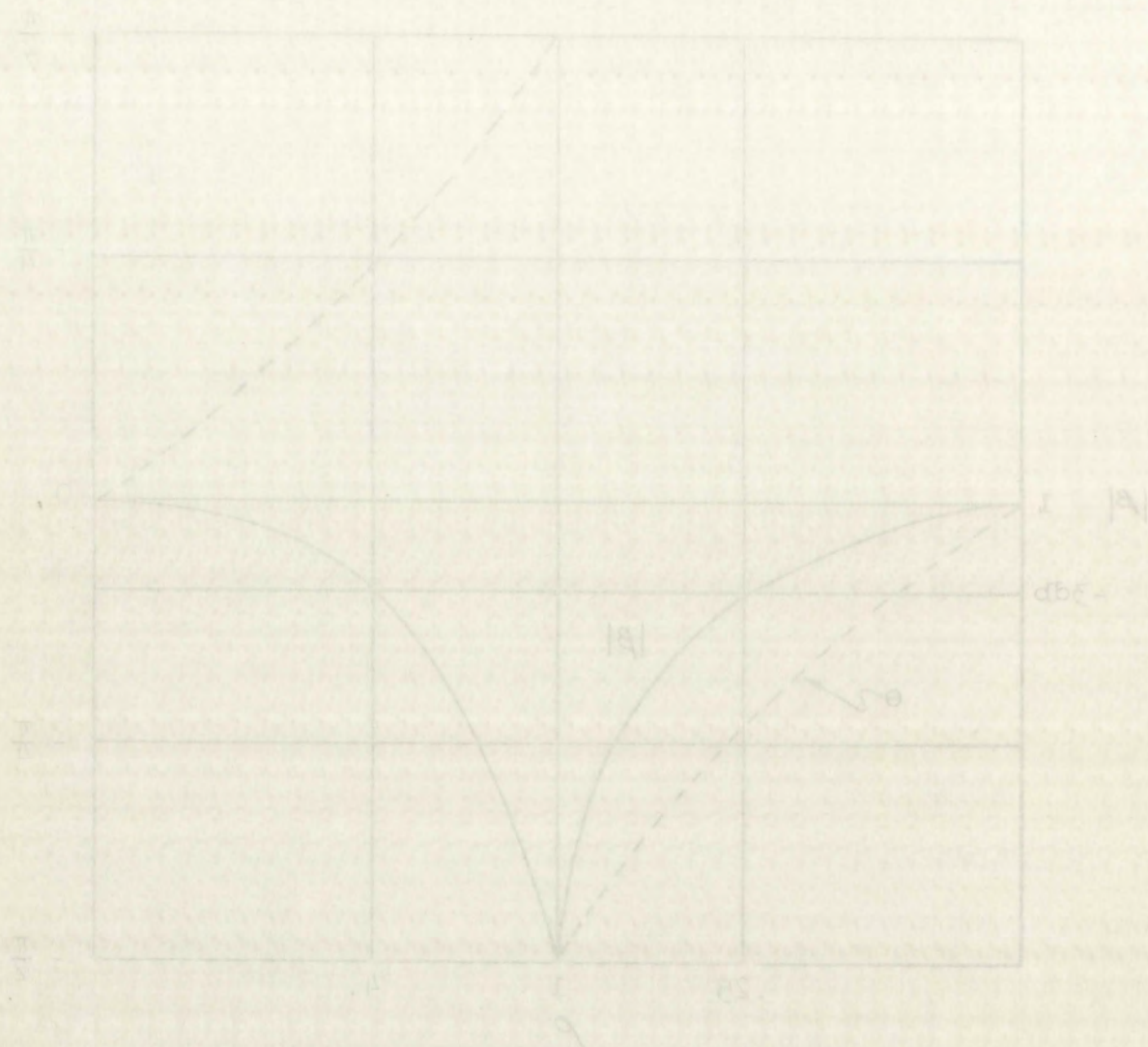


Figure 25 $|A|$ versus f

The input and output impedances affect the symmetry of the overall response.³ The equation for β , (A-55), will not be affected directly since the external impedances are intentionally related to "r" and "n" of the network to insure that the response is equal to $f = 0$ and $f = \infty$.

Consider the twin-T network in Figure A6 which is driven by a source with finite impedance (R_1) and which operates into a load (R_L).

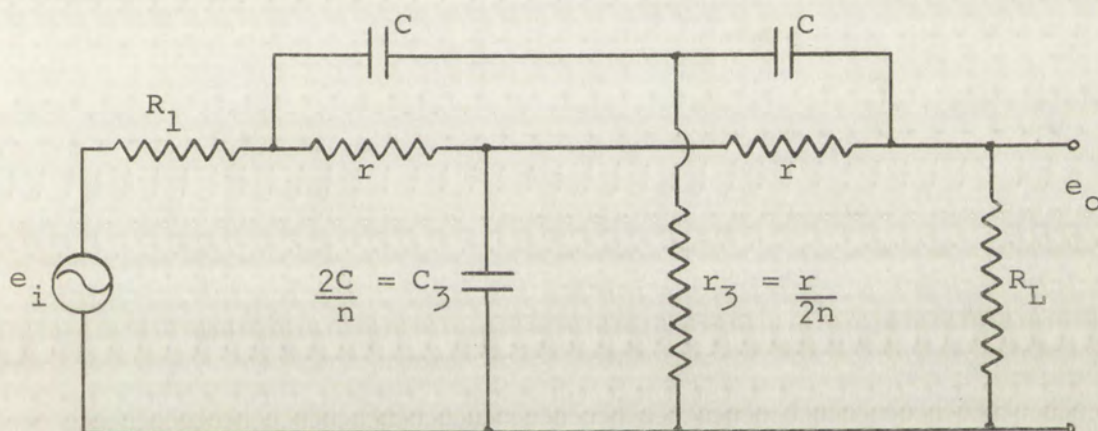


Figure A6 Twin-T network with voltage source and load

When the frequency is zero, Figure A6 reduces to the equivalent circuit shown in Figure A7.

³Cowles, L. G., "Parallel - T Resistance Capacitance Networks," Proc. I.R.E., No. 12, Dec., 1952, p. 1712.

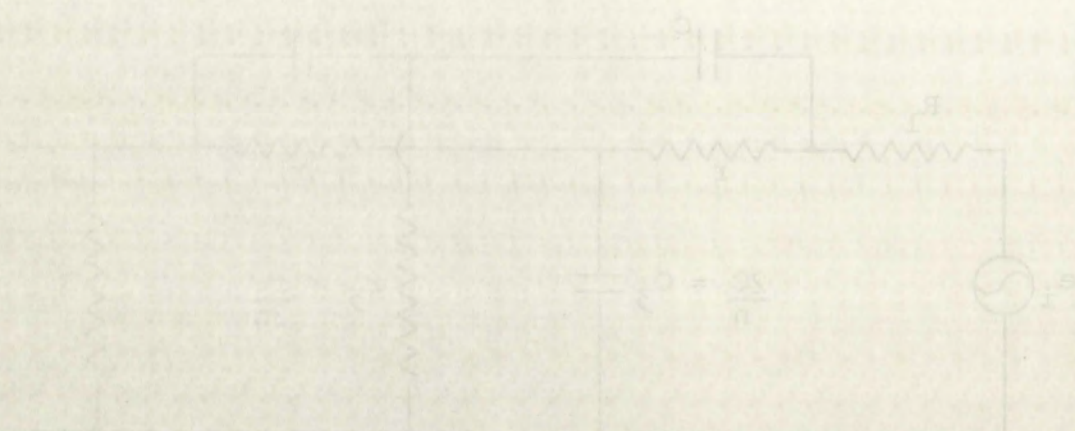


Figure 56. Twin T network with voltage source and load resistor.

When the frequency is zero, Figure 56 becomes the equivalent circuit shown in Figure 57.

Cowles, D. G., "Parallel Resonance in Twin T Networks," Proc. I.R.E., No. 41, Part 1, 1953, p. 111.

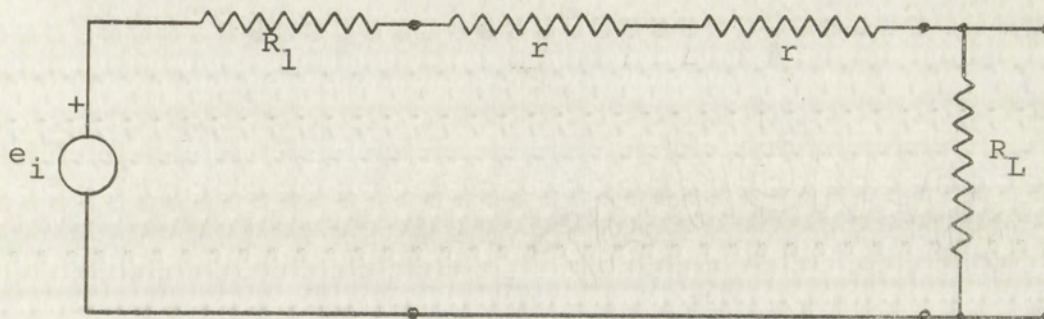
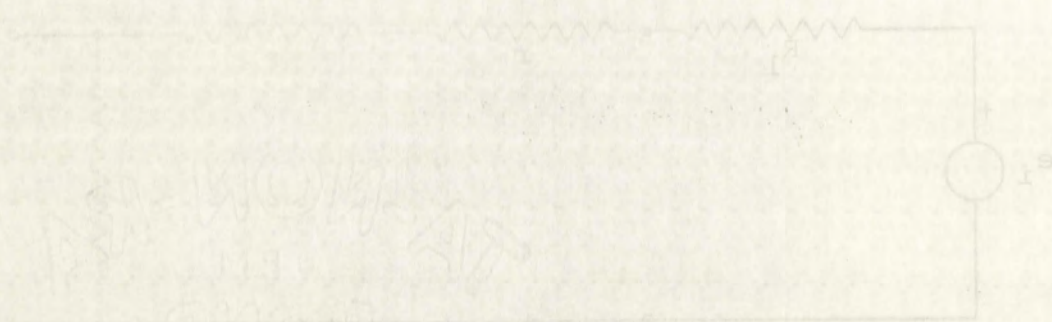


Figure A7 D-C equivalent circuit of twin-T network with source and load

The overall gain of this circuit is

$$\frac{e_o}{e_i} = \frac{R_L}{R_1 + 2r + R_1} \quad . \quad (A-63)$$

As f tends to ∞ , the circuit of Figure A6 becomes equivalent to that shown in Figure A8.



Handwritten notes:
 $V_{out} = V_{in}$
 $R_1 = R_2$
 $V_{in} = V_{out}$

Figure A7 D-C equivalent circuit of

The overall gain of the circuit is

$$\frac{e_o}{e_i} = \frac{R_1}{R_1 + R_2 + R_3}$$

As f tends to ∞ , the value of V_{out} tends to

zero

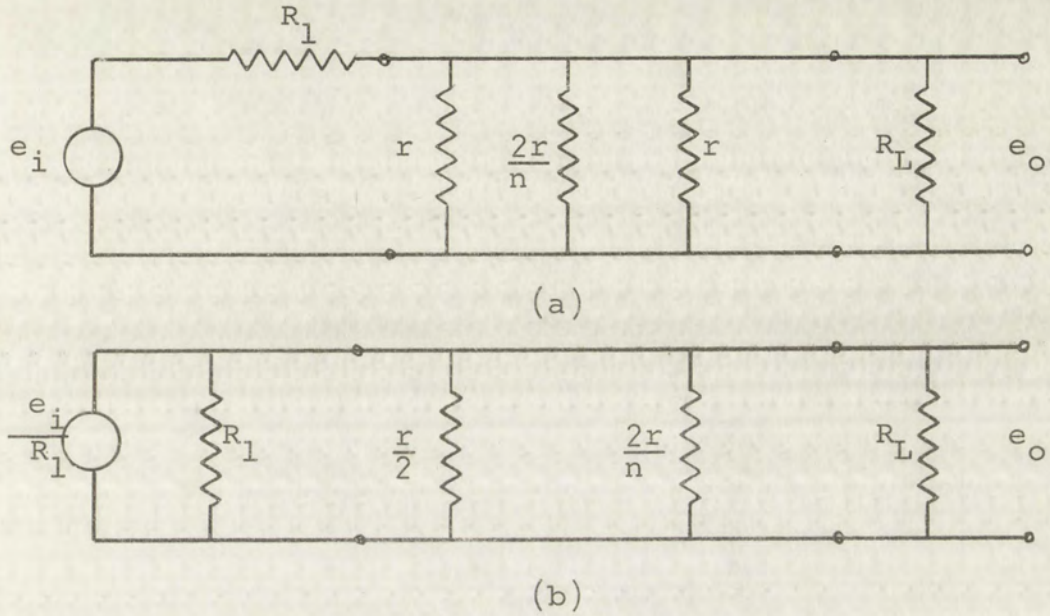


Figure A8 High frequency equivalent circuit of twin-T network with source and load

The overall gain is determined by

$$e_o \left[\frac{1}{R_L} + \frac{2}{r} + \frac{2n}{r} + \frac{1}{R_1} \right] = \frac{e_i}{R_1} \quad (\text{A-64})$$

$$\frac{e_o}{e_i} = \frac{rR_L}{rR_L + rR_1 + R_1R_L(2n + 2)}$$

Equating (A-63) and (A-64), and solving for R_1 and R_L we obtain

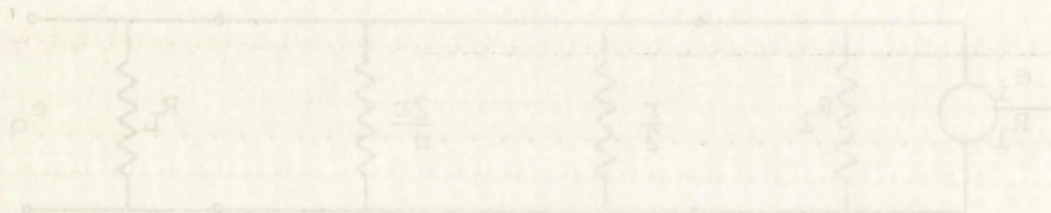
$$\frac{rR_L}{rR_L + rR_1 + R_1R_L(2n + 2)} = \frac{R_L}{R_1 + 2r + R_L}$$

$$R_1R_L^2(2n + 2) = 2r^2R_L \quad (\text{A-65})$$

$$R_1R_L = \frac{r^2}{n + 1} \quad .$$



(a)



(b)

Figure 8B High frequency equivalent circuit of Twin-T network with source and load

The overall gain is determined by

$$e_o \left[\frac{1}{R_L} + \frac{1}{R_1} + \frac{1}{R_2} + \frac{1}{R_3} \right] = \frac{e_s}{R_s}$$

(A-64)

$$\frac{e_o}{e_s} = \frac{R_s}{R_s + R_L + R_1 + R_2 + R_3}$$

Evaluating (A-63) and (A-64) and solving for R_L and

R_L we obtain

$$\frac{R_L}{R_s + R_L + R_1 + R_2 + R_3} = \frac{R_s}{R_s + R_L + R_1 + R_2 + R_3}$$

(A-65)

$$R_L R_s (2n + 2) = 2R_s R_1$$

$$R_L R_s = \frac{R_s}{n + 1}$$

Equation (A-65) relates the external impedances with the "r" and "n" of the network such that the overall response is symmetric. In general the source impedance should be small compared to "r" and the load impedance should be relatively large.

In addition to the advantage of symmetry itself, satisfying (A-65) also means that the simpler d-c relation (A-63) can be used for determining the overall gain.

Consider the situation in which circuit design has resulted in R_1 being 10 k-ohms and R_L , 2 M-ohms. By relation (A-65), with $n = 1$,

$$(10^4) \cdot 2 (10^6) = \frac{r^2}{2}$$

$$r = 2 (10^5).$$

The overall gain from (A-63) is

$$\frac{e_o}{e_i} = \frac{2(10^6)}{10^4 + 4(10^5) + 2(10^6)} = \frac{2}{2.41} \approx 0.83$$

of the gain of the twin-T itself, (β) . We are assuming here, and reasonably so, that for the value of "r" found above, the values of C , C_3 , and r_3 are practicable and can satisfy the null frequency equation for a specific " f_o ."⁴

⁴White, Gifford, "Design and Use of RC Parallel-T Networks," IRE Transactions on Audio, Vo. AV-8, Jan-Feb, 1960.

Equation (A-6) is the same as equation (A-5).

The "1" and "n" of (A-6) are the same as the "1" and "n" of (A-5). The response is symmetric in general, but the response should be small compared to the response of (A-5) if the response should be relatively large.

In addition to the response of (A-5), the response of (A-6) is also small compared to the response of (A-5).

(A-6) can be used for determining the response of (A-5).

Consider the circuit of Figure 1.

resulted in R₁ being 10 ohms and R₂ being 10 ohms.

relation (A-6) with R₁ = 10 ohms and R₂ = 10 ohms.

$$(10^4)^2 (10^6)^2 = \frac{2}{1}$$

$$10^4 = 2(10^6)$$

The overall gain from (A-6) is

$$\frac{e_o}{e_i} = \frac{2(10^6)}{10^4 + 4(10^6)} = \frac{2}{4001}$$

of the gain of the first stage. The response of (A-6) is

here, and reasonably so, since the value of R₁ is small

above, the values of R₁ and R₂ are small compared to the

can satisfy the null frequency equation for a resonant

response.

White, Gifford, "The Design of a Null Frequency Response Network," IRE Transactions on Audio, Vol. 8, October, 1960.

Considering the external impedances, a symmetrical response is obtained by equation (A-65). The series elements of the twin-T are related to the "null" frequency by

$$\omega_o^2 = \frac{n}{r^2 C^2} \quad (\text{A-66})$$

and the series and shunt elements are related by

$$r_3 = \frac{r}{2n} \quad \text{and} \quad C_3 = \frac{2C}{n} \quad . \quad (\text{A-67})$$

It is shown in Figure A9, which is based upon relation (A-66) (with $n = 1$), that for null frequencies in the 0-50 cps region there is a wide range of component values for "r" and "C" which are readily available and practical. In addition, this wide range of component values will accommodate equation (A-65) for many external impedance combinations.

Considering the above, the response is symmetrical

response is obtained by equation (A-6). The series

elements of the twin are related to the "real" frequency

by

$$\omega_0 = \frac{\omega}{\sqrt{1 - \frac{v^2}{c^2}}} \quad (A-6)$$

and the series and sum elements are related by

$$\omega_0 = \frac{\omega}{\sqrt{1 - \frac{v^2}{c^2}}} \quad (A-7)$$

It is shown in Figure A-1, which is a plot of

(A-6) (with $n = 1$) that the real frequency is the

0-50 cps region there is a wide range of component values

for "r" and "C" which are validly related to the physical

In addition, this wide range of component values will

accommodate equation (A-5) for any of the above

combinations.

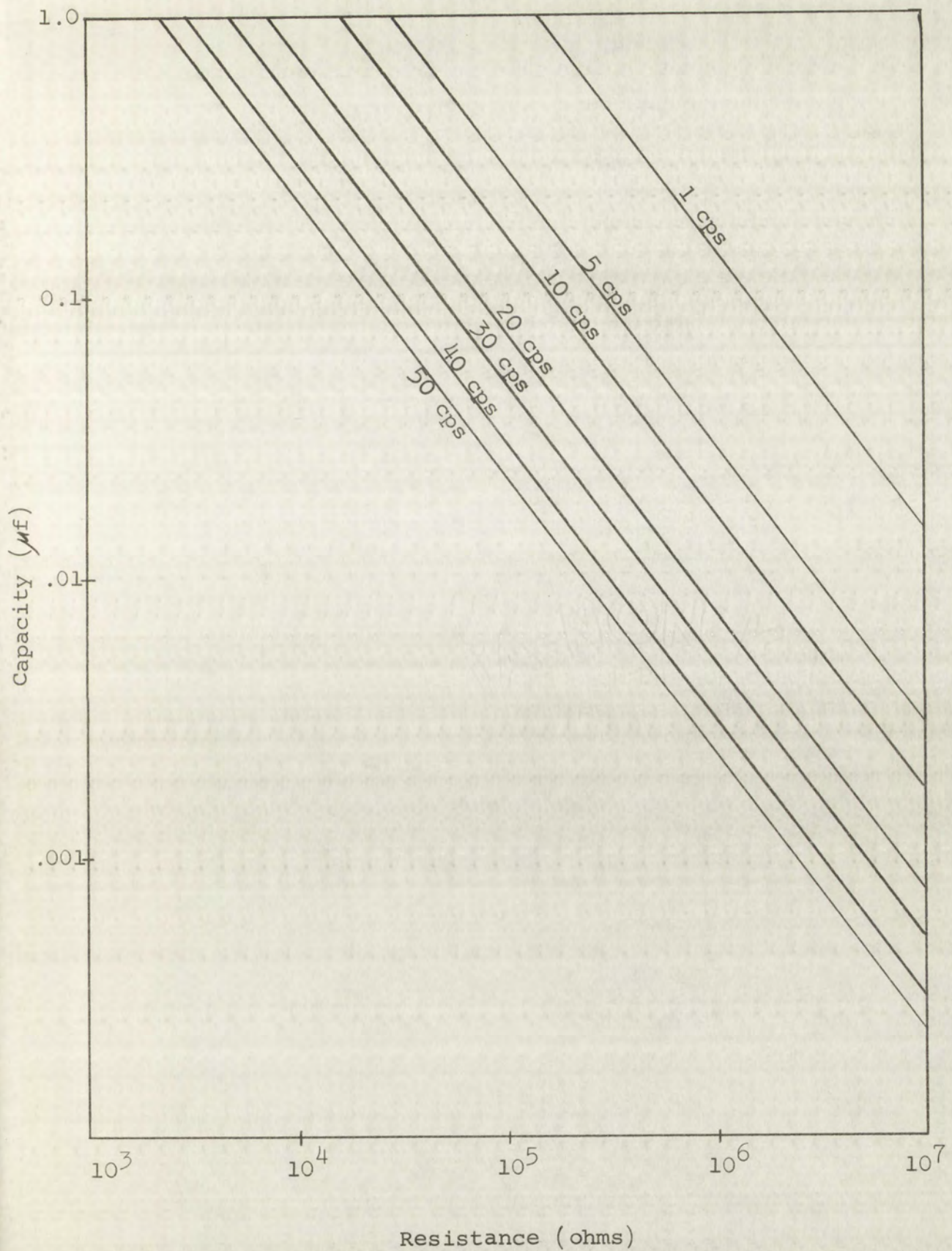


Figure A9 . Capacity and resistance for null frequencies 0-50 cps .

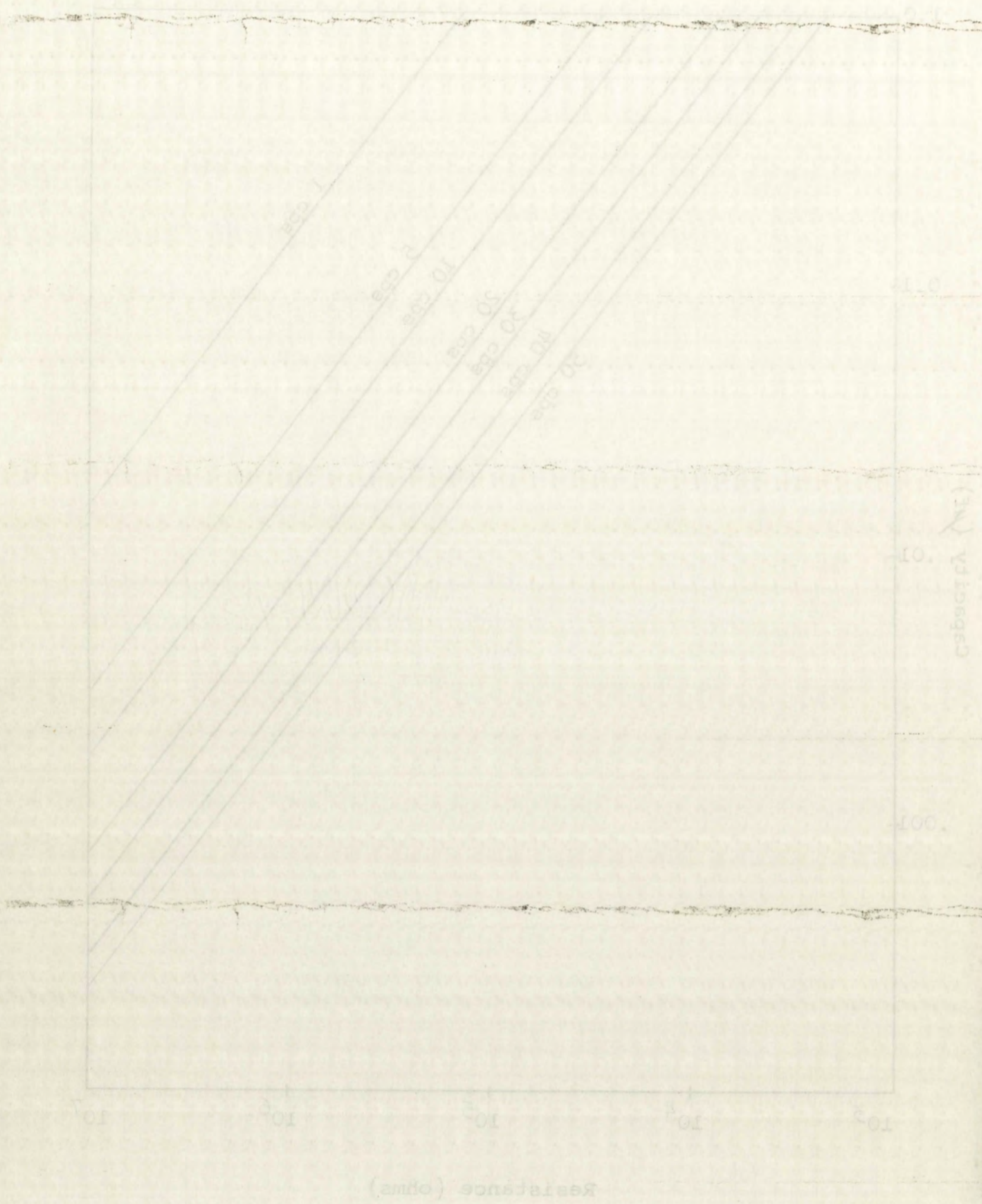


Figure A9. Capacity and resistance for null frequencies 0-50 cps.

Appendix B

Tape Recording

The objective of this article is to demonstrate the influence that varying tape speed has upon the recording and reproduction signals.

Basic Relations

During recording the magnetic material on the tape is exposed to a varying flux across the gap of the recording head. Both tape speed and flux are functions of time. Therefore interaction between the two may be analyzed at one point in space. See figure B1

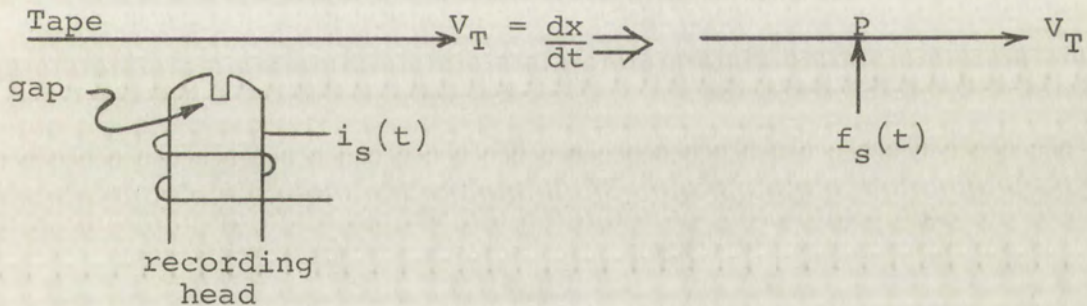


Figure B1 Interaction between tape speed and flux

The flux ϕ at point "P" is proportional to NI . Assuming $i(t)$ is periodic with frequency, f_s , then the instantaneous flux is

$$\phi = \Phi \cos \omega_s t. \quad (B-1)$$

The Recorder

The objective of this section is to determine the influence that varying tape speed has upon the recording and reproduction signals.

Basic Relations

During recording the magnetic material on the tape is exposed to a varying flux across the gap of the recording

head. Both tape speed and flux density are important factors in the recording process. Therefore interaction between the two is of great importance.

one point in space. See Figure B1.

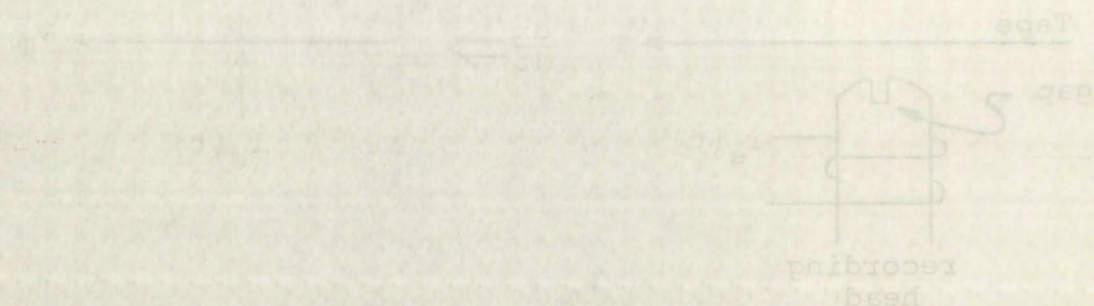


Figure B1 Interaction between tape speed and flux

The flux at point P is proportional to $i(t)$.

Assuming $i(t)$ is periodic with frequency f , then the

instantaneous flux is

$$\phi = \phi_m \cos \omega t$$

The linear velocity of the tape (v_T) is of course

$$v_T = \frac{dx}{dt} . \quad (B-2)$$

Perhaps the best way to demonstrate the relation of $\phi(t)$ and v_T is to plot both on the same time axis (Figure B2). Assuming that the frequency of the recording signal (f_{SR}) is constant, then the period (T_{SR}) of the signal and wavelength of flux in the gap ($\lambda_{\phi g}$) are constant. Figure B2 shows that the time in one wavelength on the tape (T_T) is equal to the period (T_{SR}) of the signal regardless of the tape velocity during the recording (v_{TR}). However, the space wavelength on the tape (λ_T) is proportional to tape velocity (v_{TR}). To put these relations in mathematical form, we begin by saying that

$$v_{TR} = \frac{x}{t} . \quad (B-3)$$

Considering one cycle of f_{SR} , then

$$x = \lambda_{TR}$$

$$t = T_{TR} = T_{SR} , \quad (B-4)$$

and

$$v_{TR} = \frac{\lambda_{TR}}{T_T} = \frac{\lambda_{TR}}{T_{SR}} . \quad (B-5)$$

this last expression says that

$$\lambda_{TR} = T_{SR} v_{TR} \quad (B-6)$$

The linear velocity of the tape (v_T) is of course

$$v_T = \frac{dx}{dt} \quad (B-2)$$

Perhaps the best way to demonstrate the relation of v_T

and v_R is to plot both on the same time axis (Figure B2).

Assuming that the frequency of the recording signal (f_R)

is constant, then the period (T_R) of the signal and

wavelength of flux in the gap (λ_R) are constant. Figure

B2 shows that the time in one wavelength on the tape (T)

is equal to the period (T_R) of the signal regardless of

the tape velocity during the recording (v_{TR}). However,

the space wavelength on the tape (λ_T) is proportional to

tape velocity (v_{TR}). To put these relations in mathema-

tical form, we begin by saying that

$$v_{TR} = \frac{x}{t} \quad (B-3)$$

Considering one cycle of f_R , then

$$x = \lambda_{TR}$$

$$t = T_{TR} = T_R \quad (B-4)$$

and

$$v_{TR} = \frac{\lambda_{TR}}{T} = \frac{\lambda_{TR}}{T_R} \quad (B-5)$$

This last expression says that

$$\lambda_{TR} v_{TR} = T_R \quad (B-6)$$

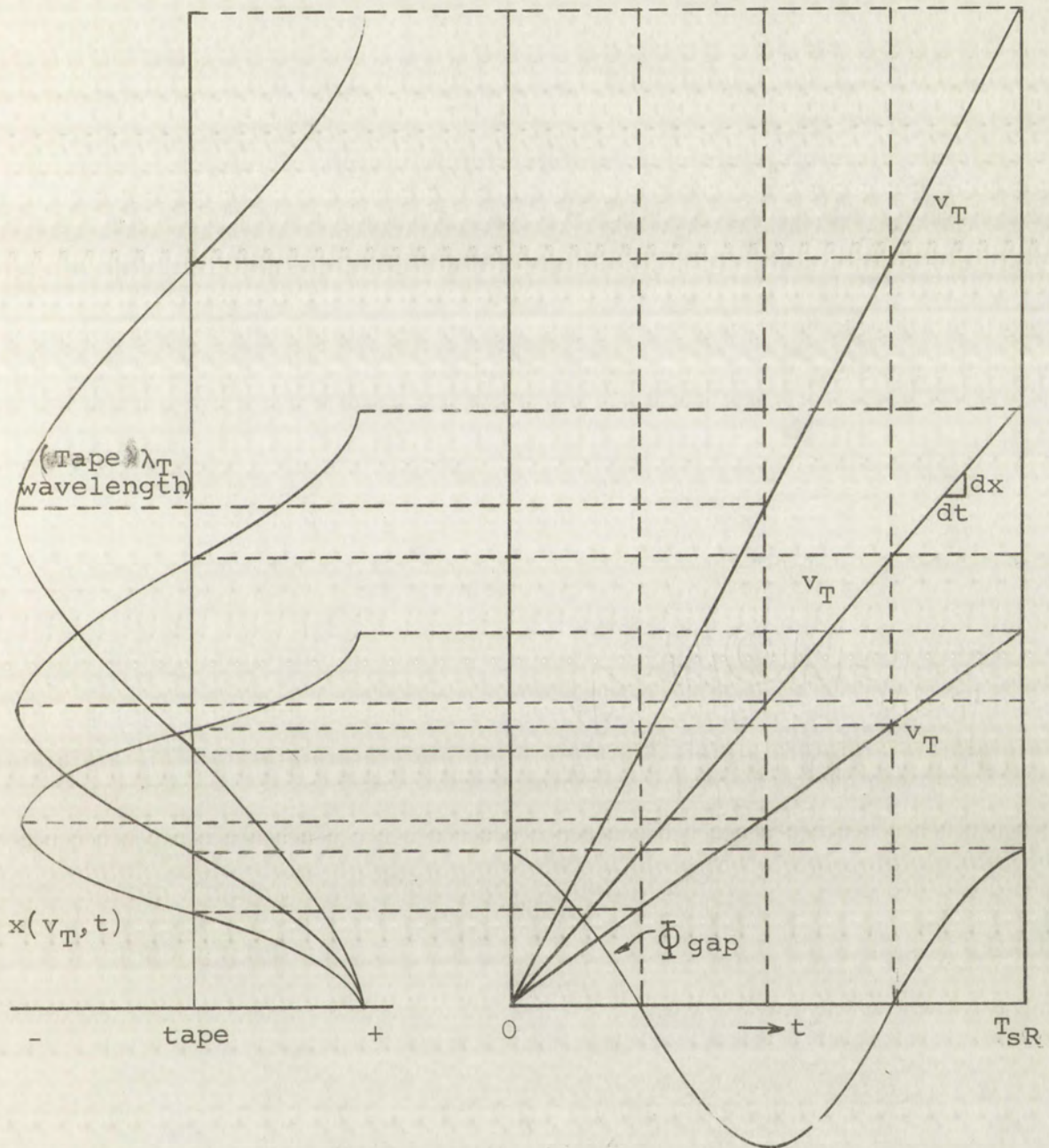


Figure B2 Recording head flux and tape speed versus time

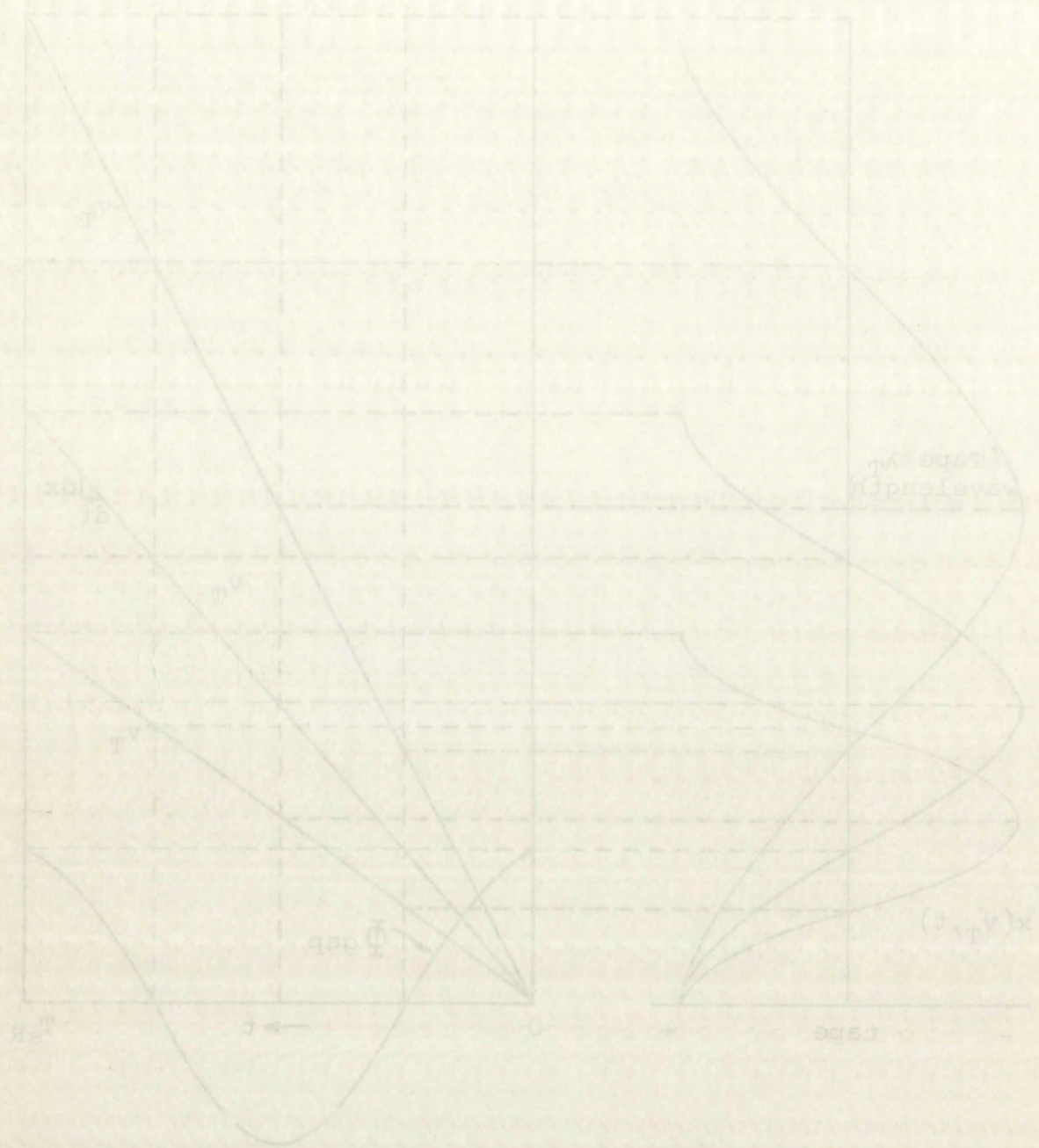


Figure B2 Recording head flux and tape speed versus time

or that

$$\lambda_{TR} = \frac{v_{TR}}{f_{sR}}$$

since

$$T_{sR} = \frac{1}{f_{sR}} . \quad (B-7)$$

We have assumed that f_{sR} is constant. If we further assume that v_{TR} is constant during the recording process; then from relation (B-7), λ_{TR} will be constant. This appears trivial until we consider the play-back situation. Once λ_{TR} is established on the tape, it is fixed, and in analyzing the play-back situation, it becomes a convenient reference parameter. Thus

$$\lambda_{Tb} = \lambda_{TR} = \lambda_T \quad (B-8)$$

where subscript (R) denotes the recording sequence and subscript (b) denoted the play-back sequence.

The basic relation (B-7) also describes the play-back process. Thus changing the subscripts (B-7) becomes

$$\lambda_T = \frac{v_{Tb}}{f_{sb}} . \quad (B-9)$$

The frequency obtained from the tape will be directly proportional to the velocity,

$$f_{sb} = \frac{v_{Tb}}{\lambda_T} \quad (B-10)$$

$$\lambda_{TR} = \frac{v_{TR}}{f_{TR}}$$

since

$$v_{TR} = \frac{v}{\lambda_{TR}}$$



We have assumed that f_{TR} is constant. If we assume that v_{TR} is constant, then from relation (8-7), λ_{TR} will be constant. This appears trivial until we consider the play-back situation. Once λ_{TR} is established on the tape, it is fixed, and analyzing the play-back situation, it is necessary to know the reference parameter, f_{TR} .

$$\lambda_{TR} = \lambda_{TB} = \lambda_{T}$$

where subscript (R) denotes the recording operation and subscript (B) denotes the play-back operation. The basic relation (8-7) also describes the play-back process. Thus changing the subscript to B becomes

$$\lambda_T = \frac{v_{TB}}{f_{TB}}$$

The frequency obtained from the tape will be directly proportional to the velocity,

$$f_{TB} = \frac{v_{TB}}{\lambda_T}$$

Or stated in another way,

$$f_{sb} = f_{sR} \quad (B-11)$$

if

$$v_{Tb} = v_{TR}.$$

Velocity Effects

The mechanism which pulls the tape past the play-back head is basically a rotating device. As a consequence, it is quite conceivable that any variation in tape velocity (v_{Tb}) would be periodic. Thus we shall assume that the tape velocity (v_{Tb}) varies about the correct tape velocity--the recording velocity (v_{TR})--in a periodic manner (Figure B3). The origin and description of this variation are of no concern at the moment.

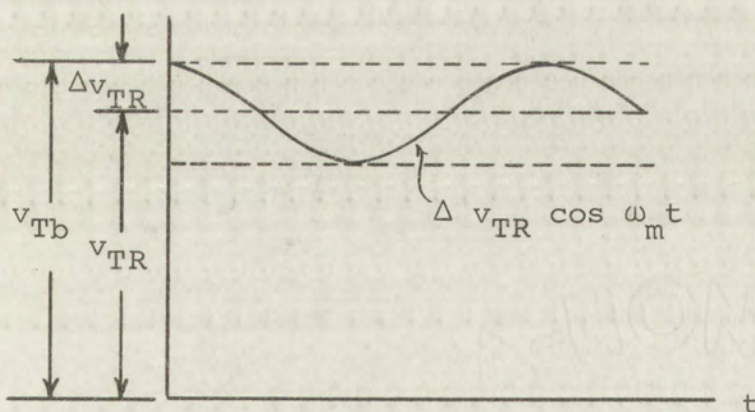


Figure B3 Playback tape speed versus time

Due to the variation tape speed,

$$v_{Tb} = v_{TR} + \Delta v_{TR} \cos \omega_m t. \quad (B-12)$$

Or stated in another way,

(B-11)

$$v_{TP} = v_{TR}$$

11

$$v_{TP} = v_{TR}$$

Velocity Effects

The mechanism which pulls the tape past the play-back head is basically a rotating device. As a consequence, its rate conceivably has any variation in tape velocity (v_{TP}) would be periodic. Thus we shall assume that the tape velocity (v_{TP}) varies about the correct tape velocity--the recording velocity (v_{TR})--in a periodic manner (Figure B5). The origin and description of this variation are of no concern at the moment.

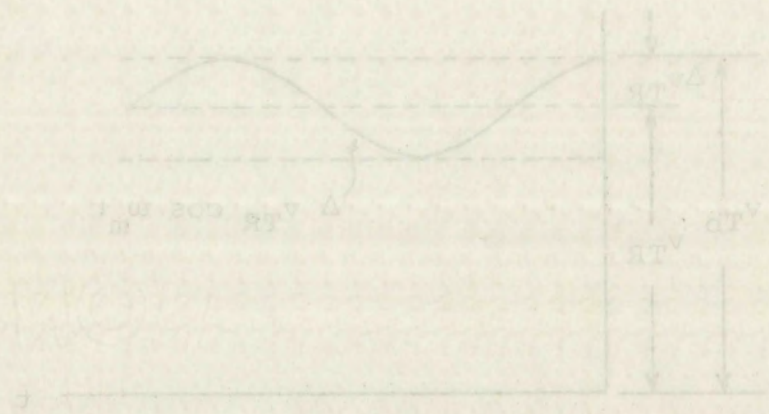


Figure B5 Play-back tape speed versus time

Due to the variation tape speed,

(B-12)

$$v_{TP} = v_{TR} + \Delta v_{TR} \cos \omega t$$

or by dividing by λ_T

$$\frac{v_{Tb}}{\lambda_T} = \frac{v_{TR}}{\lambda_T} + \frac{\Delta v_{TR}}{\lambda_T} \cos \omega_m t.$$

Recalling (B-8) and (B-10), the above equation reduces to

$$f_{sb} = f_{sR} + \Delta f_{sR} \cos \omega_m t \quad (B-13a)$$

$$f_{sb} = f_{sR} \left(1 + \frac{\Delta f_{sR}}{f_{sR}} \cos \omega_m t \right) \quad (B-13b)$$

$$\text{or } \omega_{sb} = \omega_{sR} \left(1 + \frac{\Delta \omega_{sR}}{\omega_{sR}} \cos \omega_m t \right). \quad (B-13c)$$

Equation (B-13a) is shown in Figure B4. Figure B3 and Figure B4 differ in magnitude by a factor of λ_T because of (B-10). However, the ratios are identical:

$$\frac{\Delta v_{TR}}{v_{TR}} = \frac{\Delta f_{sR}}{f_{sR}}. \quad (B-14)$$

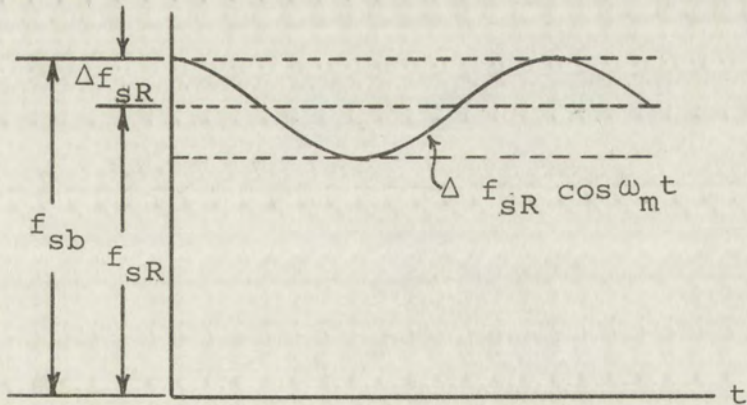


Figure B4 Playback signal frequency versus time

or by dividing by Δf_{AR}

$$\frac{v_{TR}}{\Delta f_{AR}} = \frac{v_{TR}}{\Delta f_{AR}} + \frac{v_{TR}}{\Delta f_{AR}} \cos \omega_m t$$

Recalling (B-8) and (B-10), the above equation reduces to

$$f_{AR} = f_{AR} + \Delta f_{AR} \cos \omega_m t \quad (B-12a)$$

$$f_{AR} = f_{AR} \left(1 + \frac{\Delta f_{AR}}{f_{AR}} \cos \omega_m t \right) \quad (B-12b)$$

$$\text{or } \omega_{AR} = \omega_{AR} \left(1 + \frac{\Delta \omega_{AR}}{\omega_{AR}} \cos \omega_m t \right) \quad (B-12c)$$

Equation (B-12a) is shown in Figure B4. Figure B5 and

Figure B6 differ in magnitude by a factor of 2 because

of (B-10). However, the ratios are identical:

$$\frac{\Delta v_{AR}}{v_{AR}} = \frac{\Delta f_{AR}}{f_{AR}} \quad (B-14)$$

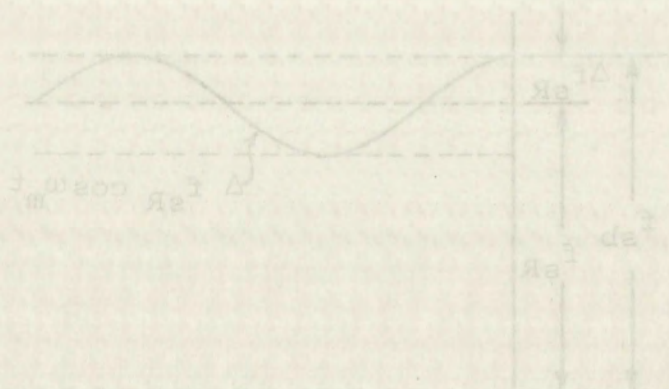


Figure B4: Playback signal frequency versus time

In other words, the percentage change in the tape velocity is equal to the percentage change in the output frequency.

Consider that the output be expressed as

$$f_{sb}(t) = A \cos \theta(t) . \quad (B-15)$$

$$\text{By definition } \frac{d\theta}{dt} = \omega \quad (B-16)$$

$$\text{or } \theta(t) = \int \omega dt + C.$$

If the angular frequency (ω) is constant, then

$$\theta(t) = \omega t + \theta_0$$

and (B-15) assumes the familiar form

$$f_{sb}(t) = A \cos (\omega t + \theta_0).$$

However, (B-13c) indicates that ω_{sb} is not constant.

Therefore (B-16), upon substituting (B-13c), becomes

$$\theta(t) = \int (\omega_{sR} + \Delta\omega_{sR} \cos \omega_m t) dt \quad (B-17)$$

or

$$\theta(t) = \omega_{sR} t + \frac{\Delta\omega_{sR}}{\omega_m} \sin \omega_m t + \theta_0$$

Letting the reference time be chosen such that $\theta_0 = 0$, and incorporating (B-17), (B-15) becomes

$$f_{sb}(t) = A \cos \left[\omega_{sR} t + \frac{\Delta\omega_{sR}}{\omega_m} \sin \omega_m t \right] \quad (B-18a)$$

in other words, the angular velocity is equal to the rate of change of the angle. Consider the angular velocity as

$$\dot{\theta}(t) = A \cos \omega t \quad (8-12)$$

By definition $\frac{d\theta}{dt} = \dot{\theta}$

$$\text{or } \theta(t) = \int A \cos \omega t \, dt$$

If the angular frequency ω is constant, then

$$\theta(t) = \omega t + \theta_0$$

and (8-12) becomes the constant term θ_0

$$\dot{\theta}(t) = A \cos(\omega t + \theta_0)$$

However, (8-12) indicates that θ_0 is constant

Therefore (8-12) can be written as (8-13)

$$\theta(t) = \int A \cos(\omega t + \theta_0) \, dt$$

or

$$\theta(t) = \frac{A}{\omega} \sin(\omega t + \theta_0)$$

Setting the reference time as $\theta_0 = 0$ and

incorporating (8-13) into (8-12) becomes

$$\dot{\theta}(t) = A \cos \left[\omega t + \theta_0 \right]$$

This is the expression for frequency modulation (FM) in which

$$\Delta\omega_{sR} - \text{the deviation} \quad (\text{B-18b})$$

and

$$\frac{\Delta\omega_{sR}}{\omega_m} = \beta - \text{the modulation index} . \quad (\text{B-18c})$$

Voltage Output During Playback

The instantaneous output voltage from the playback head is

$$e_o = -N \frac{d\phi}{dt} . \quad (\text{B-19})$$

The flux on the tape is distributed according to

$$\phi_T = \Phi \cos 2\pi f_s t \quad (\text{B-20})$$

since it is due to the flux in the gap (B-1). On playback then

$$e_o = N \Phi 2\pi f_{sb} \sin 2\pi f_{sb} t \quad (\text{B-21a})$$

or using (B-19)

$$e_o = N \Phi 2\pi \frac{v_{Tb}}{\lambda_t} \sin 2\pi \frac{v_{Tb}}{\lambda_T} t . \quad (\text{B-21b})$$

Figure B5 shows the variation of e_o due to f_{sb} or v_{Tb} .

Although the curve drops off at the higher frequencies due to losses, it is linear in the frequency range of concern.

Thus both magnitude and frequency of e_o are functions of

v_{Tb} . However, since NARTB equalization keeps $|e_o|$ constant, only the frequency of e_o changes with v_{Tb} .

This is the expression for frequency modulation (FM).

where

$$\Delta f_m = \text{the deviation} \quad (B-18c)$$

and

$$\frac{\Delta f_m}{f_m} = \beta = \text{the modulation index} \quad (B-18d)$$

Voltage Output During Playback

The instantaneous output voltage from the playback

head is

$$e_o = \frac{d\phi}{dt} \quad (B-19)$$

The flux in the tape is distributed according to

$$\phi_T = \phi_m \cos 2\pi f_c t \quad (B-20)$$

since it is due to the flux in the gap (B-1). On playback

then

$$e_o = N \frac{d\phi_T}{dt} \sin 2\pi f_c t \quad (B-21a)$$

or using (B-19)

$$e_o = N \frac{V_T}{\lambda} \sin 2\pi \frac{V_T}{\lambda} t \quad (B-21b)$$

Figure B5 shows the variation of e_o due to f_c or V_T .

Although the curve drops off at the higher frequencies due

to losses, it is linear in the frequency range of concern.

Thus both magnitude and frequency of e_o are functions of

V_T . However, since NARRB equalization keeps $|e_o|$ constant

only the frequency of e_o changes with V_T .

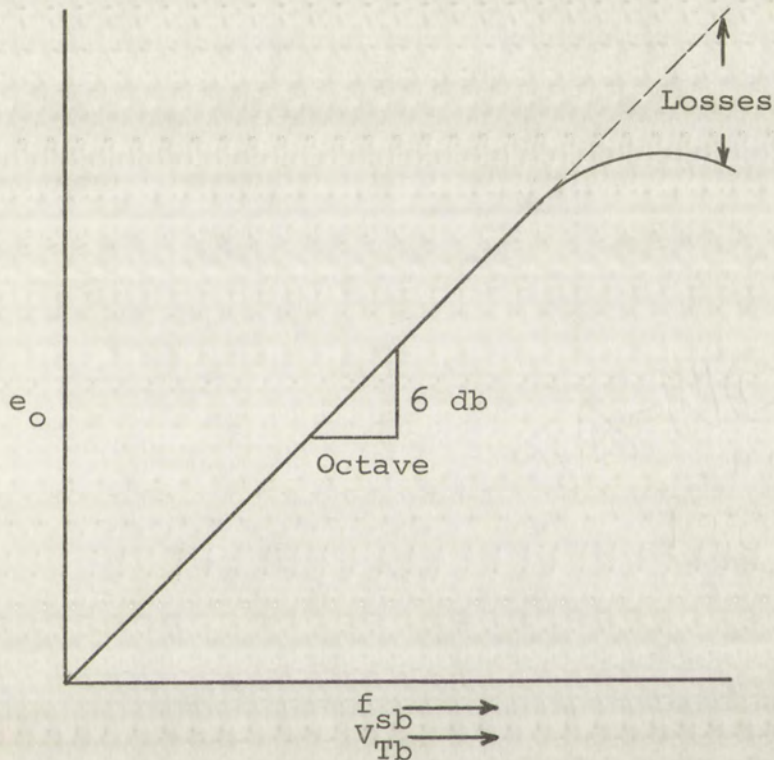


Figure B5 Output voltage versus tape playback speed

Analysis of Velocity Variations During Playback

Under idealized conditions the recording and playback velocities are identical; and therefore, the input and output frequencies are equal. Under these conditions assume a perfectly symmetric capstan pulls the tape at 7.5 ips. If the radius of the capstan is 0.5 in., then the angular velocity will be

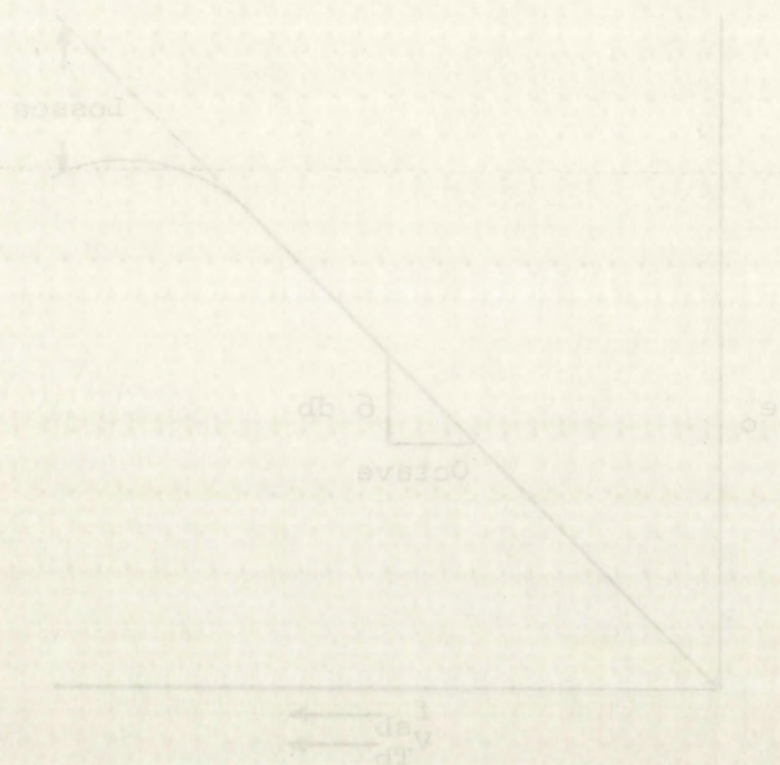


Figure B5
Output voltage versus tape
playback speed

Analysis of Velocity Variations During Playback

Under idealized conditions the recording and playback velocities are identical; and therefore, the input and output frequencies are equal. Under these conditions assume a perfectly symmetric capacitor pulsed the tape at 1.5 ips. If the radius of the capacitor is 0.5 in., then the angular velocity will be

$$\omega_m = \frac{v_{\text{Tangent}}}{r} = \frac{7.5}{0.5} = 15 \text{ rad/sec.} \quad (\text{B-22})$$

or the frequency will be

$$f_m = \frac{15}{2\pi} = 2.4 \text{ cps.} \quad (\text{B-23})$$

Now we assume that a perfect tape recorded at 7.5 ips, is played back with a non-symmetric capstan (Figure B6).

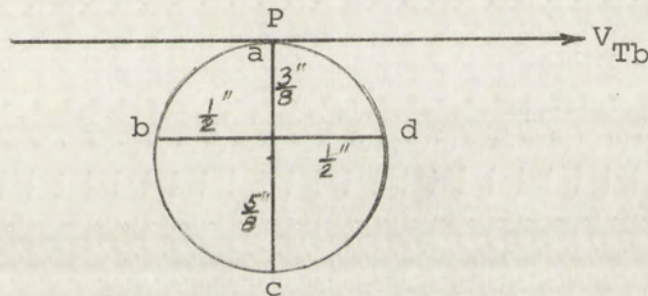


Figure B6 A non-symmetric capstan

Since no other defect is assumed, the angular velocity of this non-symmetric capstan is also 15 rad/sec. The tangential velocity or tape velocity is directly proportional to the radius,

$$v_{Tb} = \omega_m r. \quad (\text{B-24})$$

Figure B6 shows that

$$v_{Tb}(a) = 15\left(\frac{3}{8}\right) = 5.6 \text{ ips.} \quad (\text{B-25a})$$

$$\omega = \frac{v_{\text{transmit}}}{r} = \frac{1.5}{0.1} = 15 \text{ rad/s}$$

or the frequency will be

$$f_m = \frac{\omega}{2\pi} = \frac{15}{2\pi} = 2.4 \text{ cps}$$

Now we assume that a perfect tone is heard at 2.4 cps.

is played back with a non-symmetrical capacitor (Figure 1)



Figure 86. A non-symmetrical capacitor.

Since no other defect is assumed, the angular velocity of this non-symmetrical capacitor is assumed to be constant. The tangential velocity at the surface is directly proportional to the radius.

$$v_{\text{TP}} = \omega r$$

Figure 86 shows that

$$v_{\text{TP}}(a) = 15 \left(\frac{1}{2} \right) = 7.5 \text{ in/s}$$

when point "a" is in contact with the tape at "P." In a similar manner, as the capstan rotates,

$$v_{Tb}(b) = 15\left(\frac{1}{2}\right) = 7.5 \text{ ips}, \quad (\text{B-25b})$$

$$v_{Tb}(c) = 15\left(\frac{5}{8}\right) = 9.4 \text{ ips}, \quad (\text{B-25c})$$

$$v_{Tb}(d) = 15\left(\frac{1}{2}\right) = 7.5 \text{ ips}, \quad (\text{B-25d})$$

Thus the tape velocity varies about the correct velocity (7.5 ips) periodically at a frequency of 2.4 cps (B-23) and amplitude of 1.9 ips (Figure B7).

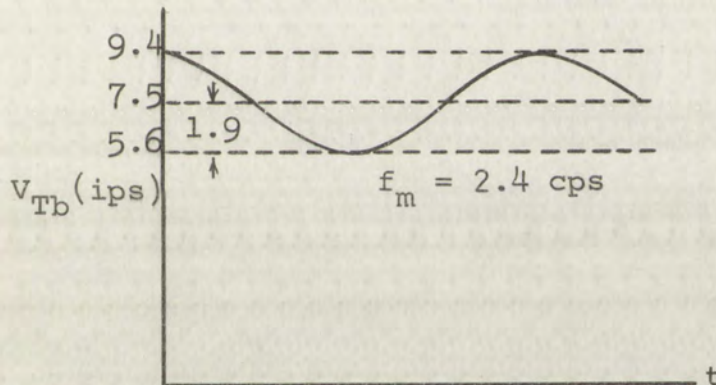


Figure B7 Tape playback speed versus time with non-symmetric capstan

From relation (B-10), we know that the output frequency (f_{sb}) is directly proportional to the tape velocity in playback (v_{Tb}) since the wavelength on the tape (λ_t) is fixed. Assuming a 1000 cps recording frequency with tape velocity of 7.5 ips., the tape wavelength is

When point "a" is in contact with the tape at "P", it is in a similar manner, as the capacitor rotates.

$$V_{TP}(a) = 15\left(\frac{1}{2}\right) = 7.5 \text{ ips}$$

$$V_{TP}(c) = 15\left(\frac{2}{3}\right) = 10 \text{ ips}$$

$$V_{TP}(d) = 15\left(\frac{1}{2}\right) = 7.5 \text{ ips}$$

Thus the tape velocity varies about the correct velocity (7.5 ips) periodically as a function of θ cps (5-10) and amplitude of 1.9 ips (Figure 8).

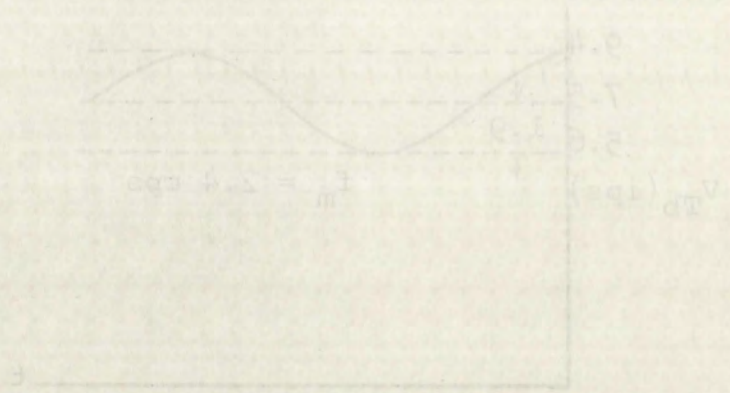


Figure 8. Tape playback speed versus time with non-symmetric capacitor

From relation (5-10), we know that the output frequency (f_{sp}) is directly proportional to the tape velocity in playback (v_{sp}) since the wavelength on the tape (λ_s) is fixed. Assuming a 1000 cps recording frequency with tape velocity of 7.5 ips, the tape wavelength is

$$\lambda_T = \frac{v_{TR}}{f_{sR}} = \frac{7.5}{10^3} = 7.5(10^{-3}) \text{ in.} \quad (\text{B-26})$$

Upon playback

$$f_{sb} = \frac{v_{Tb}}{\lambda_T} = \frac{v_{Tb}}{7.5(10^{-3})} \quad (\text{B-27})$$

The results using this relation and the values of v_{Tb} (Figure B7) are shown in Table B-I.

v_{Tb} (ips)	f_{sb} (cps)
9.4	1260
7.5	1000
5.6	740
1.9	260

Table B-I Signal frequencies at various tape speeds during playback

The output frequency (f_{sb}) varies periodically at a frequency of 2.4 cps and amplitude of 260 cps.

Figure B8 shows the correspondence indicated in Table B-I.

The frequency (f_{sb}) and velocity (v_{Tb}) axis are scaled to include the λ_T factor.

$$\lambda_T = \frac{v_{TB}}{f_{sb}} = \frac{1.5}{7.5(10^{-5})} = 2 \times 10^4 \text{ in.} \quad (B-26)$$

Upon playback

$$f_{sb} = \frac{v_{TB}}{\lambda_T} = \frac{1.5}{2 \times 10^4} = 7.5(10^{-5}) \quad (B-27)$$

The results using this relation and the values of v_{TB} (Figure B7) are shown in Table B-1.

v_{TB} (ips)	f_{sb} (cps)
2.4	1250
1.5	1000
1.6	740
1.9	260

Table B-1 Signal frequencies at various tape speeds during playback

The output frequency (f_{sb}) varies periodically at

a frequency of 2.4 cps and amplitude of 260 cps.

Figure B8 shows the correspondence indicated in Table B-1.

The frequency (f_{sb}) and velocity (v_{TB}) axis are scaled

to include the λ_T factor.

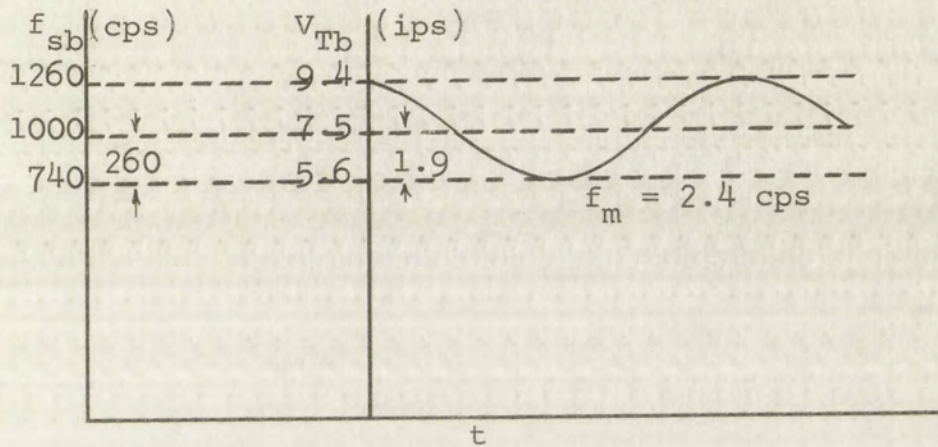


Figure B8 Tape speed and signal frequency versus time during playback

Considering the change in velocity and frequency we have from (B-27)

$$\Delta f_{sb} = \frac{\Delta v_{Tb}}{\lambda_T} . \quad (\text{B-28})$$

From (B-7) and (B-8), we have

$$\lambda_T = \frac{v_{TR}}{f_{sR}} . \quad (\text{B-29})$$

Substituting (B-29) into (B-28) gives

$$\frac{\Delta f_{sb}}{f_{sR}} = \frac{\Delta v_{Tb}}{v_{TR}} , \quad (\text{B-30})$$

which says that the percentage change in the output frequency is equal to the percentage change in the tape velocity. This expression (B-30) is general in that it



Figure 88 Tape speed and 1000 cps

Considering the circuit in Figure 87, we have

from (B-57)

$$\Delta f_{sb} = \frac{\Delta v_{Tp}}{v_T}$$

from (B-7) and (B-8), we have

$$v_T = \frac{v_{TR}}{f_R}$$

Substituting (B-29) into (B-8) or

$$\Delta f_{sb} = \frac{\Delta v_{Tp}}{v_{TR}} \cdot f_R$$

which says that the percent change in the output frequency is equal to the percent change in the tape velocity. This expression

says nothing concerning the cause of the varying tape velocity.

In arriving at (B-30), we assumed a non-symmetric capstan. We shall therefore determine the percentage of frequency change in terms of capstan asymmetry. Considering a change in velocity due to asymmetry, relation (B-24) becomes

$$\Delta v_{Tb} = \omega_m \Delta r \quad (B-31)$$

since ω is constant. Substituting (B-24) into (B-31) we have

$$\frac{\Delta v_{Tb}}{v_{TR}} = \frac{\Delta r}{r} \quad (B-32)$$

which from (B-30) gives

$$\frac{\Delta f_{sb}}{f_{sR}} = \frac{\Delta r}{r} . \quad (B-33)$$

says nothing concerning the cause of the varying type

velocity.

In arriving at (B-50), we assumed a non-symmetric

capstan. We shall therefore determine the percentage of

frequency change in terms of capstan asymmetry. Con-

sidering a change in velocity due to asymmetry, relation

(B-24) becomes

$$\Delta v_{Tp} = \omega \Delta r \quad (B-51)$$

since ω is constant. Substituting (B-24) into (B-51) we

have

$$\frac{\Delta v_{Tp}}{v_{Tp}} = \frac{\Delta r}{r} \quad (B-52)$$

which from (B-50) gives

$$\frac{\Delta f_{sp}}{f_{sp}} = \frac{\Delta r}{r} \quad (B-53)$$

Appendix C

Modulation

Single-ended Switching

A mechanical or electromechanical switch can be represented by¹

$$s(t) = \frac{1}{2} + \sum_{\substack{n=1 \\ (\text{odd})}}^{\infty} \frac{\sin \frac{n\pi}{2}}{n\frac{\pi}{2}} \cos n\omega_c t \quad (\text{C-1})$$

This switching function operating on some signal, e_i , produces an output shown in Figure C1.

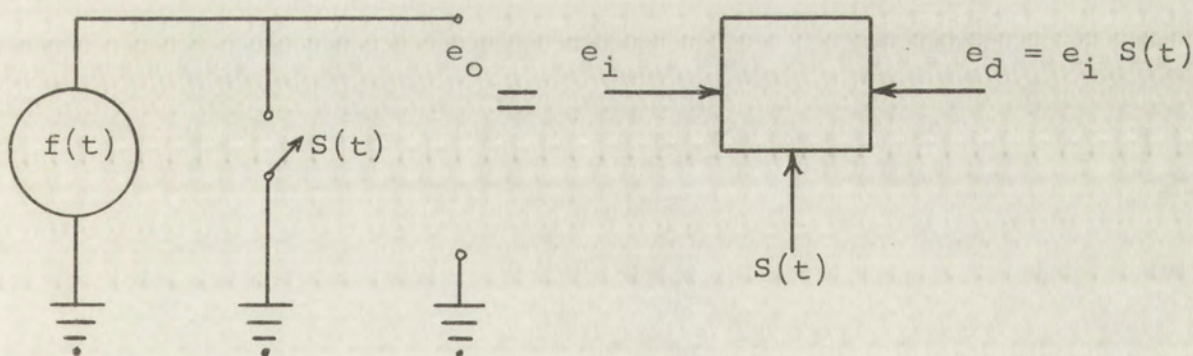


Figure C1 Single-ended switching

¹Schwartz, Mischa, Information Transmission, Modulation, and Noise, McGraw-Hill Book Company, Inc., 1959.

Figure C1 Single-ended switching



This switching function operating on some signal, e_i , produces an output shown in Figure C1.

$$s(t) = \frac{1}{2} + \sum_{n=1}^{\infty} \frac{\sin \frac{n\pi}{2}}{n\pi/2} \cos n\pi t \quad (C-1)$$

represented by

A mechanical or electromechanical switch can be

single-ended switching

Modulation

Appendix C

Assuming

$$e_i = a \cos \omega_m t \quad (C-2)$$

$$e_d = e_i S(t) = a \cos \omega_m t \left[\frac{1}{2} + \sum_{\substack{n=1 \\ \text{(odd)}}}^{\infty} \frac{\sin \frac{n\pi}{2}}{\frac{n\pi}{2}} \cos n\omega_c t \right] \quad (C-3)$$

where ω_m is the signal or modulating frequency and ω_c is the switching or carrier frequency. Expanding (C-3) and explicitly showing the "n = 1" term

$$\begin{aligned} e_d = & \frac{a}{2} \cos \omega_m t + \frac{2a}{\pi} \cos \omega_m t \cos \omega_c t \\ & + a \cos \omega_m t \sum_{\substack{n=3 \\ n \text{ odd}}}^{\infty} \frac{\sin \frac{n\pi}{2}}{\frac{n\pi}{2}} \cos n\omega_c t \end{aligned} \quad (C-4)$$

Substituting the trigonometric equivalence for the second term and letting

$$\frac{a}{2} = A \quad \text{and} \quad \frac{a}{\pi} = B, \quad (C-5)$$

equation (C-4) becomes

$$\begin{aligned} e_d = & A \cos \omega_m t + B \left[\cos (\omega_c + \omega_m)t + \cos (\omega_c - \omega_m)t \right] \\ & + a \cos \omega_m t \sum_{\substack{n=3 \\ n \text{ odd}}}^{\infty} \frac{\sin \frac{n\pi}{2}}{\frac{n\pi}{2}} \cos n\omega_c t. \end{aligned} \quad (C-6)$$

The original signal or data occupies its original position in the spectrum and in addition also becomes side bands about odd harmonics of the switching frequency.

Assuming

$$e_d = a \cos \omega_m t \quad (C-2)$$

$$e_d = a_1 s(t) = a \cos \omega_m t \left[\frac{1}{2} + \sum_{n=1}^{\infty} \frac{\sin \frac{n\pi}{2}}{\frac{n\pi}{2}} \cos n\omega_c t \right] \quad (C-3)$$

where ω_m is the signal or modulating frequency and ω_c is the switching or carrier frequency. Expanding (C-3) and explicitly showing the " $n = 1$ " term

$$e_d = \frac{a}{2} \cos \omega_m t + \frac{a}{\pi} \cos \omega_m t \cos \omega_c t + \sum_{n=2}^{\infty} \frac{\sin \frac{n\pi}{2}}{\frac{n\pi}{2}} \cos n\omega_c t \cos \omega_m t \quad (C-4)$$

Substituting the trigonometric equivalence for the second term and letting

$$\frac{a}{2} = A \quad \text{and} \quad \frac{a}{\pi} = B, \quad (C-5)$$

equation (C-4) becomes

$$e_d = A \cos \omega_m t + B \left[\cos (\omega_c + \omega_m) t + \cos (\omega_c - \omega_m) t \right] + \sum_{n=2}^{\infty} \frac{\sin \frac{n\pi}{2}}{\frac{n\pi}{2}} \cos n\omega_c t \cos \omega_m t \quad (C-6)$$

The original signal or data occupies its original position in the spectrum and in addition also becomes side bands about odd harmonics of the switching frequency.

The switching frequency and its harmonics are not present. This is double side band (DSB) modulation or carrier suppressed modulation. See Figure C2.

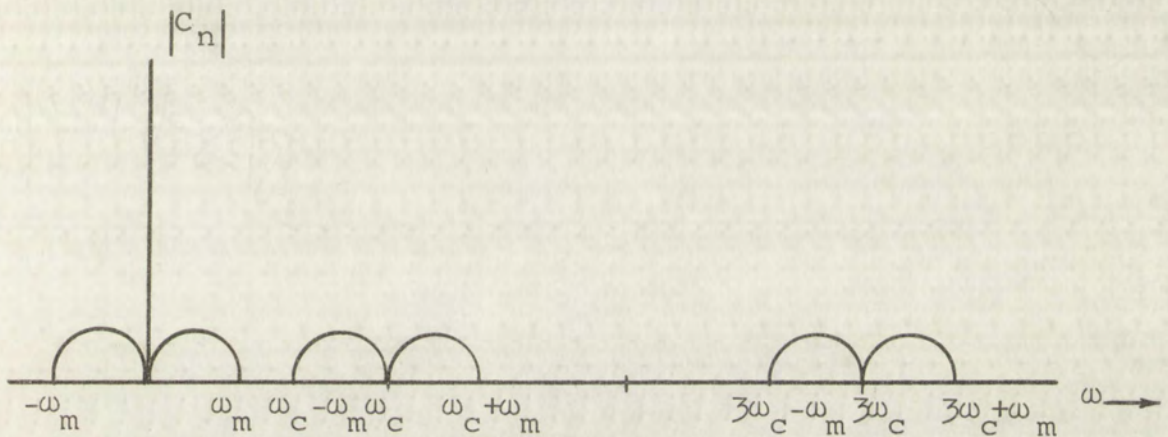


Figure C2 Spectrum of single-ended switching

It is evident from Figure C2 that filtering is made easier by increasing ω_c . Distortion occurs if $\omega_c - \omega_m < \omega_m$. Thus the minimum tolerable ω_c occurs when

$$\omega_c - \omega_m = \omega_m$$

or

$$\omega_c = 2\omega_m.$$

(C-7)

The switching frequency and its harmonics are not present.
 This is double side band (DSB) modulation or carrier
 suppressed modulation. See Figure C2.



Figure C2 Spectrum of single-ended switching

It is evident from Figure C2 that filtering is made
 easier by increasing ω_c . Distortion occurs if
 $\omega_c - \omega_m < \omega_m$. Thus the minimum tolerable ω_c occurs when

$$\omega_c - \omega_m = \omega_m$$

or

$$\omega_c = 2\omega_m$$

(C-7)

Note here that $f(t)$ has no d-c bias term. In addition, equation (C-4) and (C-6) show that the side bands are generated by the product term $\cos \omega_m t \cos \omega_c t$ which is basically

$$e_i \times \cos \omega_c t . \quad (C-8)$$

The response (assuming 100 to 4000 cps) of the tape recorder automatically filters out the ω_m (0-50 cps) in the spectrum. The fact that this occurs is the sole basis for considering switching in the first place. The frequencies above 4,000 cps are also filtered out. As a result the data actually recorded upon the tape will have the spectrum shown in Figure C3.

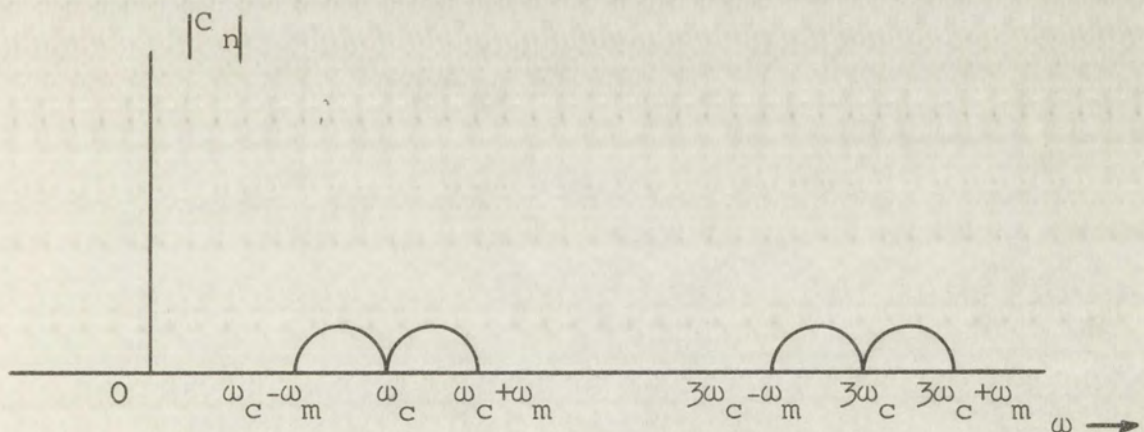


Figure C3 Spectrum of single-ended switching after filtering by tape recorder

Since the 3rd harmonics are not of interest and only complicate subsequent developments, we consider

$$e_d = B \left[\cos (\omega_c + \omega_m)t + \cos (\omega_c - \omega_m)t \right] \quad (C-9)$$

and consider only the spectrum as shown in Figure C4.

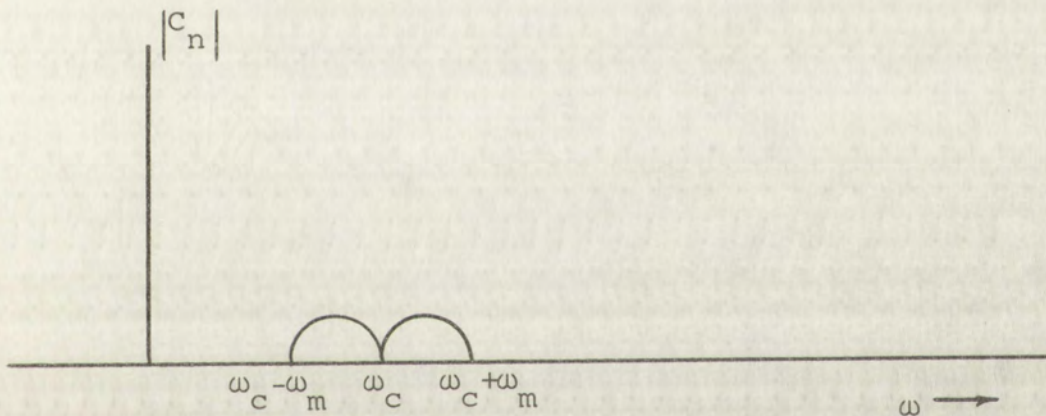


Figure C4 Spectrum of single-ended switching
used for analysis

$$e_1 = \left[\cos \left(\frac{\omega}{\omega_0} t + \cos \left(\frac{\omega}{\omega_0} t \right) \right] \right]$$

and consider only the spectrum as shown in Figure 24.



Figure 24 Spectrum of single-ended switching used for analysis

Bi-polar Switching

Bi-polar switching which is depicted in Figure C5 has a switching function $S(t)$ which is balanced with respect to ground as shown in Figure C6.

From this

$$S(t) = 2 \sum_{\substack{n=1 \\ n \text{ odd}}}^{\infty} \frac{\sin \frac{n\pi}{2}}{\frac{n\pi}{2}} \cos n\omega_c t \quad (C-10)$$

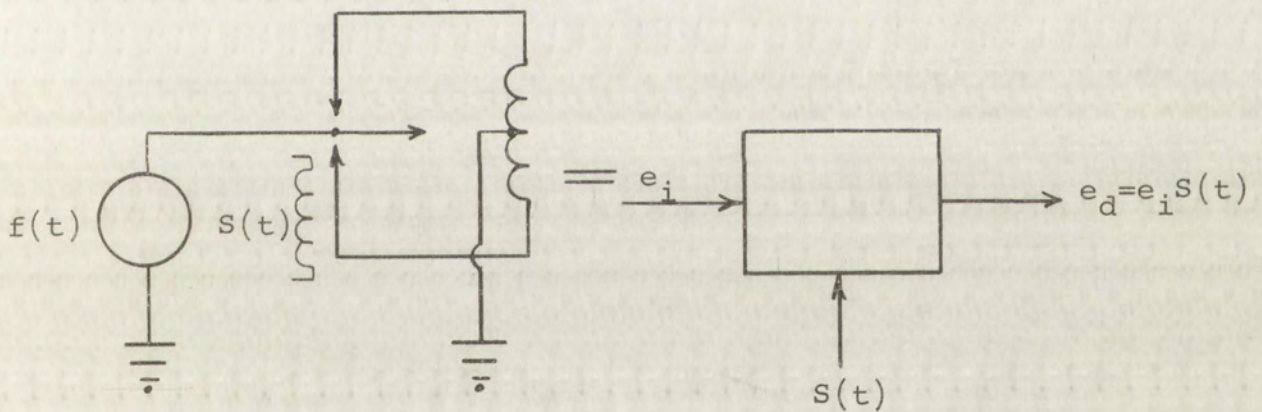


Figure C5 Bi-polar switching

Bi-polar Switching

Bi-polar switching which is depicted in Figure 65

has a switching function $S(t)$ which is balanced with

respect to ground as shown in Figure 66.

From this

$$S(t) = \sum_{n=0}^{\infty} \frac{S_n}{n!} \cos n\omega t$$

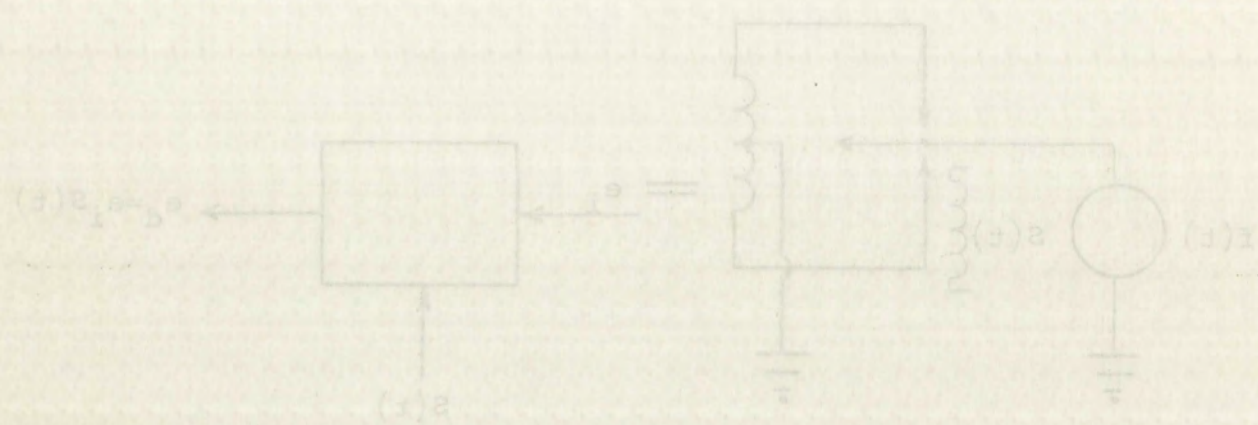


Figure 65 Bi-polar switching

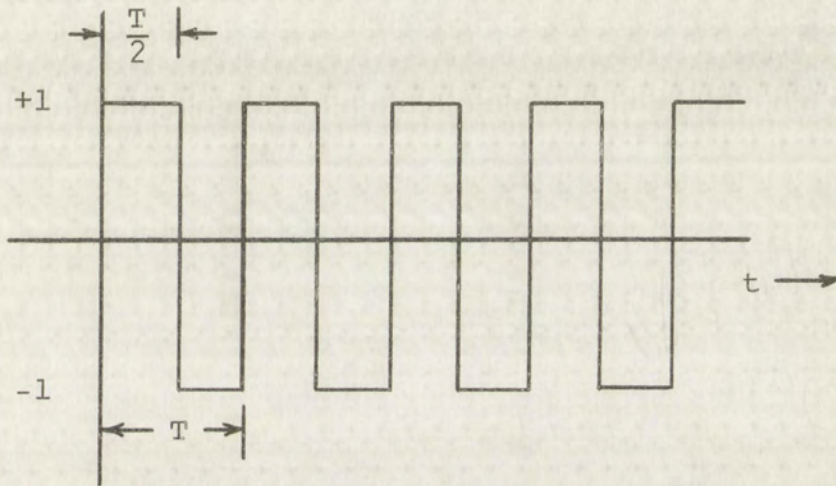


Figure C6 Bi-polar switching function

and assuming $e_i = a \cos \omega_m t$

$$e_d = a \cos \omega_m t \left[2 \sum_{\substack{n=1 \\ n \text{ odd}}}^{\infty} \frac{\sin \frac{n\pi}{2}}{\frac{n\pi}{2}} \cos n\omega_c t \right]$$

or

$$e_d = \frac{4a}{\pi} \cos \omega_m t \cos \omega_c t + a \cos \omega_m t \left[2 \sum_{\substack{n=3 \\ n \text{ odd}}}^{\infty} \frac{\sin \frac{n\pi}{2}}{\frac{n\pi}{2}} \cos n\omega_c t \right] \quad (\text{C-11})$$

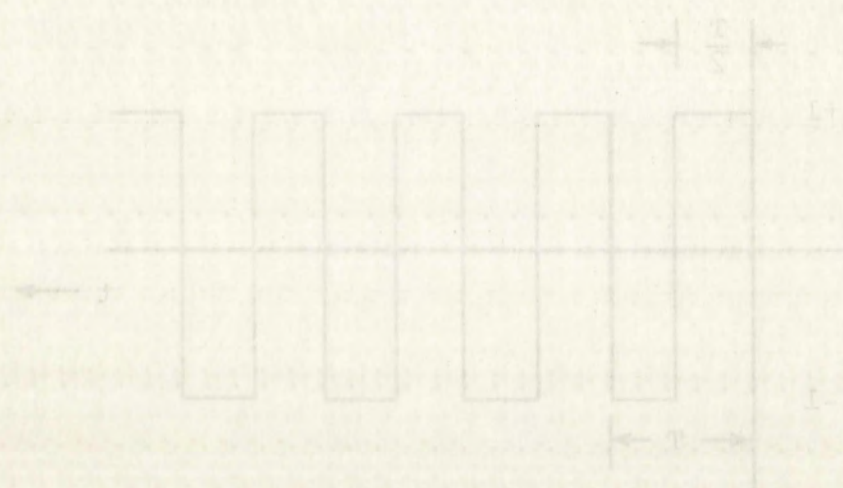


Figure 66 Bi-polar switching function

and assuming $e_1 = a \cos \omega_c t$

$$e_a = a \cos \omega_c t \left[\sum_{n=1}^{\infty} \frac{\sin \frac{n\pi}{2}}{\frac{n\pi}{2}} \cos n\omega_c t \right]$$

or

$$e_a = \frac{4a}{\pi} \cos \omega_c t \cos \omega_c t$$

$$e_a = \frac{4a}{\pi} \cos \omega_c t \left[\sum_{n=1}^{\infty} \frac{\sin \frac{n\pi}{2}}{\frac{n\pi}{2}} \cos n\omega_c t \right] \quad (C-11)$$

The spectrum, Figure C7, is identical with Figure C2, except the ω_m about zero is absent. This is due, of course, to the absence of the d-c term in $S(t)$ equation (C-10). The minimum ω_c occurs when

$$\omega_c - \omega_m = 0$$

or

(C-12)

$$\omega_c = \omega_m .$$

Since we are considering switching at 1 kc and have automatic filtering by the tape recorder, the difference in minimum switching rates and the presence or absence of ω_m spectrum at zero makes no difference here.

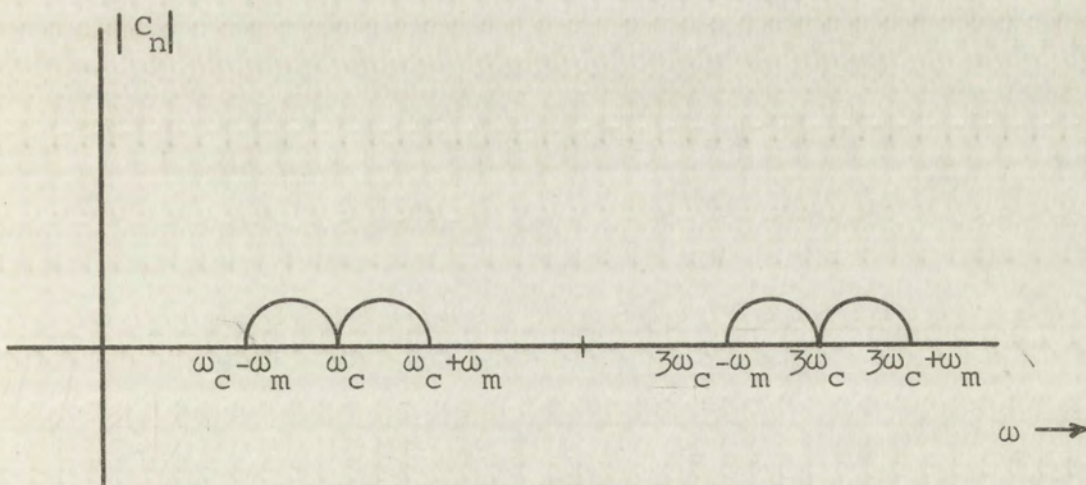


Figure C7 Spectrum of bi-polar switching

The spectrum, Figure C7, is identical with Figure C3.

except that the minimum occurs at $\omega = 0$, $\omega = \pm \omega_c$.

because of the absence of the δ -term in (5/c) equation.

(5-10). The minimum occurs when

$$\omega = 0, \omega = \pm \omega_c$$

or (C-12)

$$\omega = 0, \omega = \pm \omega_c$$

Since we are considering switching at 1 kc and have auto-

matic filtering by the tape recorder, the difference in

minimum switching rates and the presence or absence of

a spectrum at zero makes no difference here.

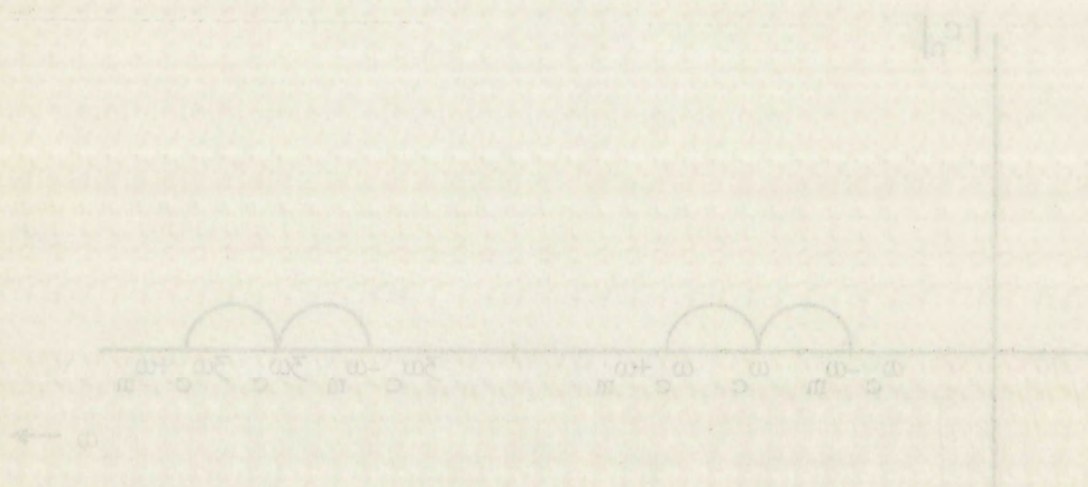


Figure C7 - Spectrum of bi-polar switching

Single-ended switching appears the simpler of the two, particularly so, if further inquiry indicates that complete carrier suppression is unnecessary. Bi-polar switching would necessitate exact balancing and, of course, would complicate construction and adjustments.

In this discussion of the two forms of switching, the analysis assumed no d-c bias on the switching device. This, of course, is easily obtainable with reed-type of mechanical switches. However, the upper frequency limit of these switches is far short of 1 kc. To satisfy other requirements, such as portability, lightweight, low battery drain, etc., some form of transistor switching would be desirable.

The typical circuit configuration shown in Figure C8 will now be analyzed. The signal input e_i fluctuates about a positive potential. The connections are made so that

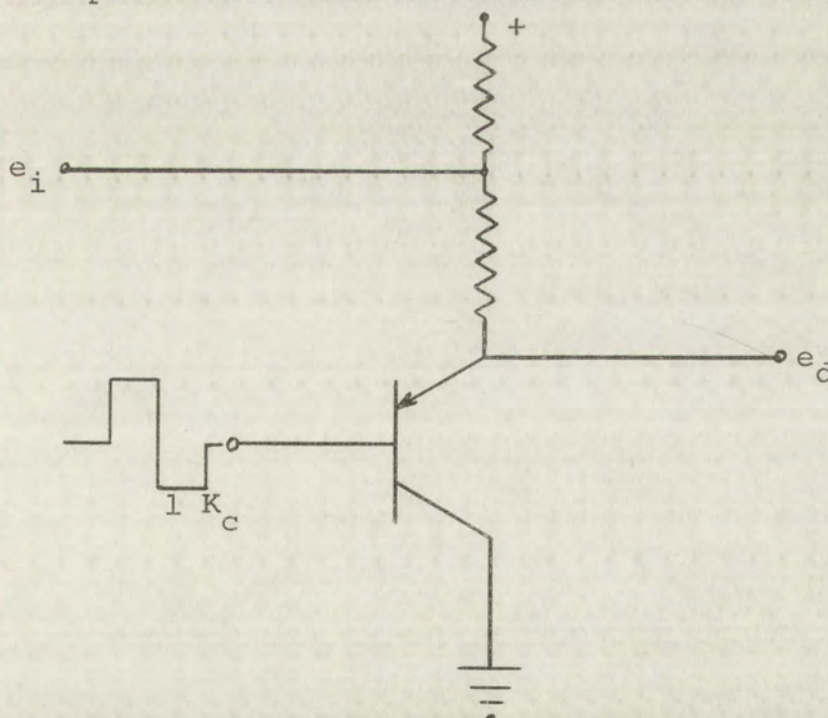


Figure C8 Transistor switch

single-ended signal appears the signal of the
 but, particularly, as it further inquiry indicates that
 complete carrier suppression is unnecessary. Bi-polar
 switching would necessitate exact balancing and of
 course, would complicate construction and adjustment.
 In this discussion of the two forms of switching,
 the analysis assumed no d-c bias on the switching device.
 This, of course, is easily obtainable with fixed-type of
 mechanical switches. However, the upper frequency limit
 of these switches is far short of 1 Mc. To satisfy other
 requirements, such as portability, lightweight, low battery
 drain, etc., some form of transistor switching would be
 desirable.

The typical circuit configuration shown in Figure C8
 will now be analyzed. The signal input e_i fluctuates about
 a positive potential. The connections are made so that

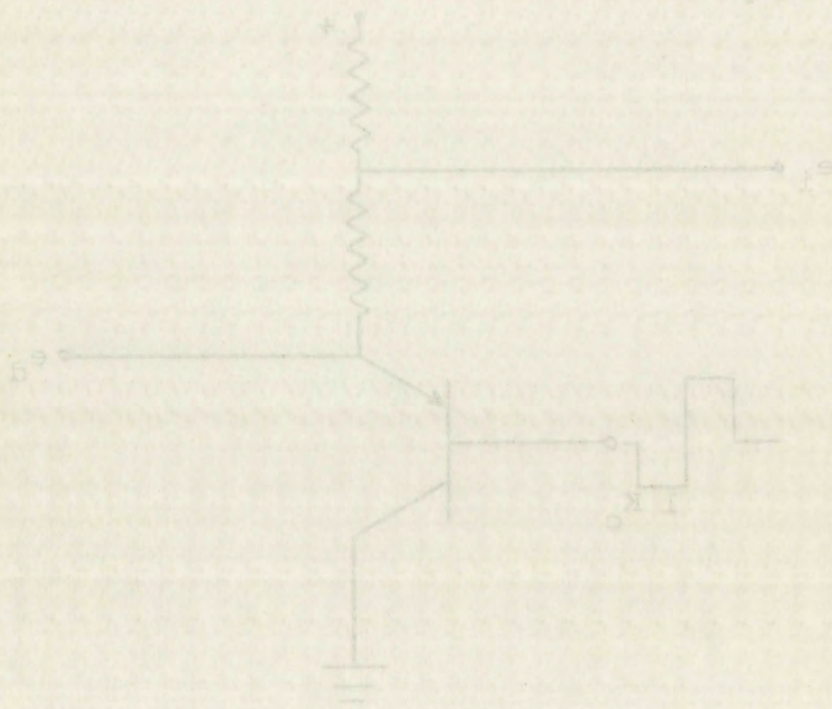


Figure C8 Transistor switch

both positive and negative excursions are preserved. The switching effect in the presence of the d-c bias can be symbolized as shown in Figure C9.

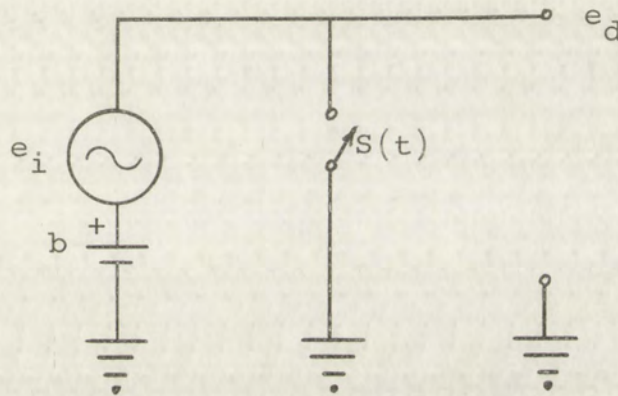


Figure C9 Equivalent circuit for transistor switch

The output voltage then is

$$e_d = [b + e_i] S(t) \quad (C-13)$$

or with $e_i = a \cos \omega_m t$

$$e_d = \left[b + a \cos \omega_m t \right] \left[\frac{1}{2} + \sum_{\substack{n=1 \\ n \text{ odd}}}^{\infty} \frac{\sin \frac{n\pi}{2}}{\frac{n\pi}{2}} \cos n\omega_c t \right]. \quad (C-14)$$

Expanding (C-14) and showing the "n = 1" terms explicitly

both positive and negative excursions are preserved. The switching effect in the presence of the d-c bias can be symbolized as shown in Figure C9.

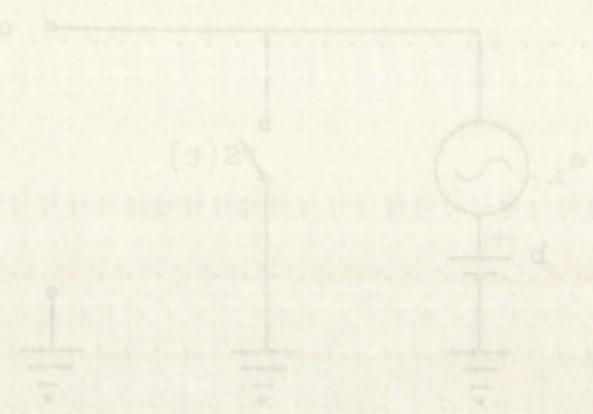


Figure C9. Equivalent circuit for transistor switch

The output voltage then is

(C-13)
$$e_2 = d + e_1 S(t)$$

or with $e_1 = a \cos \omega t$

(C-14)
$$e_2 = d + a \cos \omega t \left[\frac{1}{2} + \sum_{n=1, \text{ odd}}^{\infty} \frac{\sin \frac{n\pi}{2}}{\frac{n\pi}{2}} \cos n\omega t \right]$$

Expanding (C-14) and showing the "n = 1" terms explicitly

gives

$$e_d = \frac{b}{2} + \frac{a}{2} \cos \omega_m t + \frac{2b}{\pi} \cos \omega_c t + \frac{2a}{\pi} \cos \omega_m t \cos \omega_c t + \left[b + a \cos \omega_m t \right] \sum_{\substack{n=3 \\ n \text{ odd}}}^{\infty} \frac{\sin \frac{n\pi}{2}}{\frac{n\pi}{2}} \cos n\omega_c t. \quad (C-15)$$

The d-c term is removed by coupling capacitor and the original data term (2nd term) plus higher ordered terms will be filtered out by the tape recorder. So essentially, (ignoring the 3rd harmonic and side bands) the spectrum recorded on the tape will be

$$e_d = \frac{2b}{\pi} \cos \omega_c t + \frac{2a}{\pi} \cos \omega_m t \cos \omega_c t \quad (C-16)$$

as shown in Figure C10.

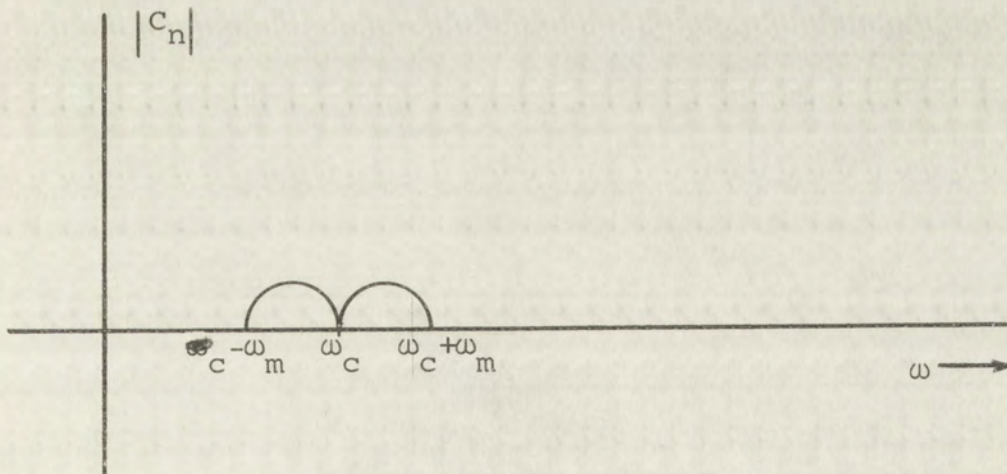


Figure C10 Spectrum of transistor switch after filtering by tape recorder

gives

$$e_0 = \frac{1}{2} + \frac{1}{2} \cos \omega_c t + \frac{1}{2} \cos \omega_c t + \frac{1}{2} \cos \omega_c t + \dots$$

$$+ \left[\frac{1}{2} + \frac{1}{2} \cos \omega_c t \right] \sum_{n=1}^{\infty} \frac{1}{n} \cos n \omega_c t \quad (C-12)$$

The δ -c term is removed by coupling capacitor and the original δ -c term (2nd term) plus higher order terms will be filtered out by the tape recorder. So essentially (ignoring the 2nd harmonic and side bands) the spectrum recorded on the tape will be

$$e_0 = \frac{1}{2} \cos \omega_c t + \frac{1}{2} \cos \omega_c t + \dots$$

as shown in Figure C10.



Figure C10. Spectrum of transmitter switch after filtering by tape recorder.

This is, of course, Amplitude Modulation (AM). The carrier, $\cos \omega_c t$, is due to the d-c bias.

One way of securing DSB modulation would be to place two such circuits as shown in Figure C8 in push-pull with transformer coupled input and output balanced to ground. This complicates the circuitry, adds to the cost, and adds to the weight.

Demodulation

Demodulation of AM modulation by switching on tape playback is now considered. A circuit identical to Figure C8 is used as the demodulator.

From equation (C-16) the output of the tape recorder will be

$$e'_d = \frac{2b}{\pi} \cos \omega'_c t + \frac{2a}{\pi} \cos \omega'_m t \cos \omega'_c t \quad (C-17)$$

where $\omega'_m \neq \omega_m$ and $\omega'_c \neq \omega_c$ due to variations in tape speed. The switching function has the same frequency (ω_c) as during modulation. Considering Figure C9, e_i is now e_d and e_d becomes e_o . Therefore

$$e_o = \left[b + e_d \right] S(t) = \left[b + \frac{2b}{\pi} \cos \omega'_c t + \frac{2a}{\pi} \cos \omega'_m t \cos \omega'_c t \right] \left[\frac{1}{2} + \sum_{\substack{n=1 \\ n \text{ odd}}}^{\infty} \frac{\sin \frac{n\pi}{2}}{\frac{n\pi}{2}} \cos n\omega_c t \right] \quad (C-18)$$

This is, of course, Amplitude Modulation (AM). The carrier $\cos \omega_c t$ is due to the B-C bias.

One way of securing DSB modulation would be to place two such circuits as shown in Figure 18 in push-pull with transformer coupled input and output balanced to ground. This complicates the circuitry, adds to the cost, and

adds to the weight.

Demodulation

Demodulation of AM modulation by switching on tape playback is now considered. A circuit identical to Figure 18 is used as the demodulator. From equation (C-16) the output of the tape recorder will be

$$e_d = \frac{2b}{\pi} \cos \omega_c t + \frac{2a}{\pi} \cos \omega_m t \cos \omega_c t \quad (C-17)$$

where $\omega_m \ll \omega_c$ and $\omega_c \approx \omega_c$ due to variations in tape

speed. The switching function has the same frequency ω_c as during modulation. Considering Figure 18, e_d is now e_o and e_g becomes e_o . Therefore

$$e_o = \left[b + a_d \right] \sum_{n=1}^{\infty} \frac{\sin \frac{n\pi}{2}}{\frac{n\pi}{2}} \cos n\omega_c t + \cos \omega_c t \left[\frac{1}{2} + \sum_{n=1}^{\infty} \frac{\sin \frac{n\pi}{2}}{\frac{n\pi}{2}} \cos n\omega_c t \right] \quad (C-18)$$

and expanding

$$\begin{aligned}
 e_o = & \frac{b}{2} + \frac{b}{\pi} \cos \omega'_c t + \frac{a}{\pi} \cos \omega'_m t \cos \omega'_c t + \frac{2b}{\pi} \cos \omega_c t \\
 & + \frac{4b}{\pi} \cos \omega'_c t \cos \omega_c t + \frac{4a}{\pi^2} \cos \omega'_m t \cos \omega'_c t \cos \omega_c t \\
 & + \left[b + \frac{2b}{\pi} \cos \omega'_c t + \frac{2a}{\pi} \cos \omega'_m t \cos \omega'_c t \right] \\
 & \left[\sum_{\substack{n=3 \\ n \text{ odd}}}^{\infty} \frac{\sin \frac{n\pi}{2}}{\frac{n\pi}{2}} \cos n\omega_c t \right].
 \end{aligned} \tag{C-19}$$

Equation (C-18) shows that the $\cos \omega'_m t$ term, the recovered data, is not isolated.

We expand the sixth term of (C-19), which is the product term, for further consideration.

This term

$$\frac{4a}{\pi^2} \cos \omega'_m t \cos \omega'_c t \cos \omega_c t \tag{C-20}$$

gives

$$\frac{2a}{\pi^2} \cos \omega'_m t \left[\cos(\omega_c + \omega'_c)t + \cos(\omega_c - \omega'_c)t \right]$$

then

$$\frac{a}{\pi^2} \left[2 \cos \omega'_m t \left[\cos(\omega_c + \omega'_c)t \right] + 2 \cos \omega'_m t \left[\cos(\omega_c - \omega'_c)t \right] \right]$$

and finally

$$\frac{a}{\pi^2} \left[\cos \left[(\omega_c + \omega'_c) + \omega'_m \right] t + \cos \left[(\omega_c + \omega'_c) - \omega'_m \right] t \right. \\ \left. + \cos \left[(\omega_c - \omega'_c) + \omega'_m \right] t + \cos \left[(\omega_c - \omega'_c) - \omega'_m \right] t \right] . \quad (C-21)$$

Now if $\omega'_c = \omega_c$, equation (C-21) becomes

$$\frac{a}{\pi^2} \left[\cos (2\omega'_c + \omega'_m) t + \cos (2\omega'_c - \omega'_m) t \right. \\ \left. + \cos \omega'_m t + \cos (-\omega'_m) t \right]$$

or

$$\frac{2a}{\pi^2} \cos 2\omega'_c t \cos \omega'_m t + \frac{2a}{\pi^2} \cos \omega'_m t . \quad (C-22)$$

With filtering, equation (C-19) reduces to

$$e_o = \frac{2a}{\pi^2} \cos \omega'_m t \quad (C-23)$$

which is the recovered data. Equation (C-23) came from (C-20) with $\omega'_c = \omega_c$ and with filtering. The assumption $\omega'_c = \omega_c$ implies $\omega'_m = \omega_m$. Therefore equation (C-23), the recovered data, is the same as the recorded data. Equation (C-20) is the only term of consequence, the product term, in (C-19). Since $\omega'_c = \omega_c$ and $\omega'_m = \omega_m$, equation (C-20) can be written symbolically

$$e_o = \cos \omega_m t \cos \omega_c t \cos \omega_c t. \quad (C-24)$$

Recalling that the original data was

$$e_i = \cos \omega_m t \quad (C-25)$$

$$\begin{aligned} \left[\cos \left(\omega_c' + \omega_m' \right) + \cos \left(\omega_c' - \omega_m' \right) \right] e &= \left[\cos \left(\omega_c' + \omega_m' \right) + \cos \left(\omega_c' - \omega_m' \right) \right] e \\ \left[\cos \left(\omega_c' + \omega_m' \right) + \cos \left(\omega_c' - \omega_m' \right) \right] e &= \left[\cos \left(\omega_c' + \omega_m' \right) + \cos \left(\omega_c' - \omega_m' \right) \right] e \end{aligned} \quad (C-21)$$

Now if $\omega_c' = \omega_m'$, equation (C-21) becomes

$$\left[\cos \left(2\omega_m' \right) + \cos \left(0 \right) \right] e = \left[\cos \left(2\omega_m' \right) + \cos \left(0 \right) \right] e$$

or

$$\cos \left(2\omega_m' \right) + \cos \left(0 \right) = \cos \left(2\omega_m' \right) + \cos \left(0 \right)$$

With filtering, equation (C-19) reduces to

$$e_c = \frac{2e}{2} \cos \omega_m' t \quad (C-22)$$

which is the recovered data. Equation (C-22) came from (C-20) with $\omega_c' = \omega_m'$ and with filtering. The assumption $\omega_c' = \omega_m'$ implies $\omega_m' = \omega_c'$. Therefore equation (C-22) the recovered data is the same as the recorded data. Equation (C-20) is the only term of consequence, the product term, in (C-19). Since $\omega_c' = \omega_m'$ and $\omega_m' = \omega_c'$, equation (C-20) can be written symbolically

$$e_c = \cos \omega_m' t \cos \omega_m' t \quad (C-23)$$

Recalling that the original data was

$$e_1 = \cos \omega_m' t \quad (C-24)$$

equation (C-24) becomes

$$e_o = e_i \cos \omega_c t \cos \omega_c t \quad (C-26)$$

which is the product of the original data, modulation carrier, and demodulation carrier. Thus if the demodulating carrier has the same frequency as the modulating carrier the original data is recovered.

Now let the demodulation carrier differ from modulation carrier by the phase angle " θ ." Equation (C-26) becomes

$$e_o = e_i \cos \omega_c t \cos(\omega_c t + \theta) \quad (C-27)$$

or

$$e_o = \frac{e_i}{2} \left[\cos[\omega_c t + (\omega_c t + \theta)] + \cos[\omega_c t - (\omega_c t + \theta)] \right]$$

and

$$e_o = \frac{e_i}{2} \left[\cos(2\omega_c t + \theta) + \cos(-\theta) \right]$$

and finally

$$e_o = \frac{e_i}{2} \cos(2\omega_c t + \theta) + \frac{e_i}{2} \cos \theta. \quad (C-28)$$

After the usual filtering (C-28) reduces to

$$e_o = \frac{e_i}{2} \cos \theta \quad (C-29)$$

and from (C-25)

$$e_o = \frac{1}{2} \cos \omega_m t \cos \theta. \quad (C-30)$$

This shows that the recovered data is a function of phase difference between the modulating and demodulating carriers. If $\theta = \pi/2$, the data is, of course, lost.

equation (C-24) becomes

$$e_o = e_i \cos \omega_c t \cos \theta \quad (C-25)$$

which is the product of the original data, modulation carrier, and demodulation carrier. Thus if the demodulation carrier has the same frequency as the modulation carrier the original data is recovered.

Now let the demodulation carrier differ from modulation

carrier by the phase angle " θ ". Equation (C-25) becomes

$$e_o = e_i \cos \omega_c t \cos(\omega_c t + \theta) \quad (C-26)$$

or

$$e_o = \frac{e_i}{2} \left[\cos(\omega_c t + (\omega_c t + \theta)) + \cos(\omega_c t - (\omega_c t + \theta)) \right]$$

and

$$e_o = \frac{e_i}{2} \left[\cos(2\omega_c t + \theta) + \cos(-\theta) \right]$$

and finally

$$e_o = \frac{e_i}{2} \cos(2\omega_c t + \theta) + \frac{e_i}{2} \cos \theta \quad (C-28)$$

After the usual filtering (C-28) reduces to

$$e_o = \frac{e_i}{2} \cos \theta \quad (C-29)$$

and from (C-25)

$$e_o = \frac{1}{2} \cos \omega_c t \cos \theta \quad (C-30)$$

This shows that the recovered data is a function of phase difference between the modulating and demodulating carriers. If $\theta = \pi/2$, the data is, of course, lost.

Thus the requirements for demodulation of AM modulation by switching are that the frequency and phase be the same for both carriers. These are also the same requirements for DSB demodulation.

To ensure that the demodulating carrier is always of the same frequency and in phase with the modulating carrier, the modulating carrier is recorded as a synchronizing signal on the second track of the duo-track tape simultaneously with the data-modulated carrier on the first track. In the playback mode, the synchronizing signal becomes the demodulating carrier. Thus regardless of tape speed variations, the modulating and demodulating carriers are always of same frequency, and in phase.

These speed variations cause ω'_m to differ from ω_m . Since the percentage change in the data frequency and the synchronizing signal are equally proportional to speed variations, monitoring the synchronizing signal is tantamount to monitoring ω'_m . This monitoring is accomplished by using filters of same percentage bandpass for the data frequencies and synchronizing signal. The fact that the synchronizing signal remains within the filter bandpass ensures that the data-frequencies are within their filters and that the data is being recovered. Furthermore, should the speed variations become excessive, this synchronizing signal is available as a control signal for a speed control servo system.

Thus the requirements for demodulation of FM mod-

ulation by synchronous are that the frequency and phase be

the same for both carriers. There are also the same

requirements for DSS demodulation.

To ensure that the demodulating carrier is always of

the same frequency and in phase with the modulating carrier

the modulating carrier is recorded as a synchronizing

signal on the second track of the dup-track tape simultane-

ously with the data-modulated carrier on the first track.

In the playback mode, the synchronizing signal becomes the

demodulating carrier. This regardless of tape speed

variations, the modulating and demodulating carriers are

always of same frequency and in phase.

These speed variations cause ω_m to differ from ω_c .

Since the percentage change in the base frequency and the

synchronizing signal are equally proportional to speed

variations, monitoring the synchronizing signal is tantamount

to monitoring ω_m . This monitoring is accomplished

by using filters of same percentage bandwidth for the data

frequencies and synchronizing signal. The fact that the

synchronizing signal remains within the filter bandwidth

ensures that the data-frequencies are within their filters

and that the data is being recovered. Furthermore, should

the speed variations become excessive, this synchronizing

signal is available as a control signal for a speed

control servo system.

Appendix D

Antenna

On the basis of portability, the loop antenna seems to be the proper type to use for the data-collecting system. Nevertheless, a further inquiry is advisable before the final selection is made.

Initial computations for a loop antenna may be performed by line integration or by Faraday's Law.

Figure D1 shows the antenna configuration and symbolism. Letting $\theta = 0$,

$$e_o = \int \vec{E} \cdot d\vec{l} = \int_0^h \vec{E} \cdot \vec{k} dl + 0 + \int_{-h}^0 \vec{E} \cdot -\vec{k} dl + 0 \quad (D-1)$$

and

$$\begin{aligned} e &= hE_z e^{-jk(r - \frac{W}{2})} - hE_z e^{-jk(r + \frac{W}{2})} \\ &= hE_z e^{-jkr} \left[e^{j\frac{kW}{2}} - e^{-j\frac{kW}{2}} \right] = 2jh E_z e^{-jkr} \sin \frac{kW}{2} . \end{aligned} \quad (D-2)$$

Now with $W \ll \lambda$,

$$e = jkWh E_z e^{-jkr} . \quad (D-3)$$

Since the area is

$$A = Wh \quad (D-4)$$

Appendix B

Antenna

On the basis of portability, the loop antenna seems to be the proper type to use for the data-collecting system. However, a further study is advisable before the final selection is made. Initial computations for a loop antenna may be performed by using integration or by Faraday's Law.

Figure B1 shows the antenna configuration and

$$E_{\theta} = \int_0^h E_r dl + 0 + \int_{-h}^0 E_r dl + 0 \quad (B-1)$$

and

$$E_{\theta} = h E_0 e^{-jkr} \left(r - \frac{W}{2} \right) - h E_0 e^{-jkr} \left(r + \frac{W}{2} \right) = h E_0 e^{-jkr} \left[e^{-jkr} \left(r - \frac{W}{2} \right) - e^{-jkr} \left(r + \frac{W}{2} \right) \right] = h E_0 e^{-jkr} \left[-\frac{W}{2} e^{-jkr} \right] = -\frac{h W E_0}{2} e^{-jkr} \sin \frac{kr}{2} \quad (B-2)$$

Now with $W \ll \lambda$

$$E_{\theta} = j k W h E_0 e^{-jkr} \quad (B-3)$$

Since the area is

$$A = W h \quad (B-4)$$

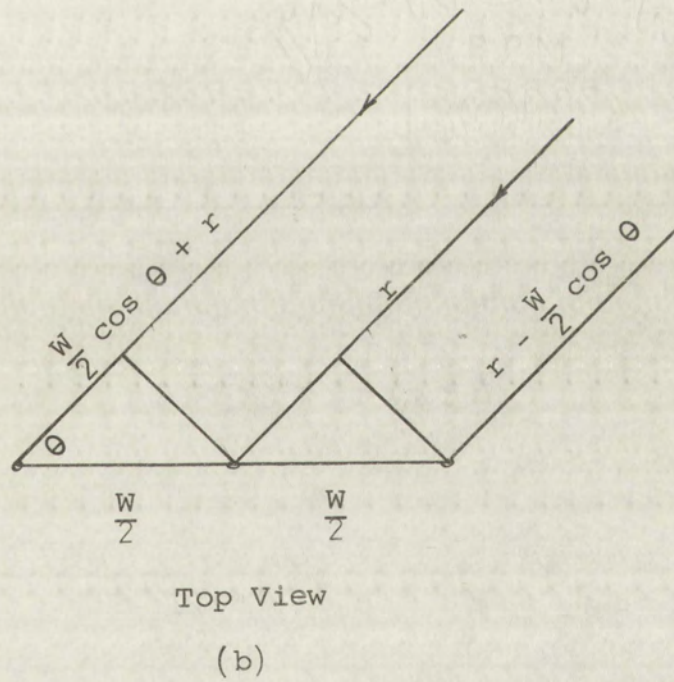
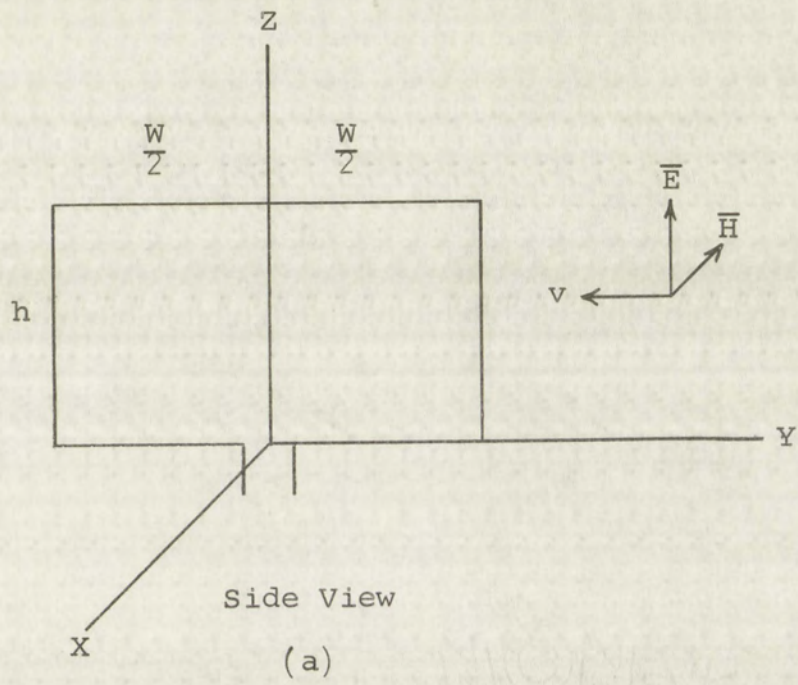


Figure D1 Loop antenna configuration

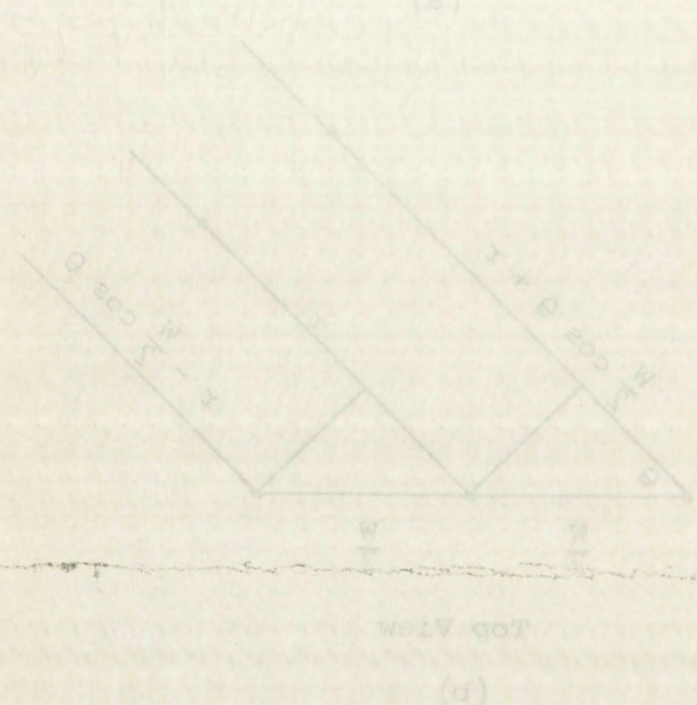
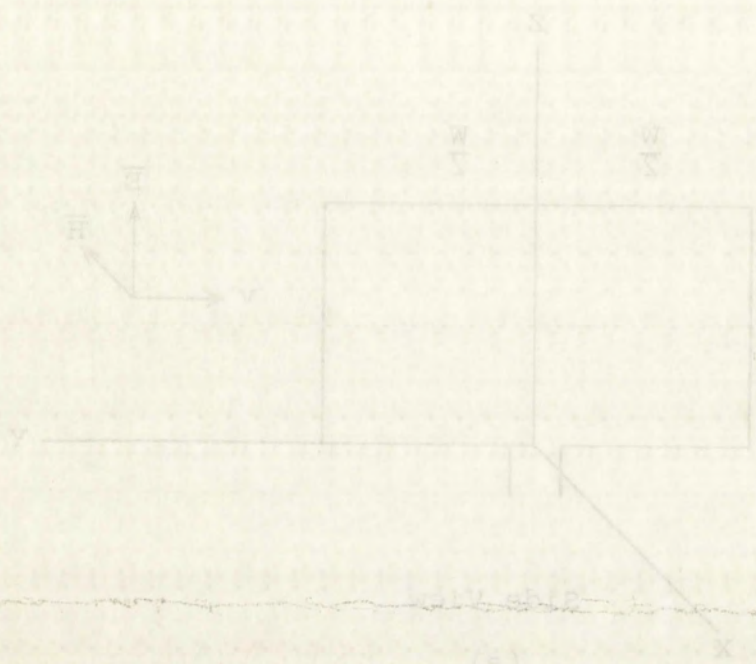


Figure B1 Loop antenna configuration

$$\text{and } k = \frac{2\pi}{\lambda} = 2\pi f \sqrt{\mu\epsilon} = \omega \sqrt{\mu\epsilon} , \quad (\text{D-5})$$

$$e = j A \omega \sqrt{\mu\epsilon} E_z e^{-jkr} \quad (\text{D-6})$$

For "N" turns, then

$$e = j NA \omega \sqrt{\mu\epsilon} E_z e^{-jkr} , \quad (\text{D-7})$$

By Faraday's Law and with $\theta = 0$,

$$e = - NA \frac{\partial \bar{B}}{\partial t} = - NA \mu \frac{\partial \bar{H}}{\partial t} . \quad (\text{D-8})$$

In free space,

$$\eta = \frac{E_v}{H_H} \quad (\text{D-9})$$

and upon substitution

$$e = - \frac{NA\mu}{\eta} \frac{\partial E_z}{\partial t} = \frac{NA\mu}{\eta} j\omega E_z e^{-jkr} . \quad (\text{D-10})$$

Since the relation

$$\eta = \sqrt{\frac{\mu}{\epsilon}} \quad (\text{D-11})$$

holds,

$$e = jNA \omega \sqrt{\mu\epsilon} E_z e^{-jkr} . \quad (\text{D-12})$$

Using either (D-7) or (D-12),

$$|e| = \frac{2\pi}{\lambda} E_z AN \quad (\text{D-13})$$

with $\theta = 0$ and with $W \ll \lambda$. The AN-product becomes

$$AN = \frac{\lambda}{2\pi} \frac{|e|}{E_z} . \quad (\text{D-14})$$

$$\text{and } k = \frac{\omega}{v} = \frac{\omega}{\sqrt{v_0^2 - v^2}} = \frac{\omega}{v_0} \sqrt{1 - \frac{v^2}{v_0^2}} \quad (D-5)$$

$$e = j \omega \sqrt{\epsilon} E_0 e^{-j k x} \quad (D-6)$$

For "N" turns, then

$$e = j \omega N \sqrt{\epsilon} E_0 e^{-j k x} \quad (D-7)$$

By Faraday's law and with $\theta = 0$,

$$e = - N A \frac{\partial H}{\partial t} = - N A \frac{\partial}{\partial t} \left(\frac{E}{H} \right) \quad (D-8)$$

In free space,

$$\frac{E}{H} = \frac{v}{\omega} \quad (D-9)$$

and upon substitution

$$e = - \frac{N A \omega}{v} \frac{E}{H} e^{-j k x} = \frac{N A \omega}{v} \frac{E}{H} e^{-j k x} \quad (D-10)$$

Since the relation

$$v = \sqrt{\epsilon} v_0 \quad (D-11)$$

holds,

$$e = j \omega \sqrt{\epsilon} E_0 e^{-j k x} \quad (D-12)$$

Using either (D-7) or (D-12),

$$|e| = \frac{\omega}{k} E_0 \quad (D-13)$$

with $\theta = 0$ and with $k \ll \lambda$. The $N A$ product becomes

$$N A = \frac{\lambda}{2\pi} \quad (D-14)$$

Considering $\lambda = 3 \times 10^7 \text{ m}$, $E_z = 1 \mu\text{v/m}$, and $|e| = 1 \mu\text{v}$, equation (D-14) becomes

$$AN \approx 5 \times 10^6 [\text{m}^2]. \quad (\text{D-15})$$

This AN-product is obviously too large. For any combination of area and turns, the resultant loop is certainly not portable.

A possible alternative is to restrict the loop area to a size that is portable and consider core material to reduce the required turns. A few calculations show that the weight of the core material is excessive for portability.

In view of this inability to meet the portability requirements, further investigation into the characteristics of the loop antenna was abandoned.

Perhaps the most important aspect of a vertical antenna is the capacity to ground. This capacity is given by¹

$$C = \frac{7.36 \text{ m}}{\log_{10} \frac{2m}{d} - k} \mu\mu\text{fd} \quad . \quad (\text{D-16})$$

where

m = length in feet

d = diameter in feet

h' = height of lower end above ground

¹Terman, F. E., Radio Engineers' Handbook, McGraw-Hill Book Company, Inc., New York, 1943, p. 116.

Considering $\lambda = 3 \times 10^8$ m, $E = 1$ mV/m, and $h = 1$ m, equation (11-1) reduces

$$W \approx 5 \times 10^{-6} \text{ (D-12)}$$

This EM-product is obviously too large for any combination of size and shape. The resultant loop is certainly not portable.

A possible alternative is to restrict the loop size to a size that is portable and consider core material to reduce the required turns. A few calculations show that

the weight of the core material is excessive for portability. In view of this inability to meet the portability requirements, further investigation into the characteristics of the loop antenna was abandoned.

Perhaps the most important aspect of a vertical antenna is the capacity to ground. This capacity is given by

$$C = \frac{7.56 \times 10^{-12} \text{ m}}{\log \frac{2m}{d} - \frac{2m}{d}} \quad \text{(D-13)}$$

where

m = length in feet

d = diameter in feet

h' = height of lower end above ground

and $k = \frac{h'}{m}$ or $\frac{m}{h'}$, whichever is less than unity, from Table 30.²

Table D-1 shows the antenna capacity for various values in equation (D-16). In general, the capacity doubles with doubling the height or with increasing the diameter by a factor of 10. Lowering the height above the ground increases the capacity only slightly.

m (ft)	d (ft)	h' (ft)	k *	C ($\mu\mu\text{fd}$)
20	1/12	1	.376	64.
20	1	1	.376	120.
20	1/6	1	.376	73.6
20	1/12	2	.345	60.6
40	1/12	1/2	.418	115.
40	1/12	1	.398	114.
30	1/12	1/2	.403	90.1
30	1/12	1	.3935	89.8

* See equation (D-16)

Table D-I Capacity of a vertical antenna with variations in dimensions

²
Ibid., p. 116.

and $k = \frac{1}{m} \ln \frac{1}{h}$ whichever is less than unity. From Table 2 to 5.

Table D-1 shows the antenna capacity for various values in equation (D-16). In general, the capacity doubles with doubling the height or with increasing the diameter by a factor of 10. Lowering the height above the ground increases the capacity only slightly.

a (ft)	b (ft)	h (ft)	k	C (pF)
20	$\sqrt{12}$	1	.576	64
20	1	1	.576	120
20	$\sqrt{6}$	1	.576	73.6
20	$\sqrt{12}$	2	.545	60.6
40	$\sqrt{12}$	$\sqrt{2}$.418	115
40	$\sqrt{12}$	1	.398	114
30	$\sqrt{12}$	$\sqrt{2}$.403	90.1
30	$\sqrt{12}$	1	.3955	89.8

* See equation (D-16)

Table D-1. Capacity of a vertical antenna with variations in dimensions

The last entry in Table D-I shows that a 30-ft antenna, 1 inch in diameter, and mounted 1 ft above the ground has a capacity of approximately $90\mu\mu\text{fd}$. The reactance of this antenna in the 0-50 cps region is obviously quite large. In fact, the magnitude of the reactance implies that matching to a receiving device is a problem.

Methods such as capacity top-loading and inductive loading which are used to increase antenna capacity are not applicable here because of the portability requirement.

In spite of the high reactance, the vertical antenna has some advantages. Perhaps the foremost is that the reception pattern is omnidirectional. And in addition, it can be made quite portable by using lightweight material and telescoping sections of convenient length.

A Hall device was also considered as an antenna or sensing element. The impedance is resistive; and therefore is relatively independent of frequency.³ However, in addition to being directional, it also requires much higher signal levels than either a loop or whip antenna for unity signal-to-noise ratio.

³Monsen, G. J., "Pickup Devices for Very-Low Frequency Reception," Electronics, April 14, 1961, p. 68.

The last entry in Table D-1 shows that a 30-ft antenna 1 inch in diameter, and mounted 1 ft above the ground has a capacity of approximately 90 pF. The resistance of this antenna in the 0-50 cps region is obviously quite large. In fact, the magnitude of the resistance implies that matching to a receiving device is a problem.

Methods such as capacity loading and inductive loading which are used to increase antenna capacity are not applicable here because of the portability requirements. In spite of the high resistance, the vertical antenna has some advantages. Perhaps the foremost is that the reception pattern is omnidirectional. And in addition, it can be made quite portable by using lightweight material and telescoping sections of convenient lengths.

A half device was also considered as an antenna or sensing element. The impedance is resistive and therefore is relatively independent of frequency. However, in addition to being directional, it also requires much higher signal levels than either a loop or whip antenna for unity signal-to-noise ratio.

Antenna Capacitance

The vertical antenna finally constructed had the following dimensions:

$$m(\text{ height}) = 28.96 \text{ ft.} = 4.4 \text{ meters}$$

$$h'(\text{ height above ground}) = 0.375 \text{ ft.}$$

$$d(\text{ diameter}) = 0.11 \text{ ft.}$$

From these dimensions,

$$\frac{h'}{m} = 0.013 .$$

The value,

$$k = 0.413,$$

was determined by extending the curve, Figure D2, which was drawn from Table 30 referred to previously.

Using relation (D-16), the capacity was found to be $92.33 \mu\text{mfd.}$ From this, the reactance, as shown in Figure D3, was determined.

Since $m \ll \lambda$ in the 0-50 cps region, the effective height " h_e " can be considered as equal to $m/2$ or 2.2 meters.

Antenna Capacitance

The vertical antenna typically constructed had the

following dimensions:

$$m \text{ (height)} = 38.50 \text{ ft} = 4.4 \text{ meters}$$

$$h' \text{ (height above ground)} = 0.375 \text{ ft}$$

$$d \text{ (diameter)} = 0.11 \text{ ft}$$

From these dimensions

$$\frac{h'}{m} = 0.015$$

$$k = 0.413$$

was determined by extending the curve Figure D2, which

was drawn from Table 30 referred to previously.

Using relation (D-16), the capacity was found to be

92.35 pF. From this, the reactance, as shown in

Figure D3, was determined.

Since $m \ll \lambda$ in the 0-50 cps region, the effective

height "h" can be considered as equal to $m/2$ or 2

meters.

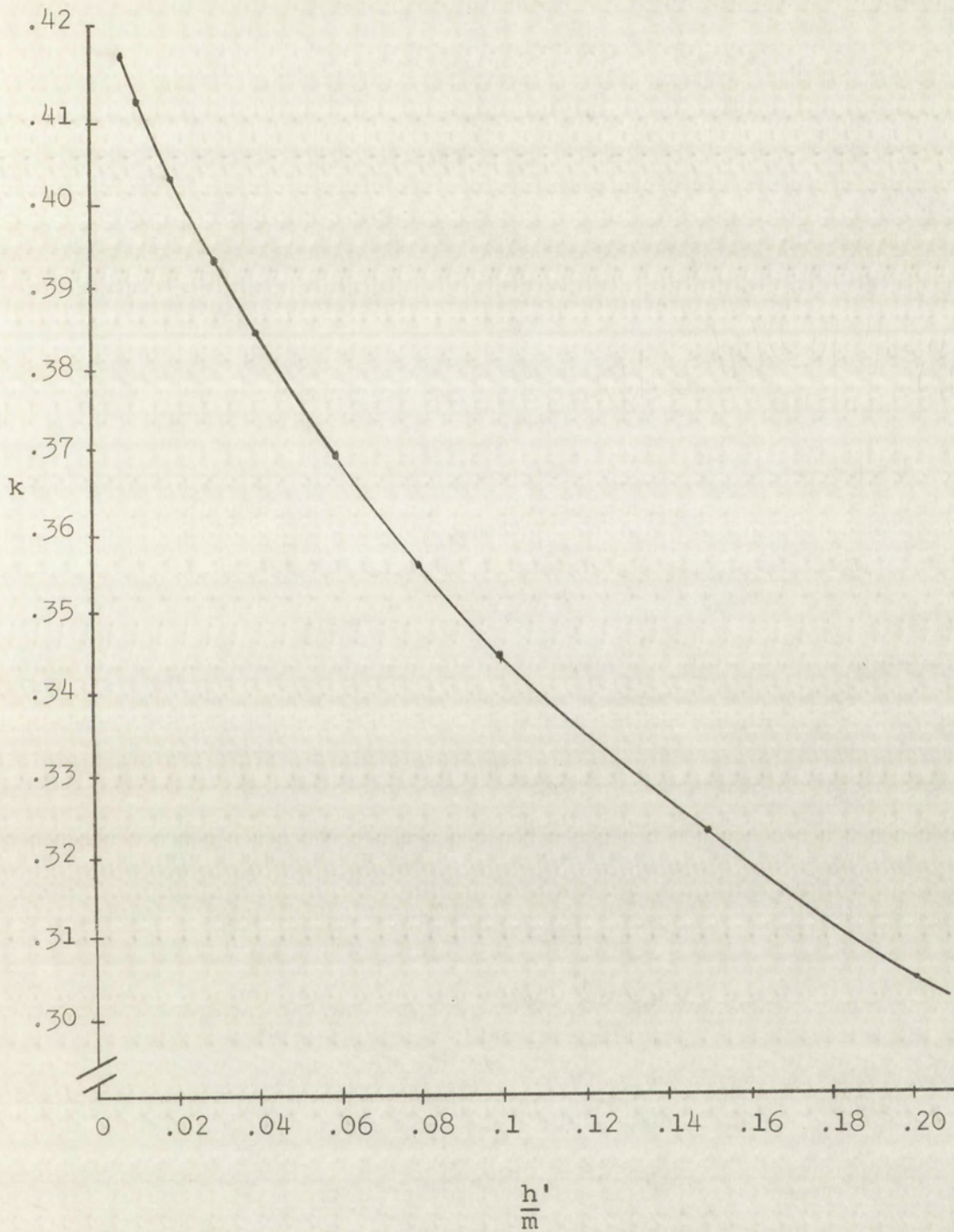


Figure D2 Values of the constant k for $\frac{h'}{m}$

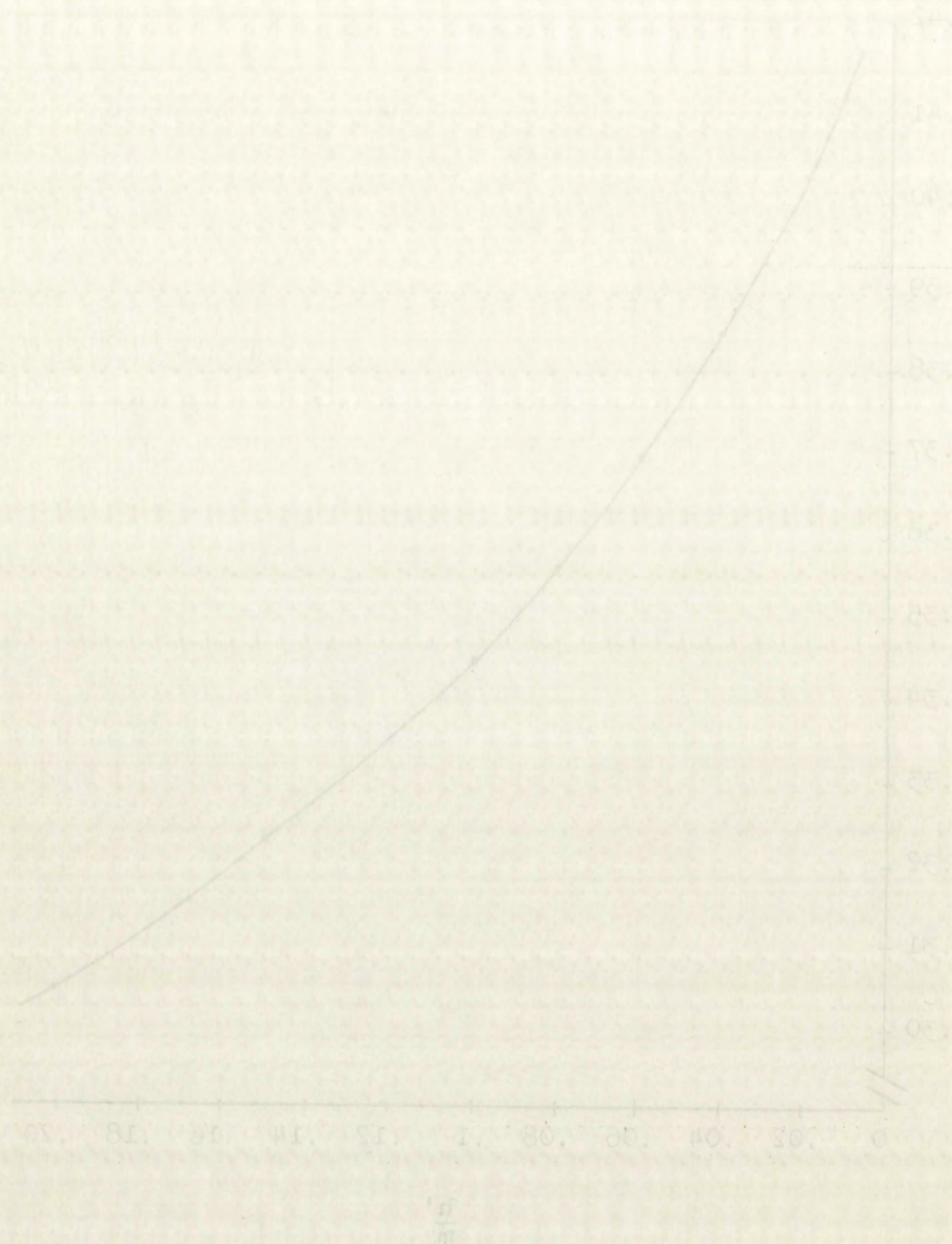


Figure 12 Values of the constant k for $\frac{h'}{m}$

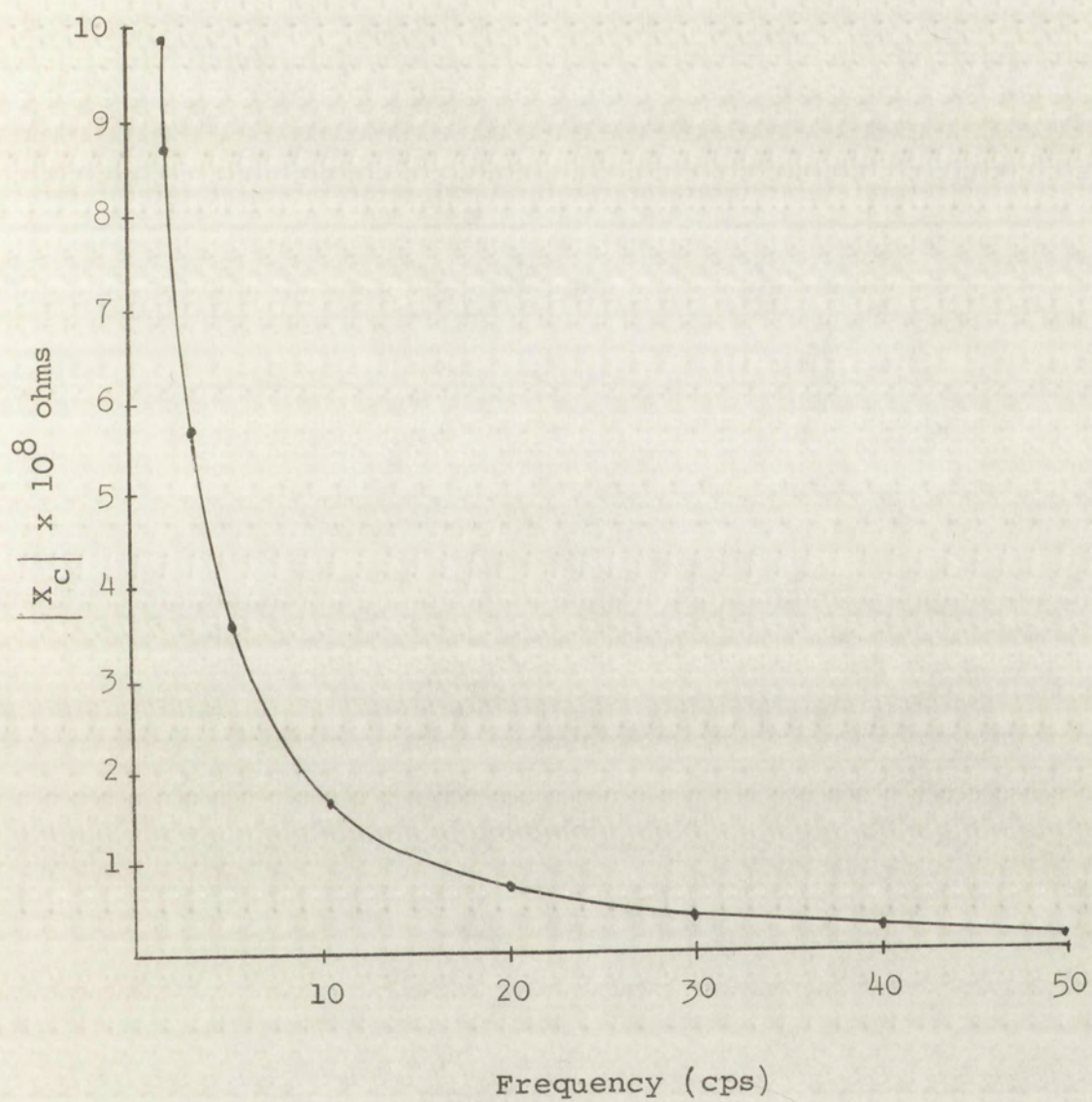


Figure D3 Antenna reactance versus frequency

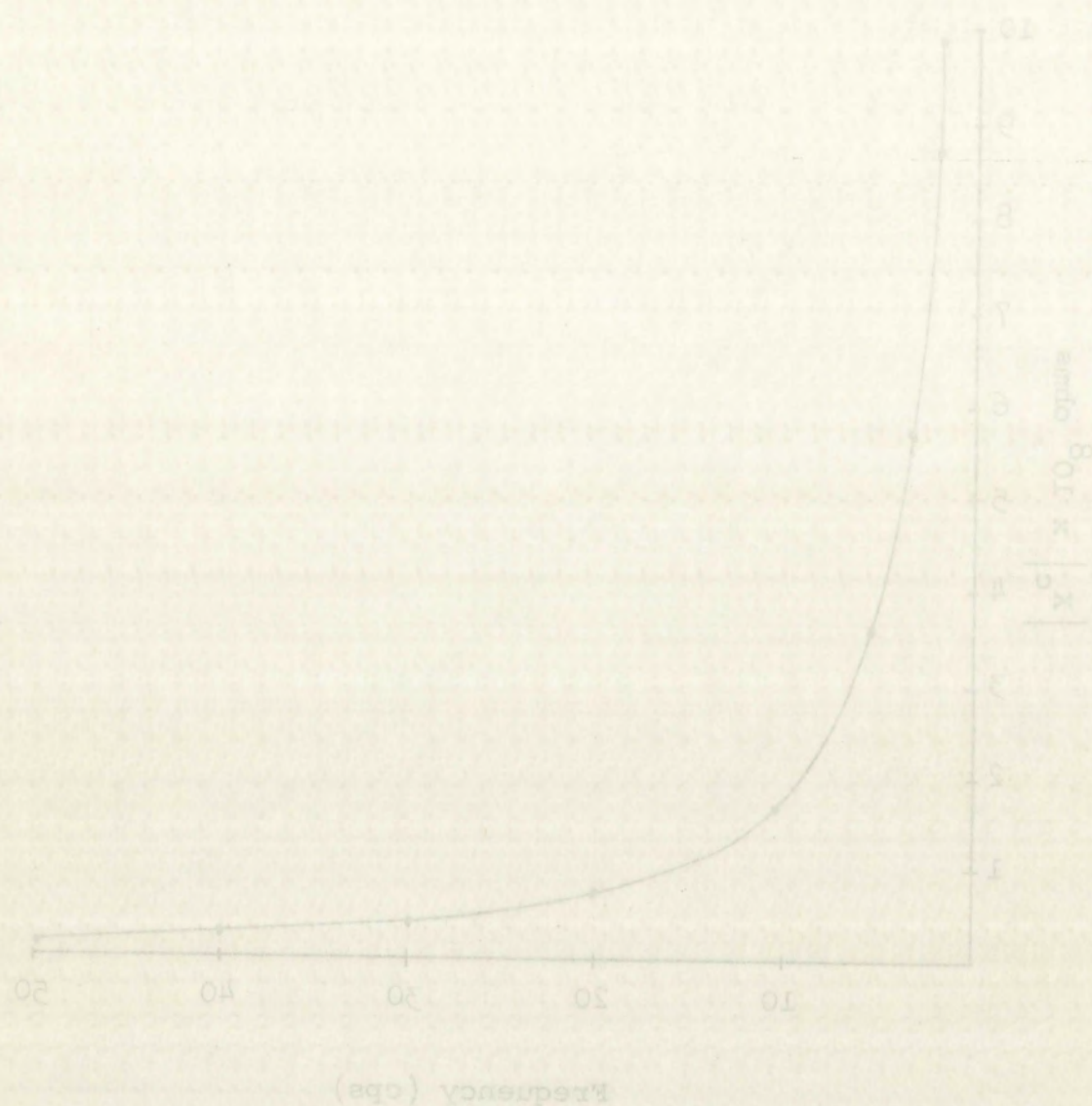


Figure D3. Antenna resistance versus frequency

LIST OF REFERENCES

- Aarons, J., "Low Frequency Electromagnetic Radiation 10 to 900 cps," Jour. Geophys. Res., 61, 647 (1956).
- Aarons, J., G. Gustafsson, and A. Egeland, "Correlation of Audio-Frequency Electromagnetic Radiation with Auroral Zone Micropulsations," Nature, 185, 148, (1960).
- Aarons, J., and M. Henissart, "Low Frequency Noise in the Range 0.5 to 20 cps," Nature 172, part 2, 682 (1953).
- Anderson, Wallace L., Doctoral Dissertation, The Fields of Electric Dipoles in Sea Water--The Earth-Air-Ionosphere Problem, University of New Mexico, 1961.
- Austin and Cohen, Bulletin of Bureau of Standards 7, 315 (1911).
- Appleton, E. V., and F. W. Chapman, "The Nature of Atmospheric," Proc. Roy. Soc. A 158, 1 (1937).
- Balser, M., and C. A. Wagner, "Measurements of Spectrum of Radio Noise from 50 to 100 Cycles per Second," Journal of Research NBS, 64D, No. 4 (1960).
- Barber, N. F., and D. D. Crombie, "VLF Reflections from the Ionosphere in the Presence of a Transverse Magnetic Field," Jour. Atmos. Terr. Phys., 16, 37 (1959).
- Boothe, R. R., B. M. Fannin, and F. X. Bostick, "A Geomagnetic Micropulsation Measuring System Utilizing Air-Core Coils as Detectors," Report Nr. 115, Electrical Engineering Research Laboratory, University of Texas, August 1, 1960.
- Campbell, Wallace H., "Studies of Magnetic Field Micropulsations with Periods of 5 to 30 seconds," Jour. Geophys. Res. 64, 1819 (1959).
- Chapman, F. W., and A. G. Edwards, Proc. U.R.S.I. 8, part 2, 351 (1950).
- Chapman, F. W., and A. Jolley, Proc. U.R.S.I. 10, part 4, 33 (1954).
- Chapman, F. W., and R. C. V. Macario, "Propagation of Audio Frequency Radio Waves to Great Distances," Nature 177, 930 (1956).
- Chapman, F. W., and W. D. Mathews, "Audio-frequency Spectrum Atmospherics," Nature 172, 495 (1953).

LIST OF REFERENCES

- Arnsperg, C. G. "Low Frequency Electromagnetic Radiation in the
900 cps." Journal of Geophysics, 61, 547 (1956).
- Arnsperg, C. G., Gustafsson, and A. Berglund. "Correlation of
Radio-Frequency Electromagnetic Radiation with Auroral
Noise Microfluctuations." Nature, 185, 148 (1960).
- Arnsperg, C. G., and M. Helliwell. "Low Frequency Noise in the
Range 0.5 to 50 cps." Nature 172, part 2, 682 (1953).
- Arnsperg, Wallace L. "Doctoral Dissertation, The Fields of
Electric and Magnetic Fields in Sea Water. The Earth-Air-Ionosphere
Problem. University of New Mexico, 1961.
- Arnsperg, Wallace L. "Bulletin of Bureau of Standards" 16, 315 (1911).
- Arnsperg, E. V., and E. W. Chapman. "The Nature of Atmospheric
Radio Noise." Proc Roy Soc A 158, 1 (1937).
- Baker, M., and C. A. Wagner. "Measurements of Spectrum of
Radio Noise from 50 to 100 Cycles per Second." Journal
of Research NBS, 64D, No. 4 (1960).
- Barber, W. F., and D. B. Crombie. "VLF Reflections from the
Ionosphere in the Presence of a Transverse Magnetic Field."
Journal Atmos. Terr. Phys., 10, 37 (1959).
- Bostick, R. E., E. M. Farnin, and R. K. Bostick. "A Geomagnetic
Micropulsation Measuring System Utilizing Air-Core
Coils as Detectors." Report No. 115, Electrical Engineering
Research Laboratory, University of Texas, August 1, 1960.
- Campbell, Wallace H. "Studies of Magnetic Field Micropulsations
with Periods of 5 to 50 seconds." Journal Geophysics, 64,
1819 (1959).
- Chapman, F. W., and A. G. Edwards. Proc. U.R.S.I., 8, part 2,
351 (1950).
- Chapman, F. W., and A. Jolley. Proc. U.R.S.I., 10, part 4,
33 (1954).
- Chapman, F. W., and R. C. V. MacLeod. "Propagation of Audio
Frequency Radio Waves to Great Distances." Nature 177,
930 (1956).
- Chapman, F. W., and W. D. Mathews. "Audio-Frequency Spectrum
Atmospheric" Nature 172, 405 (1953).

- Chapman, J., and E. T. Pierce, "Relations Between the Character of Atmospherics and Their Place of Origin," Proc. Inst. Radio Engr., 45, 804 (1957).
- Cowles, L. G., "Parallel-T Resistance Capacitance Networks," Proc. IRE, No. 12, Dec., 1952, p. 1712.
- Crary, J. H. and R. A. Helliwell, "Calculations and Interpretation of VLF Field Strengths, Polarizations and Angles of Arrival," U.R.S.I. Conference Georgetown University Abstracts, May 1-4, 1961, p. 40.
- Crombie, D. D., "Differences Between the East-West and West-East Propagation of VLF Signals Over Long Distances," Jour. Atmos. Terrest. Phys., 12, 110 (1958).
- Davis, Robert C., "The Average Rate of Lightning Flashes to Ground," U.R.S.I. Conference Georgetown University Abstracts, May 1-4, 1961, p. 23.
- Duffus, H. J., P. W. Nasmyth, J. A. Shand, and Sir Charles Wright, "Note on Low Frequency Electromagnetic Studies at P.N.L.," P.N.L. (Pacific Naval Laboratory), VLF Symposium, NBS Boulder, Vol. II, paper 19, 1957.
- Duffus, H. J., P. W. Nasmyth, J. A. Shand, C. S. Wright, "Sub-audible Geomagnetic Fluctuations," Nature, 181, part 2, 1258 (1958).
- Fitchen, F., R. Dubois, and C. Polk, "Schumann Resonances of the Earth-Ionosphere Cavity," U.R.S.I. Conference University of Texas, October 1961.
- Gallet, Roger M., "Very-low-frequency Emissions Generated in the Earth's Exosphere," Proc. IRE, 47, 211 (1959).
- Gallet, R. M., and R. A. Helliwell, "A Theory of the Production of VLF Noise (so-called Dawn Chorus) by Traveling Wave Amplification in the Exosphere of the Earth," VLF Symposium Vol. II, paper 20, 1957.
- Gallet, R. M., and R. A. Helliwell, "Origin of Very-low-frequency Emissions," Jour. Res. NBS, 63D, 21 (1959).
- Goldberg, P. A., "Electromagnetic Phenomena of Natural Origin in the 1.0-150 cps Band," Nature, 177, 1219 (1956).
- Grierson, J. K., "A Technique for Rapid Analysis of Whistlers," Proc. IRE, 45, 806 (1957).
- Gruentz, O.O., "8000 Cycle Sound Spectrograph," Bell Lab. Review, Vol. 29, 256, June 1951.

- Gustafsson, G., A. Egeland, and J. Aarons, "Audio-frequency Electromagnetic Radiation in the Auroral Zone," Jour. Geophys. Res. 65, No. 9 (1960).
- Hales, A. L., "A Possible Mode of Propagation of the "Slow" or Tail Component in Atmospherics," Proc. Roy. Soc. A 193, 60, (1948).
- Helliwell, R. A., "Whistlers and Very Low Frequency Emissions," Geophysics and the IGY, Geophysical Monograph No. 2, American Geophysic Union, Washington D. C., July, 1958.
- Helliwell, R. A., "Low Frequency Propagation Studies, Part I-Whistlers and Related Phenomena," June, 1953-Sept., 1956, Report, (Revised May, 1958) Final Report, Stanford Electronics Laboratories, Stanford University.
- Helliwell, R. A., J. H. Crary, J. H. Pope, and R. L. Smith, "The Nose Whistler-a New High-Latitude Phenomenon," Jour. Geophys. Res. 61, 139 (1956).
- Helliwell, R. A., and M. G. Morgan, "Atmospheric Whistlers," Proc. IRE, 47, No. 2 (1959).
- Hepburn, F., "Wave-guide Interpretation of Atmospheric Waveforms," Jour. Atmos. Terrest. Phys., 10, 121 (1957a).
- Hepburn, F., "Atmospheric Waveforms with Very-low-frequency Components below 1 kcs Known as Slow Tails," Jour. Atmos. Terrest. Phys., 10, 266 (1957b).
- Hepburn, F., "Classification of Atmospheric Waveforms," Jour. Atmos. Terrest. Phys., 12, 1 (1958).
- Hepburn, F., and E. T. Pierce, "Atmospherics with Very-low Frequency Components," Nature, 171, 837, (1953).
- Holzer, R. E., and O. E. Deal, "Low Audio-frequency Electromagnetic Signals of Natural Origin," Nature, 177, 536 (1956).
- Hopkins, Geo. H. Jr., "A Survey of Past and Present Investigations of the Natural Earth Currents," Report No. 113, Electrical Engineering Research Laboratory, University of Texas, April 1, 1960.
- Large, M. I., Dissertation, Some Investigations in Atmospheric Electricity, Cambridge University, 1957.
- Large, M. I., and T. W. Wormell, "Fluctuations in the Vertical Electric Field in Frequency Range from 1 cps to 500 cps," Recent Advance Atmospheric Electricity, Pergamon Press Ltd., New York, 1958, p. 603.

Chapman, G. A., "The Earth's Magnetic Field," *Journal of Geophysical Research*, Vol. 65, No. 3, 1960.

Chapman, G. A., "The Earth's Magnetic Field," *Journal of Geophysical Research*, Vol. 65, No. 3, 1960.

Hellweger, E. A., "The Earth's Magnetic Field," *Journal of Geophysical Research*, Vol. 65, No. 3, 1960.

Hellweger, E. A., "The Earth's Magnetic Field," *Journal of Geophysical Research*, Vol. 65, No. 3, 1960.

Hellweger, E. A., "The Earth's Magnetic Field," *Journal of Geophysical Research*, Vol. 65, No. 3, 1960.

Hellweger, E. A., "The Earth's Magnetic Field," *Journal of Geophysical Research*, Vol. 65, No. 3, 1960.

Hellweger, E. A., "The Earth's Magnetic Field," *Journal of Geophysical Research*, Vol. 65, No. 3, 1960.

Hellweger, E. A., "The Earth's Magnetic Field," *Journal of Geophysical Research*, Vol. 65, No. 3, 1960.

Hellweger, E. A., "The Earth's Magnetic Field," *Journal of Geophysical Research*, Vol. 65, No. 3, 1960.

Hellweger, E. A., "The Earth's Magnetic Field," *Journal of Geophysical Research*, Vol. 65, No. 3, 1960.

Hellweger, E. A., "The Earth's Magnetic Field," *Journal of Geophysical Research*, Vol. 65, No. 3, 1960.

Hellweger, E. A., "The Earth's Magnetic Field," *Journal of Geophysical Research*, Vol. 65, No. 3, 1960.

Hellweger, E. A., "The Earth's Magnetic Field," *Journal of Geophysical Research*, Vol. 65, No. 3, 1960.

Hellweger, E. A., "The Earth's Magnetic Field," *Journal of Geophysical Research*, Vol. 65, No. 3, 1960.

- Liebermann, L. N., "Anomalous Propagation Below 500 c/s,"
VLF Symposium NBS, Boulder, Vol. III, paper No. 25, 1957.
- Liebermann, L. N., "Extremely Low Frequency Electromagnetic
Waves, I. Reception From Lightning," Jour. Appl. Phys.
27, 1473 (1956a).
- Liebermann, L. N., "Extremely Low Frequency Electromagnetic
Waves, II. Propagation Properties," Jour. Appl. Phys. 27,
1477 (1956b).
- Lutkins, F. E., "The Nature of Atmospherics," Proc. Roy. Soc.
171A, 285 (1939).
- Maple, Elwood, "1 to 50 cps Geomagnetic Fluctuations," U.R.S.I.
Conference Abstracts, University of Texas, Oct.20-21,
1961, p. 14.
- Martin, L. H., R. A. Helliwell, and K. R. Marks, "Association
Between Aurorae and Very Low-frequency Hiss Observed at
Byrd Station, Antarctica," Nature, 187, 751 (1960).
- Menzel, D. H., and W. W. Salisbury, "Audio-frequency Radio
Waves from the Sun," Nature, 161, 91 (1948).
- Monsen, G. J., "Pickup Devices for Very-Low Frequency Reception,"
Electronics, April 14, 1961, p. 68.
- Pierce, E. T., "Electrostatic Field-changes due to Lightning
Discharge," Quart. Jour. Roy. Met. Soc., 81, 211 (1955).
- Pierce, E. T., "The Propagation of Radio Waves at Frequencies
Less than 1 kcs," Proc. IRE, 48, 329 (1960a).
- Pierce, E. T., "Some ELF Phenomena," Jour. Res. NBS, 64D,
No. 4, (1960b).
- Pierce, E. T., "Attenuation Coefficients at Very Low Frequencies
(VLF) During a Sudden Ionospheric Disturbance (SID),"
U.R.S.I. Conference Georgetown University Abstracts,
May 1-4, 1961, p. 40.
- Potter, R. K., "Visible Patterns of Sound," Science, 102,
463 (1945).
- Raemer, H. R., "Extremely Low Frequency Terrestrial Noise as a
Propagation Research Tool," U.R.S.I. Conference Georgetown
University Abstracts, May 1-4, 1961, p. 39.
- Schumann, W. O., "The Propagation of Very Long Radio Waves
Around the Earth and Signals from Lightning," Nuovo
Cimento, 9, 1116, (1952a).

Liebermann, L. W., "Anomalous Propagation Below 500 c/s,"
VLF Symposium NBS, Boulder, Vol. III, paper No. 25, 1957.

Liebermann, L. W., "Extremely Low Frequency Electromagnetic
Waves, I. Reception from Lightning," Jour. Appl. Phys.
27, 1473 (1956).

Liebermann, L. W., "Extremely Low Frequency Electromagnetic
Waves, II. Propagation Properties," Jour. Appl. Phys. 27,
1477 (1956).

Luckins, F. E., "The Nature of Aurorae," Proc. Roy. Soc.
171A, 285 (1939).

Maple, R. Wood, "1 to 50 cps Geomagnetic Fluctuations," U.S.S.I.
Conference Abstracts, University of Texas, Oct. 20-21,
1961, p. 14.

Martin, J. H., R. A. Helliwell, and K. R. Marke, "Association
Between Aurorae and Very Low-Frequency Hiss Observed at
Byrd Station, Antarctica," Nature, 187, 751 (1960).

Menzel, D. H., and W. W. Salisbury, "Audio-frequency Radio
Waves from the Sun," Nature, 161, 91 (1948).

Morse, G. J., "Pickup Devices for Very-Low Frequency Reception,"
Electronics, April 14, 1961, p. 68.

Pierce, E. T., "Electrostatic Field-changes due to Lightning
Discharges," Quart. Jour. Roy. Met. Soc., 81, 211 (1955).

Pierce, E. T., "The Propagation of Radio Waves at Frequencies
Less than 1 Mc," Proc. IRE, 48, 529 (1960a).

Pierce, E. T., "Some ELF Phenomena," Jour. Res. NBS, 64D,
No. 4, (1960b).

Pierce, E. T., "Attenuation Coefficients at Very Low Frequencies
(VLF) During a Sudden Ionospheric Disturbance (SID)," U.S.S.I.
Conference Abstracts, Georgetown University Abstracts,
May 1-4, 1961, p. 40.

Potter, R. K., "Visible Patterns of Sound," Science, 102,
463 (1945).

Raezer, H. R., "Extremely Low Frequency Terrestrial Noise as a
Propagation Research Tool," U.S.S.I. Conference Georgetown
University Abstracts, May 1-4, 1961, p. 39.

Schumann, W. G., "The Propagation of Very Long Radio Waves
Around the Earth and Signals from Lightning," Nuovo
Cimento, 9, 1116, (1952a).

- Schumann, W. O., "Über die strahlungslosen Eigenschwignungen einer leitenden Kugel, die von einer Luftschicht und einer Ionosphärenhülle umgeben ist," Zeitschrift für Naturforschung, 7A, 149 (1952b).
- Schumann, W. O., "Über die oberfelder bei der ausbreitung langer, elektrischer wellen im system erde-luft-ionosphere und z anwendungen (horizontaler und senkrechter dipol)," Zeits fur ante, Phys, 6, 34, (1954a).
- Schumann, W. O., "On the Radiation of Long Waves from a Horizontal Dipole in the Cavity Between the Earth and Ionosphere," Zeitz fur ange, Phys, 6, 225 (1954b).
- Schwartz, Mischa, Information Transmission, Modulation, and Noise, McGraw-Hill Book Company, Inc., 1959.
- Seshu, S. and N. Balabanian, Linear Network Analysis, John Wiley and Sons, Inc., 1959.
- Smith, H. W., L. D. Provazek, and F. X. Bostick, Jr., Directional Properties and Phase Relations of the Magneto-telluric Fields at Austin, Texas, Report No. 116, Electrical Engineering Research Laboratory, University of Texas, October 10, 1960.
- Storey, L. R. O., "A Method to Interpret the Dispersion Curves of Whistlers," VLF Symposium, NBS, Boulder, Vol. I, Paper 9, 1957.
- Taylor, W. L., "Radiation Field Characteristics of Lightning Discharges in the Band 1 kc to 100 kc," U.R.S.I. Conference Georgetown University Abstracts, May 1-4, 1961.
- Tepley, L. R., "A Comparison of Sferics as Observed in the VLF and ELF Bands," Jour. Geophys. Res. 64, 2315 (1959).
- Tepley, L. R., "Sferics from Intracloud Lightning Strokes," Jour. Geophys. Res. 66, No. 1, (1961a).
- Tepley, L. R., "Observations of Hydromagnetic Emissions," Jour. Geophys. Res. 66, No. 6 (1961b).
- Terman, F. E., Radio Engineers' Handbook, McGraw-Hill Book Company, Inc., New York, 1943, p. 116.
- Valley, G. E., Jr., and H. Wallman, Vacuum Tube Amplifiers, Vol. 18, Radiation Laboratory Series, McGraw-Hill Book Company, Inc., 1948.
- Wait, J. R., On the Mode Theory of VLF Ionospheric Propagation, NBS Report No. 5022, October, 1956.

Schumann, W. O. "The ... of ..."

Schumann, W. O. "The ... of ..."

Schumann, W. O. "The ... of ..."

Schumann, W. O. "The ... of ..."

Schumann, W. O. "The ... of ..."

Schumann, W. O. "The ... of ..."

Schumann, W. O. "The ... of ..."

Schumann, W. O. "The ... of ..."

Schumann, W. O. "The ... of ..."

Schumann, W. O. "The ... of ..."

Schumann, W. O. "The ... of ..."

- Wait, J. R., "The Attenuation vs. Frequency Characteristics of VLF Radio Waves," Proc. IRE, 45, 768 (1957).
- Wait, J. R., "Terrestrial Propagation of Very-Low Frequency Radio Waves," Jour. Res. NBS, 64D, No. 2, 153 (1960a).
- Wait, J. R., A Survey and Bibliography of Recent Research in the Propagation of VLF Radio Waves, NBS Technical Note No. 58, (1960b).
- Wait, J. R., "Preface to ELF Papers," Conference on Propagation of Electromagnetic Waves at ELF, NBS, Boulder, Jan. 26, 1960, Jour. Res. NBS, 64D, No. 4, p. 381 (1960c).
- Wait, J. R., "Mode Theory of the Propagation of ELF Radio Waves," Jour. Res. NBS, 64D, July-August (1960d).
- Wait, J. R., Report of U.S. Commission 4, U.R.S.I. "Radio Noise of Terrestrial Origin," Part 4, A Summary of VLF and ELF Propagation Research. Jour. Res. NBS, 64D, No. 6, (1960e).
- Wait, J. R., and N. F. Carter, Field Strength Calculation for ELF Radio Waves, NBS Technical Note No. 52 (1960).
- Watson-Watt, R. A., J. F. Herd, and F. E. Lutkin, "On the Nature of Atmospherics," Proc. Roy. Soc. A 162, 267 (1937).
- Watt, A. D., "ELF Electric Fields from Thunderstorms," Jour. Res. NBS, 64D, No. 5, (1960).
- Watt, A. D., and E. L. Maxwell, "Measurement of Statistical Characteristics of VLF Atmospheric Radio Noise," Proc. IRE, 45, part 1, p. 55 (1957).
- Watts, J. M., "An Observation of Audio-frequency Electromagnetic Noise During a Period of Solar Disturbance," Jour. Geophys. Res. 62, 199 (1957a).
- Watts, J. M., "Audio-frequency Electromagnetic Hiss Recorded at Boulder in 1956," VLF Symposium, NBS, Boulder, Vol. II, Paper No. 17 (1957b).
- White, Gifford, "Design and Use of RC Parallel-T Networks," IRE Transactions on Audio, Vol. AV-8, Jan-Feb, 1960.
- Whitson, A. L., Arctic Atmospheric Noise and Propagation Studies Part A: Arctic Sferic Data--August 1958 to March 1959, a final report on Contract AF 19(604)-2409, February, 1960.
- Willis, H. F., "Audio-frequency Magnetic Fluctuations," Nature, 161, 887 (1948).
- Wilson, C. T. R., Phil. Trans. A, 221, p. 75 (1920).

Wait, J. R., "The Atmosphere as a Waveguide for VLF Radio Waves", Proc. IRE, 45, 10, 1450-1454 (1957).

Wait, J. R., "Theoretical Investigation of the Propagation of VLF Radio Waves", Radio Waves, 1, 1, 1-10 (1957).

Wait, J. R., A. Suvorov and R. F. Millington, "The Propagation of VLF Radio Waves", Radio Waves, 1, 1, 1-10 (1957).

Wait, J. R., "Reference to the Propagation of Electromagnetic Waves in the Earth's Ionosphere", 1960, Jour. Res. NBS, 64D, 1, 1-10 (1960).

Wait, J. R., "Mode Theory of the Propagation of VLF Radio Waves", Jour. Res. NBS, 64D, 1, 1-10 (1960).

Wait, J. R., Report to the Commission of the European Communities, "Terrestrial Origin of VLF Radio Waves", Jour. Res. NBS, 64D, 1, 1-10 (1960).

Wait, J. R., and R. F. Millington, "The Propagation of VLF Radio Waves", Radio Waves, 1, 1, 1-10 (1957).

Watson-Watt, R. A., J. E. Hill, and J. E. Hill, "The Propagation of VLF Radio Waves", Radio Waves, 1, 1, 1-10 (1957).

Watt, A. D., "The Electric Fields from Thunderstorms", Res. NBS, 64D, 1, 1-10 (1960).

Watt, A. D., and E. L. Munn, "The Propagation of VLF Radio Waves", Radio Waves, 1, 1, 1-10 (1957).

Watts, J. M., "An Observation of the Propagation of VLF Radio Waves", Res. NBS, 62, 109 (1957).

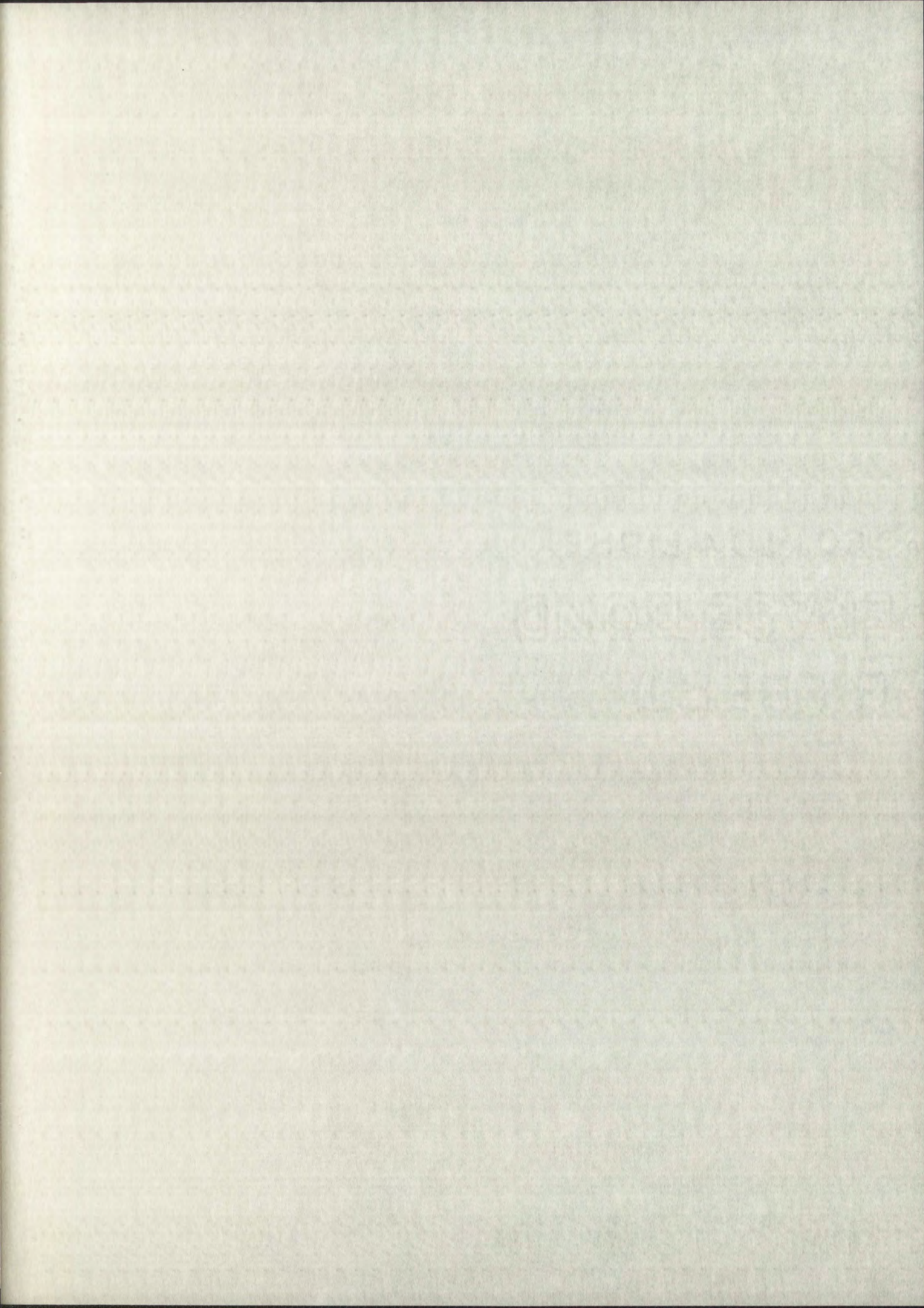
Watts, J. M., "VLF Propagation in 1956", Boulder Jour. Paper No. 17 (1957).

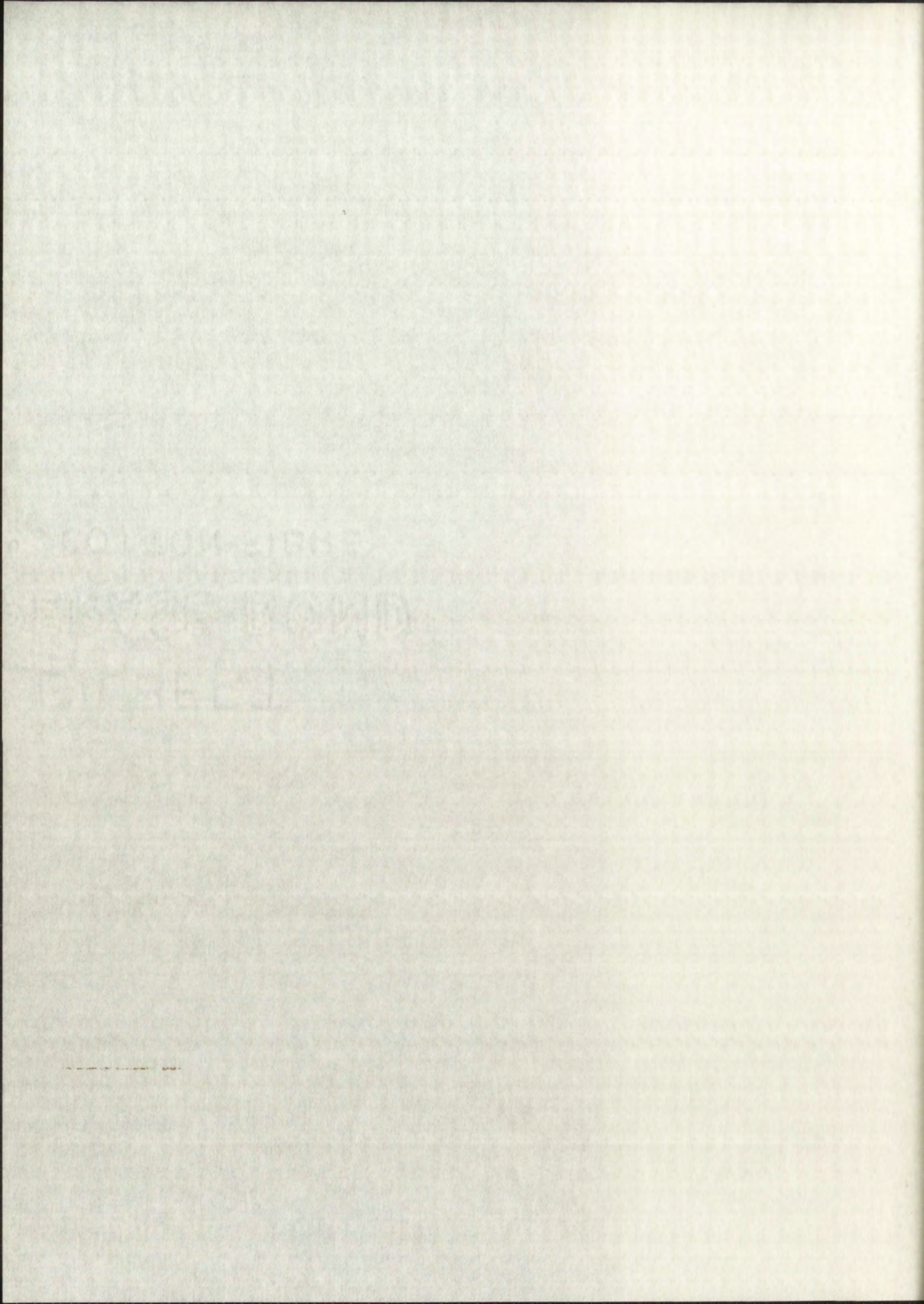
White, Gifford, "Design and Use of an Earthed-Loop Network", IRE Transactions on Audio, Vol. 44, Part 1, 1-10 (1957).

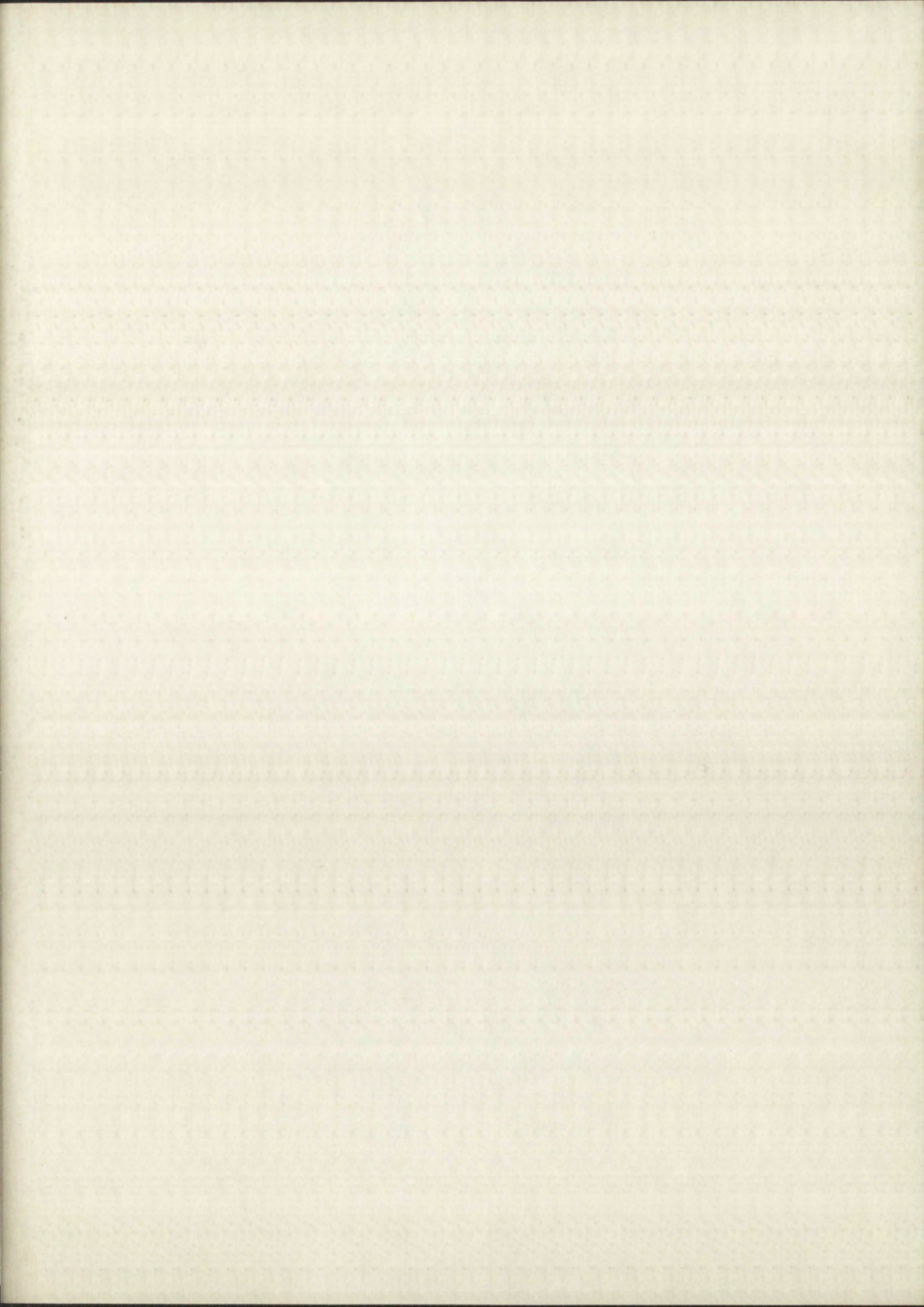
Wilson, A. L., "Arctic Atmosphere Research and Propagation of VLF Radio Waves", Part A: Arctic Atmosphere Research and Propagation of VLF Radio Waves, a final report on Contract No. 44-1-109, 1-10 (1957).

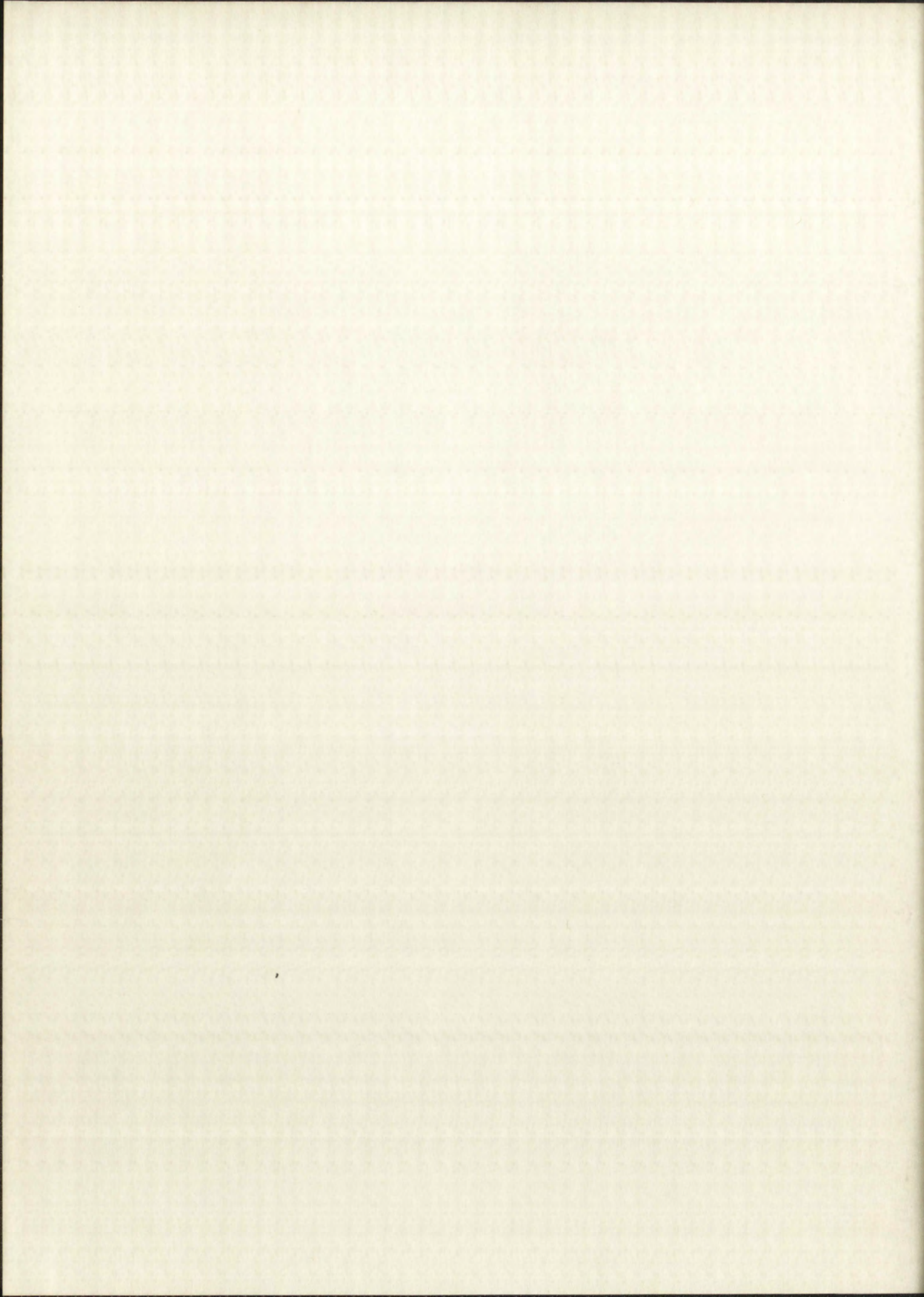
Willis, H. F., "Radio Frequency Measurements in the Ionosphere", 161, 887 (1948).

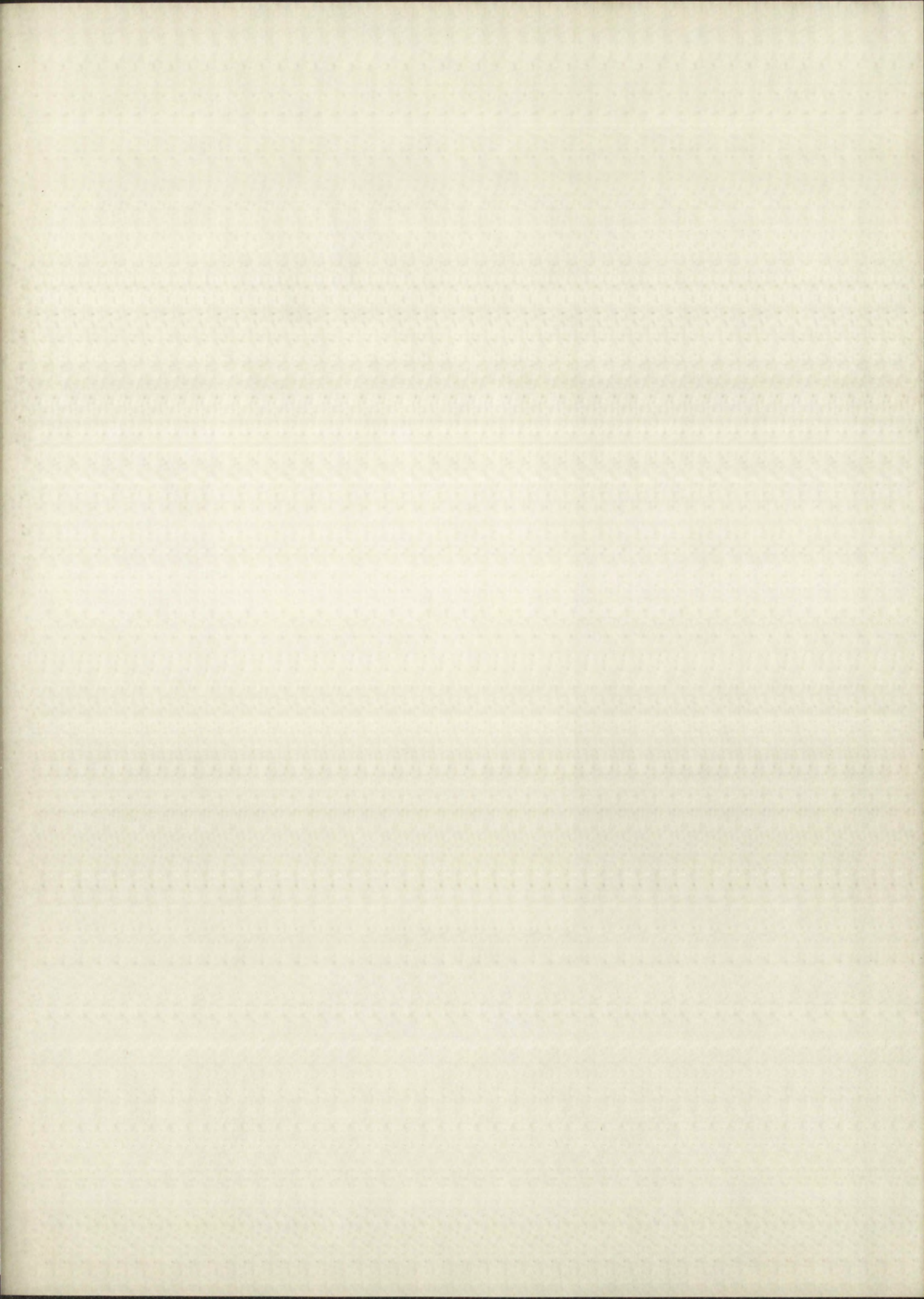
Wilson, C. T. R., "The Propagation of VLF Radio Waves", Radio Waves, 1, 1, 1-10 (1957).











IMPORTANT!

Special care should be taken to prevent loss or damage of this volume. If lost or damaged, it must be paid for at the current rate of typing.

DATE DUE			
GAYLORD			PRINTED IN U.S.A.

